Non-Covalent Binding

Rotaxane-Based Molecular Machines, Molecular Motion and Ion Sensing

Dissertation zur Erlangung des akademischen Grades des Doktors der Naturwissenschaften (Dr. rer. nat.)

eingereicht im Fachbereich Biologie, Chemie, Pharmazie der Freien Universität Berlin

vorgelegt von

Dominik P. Weimann

aus München

2012

Die vorliegende Arbeit wurde im Zeitraum von Mai 2007 bis August 2012 am Institut für Chemie und Biochemie der Freien Universität Berlin unter Betreuung von Herrn Prof. Dr. Christoph A. Schalley erstellt.

1. Gutachter: Prof. Dr. Christoph Schalley

2. Gutachter: Prof. Dr. Rainer Haag

Disputation am 31. Oktober 2012

“In the beginning there was nothing, which exploded.”

Terry Pratchett (*1948), “Lords and Ladies”

“Science may set limits to knowledge, but should not set limits to imagination.”

Bertrand Russell (1872 - 1970)

Summary

Non-covalent interactions play a key role in nature as their reversible formation and dynamic nature allows the control of almost all biological processes. This thesis deals with several projects about the exploration of the potential of non-covalent interactions for the creation and analysis of ion receptors, the templation of the self-assembly of supramolecular encapsulation complexes, and the construction and control of molecular machines. The detailed achievements can be summarized as follows:

- The well-known Hunter/Vögtle-type tetralactam macrocycle could be modified accordingly so that a change of the solution's acidity from neutral to strongly basic induces a conformational switch of the macrocycle's conformation causing it to contract and also to turn one of the four amide protons outwards the macrocyclic cavity. This effect was used to control the shuttling rate in bistationary [2]rotaxane-based molecular shuttles prepared from this switchable macrocycle. Depending on the central spacer separating the two ethylene diamide stations in the axle, the shuttling rate is influenced either by the shrinking of the macrocycle's inner cavity or the weakening of the hydrogen bonding interactions between macrocycle and axle.
  Furthermore, it was found that the 4,6-dialkoxy functionalization of the isophthaloyl moiety used in the design of the switchable tetralactam macrocycle, works as an integrated template to direct Hunter/Vögtle-type macrocyclization reactions towards the selective formation of octalactam macrocycles. This class of larger macrocycles accommodating two instead of just one recognition sites for hydrogen-bond acceptor guest molecules has been only observed as a side product of the corresponding tetralactam macrocycle so far.

- Gas-phase H/D exchange experiments were employed to track the highly dynamic motion of 18-crown-6 along oligolysine peptide chains and over the periphery of POPAM dendrimers in what could be called a "spacewalk" on the molecular level. Furthermore, mechanistic studies with suitable model compounds showed the crown ethers to move together with a proton from an ammonium to an amino group. Finally, the zwitterionic structure of crown complexes of acid-terminated oligolysine peptides is expressed by the isotope exchange behaviour.

Only the unique environment-free conditions of the highly diluted gas phase inside a mass spectrometer provide the ideal means required to investigate the dynamics within non-covalent complexes, as intermolecular dissociation/reassociation processes that may likely occur in solution can be ruled out completely here. Consequently, gas-phase chemistry provides insight into a completely new reactivity of weakly bound supramolecular complexes and suggests many non-covalent complexes to exhibit a more pronounced dynamic behaviour than commonly recognized.

- It was shown that mass spectrometry and gas-phase experiments are perfectly suited for the analysis of the binding of anions to different receptor molecules through hydrogen bonding and anion-π interactions, respectively. Not only do these experiments complement results from experiments in solution (e.g. from NMR), but rather extend the view on recognition phenomena.
  For the first time, it was possible to observe anion-π interactions at work under the environment-free conditions in the highly diluted gas phase. Furthermore, working in the gas phase allows the exclusive study of the intrinsic properties of a receptor without any solvation effects: Tandem MS experiments allowed the determination of the influence of the substitution pattern of monomeric naphthalene diimide systems (NDIs) on the anion binding behavior through anion-π interactions, whereby π-acidification and active-site decrowding increased the binding strenghth.

- The investigation of the formation of resorcinarene hexamers by complementary gas-phase and solution NMR studies revealed that the hexamers encapsulating pseudooctahedral transition metal complexes (e.g. $Ru(bpy)_3^{2+}$ as well as singly charged and neutral Ir-based analoga, each with differently strongly coordinating anions) are only formed under special conditions: In solution, larger aggregates are only formed with the doubly charged $Ru(bpy)_3^{2+}$ complex in combination with the extremely weakly coordinating $[Al(OC(CF_3)_3)_4]^-$ anion. However, even this does not lead to the exclusive formation of 6:1 complexes, but rather to a mixture of different ones. In marked contrast, the ESI-FTICR-MS experiments show a strong preference for exactly these 6:1 complexes indicating a stepwise clipping of resorcinarene monomers to the $Ru(bpy)_3^{2+}$ complex as the mechanistic pathway, which can only be concluded by the comparison of gas-phase and solution results.

- In the last project, the binding of tetramethylammonium (TMA) to upper-rim substituted resorcinarenes was examined. Whereas gas-phase tandem-MS experiments exposed the pure intrinsic properties of the different receptors based on the substituents electronic effects, NMR titrations unraveled a significant influence of the counteranion on the binding situation in a competitive solvent. It was found that halogen substituents on the resorcinarene's upper rim render the adjacent OH groups more acidic, which allows the halogenated resorcinarenes to from stronger Ar-OH•••anion hydrogen bonds than the other non-halogenated analoga. Consequently, the additional binding of the anion increases the binding constant of the TMA cation, as it is bound together with its anion to the resorcinarene.

  These results clearly point out the importance of considering more than just one analytical method for the investigation of supramolecular recognition and complexation events. The comparison results from different methods initially appearing contradictory may open an entirely new view on the basic interactions affecting the binding.

Zusammenfassung

Nichtkovalente Wechselwirkungen spielen eine Schlüsselrolle in der Natur, da ihre reversible Bildung und dynamische Natur die Kontrolle fast aller biologischer Prozesse erlauben. Die vorliegende Arbeit befasst sich mit mehreren Projekten bezüglich der Erforschung des Potentials nichtkovalenter Wechselwirkungen für die Gestaltung und Analyse von Ionenrezeptoren, die templatgesteuerte Selbstorganisation von supramolekularen Einkapselungskomplexen sowie für die Konstruktion und kontrollierte Steuerung von molekularen Maschinen. Die detaillierten Erfolge können wie folgt zusammengefasst werden:

- Der wohlbekannte Hunter/Vögtle-Tetralactammakrozyklus konnte derart modifiziert werden, dass die Änderung der Azidität der Lösung von neutral in Richtung stark basisch eine Konformationsänderung im Makrozyklus induziert, die diesen dazu veranlasst, zu kontrahieren und außerdem eines der vier Amidprotonen aus der makrozyklischen Kavität nach außen zu drehen. Dieser Effekt wurde dafür genutzt, die Pendelrate in [2]Rotaxan-basierten molekularen Shuttles – bestehend aus diesem schaltbaren Makrozyklus und verschiedenen Achsen mit jeweils zwei identischen Bindungsstationen – zu kontrollieren. Abhängig von der zentralen Spacereinheit zwischen den beiden Diamidstationen in der Achse wird die Pendelrate entweder durch die Kontraktion der inneren Kavität des Makrozyklus oder aber durch die Schwächung der wasserstoffbrückenbasierten Wechselwirkungen zwischen Makrozyklus und Achse beeinflusst.

  Weiterhin wurde entdeckt, dass die 4,6-Dialkoxy-Funktionalisierung der Isophthalsäureeinheit, die für das Design des schaltbaren Tetralactammakozyklus verwendet wurde, als integriertes Templat fungiert, welches Makrozyklisierungsreaktionen des Hunter/Vögtle-Typs in Richtung der selektiven Bildung der entsprechenden Octalactammakrozyklen dirigiert. Diese Klasse von größeren Makrozyklen, die zwei Bindungsstellen für Wasserstoffbrückenakzeptoren aufweisen statt nur einer, wurde bisher nur als Nebenprodukt der Synthese der entsprechenden Tetralactammakozyklen beobachtet.

- Gasphasen-H/D-Austausch-Experimente wurden angewendet, um die hochdynamische Bewegung von 18-Krone-6 entlang von Oligolysin-Peptidketten sowie über die Peripherie von POPAM-Dendrimeren zu verfolgen, was man als

„Weltraumspaziergang“ auf molekularer Ebene bezeichnen könnte. Weiterhin konnte durch mechanistische Studien mit adäquaten Modellverbindungen gezeigt werden, dass die Kronenether zusammen mit einem Proton von einer Ammonium- zu einer benachbarten Aminogruppe wandern. Schließlich wurde die zwitterionische Struktur von Kronenetherkomplexen von säureterminierten Oligolysinpeptiden durch ihr Isotopenaustauschverhalten nachgewiesen.

Nur die einzigartigen umgebungsfreien Bedingungen in der hochverdünnten Gasphase innerhalb eines Massenspektrometers bieten die idealen Voraussetzungen, um die Dynamik innerhalb nichtkovalenter Komplexe zu untersuchen, da intermolekulare Dissoziation/Reassoziationsprozesse im Gegensatz zur Untersuchung in Lösung hier vollständig ausgeschlossen werden können. Folglich bietet die Gasphasenchemie einen Einblick in eine komplett neue Reaktivität von schwach gebundenen supramolekularen Komplexen und legt nahe, dass viele nichtkovalente Komplexe ein stärker ausgeprägtes dynamisches Verhalten aufweisen könnten als gemeinhin bekannt.

- Es konnte gezeigt werden, dass Massenspektrometrie und Gasphasenchemie perfekt für die Analyse der Bindung von Anionen an verschiedene Rezeptoren über Wasserstoffbrückenbindung oder Anion-π-Wechselwirkungen geeignet sind. Diese Experimente ergänzen nicht nur Ergebnisse von Experimenten in Lösung; vielmehr erweitern sie die Sicht auf Erkennungsphänomene.

  Erstmals war es möglich, unter den umgebungsfreien Bedingungen in der hochverdünnten Gasphase Anion-π-Wechselwirkungen „bei der Arbeit“ zu beobachten. Weiterhin erlaubt die Arbeit in der Gasphase die exklusive Untersuchung der intrinsischen Eigenschaften eines Rezeptors ohne jegliche Solvatisierungseffekte. Tandem-MS-Experimente erlauben die Bestimmung des Einflusses des Substitutionsmusters von monomeren Naphthalindiimidsystemen (NDIs) hinsichtlich ihres Anionbindungsverhaltens durch Anion-π-Wechselwirkungen, wobei π-Azidifizierung sowie die Reduzierung des sterischen Anspruchs am aktiven Zentrum in einer Erhöhung der Bindungsstärke resultieren.

- Die Untersuchung der Bildung von Resorcinaren-Hexameren durch komplementäre Gasphasen- und Lösungs-NMR-Studien offenbarte, dass die Hexamere mit eingekapselten pseudooktaedrischen Übergangsmetallkomplexen (z.B. $Ru(bpy)_3^{2+}$ wie

auch einfach geladene und neutrale Ir-basierte Analoga, jeweils mit verschieden stark koordinierenden Anionen) nur unter ganz bestimmen Bedingungen gebildet werden: In Lösung werden größere Aggregaten ausschließlich mit dem doppelt geladenen $Ru(bpy)_3^{2+}$-Komplex in Verbindung mit dem extrem schwach koordinierenden Anion $[Al(OC(CF_3)_3)_4]^-$ gebildet. Dennoch führt selbst dies nicht zur ausschließlichen Bildung von 6:1-Komplexen, sondern vielmehr zu einer Mischung verschiedener Komplexe. In krassem Gegensatz dazu zeigen die ESI-FTICR-MS-Experimente eine deutlich Präferenz für eben jene 6:1-Komplexe, was darauf hindeutet, dass die Bildung mechanistisch über schrittweises „Anklammern" von Resorcinaren-Monomeren an den $Ru(bpy)_3^{2+}$-Komplex verläuft. Diese Schlussfolgerung kann nur durch die Kombination der Ergebnisse aus Gasphase und Lösung gezogen werden.

- Im letzten Projekt dieser Arbeit wurde die Bindung von Tetramethylammonium (TMA) an am oberen Rand substituierte Resorcinarene untersucht. Während Tandem-MS-Experimente die unverfälschten intrinsischen Eigenschaften der verschiedenen Rezeptoren basierend auf den elektronischen Eigenschaften der Substituenten zeigten, offenbarten NMR-Titrationen einen entscheidenden Einfluss des Gegenanions auf die Bindungssituation in einem kompetitiven Lösungsmittel. Es wurde gezeigt, dass Halogensubstituenten am oberen Rand des Resorcinarens die Azidität der benachbarten OH-Gruppen verstärkt, was den halogenierten Resorcinarenen erlaubt, stärkere Ar-OH•••Anion-Wasserstoffbrückenbindungen auszubilden als die anderen nicht-halogenierten Analoga. Infolgedessen erhöht die zusätzliche Bindung des Anions die Bindungskonstante des TMA-Kations, da dieses zusammen mit seinem Anion an das Resorcinaren gebunden wird.

  Diese Ergebnisse zeigen deutlich die Wichtigkeit auf, mehr als nur eine analytische Methode für die Untersuchung von supramolekularen Erkennungs- und Komplexierungsvorgängen in Betracht zu ziehen. Der Vergleich der Ergebnisse verschiedener Methoden, die anfänglich widersprüchlich erscheinen mögen, kann einen gänzlich neuen Blick auf die grundlegenden Wechselwirkungen, die den Bindungsvorgang beeinflusssen, eröffnen.

Table of Contents

1. INTRODUCTION 2

2. AIMS OF THIS THESIS 5

2.1 Construction of a pH-controllable Molecular Shuttle Rotaxane 5

2.2 Investigation of Molecular Motion in Supramolecular Crown Ether/Ammonium Complexes in the Gas Phase 5

2.3 Investigation of the Binding Properties of Different Anion and Cation Receptors in the Gas Phase and in Solution 6

3. THEORETICAL BACKGROUND 8

3.1 Rotaxanes and Catenanes 8

3.1.1 Definition and Nomenclature of Rotaxanes 8

3.1.2 Topology of Interlocked Molecules 9

3.1.3 Templated Synthesis of Rotaxanes 12

3.1.3.1 General Remarks on Templates and Rotaxane Synthesis 12

3.1.3.2 Historic Roots: Rotaxane Synthesis without Template 14

3.1.3.3 Rotaxane Synthesis through Neutral Amide Templates 15

3.1.3.4 Rotaxane Synthesis through Anionic Templates 18

3.1.3.5 Rotaxane Synthesis through Cationic Templates 21

3.1.3.6 Rotaxane Synthesis through Paraquat-Arene Templates 24

3.2 Mass Spectrometry as a Tool in Supramolecular Chemistry 26

3.2.1 Basics of Mass Spectrometry 26

3.2.2 Ionization Techniques 26

3.2.3 Mass Analyzation and Detection Techniques 30

3.2.3.1 Quadrupole Instruments and Quadrupole Ion Traps 31

3.2.3.2 Time-Of-Flight (TOF) 32

3.2.3.2 Ion Cyclotron Resonance (ICR) 33

4. RESULTS AND DISCUSSION 37

4.1 A pH-controllable Rotaxane-based Molecular Shuttle 37

4.1.1 Introduction and Idea of the Project 37

4.1.2 Design of the Macrocycle 40

4.1.3 Design of the Axle 44

4.1.4 Construction of the Rotaxane Shuttles 47
4.1.5 Analysis and Control of the Shuttling Dynamics in the Rotaxane Shuttles 61
4.1.6 Fluocescence Properties of the Rotaxane Shuttles R3 and R5 69
4.1.7 Conclusion 71

4.2 Influence of Alkoxy-Substitution of the Isophthalic Acid Moiety on Macrocycle Formation – Tetra- vs. Octalactam Macrocyle 73

4.3 A "Spacewalk" on the Molecular Scale - Highly Dynamic Motion of Crown-Ethers in Non-Covalent Complexes 84
4.3.1 The Idea of the "Spacewalk" 84
4.3.2 Gas-Phase H/D Exchange as the Method of Choice to Track Molecular Motion in 18-Crown-6/Ammonium Complexes 86
4.3.3 Molecular Motion of 18-Crown-6 on Oligolysine Peptides 88
4.3.4 Molecular Motion of 18-Crown-6 on POPAM Dendrimers 98
4.3.5 Mechanism of the Crown-Ether Transfer 103
4.3.6 Are Oligolysine Peptides Zwitterions in the Gas Phase? 107
4.3.7 Conclusion 110

4.4 Mass Spectrometric Studies of the Binding Properties of a Resorcinarene-based Anion Receptor 111

4.5 Gas-Phase Studies of Anion Binding to Naphthalene Diimide Systems 119
4.5.1 Basic Mass Spectrometric Studies of the Anion Binding to Monomeric and Dimeric Naphthalene Diimide Hosts 121
4.5.2 Gas-Phase Competition Experiments with Monomeric Naphthalene Diimide Systems 125
4.5.3 The Unexpected Formation of Heptameric Complexes with Monomeric Naphthalene Diimides ($[NDI_7 \bullet Cl]^-$) 131
4.5.4 Anion Binding to Substituted Dimeric Naphthalene Diimide Systems 138
4.5.5 Ion-Pair Binding to Crown Ether Substituted Naphthalene Diimides? 143
4.5.6 Conclusion 151

4.6 Encapsulation Complexes of Resorcinarene Hexamers 153
4.6.1 Basic Idea of the Project 153
4.6.2 Solution Studies on Resorcinarene Hexamer Formation 156
4.6.3 Gas-Phase Studies on Resorcinarene Hexamer Formation 168
4.6.4 Conclusions drawn from the Comparison of the Solution and Gas-Phase Studies on Resorcinarene Hexamer Formation 171

4.7 The Influence of the counteranion on the Cation Binding towards Upper-Rim substituted Resorcinarenes 172

5. CONCLUSION AND OUTLOOK 183

6. EXPERIMENTAL SECTION 186

6.1 General Methods 186

6.1.1 Analytical Methods 186

6.1.2 Preparative Methods 187

6.1.3 Description of the Gas-Phase Experiments in Chapter 4.3 (Molecular "Spacewalk") 187

6.1.4 Description of the Gas-Phase Experiments in Chapter 4.4 (Resorcinarene-based Anion Receptor) 188

6.1.5 Description of the Gas-Phase Experiments in Chapter 4.5 (Anion Binding to Naphthalene Diimides) 189

6.1.6 Description of the Gas-Phase Experiments in Chapter 4.6 (Formation of Resorcinarene Hexamers) 189

6.1.7 Description of the Gas-Phase Experiments in Chapter 4.7 (Ion-Pair Binding to Halogenated Resorcinarenes) 190

6.2 Synthesis of Tetra- and Octalactam Macrocycles 191

6.2.1 Synthesis of Isophthaloyol Building Blocks 191

6.2.2 Synthesis of Extended Diamine Building Blocks 200

6.2.3 Synthesis of Macrocycles 208

6.3 Synthesis of Axle Components 216

6.4 Synthesis of Rotaxanes 225

6.5 Synthesis of Metal Complexes 234

6.6 Synthesis of Oligolysine Peptides 236

7. ACKNOWLEDGEMENTS 237

8. LIST OF PUBLICATIONS 239

9. REFERENCES 240

List of Abbrevations

ADP	adenosine diphosphate
ATP	adenosine triphosphate
$CBPQT^{4+}$	cyclobis(paraquat-para-phenylen) tetracation
δ	chemical shift
DCM	dichloromethane
DMF	dimethylformamide
DMSO	dimethylsulfoxide
EE	ethyl acetate
EI	electron impact
eq.	stoichiometric equivalent(s)
ESI	electrospray ionization
FT-ICR	fourier transform ion cyclotron resonance
HV	high vacuum
MS	mass spectrometry
NDI	naphthalene diimide
NMR	nuclear magnetic resonance
ppm	parts per million
r.t.	room temperature
THF	tetrahydrofuran
TLC	thin layer chromatography

1. Introduction

Non-covalent interactions play a crucial role in nature as they control almost all biological processes likely because of their reversible formation and highly dynamic nature that allow fast processes to occur much more easily than covalent bond formation.
For example during peptide (re-)folding, structural elements move relative to each other exploring part of the available conformational space and thus optimizing their mutual interactions. The dynamics of non-covalent complexes is also the basis for the geometry changes mediating induced-fit binding, cooperativity and effector-controlled allosteric interactions.

interaction	bond energy [kJ/mol]
covalent C-X bond	160 - 500
coordinative bond	80 - 400
ion-ion interaction	40 - 375
ion-dipole interaction	40 - 200
hydrogen bond	5 - 120
cation-π intercation	5 - 80
anion-π intercation	5 - 40
dipole-dipole intercation	5 - 40
π-π intercation	5 - 20
van-der-Waals intercation	<5 - 20

Table 1.1 *Non-covalent intermolecular interactions and typical ranges of their bond energies as related to typical covalent bonds.*[1]

The research field dealing with the exploration of the power of non-covalent interactions in natural as well as in synthetic systems is generally referred to as "supramolecular chemistry".[2] The roots of this discipline can be traced back to Emil Fischer's theory of the "key-and-lock" principle for enzyme-substrate interaction anticipating the concepts of host-guest chemistry and molecular recognition.[3] With the growing insight into natural bonding structures like the first descriptions of the concept of the hydrogen bond[4] and the elucidation

of the double helical structure of DNA strands,[5] the interest in the study of supramolecular interactions began to rise. This was also supported by the advances on the analytical field.
Table 1.1 gives an overview on the different nature and an estimation of the relative strength of the most important non-covalent interactions.

The diversity of how nature achieves to regulate all of life's sequences e.g. by self-assembly processes appears to be nearly infinite.
One of the most impressive examples for this in nature is ATP synthase, an enzyme complex that catalyzes the synthesis of adenosine triphosphate (ATP) from adenosine diphosphate (ADP) and phosphate. In this enzyme, the catalysis involves a circular movement of a wheel-like subunit around an axle-like stator, which is driven by a proton gradient between two sides of a membrane. [6]
The insight into such nanoscaled structures prompted researchers to mimic complex natural design and function by creating simplified model systems to establish a basis for understanding the natural processes[7,8] on the way to possible applications e.g. in molecular computers[9].

One approach towards switchable systems on the molecular scale is the class of so called rotaxanes. A rotaxane – the name is derived from the Latin words for wheel (rota) and axle (axis) – is defined as a dumbbell-shaped molecule, in which a so called axle (also referenced as thread) is threaded through a macrocyclic molecule (Figure 1.1), whereas the axle is kinetically hindered from dethreading by covalently attached bulky "stopper" groups that are larger than the interior diameter of the macrocycle thus creating a mechanically interlocked structure. A related structure is the so called catenane, which is formed by connecting the two ends of the thread thus creating two mechanically interlocked macrocycles.

Figure 1.1 *Schematic representation of the threaded and mechanically interlocked structure of a [2]rotaxane.*

A rotaxane structure fulfills the requirements for a linear molecular switch, if the axle contains two stations between which the ring may shuttle depending on outside influences, e.g. oxidation/reduction or change of the pH value.

The synthesis of such a system has to be guided to some degree to ensure, that the axle is effectively threaded through the cavity of the ring. For this purpose, axle as well as wheel have to be designed in such a fashion, that they undergo a process of self assembly with the purpose of pre-arrangement of the components of the desired rotaxane.
The most important templates commonly applied will be discussed in chapter 3.1.3.

2. Aims of this Thesis

2.1 Construction of a pH-controllable Molecular Shuttle Rotaxane

The first goal of this thesis is the construction of a [2]rotaxane-based molecular shuttle, in which the macrocyclic component performs an oscillating motion between two equal "stations" on the axle component. For this purpose, the Hunter/Vögtle-type tetralactam macrocycle will be modified so that a change in pH can induce a conformational change from a conformation with all four amide hydrogen atoms pointing inwards the macrocyclic cavity towards a structure in which three of them point inwards and the other one point outwards. This conformational change would then reduce the interactions between macrocycle and axle thus accelerating the shuttling motion.

These effects of the macrocycle's switching on the change of the shuttling rate will be examined on the basis of two different axle components (unsubstituted as well as OH substituted aromatic spacer between the two diamide stations) by means of two-dimensional EXSY NMR spectroscopy.

As a side-effect of the modification of the tetralactam macrocycle (OH substitution on the isophthaloyl moiety), the effect of this modification on the formation of larger octalactam macrocycles will be examined.

The results of these projects are described in chapter 4.1 (pH-controllable molecular shuttle) and 4.2 (enhanced preparation method for octalactam macrocycles).

2.2 Investigation of Molecular Motion in Supramolecular Crown Ether/Ammonium Complexes in the Gas Phase

Although molecular mobility has attracted considerable attention in supramolecular chemistry and biochemistry, the simple question of whether a small molecule can move directly between different binding sites of a multitopic host without intermediate dissociation so far has only been addressed in rotaxane-based molecular shuttles in which dissociation is prevented by the mechanically interlocked structure. To study such a process, H/D exchange experiments on a model system comprising complexes formed between 18-crown-6 and oligolysine peptides and POPAM dendrimers, respectively, were considered to

represent the appropriate method to track such a motion. Since in solution, direct binding-site hopping is indistinguishable from a dissociation/reassociation mechanism, here, the high vacuum inside a mass spectrometer is shown to offer a unique environment for probing such processes.

Furthermore, the mechanism of the highly dynamic motion of the crown ethers on multitopic hosts will be examined employing suitable ditopic model systems to distinguish the two different mechanistic possibilities.

The results of this project are described in chapter 4.3.

2.3 Investigation of the Binding Properties of Different Anion and Cation Receptors in the Gas Phase and in Solution

The triggering of switching events as well as responsiveness in supramolecular complexes require the effective binding of an effector. Therefore, the third part of this thesis deals with the investigation of the binding properties of several anion, cation, and ion pair receptors provided by different cooperation partners. For these studies, various analytical methods are employed, namely ESI-FTICR mass spectrometry, but also different NMR techniques such as NMR titration or DOSY experiments.

a) The goal of the first project comproses the investigation of the anion binding properties of an *o*-phenylenediamine substituted resorcinarene prepared in the group of Prof. Maija Nissinen (Nanoscience Center, University Jyväskylä, Finland) to verify that anions actually are bound to the receptor thus confirming the results from NMR experiments and furthermore the detection of additional anions, which are bound less strongly so that this can only be monitored in the gas phase and not in solution. Furthermore, the binding situation will be examined by gas-phase H/D exchange experiments.

   The results of this project are described in chapter 4.4.

b) Although anion-π interactions have been shown to exist by theoretical calculation, they have never been observed at work. Therefore, in this project, a series of differently substituted monomeric naphthalene diimides (NDIs) prepared in the groups of of Prof. Stefan Matile (University of Geneva, Switzerland) and Prof. Marcel Mayor (University of Basel, Switzerland) as well as some differently substituted macrocyclic naphthalene

diimide dimers (NDIMs) will be examined by ESI-FTICR mass spectrometry with respect to their anion binding behavior. To compare the influence of substitution of the NDI systems, tandem mass spectrometric experiments are employed.
The results of this project are described in chapter 4.5.

c) Resorcinarene hexamers have been extensively studied, mainly in solution and in the solid state, but have also been shown to be formed in the gas phase, if a suitable template (i.e.$[Ru(bpy)_3]^{2+}$) is present.
This project deals with the question, if resorcinarene hexamers encapsulating pseudooctahedral metal complexes can also be formed in solution. For this purpose, several of these complexes will be prepared in charge states 0, +I, and +II with different counter anions and investigated with respect to their templating ability by means of mass spectrometry as well as different NMR spectroscopic techniques.
The results of this project are described in chapter 4.6.

d) Resorcinarenes are widely known to bind cations through cation-π interactions. In this last project, the question is addressed, how substitution of the upper rim of a resorcinarene influences its binding properties. For this purpose, a series of five differently substituted resorcinarenes (provided by Kodiah Beyeh from the group of Prof. Kari Rissanen, University of Jyäskylä, Finland) is investigated with respect to the binding behavior towards different ammonium salts subject to the influence of the counteranion.

3. Theoretical Background

3.1 Rotaxanes and Catenanes

3.1.1 Definition and Nomenclature of Rotaxanes

The term rotaxane describes the class of supramolecular non-covalently linked compounds, which basically consist of (at least) one macrocyclic wheel-like molecule and one or more axle-like molecules threaded through the former. To prevent the non-covalently bound axle from de-threading, bulky stopper groups can be attached at its ends. If not, the compound is called a pseudorotaxane (Figure 3.1.1).

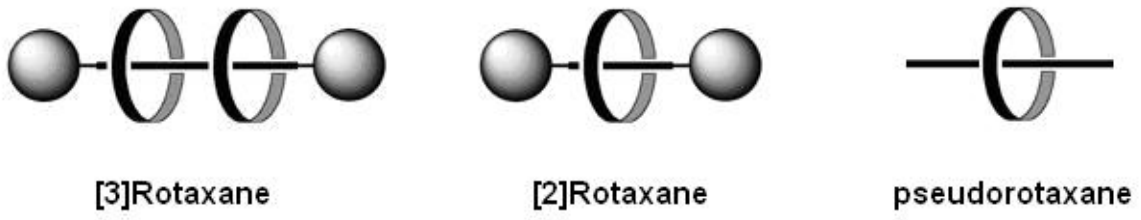

Figure 3.1.1 *Basic structures of rotaxanes/pseudorotaxanes.*

According to the nomenclature rules developed by Vögtle et al.,[10] an [n]rotaxane consists of a total of n linear and cyclic compounds (n = 1, 2, 3, …). However, this basic rule only describes the more simple rotaxanes as depicted in Figure 3.1.1 and not the exact constitution. For more complex structures with multiple macrocycles on one axle, multiple axles threaded through one macrocycle, or rotaxane structures with covalently linked subunits (some examples are schematically shown in Figure 3.1.2), one has to introduce more information about the connectivity of the rotaxane's constituents. Axles and wheels are entitled "ax" and "cy" respectively, whereas the different bonding types are classified as "mec" (mechanical bond) and "cov" (covalent bond).

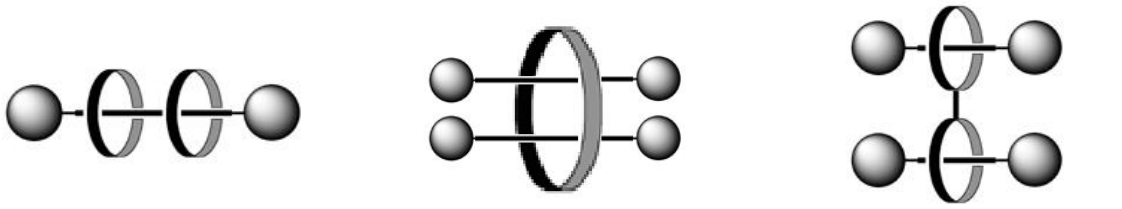

[$3^{ax1meccy2,ax1meccy3}$] rotaxane

[$3^{ax1meccy2,cy2mecax3}$] rotaxane

[$2^{ax1meccy2}$-(cy2covcy3)-$_{cy3mecax4}$] rotaxane

Figure 3.1.2 *More complex types of rotaxanes consisting of multiple axle and/or macrocycle components and their denomination according to Vögtle et al.*[10]

3.1.2 Topology of Interlocked Molecules

In contrast to the classical Euclidian geometry, the mathematical branch of topology (greek: τόπος = "place" and λόγος = "study") describes geometry without regard to exact lengths or precise angels. The focus rather lies on allowed and non-allowed transformations, whereas the allowed transformations are only those that stretch an object without tearing it apart or connecting distinct parts.[11] In this regard, a cup and a torus are topologically equivalent, even if the spatial appearance is considerably different (Figure 3.1.3).

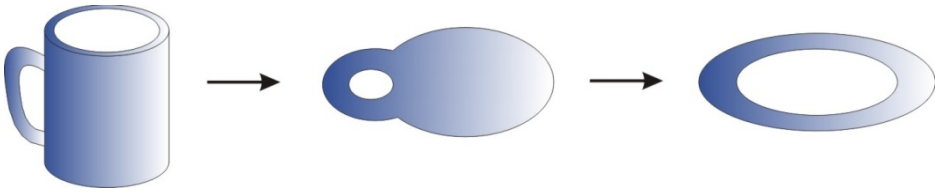

Figure 3.1.3 *Topologically equivalent representions of a cup.*

Applied to supramolecular assemblies, a [2]rotaxane as well as a [2]pseudorotaxane are topologically equivalent to the completely non-threaded structure (Figure 3.1.4), since all transformations are continuous and no covalent bond is broken, even if usually this deslipping is mechanically prevented by the size of the stopper groups.

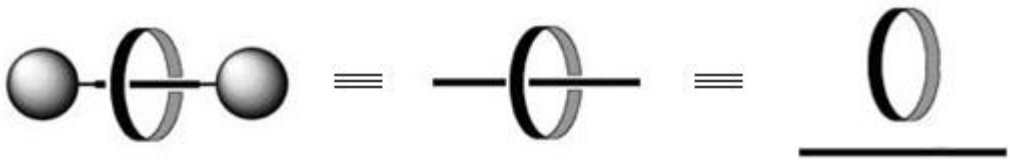

Figure 3.1.4 *Topologically equivalent transformations of a [2]rotaxane and a [2]pseudorotaxane.*

On the other hand, a catenane cannot be converted into two separated rings without breaking at least one bond. The same is true for a trefoil knot, which – topologically speaking – is not equivalent to a macrocycle, since the knot cannot be unfolded without cutting it (Figure 3.1.5).

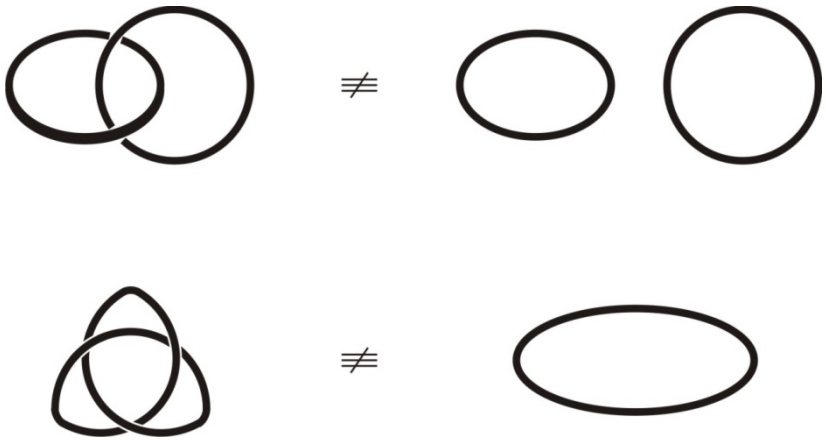

Figure 3.1.5 *Topologically non-equivalent transformations for a [2]catenane and a trefoil knot.*

If a certain atom sequence is introduced into ring and/or axle of a [2]rotaxane, two chiral enantiomers are resulting from this directionality (Figure 3.1.6). Although the two rotaxanes depicted in Figure 3.1.6 are chiral, they can be interconverted into each other by continuous transformations and therefore are topologically equivalent; more precisely they are cycloenantiomers.

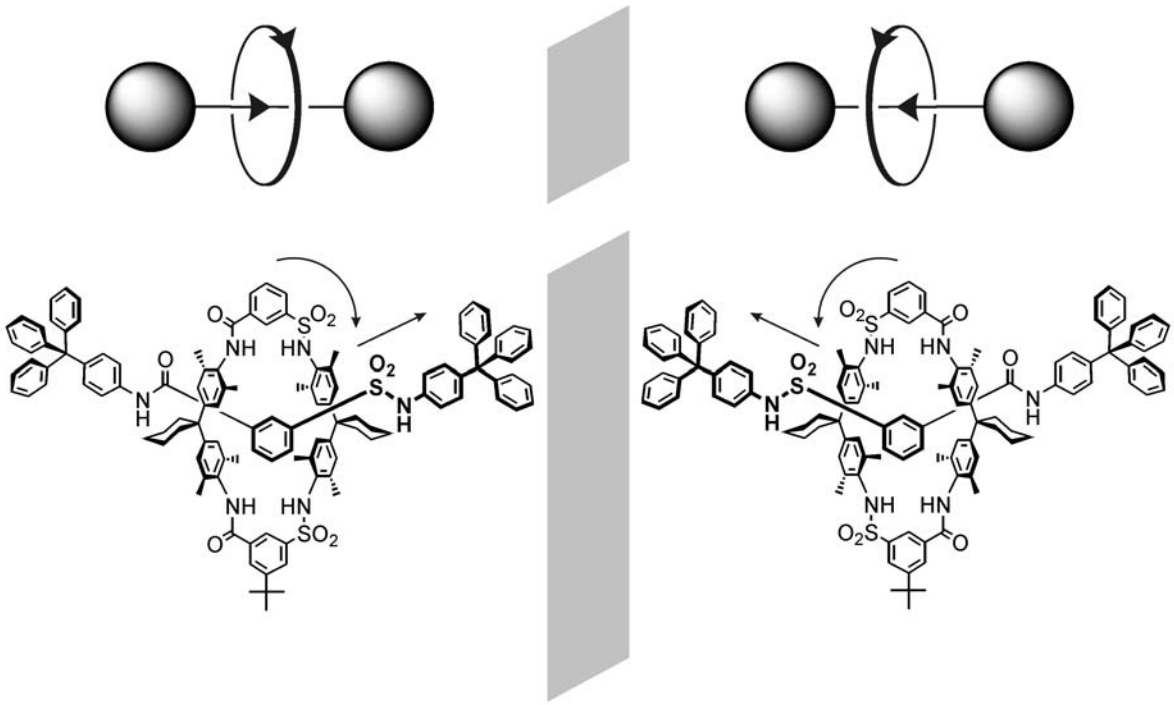

Figure 3.1.6 *Two cycloenantiomers of an amide [2]rotaxane, with each one amide in both, macrocycle and axle, substituted for a sulfonamide.*[12]

3.1.3 Templated Synthesis of Rotaxanes

3.1.3.1 General Remarks on Templates and Rotaxane Synthesis

If one aims at designing supramolecular architectures such as a rotaxane, a certain pre-organization of the constituents is required to ensure the formation of the desired structure. For this purpose, a template needs to bind somehow to the substrates to assure a certain pre-organization. This binding may occur in a lot of different fashions, e.g. through hydrogen bonding to amides (chapter 3.1.3.3) or anions (chapter 3.1.3.4), through binding of crown ethers to secondary ammonium ions (chapter 3.1.3.5), or pre-organization by π-donor π-acceptor interactions (chapter 3.1.3.6).

Basically, it is possible to differentiate between templates that are removed after a template-assisted synthesis (Figure 3.1.7) and templates that become a part of the desired supramolecular assembly (Figure 3.1.8). A very prominent example for the first strategy is the rotaxane (or catenane) formation through Cu(I)-mediated template effect:[13] Axle and macrocycle are oriented in the desired way by coordination of bipyridine, terpyridine, or phenanthroline moieties to a suitable metal ion followed by attachment of the stoppers. The free rotaxane/catenane can then be obtained by demetallation with e.g. cyanide.

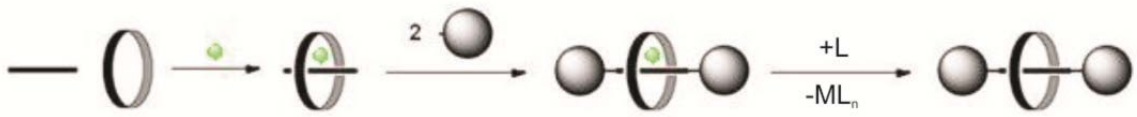

Figure 3.1.7 *Metal-ion templated synthesis of a [2]rotaxane. The metal ion (e.g. Cu(I)) can be removed after rotaxane synthesis by adding stronger ligands (e.g. cyanide).*

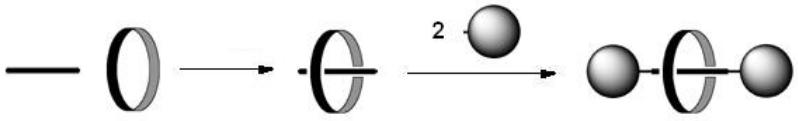

Figure 3.1.8 *Schematic representation of the synthesis of a [2]rotaxane with the template remaining part of the product.*

If in the templated synthesis of a [2]rotaxane, first an axle center piece is threaded through a wheel – directed by a specific bonding between these two components – and then the axle center piece is equipped with two bulky stopper groups, the axle center piece as the template of course remains a part of the entire rotaxane.[14]

The general strategies for the synthesis of a [2]rotaxane are outlined in Figure 3.1.9, whereas the focus in supramolecular chemistry definitely lies on the clipping strategy and the trapping/threading strategy as in this thesis. The difference between trapping and threading is just marginal, since both strategies proceed via a semirotaxane equipped with only one stopper.

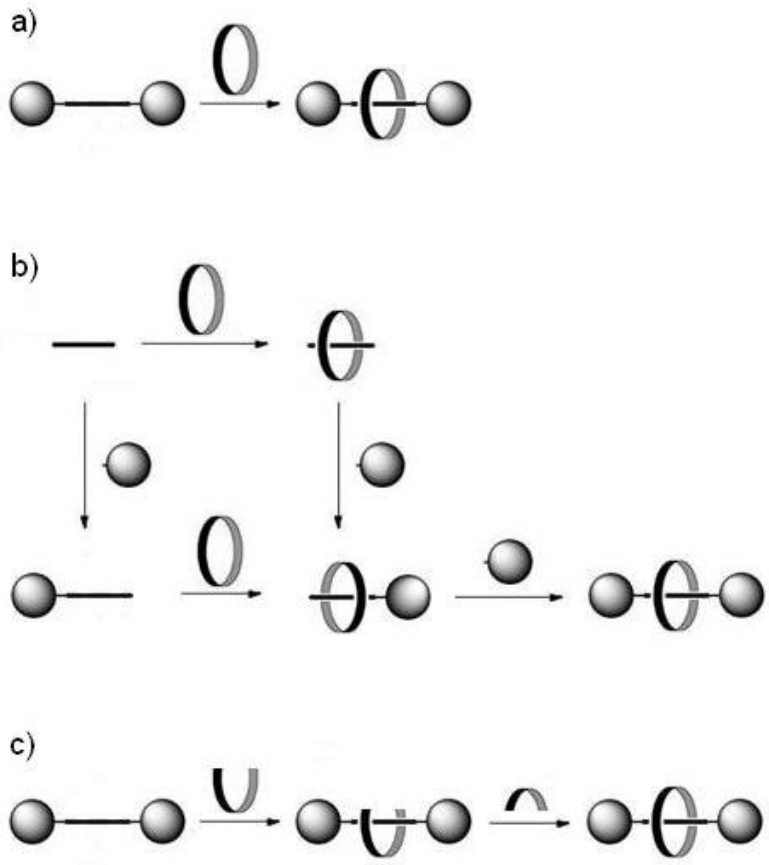

Figure 3.1.9 *Schematic representation of different synthesis strategies towards a [2]rotaxane:* ***a)*** *slipping,* ***b)*** *threading followed by trapping, and* ***c****) clipping.*

The following chapters will provide an overview of the most famous template effects for the preparation of rotaxanes.

3.1.3.2 Historic Roots: Rotaxane Synthesis without Template

The synthesis of a rotaxane without any preorganization of axle and wheel is only of historic interest after the discovery of template effects.

The first rotaxane structure, however, was obtained by covalent attachment of a C30 ring to a Merrifield resin and then 70 repetitive steps of washing with a solution of dodecanedioyl dichloride (axle) and triphenylmethanol (stopper). Following this procedure, the rotaxane depicted in Figure 3.1.10 could be obtained with a yield of 6 %.[15]

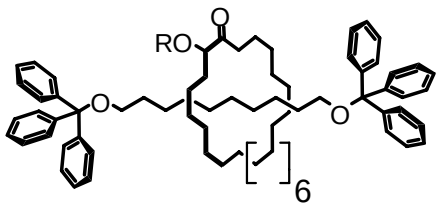

Figure 3.1.10 *The first [2]rotaxane (R = linker & Merrifield resin).*

3.1.3.3 Rotaxane Synthesis through Neutral Amide Templates

For rotaxane synthesis through an amide template, usually a tetralactam macrocycle as shown in Figure 3.1.11 is used as the wheel component. This kind of macrocycles originally had been designed as host for the molecular recognition of *p*-benzoquinone (Figure 3.1.12).[16]

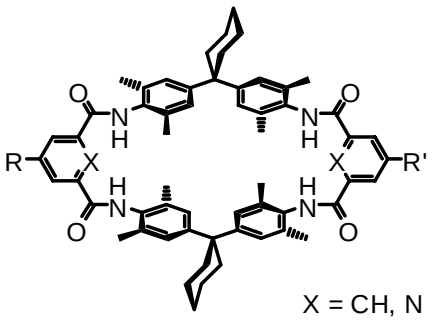

Figure 3.1.11 *Hunter/Vögtle-type tetralactam macrocycle.*

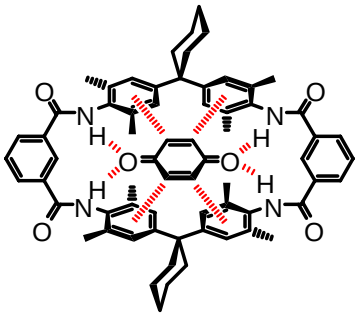

Figure 3.1.12 *Binding of p-benzoquinone in a Hunter/Vögtle-type tetralactam macrocycle through a combination hydrogen bonding and C-H•••π interaction.*

This type of tetralactam macrocycles features four amide groups, which can act as excellent hydrogen-bond donors for the incorporation of hydrogen-bond acceptors, because the N-H bonds point into the cavity of the macrocycle in the two most stable conformations (all in) as shown by density functional calculations.[17] The four hydrogen atoms are not situated in a plane with the isophthalic aromatic rings; rather each two of them are located above and below this plane respectively (Figure 3.1.13).

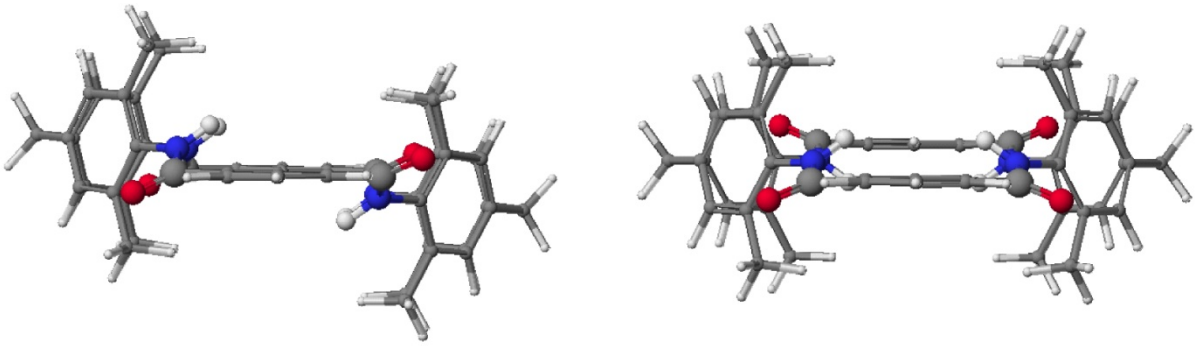

Figure 3.1.13 *The two most favorable conformations of a Hunter/Vögtle-type tetralactam macrocycle.*[17]

Vögtle *et al.* were first to discover that these macrocyclic amides could be used to accommodate suitable amide guests inside the macrocycle through hydrogen bonding to allow for rotaxane formation.[18]

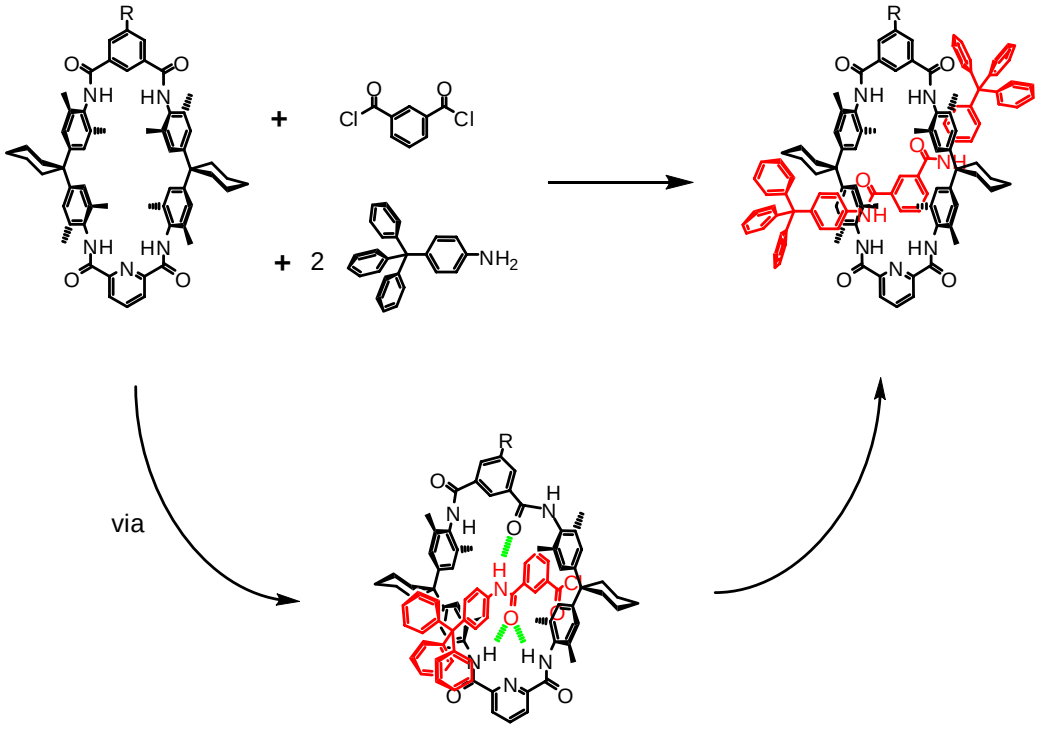

Figure 3.1.14 *Kinetically controlled synthesis of a [2]rotaxane through an amide template.*

Figure 3.1.14 shows the synthesis of a [2]rotaxane using the previously described ability of a tetralactam macrocycle to form hydrogen bonds to molecules that are complementary with the cavity size of the macrocycle. In this case, the amide guest is generated from the condensation reaction of isophthaloyl dichloride with triphenylmethylaniline in the first step. This half-axle is then bound to the macrocycle through three hydrogen bonds (see Figure 3.1.14 for the binding pattern). The reaction of this intermediate complex with a second equivalent of triphenylmethylaniline stopper leads to the formation of the mechanically interlocked rotaxane.[19a] On this basis, a large variety of rotaxane species was prepares based on the amide template effect.[19]

A similar approach was developed by Leigh *et al.* based on the smaller tetralactam macrocycle shown in Figure 3.1.15.[20] As its larger analogue, this macrocycle is able to bind amides through up to four converging hydrogen bonds. The range of possible guests is limited to smaller aliphatic amides that are still able to penetrate the macrocyclic cavity.

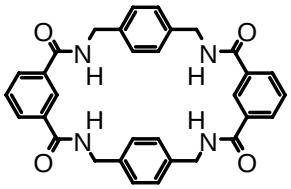

Figure 3.1.15 *Small Leigh-type tetralactam macrocycle.*

Figure 3.1.16 shows one possible example of a [2]rotaxane based on the Leigh-type tetralactam macrocyle formed via clipping the macrocycle around a fumaramide axle component.

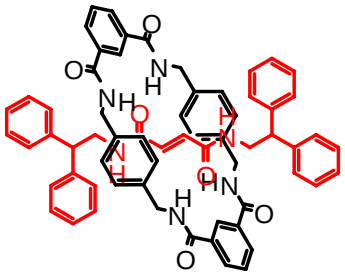

Figure 3.1.16 *[2]rotaxane based on the Leigh-type tetralactam macrocycle and a fumaramide axle.*

3.1.3.4 Rotaxane Synthesis through Anionic Templates

The synthesis of a [2]rotaxane through anionic templates is based on the same principles as the synthesis through amide templates, namely the pre-organization of macrocycle and stopper or macrocycle and half-axle, respectively, through hydrogen bonding.

Unlike the amide template synthesis, the anion template synthesis involves hydrogen bonding between a tetralactam macrocycle and a stopper phenolate anion, which can easily be generated by deprotonation of a suitable precursor as shown in Figure 3.1.17 as first reported by Vögtle *et al.* in 1999.[21]

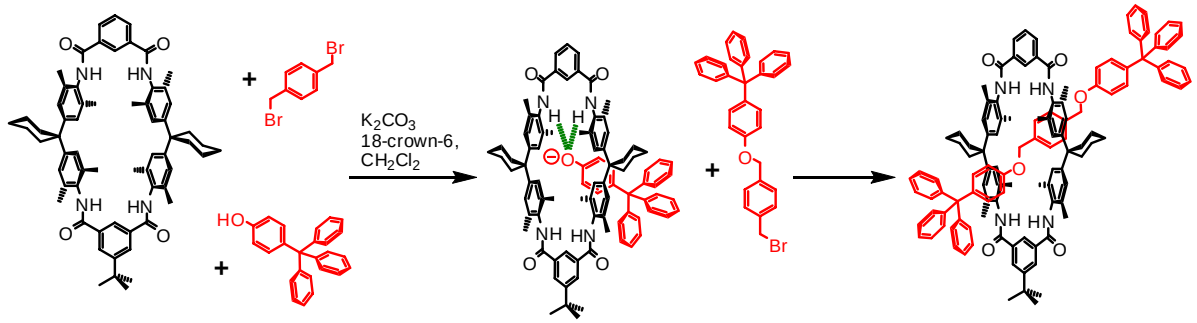

Figure 3.1.17 *Kinetically controlled synthesis of a [2]rotaxane through Vögtle-type anion template.*

Generally, anion-templated rotaxane syntheses result in higher yields than amide templated ones, because hydrogen bonding from the tetralactam macrocycle to an anion is supposed to be much stronger than to an amide. Consequently, the equilibrium in the threading step lies far on the side of anionic stopper bound to the macrocycle instead of the corresponding free components.

In 2002, Schalley *et al.* reported the synthesis of a [2]rotaxane through a novel anionic template involving a phenolate ion for threading, which is only used for threading through hydrogen bonding and not directly involved as a reactant for stoppering. In this case, stoppering is achieved by reaction of terminal amine functionalities with bulky acid chlorides (Figure 3.1.18).[22]

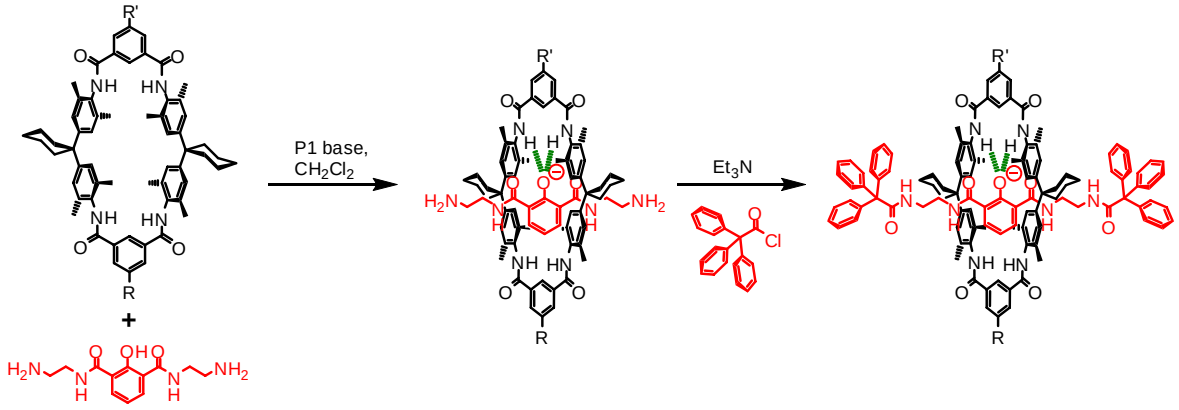

Figure 3.1.18 *Kinetically controlled synthesis of a [2]rotaxane through Schalley-type anion template.*

Furthermore, this rotaxane possesses very interesting properties regarding intramolecular dynamic movements: The macrocycle performs a shuttling motion between the two identical diamide stations in the axle, whereas the shuttling rate can be controlled by protonation and deprotonation of the phenol-OH in the middle of the axle.[23]

In the protonated state, the macrocycle performs a shuttling motion between the two diamide stations in the axle. Deprotonation of the phenol-OH with P1 base significantliy slows down this movement, as the strong phenolate/P1 cation ion pair acts as a "brake" for the macrocycle's shuttling (Figure 3.1.19). To switch the macrocycle from one diamide station to the other, the phenolate/P1 cation ion pair has to be separated, which raises the barrier for this shuttling movement.

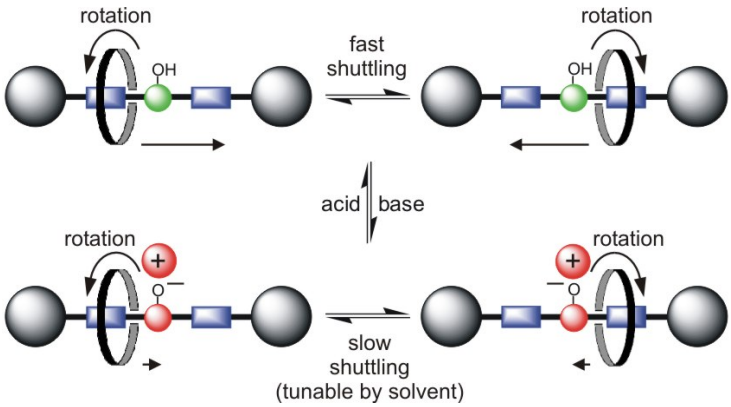

Figure 3.1.19 *Control of the shuttling rate in the [2]rotaxane molecular shuttle described in Figure 3.1.18.*[23]

Recently, Beer *et al.* developed another approach for the preparation of interlocked molecules based on the recognition of halide anions by a combination of an isophthalamide and a methylpyridinium cation (Figure 3.1.20).[24]

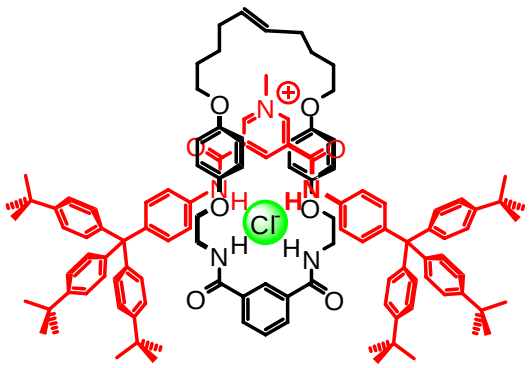

Figure 3.1.20 *Synthesis of a [2]rotaxane through combination of anion template and π-π-stacking. The macrocyle is closed by Grubbs-type ring closing metathesis.*

3.1.3.5 Rotaxane Synthesis through Cationic Templates

The first template effect based on transition metal coordination developed by Sauvage *et al.* has been used for the synthesis of a [2]catenane.[13]

The coordination of two 2,2'-bipyridine moieties to a copper(I) ion (tetrahedral geometry) can also be used for the synthesis of rotaxanes such as the one depicted in Figure 3.1.21. In this special case, the additional incorporation of a terpyridine moiety allows the control of the rotation of the macrocycle around the axle by oxidation and reduction of the copper ion template. According to its oxidation state, the copper ion prefers tetrahedral (for Cu(I)) or trigonal bipyramidal coordination (for Cu(II)), respectively, which results in two different positions of the wheel.[25]

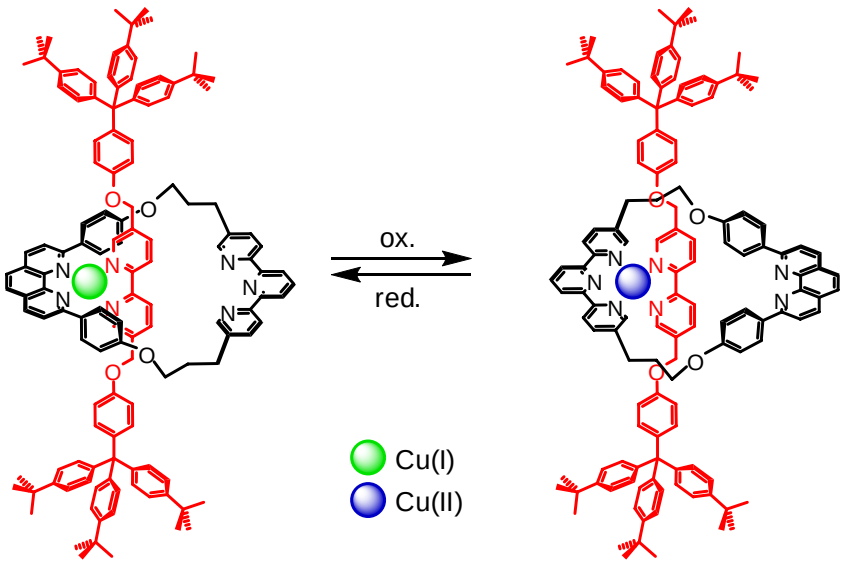

Figure 3.1.21 *A redox switchable [2]rotaxane prepared through cationic copper(I) template.*

One of the most popular ways of rotaxane synthesis through cationic templation is represented by the threading of secondary ammonium ions through crown ethers; the minimum size of the macrocyclic component is 21-crown-7, which allows the threading of aliphatic chains, but mostly 24-crown-8 is used, which also allows the threading of phenyl rings.[26,27] The interaction is based on a combination of strong N-H•••O and weaker N-C-H•••O hydrogen bonds.

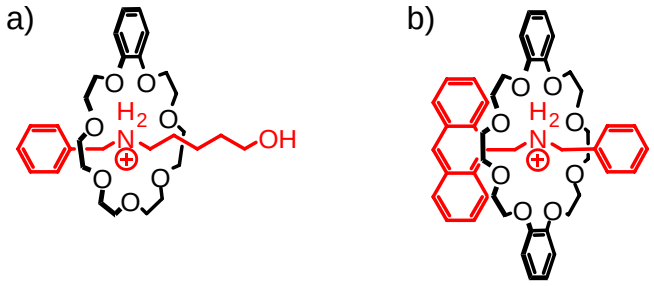

Figure 3.1.22 *Illustration of common binding motifs based on the crown ether/ammonium template for a) 21-crown-7 and b) 24-crown-8.*

Recently, Schalley *et al.* developed the concept of "integrative self sorting" based on the crown ether/ammonium template.[28] This concept makes use of the fact that differently sized crown ethers preferably bind specific secondary ammonium guests (Figure 3.1.23).

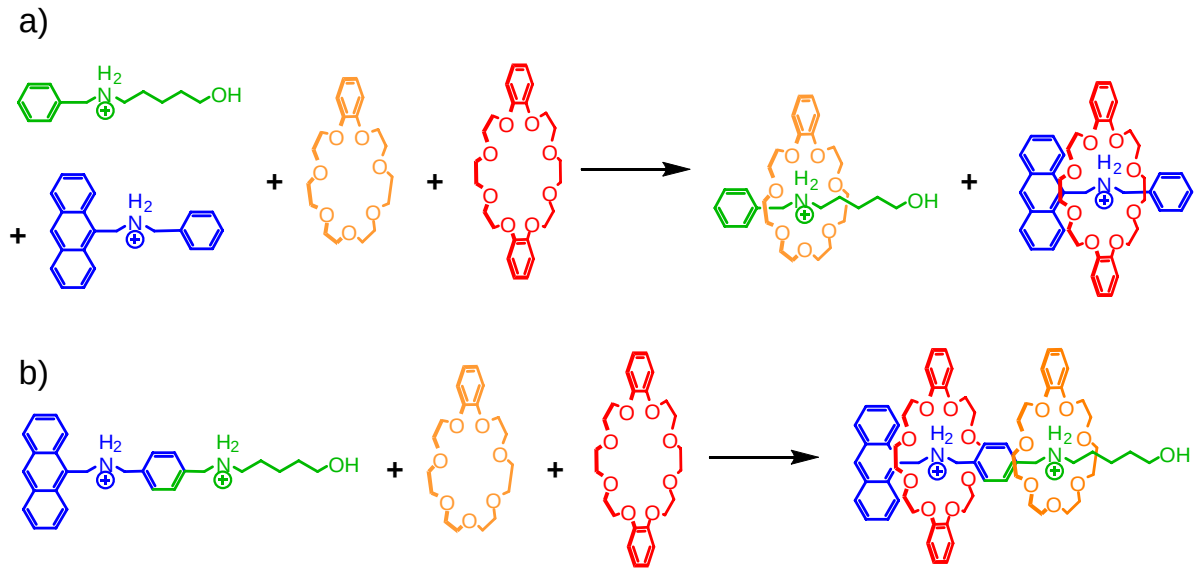

Figure 3.1.23 *Illustration of the concept of "integrative self sorting" based on the crown ether/ammonium binding motifs: a) Benzo-21-crown-7 preferably binds the green secondary ammonium ion with one benzyl and one aliphatic substituent, whereas dibenzo-24-crown-8 preferably binds the blue secondary ammonium ion with one benzyl and one anthracene substituent. b) If the green and the blue binding site are joined together, this leads to a specific sequence of benzo-21-crown-7 and dibenzo-24-crown-8 threaded onto the axle.*[28]

Stoddart *et al.* used the combination of ammonium ions and paraquat dications for the construction of a "molecular elevator" with each one ammonium and one paraquat binding station in every axle of a trivalent guest molecule (Figure 3.1.24).[29] The three covalently connected 24-crown-8 macrocycles preferably bind to the secondary ammonium ions, whereas deprotonation of the latter leads to a shift of the trivalent crown ether towards the paraquat moieties.

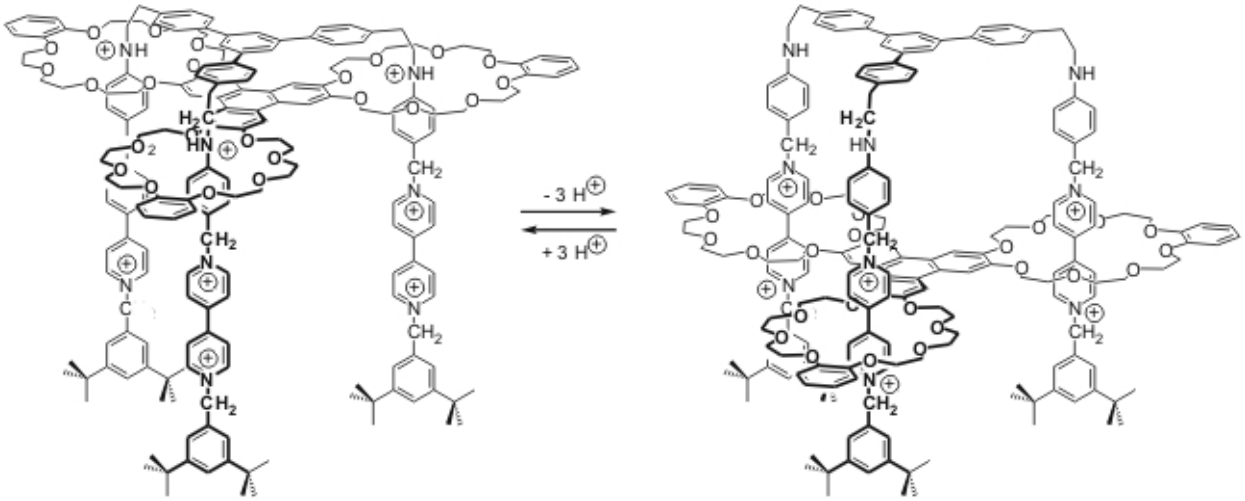

Figure 3.1.24 *A "molecular elevator" based on [2]rotaxanes. The position of the trivalent crown ether can be controlled by the protonation state of the ammonium ions in the axles.*[30]

3.1.3.6 Rotaxane Synthesis through Paraquat-Arene Templates

Another very common way of synthesizing rotaxanes is the synthesis through paraquat/arene template effect based on π-donor/π-acceptor interactions.[31]

The general procedure follows the way of forming a $CBPQT^{4+}$ (cyclo-bis-paraquat tetracation) macrocycle by clipping two adequate precursors together, whereas the electron-poor dicationic macrocycle precursor is coordinated to an electron-rich aromatic system incorporated in the axle, which for example can be a tetrathiafulvalene (TTF) moiety (Figure 3.1.25).[32,33] Also, a templated synthesis of the $CBPQT^{4+}$ macrocycle followed by threading rotaxane synthesis is possible.[34,35]

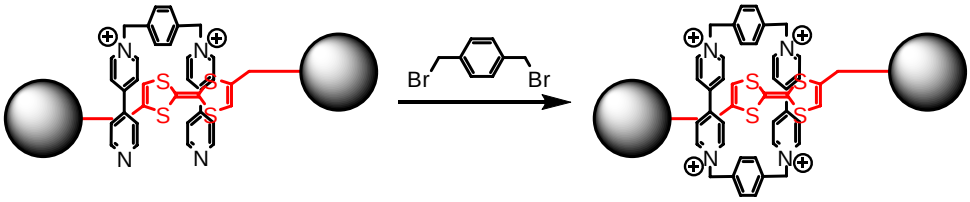

Figure 3.1.25 *Synthesis of a $CBPQT^{4+}$ rotaxane through clipping of the macrocycle around the axle.*

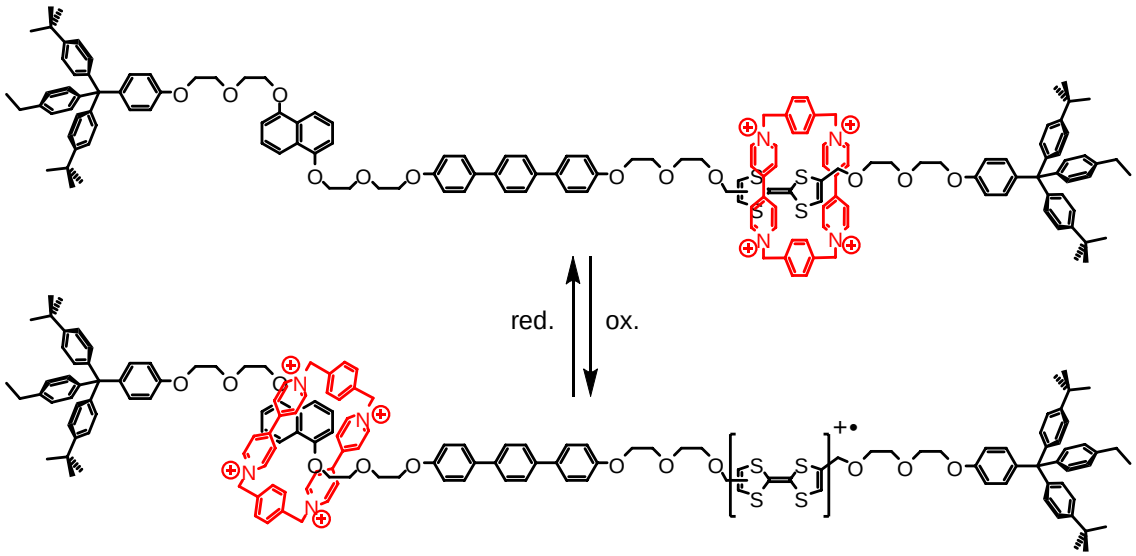

Figure 3.1.26 *A redox switchable bistable rotaxane based on the $CBPQT^{4+}$ macrocycle. If the axle is electrically neutral, the $CBPQT^{4+}$ macrocycle prefers to stick to the TTF moiety, whereas oxidation of the TTF leads to electrostatic repulsion of the two cationic species and switching of the macrocycle towards the naphthalenediol station.*

The rotaxane depicted in Figure 3.1.26 can be prepared through clipping synthesis as described above. The axle contains two possible stations – one TTF and one naphthalene-1,5-diol ether. In the electronically neutral state of the axle, the $CBPQT^{4+}$ macrocycle prefers to stick to the more electron-rich TTF station, whereas oxidation of the TTF leads to electrostatic repulsion of the two cationic species ($TTF^{+\bullet}$ and $CBPQT^{4+}$), which causes the macrocycle to switch towards the naphthalenediol station.[36,37]

3.2 Mass Spectrometry as a Tool in Supramolecular Chemistry[*]

3.2.1 Basics of Mass Spectrometry

Mass spectrometry has recently gained importance in the field of supramolecular chemistry.[38] Especially the development of softer ionization methods contributed to make mass spectrometry a useful tool for the examination of non-covalent structures beyond the mere determination of the mass-to-charge ratio. Whereas the study of supramolecular complexes in the environment-free gas phase may deliver information about the intrinsic properties of the analyte ions, the comparison with solution data can unravel solvation-based effects. Furthermore, collision- or laser-induced fragmentation reactions as well as gas-phase reactions with a neutral reactant gas can provide additional information about the topological superstructure and on the reactivity.[39,40,41]

As mass spectrometry plays a key role in many of the projects investigated in the present work, the most important aspects and methods of ionization and detection during a mass spectrometric experiment will be discussed in the following (chapter 3.2.2 and 3.2.3) with a main focus on electrospay ionization (ESI)[48,49] and fourier transform ion-cyclotron resonance (FTICR)[53] detection.

3.2.2 Ionization Techniques

To allow for mass-spectrometric investigation of a sample, the analyte molecules have to be ionized and transferred into the gas-phase. Over the past decades, numerous ionization methods have been developed, of which the most important will be summarized in the following.

---

[*] The overview on mass spectrometry has been similarly published in:

Mass Spectrometry and Gas Phase Chemistry of Supramolecules, D. P. Weimann, M. Kogej, C. A. Schalley in *Analytical Methods in Supramolecular Chemistry, 2nd Edition*, C.A. Schalley (ed.), Wiley-VCH, Weinheim, 2012

The probably most classical ionization method is the **Electron Impact** (EI)[42] ionization. With this method, the sample is vaporized by heating in high vacuum and then subjected to a fast electron beam. The molecule-electron collisions produce radical cations ($M + e^- \rightarrow M^{+\bullet} + 2\ e^-$). The main disadvantages of this method are limitation of the mass range determined by sample volatility (M < approx. 800 Da) and the high degree of fragmentation caused by the high internal energies of the radical cations.

Chemical Ionization (CI)[43] uses a similar ionization principle as EI; prior to ionization, the sample has to be vaporized in a high vacuum. Analyte ions are then generated by collisions with ions of a suitable reagent gas (H_2, CH_4, NH_3, …). The reagent gas ions themselves are generated by collisions with electrons. E.g. electron bombardment of methane produces CH_5^+ ions that are able to protonate the analyte. As mostly the high excess of reagent gas is ionized in the first place, this method limits the amount of fragmentation reactions due to the lower energy transferred to the analyte molecules. However, the mass range is limited by sample volatility as described above for EI.

For **Atmospheric Pressure Chemical Ionization** (APCI),[44] a solution of the analyte is nebulized in a nitrogen gas stream and then dried in a high temperature chamber and subjected to corona discharge creating primary (solvent) ions. Analyte ions are created by contact with the primary ions through protonation, deprotonation, or charge exchange. As desolvation occurs in a heated vaporization chamber, fragmentations are still rather prominent.

For **Fast Atom Bombardment** (FAB)[45] ionization, an analyte solution in a liquid matrix with high boiling point (e.g. glycerol) is bombarded with a high-energy beam of atoms, which produces protonated or deprotonated ions. Fragmentation reactions are much less prominent than for EI and CI, but still occur to a lower extent.

Matrix-assisted laser desorption/ionization (MALDI)[46] is based on the vaporization and ionization of an analyte embedded in a suitable crystalline matrix by laser irradiation. For sample preparation, a mixture of analyte and a large excess of matrix are co-crystallized on a target plate. The matrix serves several purposes: a) It absorbs the laser radiation; therefore, typically small aromatic molecules are used (e.g. 2,5-dihydroxybenzoic acid, α-cyano-4-hydroxycinnamic acid, dithranol, or sinapinic acid). They perfectly fit the mostly used UV

lasers, e.g. N_2 lasers with a wavelenghth of 337 nm. b) Acidic matrices can act as proton donors. However, other ionization pathways such as photoionization, charge transfer, self-protonation of the matrix, or adduct formation with background cations are also possible, especially in non-protic matrices.[47] Like this, mostly singly charged ions are generated.
The mass range of MALDI is technically nearly unlimited; also the ions are generated in a pulsed way instead of continuously. Therefore, MALDI ion sources are mostly coupled with time-of-flight (TOF) analyzers (see chapter 3.2.3).
Although most of the laser energy is absorbed by the matrix molecules, the conditions during the MALDI process are rather harsh so that the intact transfer of weakly-bound non-covalent complexes is at least not very trivial.

For **Electrospray ionization** (ESI),[48,49] a solution of the analyte in a volatile solvent is pumped through an electrically charged needle creating micrometer-sized charged droplets (Figure 3.2.1). At the needle tip, the sprayed solution forms the so-called Taylor cone due to the high voltage that is applied to the needle. From the tip of the Taylor cone, a jet is formed in which charged droplets are generated. The charge of the droplets depends on the charge that is applied to the spray needle (excess positive charge in the droplets for positively charged needle and vice versa). To support the evaporation of the solvent, the needle is embedded into a heatable stream of so-called nebulizing gas (usually N_2). Once the droplets are formed, they are driven away from each other due to Coulomb repulsion. Upon the preceeding evaporation of solvent, the droplets shrink and undergo Colomb explosion, when they reach the Rayleigh limit, which leads to the formation of smaller droplets.

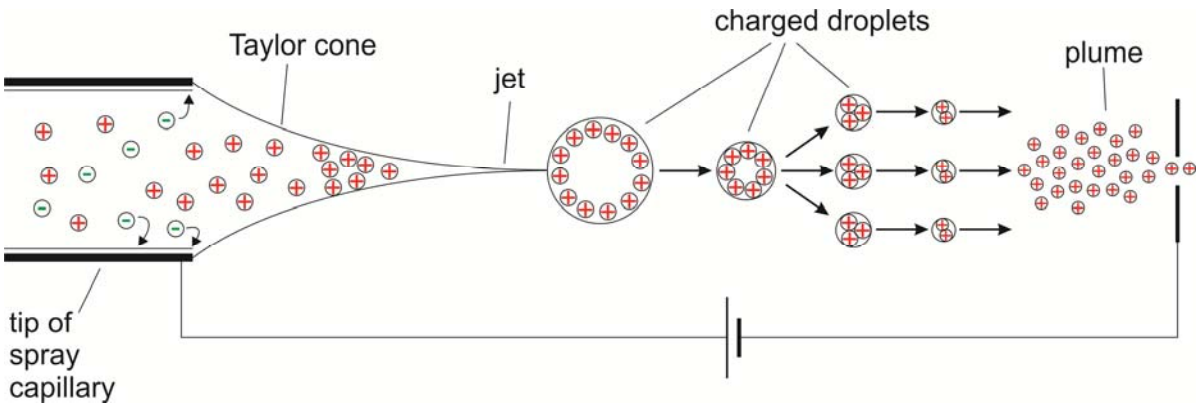

Figure 3.2.1 *Schematic representation of the electrospray ionization (ESI) process.*

The final formation of single fully desolvated ions can be explained by two different mechanisms: a) According to the **charge residue model** (CRM),[50] the process of solvent evaporation and Coulomb explosions continues until only one ion remains in one droplet. This is then desolvated completely by evaporation of the remaining solvent molecules. b) According to the **ion evaporation model** (IEM),[51] single ions can already be emitted from the droplets, when charge repulsion becomes too strong on the droplet surface.

The ions are then guided to the detection unit through the potential difference between spray capillary and orifice.

ESI as one of the softest ionization methods usually produces quasi-molecular ions via protonation, deprotonation, or the addition of (background) cations like sodium or potassium or anions such as chloride. Also labile molecules as well as non-covalent (supramolecular) aggregates can be intactly transferred into the gas phase by ESI. Especially for larger analytes, broad distributions of multiply charged ions are observed.

3.2.3 Mass Analyzation and Detection Techniques

Table 5.2: *Overview on the common mass analyzers and their ion separation principles.*[52]

type of analyzer	ion separation principle	comments	accuracy	m/z range	resolution
sector field (B, E, BE, EB...)[a)]	magnetic sector: Lorentz force; impulse selection electrostatic sector: kinetic energy selection	limited resolution in MS/MS experiments[b)], high-energy collisions; usually coupled to EI/CI, FAB	< 5 ppm	10,000	30,000
Quadrupole (Q)	superposition of a constant electric field (U) and a radiofrequency field (V) on four parallel metal rods, stable ion trajectories require appropriate settings of U and V, scanning voltages separates different m/z	low cost instruments which can favorably be coupled to continuously operating ESI ion sources; MS/MS capable, if e.g. three quadrupols are used for mass selection, collisional activation and product ion scan	100 ppm	4,000	4,000
Ion Trap (IT)	similar to Q, traps have a ring electrode and two capping electrodes	low cost instruments; collision gases can be subjected into the trap for MS/MS and beyond (MS^n)	100 ppm	4,000	4,000
Time-of-flight (TOF)	all ions accelerated at the same time by a high voltage pulse, travel time corresponds to m/z	pulsed analyzer typically used together with MALDI ion sources, not generally applicable for MS/MS	200 ppm	> 300,000	8,000
Time-of-flight (reflectron)	similar to TOF, but ions are reflected and thereby refocussed by reflectron thus providing higher accurracy	TOF/TOF analyzers permitting MS/MS experiments available, growing number of applications	10 ppm	10,000	15,000
Ion-cyclotron resonance (ICR)	cyclotron frequency of ions orbiting inside a cell within a superconducting magnet (4.7 - 12 T field strength) is measured	costly equipment, highest accuracy and resolution, in principle unlimited MS^n capabilities (as long as ion intensity suffices), bimolecular reactions possible	< 2 ppm	10,000	>> 100,000

[a)] B indicates a magnetic sector, E an electrostatic sector. The most common setups are double-focussing instruments with either a Nier-Johnson geometry (EB) or an inverse Nier-Johnson configuration (BE). Extended setups such as BEBE are available and can be used for up to MS^3 experiments.

[b)] MS/MS, tandem MS and MS^n are expressions referring to experiments in which the ion of interest is mass-selected, then subjected to a gas-phase experiment, and finally examined with respect to the product ions formed in fragmentation reactions.

3.2.3.1 Quadrupole Instruments and Quadrupole Ion Traps

A quadrupole mass analyzer consists of four parallel metal rods that are connected to an alternating electric potential with each two opposing rods likely charged. The potential Φ that is applied to the first pair of rods consists of a constant potential U and an alternating potential V cos(ωt) (equation 3.2.1). The potential of the other pair of opposite rods corresponds to -Φ.

$$\Phi = \left(U - V\cos\omega t\right) \tag{3.2.1}$$

The ions pass this analyzer in z-direction in a wavelike trajectory, which is expressed by the Mathieu differential equations (equation 3.2.2 and 3.2.3). In these equations, e is the elemental charge, m is the mass of the corresponding ion, and 2r describes the distance between two opposite rods.

$$\ddot{x} + \frac{2e}{mr^2}\left(U + V\cos\omega t\right)x = 0 \tag{3.2.2}$$

$$\ddot{y} - \frac{2e}{mr^2}\left(U + V\cos\omega t\right)y = 0 \tag{3.2.3}$$

The solution of these differential equations gives stable trajectories for specific *m/z* values depending on the corresponding potentials. All other ions have unstable trajectories and collide with the rods, where they are neutralized. The ions with stable trajectories, however, can be detected at the end of the quadrupole, for example by means of a secondary electron multiplier. By variation of the DC and AC voltage, a certain range of *m/z* values can be scanned.

If at least three quadrupoles are connected in a row, this setup can be used for tandem mass-spectrometric experiments: In the first quadrupole, ions of a specific *m/z* value are mass-selected by applying a certain potential. In the second quadrupole, the ions can be reacted with a reagent or collision gas and the products subsequently detected in the third quadrupole as described above.

3.2.3.2 Time-Of-Flight (TOF)

In a time-of-flight mass spectrometer, the ions are accelerated in an electric field, which results in all ions of the same charge (z) having the same kinetic energy E_{kin}. However, they differ with respect to their velocity; therefore, they can be distinguished by the time they need to reach the detector.

$$E_{kin} = zeU = \frac{1}{2}mv^2 \tag{3.2.4}$$

Rearrangement of equation 3.2.4 results in a relationship between *m/z* ratio and the flight time t. So if the flight time is measured and acceleration voltage U and flight path d are known, the corresponding *m/z* values can be calculated (equation 3.2.6).

$$v = \frac{d}{t} = \sqrt{\frac{2zeU}{m}} \tag{3.2.5}$$

$$\frac{m}{z} = \frac{2eUt^2}{d^2} \tag{3.2.6}$$

This principle can be used in TOF analyzers, if the starting time is the same for all ions within one ion package. In modern instruments, this is achieved by accelerating the ions by a high-voltage pulse through a so-called deflector electrode perpendicular to the ions' flight path arriving from the ion source.

Furthermore, one distinguishes simple linear TOF analyzers and reflectron TOF (ReTOF) analyzers. The reflectron unit reflects the ion beam in a constant electrostatic field opposed to the acceleration voltage, which elongates the flight path and also refocuses the ion beam and therefore leads to higher resolution than in linear TOF analyzers. However, the use of a reflectron limits the mass range, which in linear TOF analyzers is technically unlimited.

Connecting two TOF subunits with intermediate mass selection allows for MS/MS experiments.

3.2.3.2 Ion Cyclotron Resonance (ICR)

In **Ion Cyclotron Resonance** (ICR)[53] instruments, the ions are held on small orbits in the analyzer cell within the magnetic filed of a superconducting magnet (magnetic flux density up to B = 15 T in commercial instruments). Ions with the charge *q* and the velocity $\vec{v}$ in the ICR cell are affected by the Lorentz force (equation 3.2.7) perpendicular to the magnetic field axis z, which traps the ions in x and y direction.

$$\vec{F}_L = q \bullet \vec{v} \times \vec{B} \tag{3.2.7}$$

The cylindrically shaped cell itself consists of each one pair of trapping, excitation, and detection plates. The trapping plates are likely charged as the ions under study to keep them inside the ICR cell in z direction.

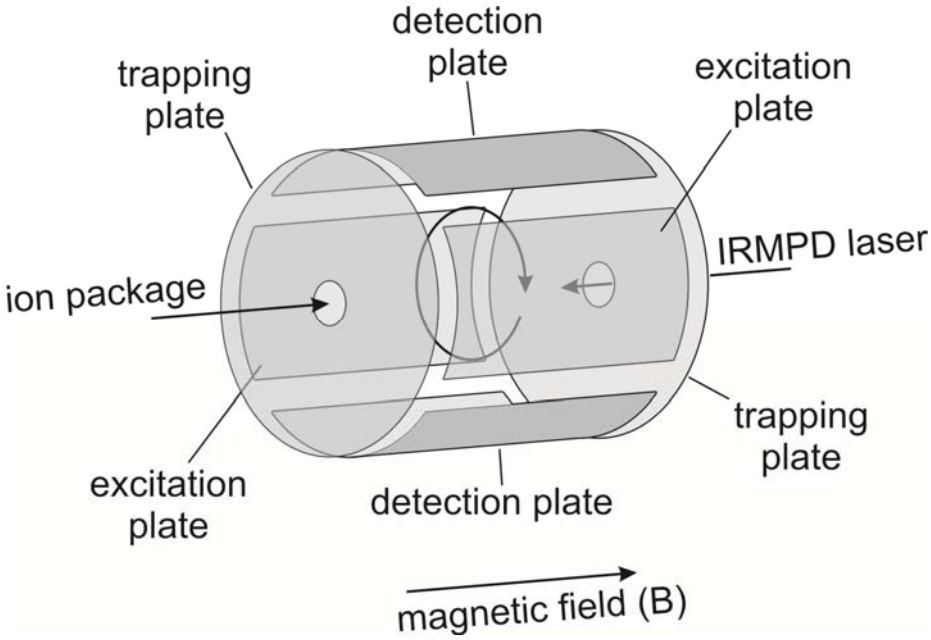

Figure 3.2.2 *Schematic representation an ICR analyzer cell.*

If the ions move on stable orbits, the Lorentz force F_Z equals the centripetal force F_C (equation 3.2.8).

$$\vec{F}_L = q\vec{v}\vec{B} = \frac{m\vec{v}^2}{r} = \vec{F}_c \tag{3.2.8}$$

Therefore, the radius *r* of the ions' orbits inside the ICR cell – given by equation 3.2.9 – is directly proportinal to its mass-to-charge ratio.

$$r = \frac{m\vec{v}}{ze\vec{B}} \tag{3.2.9}$$

Substitution of $\vec{v} = r\omega$ in equation 3.2.9 gives the angular frequency ω (equation 3.2.10).

$$\omega = \frac{ze\vec{B}}{m} \tag{3.2.10}$$

As the magnetic field is kept constant, the angular frequency ω of an ion – and therefore also every ion's particular cyclotron frequency – only depends on its mass-to-charge ratio and is independent of its initial velocity *v*.

If now the ions inside the cell are excited by applying a high-frequency pulse via the excitation plates (see Figure 3.2.2), the ions are forced to an orbit with larger radius, while the cyclotron frequency remains the same. This effect can be used for different purposes:

a) The excited ion packages induce a small image current at the detection plates, which allows the measurement of the cyclotron frequency of each ion, from which the corresponding *m/z* ratios can be calculated according to equation 3.2.10. As ion packages with different *m/z* ratio orbit inside the cell – each one with a unique cyclotron frequency – the measured signal consists of a superposition of different frequencies, which can all be detected simultaneously as a transient *free induction decay* (FID; similar to NMR instruments). Fourier transformation of the FID transforms the time domain into the frequency domain finally resulting in the corresponding *m/z* values. As the frequencies can be measured with extreme precision, are able to provide very high resolutions (up to the 10^6 region) and high mass accuracy.

b) Besides detection, the emission of appropriately chosen high frequency pulses may excite specific ions to radii larger than the cell diameter, which leads to neutralization of these ions, when they collide with the cell walls. This allows the isolation and mass-selection of specific ions, which then may be used for tandem-MS experiments.[54] Technically, these experiments are unlimited with respect to the number of MS^n steps, but practically limited by the actual ion abundances caused by collisions with residual gas

Fragmentation may be induced by a variety of different methods:

For **Collision Induced Dissociation** (CID), sometimes also referred to as **Collision Activated Decay** (CAD), mass-selected ions are allowed to collide with an inert gas – e.g. helium, argon, or nitrogen – which leads to bond cleavage and fragmentation.[55] A special case of this method is represented by the so-called **Sustained Off-Resonance Irradiation Collision Induced Dissociation** (SORI-CID)[56]: Here, the ions are accelerated by applying an off-resonance electric field pulse, which leads to lower collision energies as compared to on-resonance activation so that decomposition more likely occurs via the lowest energy fragmentation pathway.

The usage of non-inert collision gases (or at least volatile reagents) allows the study of bimolecular reactions in the gas phase, e.g. H/D exchange (→ chapter 4.3).

In an **Infrared Multiphoton Dissociation** (IRMPD) experiment,[57] the ions of interest are excited by an IR laser, which requires the ions to absorb in the applied wavelength region (the mass spectrometer employed for the experiments described in this thesis uses a 25 W laser with a fixed wavelength of $\lambda = 10.6$ μm). The application of wavelength tunable lasers (e.g. free electron laser) allows the measurement of IR spectra of species only stable in the gas phase by studying the wavelength-dependent fragmentation yield.[58]

Hence, FTICR instruments do not only combine the advantage of extremely high mass accuracy and resolution, but also offer the ideal prerequisites for gas-phase chemistry beyond mere analytical characterization.

This makes FTICR mass spectrometry an extremely useful tool for the investigation of non-covalent interactions in supramolecular aggregates and molecular recognition processes.[59-63]

“The most exciting phrase to hear in science, the one that heralds new discoveries, is not 'Eureka!' (I found it!) but 'That's funny ...'”

Isaac Asimov (1920 - 1992)

4. Results and Discussion

4.1 A pH-controllable Rotaxane-based Molecular Shuttle

4.1.1 Introduction and Idea of the Project

The Hunter-type tetralactam macrocycle described above (chapter 3.1) is able to adopt several different conformations with respect to the orientation of the four amide groups (Figure 4.1.1). DFT calculations show that the two most stable conformations are the ones with all four amide N-H protons pointing inside the macrocyclic cavity (**A** and **B** in Figure 4.1.1).

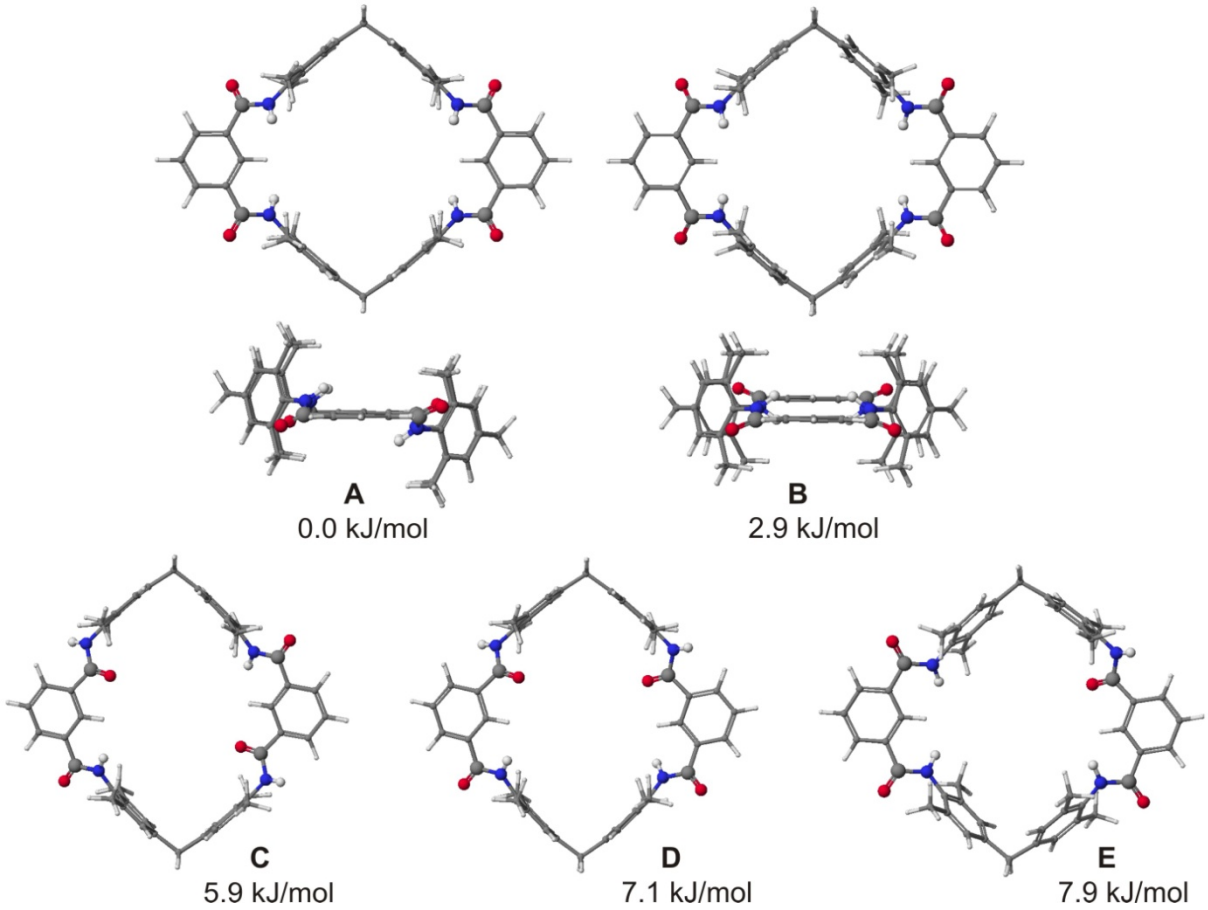

Figure 4.1.1 *Five different conformers of an unsubstituted tetralactam macrocycle optimized with the B3LYP density functional hybrid and a DZP basis. Structures* **A** *and* **B** *are also shown from the side of a plane parallel to the two isophthaloyl rings moieties to show the NH groups above and below the macrocyclic plane. The relative energies of these five conformations are very close to each other.*[64] *The cyclohexyl rings were replaced by methylene groups to simplify the calculations.*

In both of these two structures, each two of the amide protons point above and below of the macrocyclic plane, respectively, which is coplanar with the isophthaloyl rings. The energetic difference between the two "all-in" macrocycles is only 2.9 kJ/mol. Also the two different "two-in-two-out" conformations (**C** and **D** in Figure 4.1.1) as well as the "three-in-one-out" conformation (**E** in Figure 4.1.1) lie within a range of less than 8 kJ/mol.
Furthermore, the calculated barrier for the in-to-out transformation of one amide group is relatively low requiring an activation energy of 29 kJ/mol.

In the crystal structure of a similar tetralactam macrocycle incorporating a pyridine-3,5-dicarbonyl moiety instead of an isophthaloyl ring, the "all-in" conformer **B** as well as the "two-in-two-out" conformer **C** are found in a 1:1 ratio (Figure 4.1.2).[65] This confirms the prediction of the different conformers as obtained from the theoretical studies.

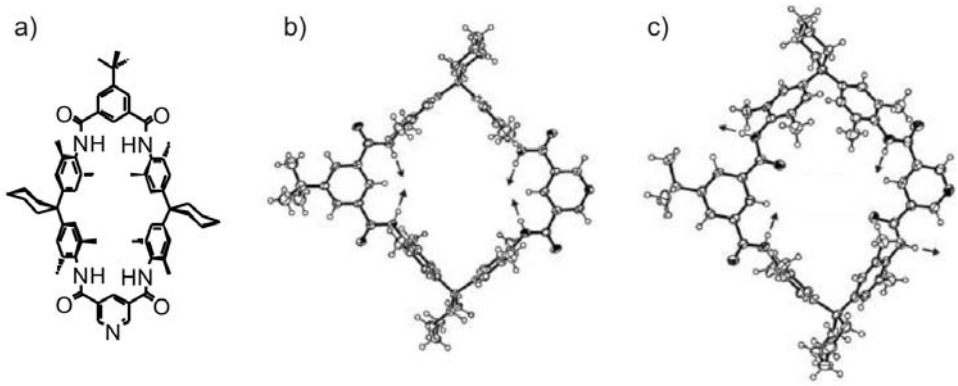

Figure 4.1.2 *a) Chemical structure of a tetralactam macrocycle incorporating a pyridine-3,5-dicarbonyl moiety, b) "all-in" conformer and c) "two-in-two-out" conformer of this macrocycle as observed in the solid state structure in 1:1 ratio.*[65]

These findings raised the question, whether the tetralactam macrocycle's transition from the "all-in" conformation to the "two-in-two-out" conformation can be controlled. A convenient way to achieve conformation switchability by change of the pH value appeared to be hydroxy substitution of the isophthalic acid moieties in position 4 and/or 6. Substitution of all four positions in the macrocycle should be the easiest way due to the higher symmetry (Figure 4.1.3a).
Deprotonation of the macrocycle's OH groups would the induce a conformational change from a conformation with all four amide hydrogen atoms pointing inwards the macrocyclic

cavity towards a structure in which two of them point inwards and the other two point outwards. This conformational change would then be expected to reduce the interactions between macrocycle and axle thus accelerating the shuttling rate in a bistationary [2]rotaxane (Figure 4.1.3c).[66]

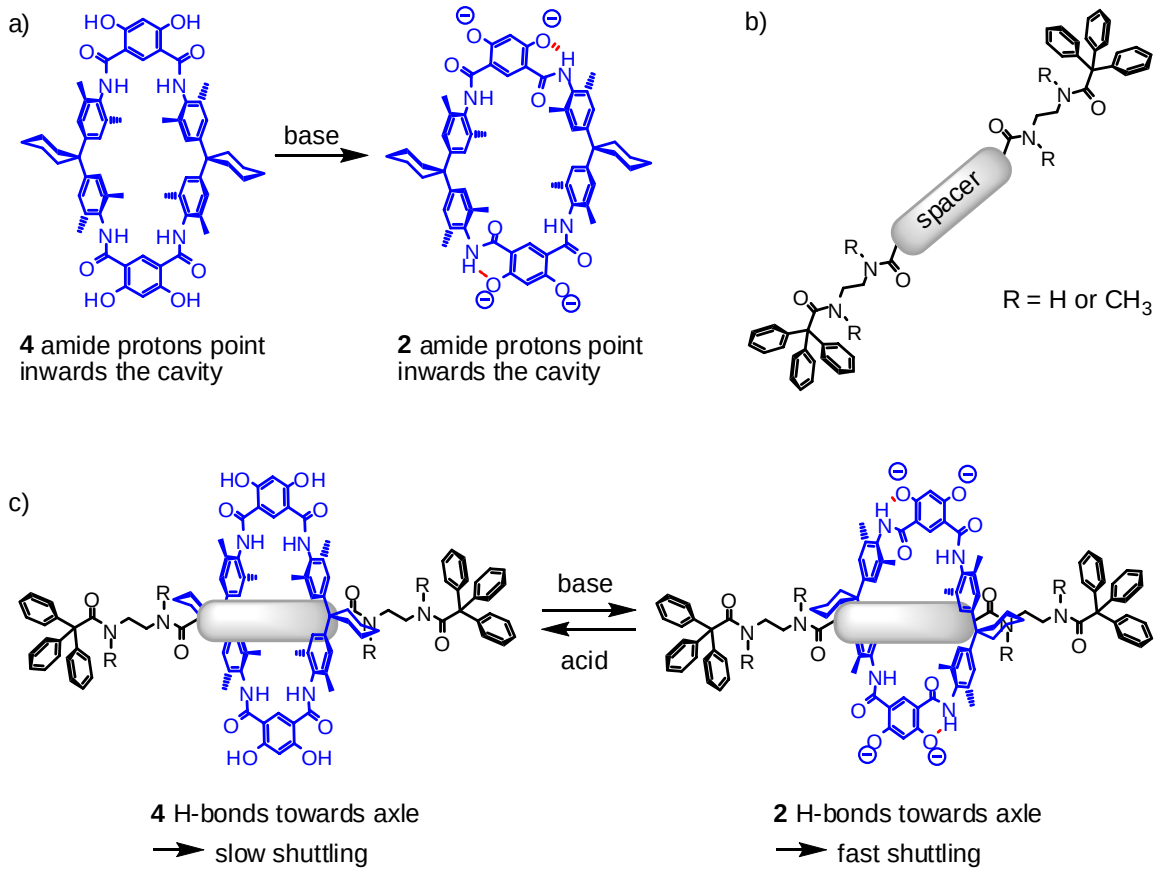

Figure 4.1.3 ***a****) Deprotonation-induced conformational change of a modified Hunter/Vögtle-type tetralactam macrocycle;* ***b)*** *suggestion for a bistationary diamide axle for the construction of a molecular shuttle rotaxane;* ***c)*** *control of the shuttling rate in a molecular shuttle rotaxane through deprotonation-induced conformational change of the macrocycle.*

4.1.2 Design of the Macrocycle

The 4,6-dihydroxy-substituted isophthalic acid required for the preparation of the tetra-hydroxy substituted macrocycle presented above (Figure 4.1.3c) is literature known and can be prepared by reaction of resorcinol with potassium carbonate at high pressure.[67]
As the phenolic hydroxyl groups would interfere with macrocycle synthesis, they need to be protected with a suitable protective group. This protective group should fulfill certain requirements: a) protection of the hydroxyl groups against reaction with an electrophile during the different steps of macrocycle synthesis, b) stability under strongly basic conditions, c) stability under slightliy acidic conditions to allow purification on silica columns, and d) a rather facile method of deprotection that does not affect amide bonds used to construct the macrocycle and the rotaxane. Futhermore, the protective group should provide a certain solubility of the corresponding protected macrocycle in non-polar organic solvents like dichloromethane to allow for rotaxane formation.

Based upon these preliminary considerations, there are three feasible alternatives (Figure 4.1.4):
a) The methyl protective group can be easily introduced by reaction with either methyl iodide or the less dangerous dimethyl sulfate, whereas cleavage is usually performed by reaction with BF_3, which would not interfere with amide bonds. Also, the methyl ether would be stable under both, basic and acidic conditions. Furthermore, two methoxy groups per isophthaloyl moity should suffice to prevent π-π-stacking of the isophthalic aromatic rings, which was found to cause very low soubility of tetralactam macrocycles in case of unsubstituted isophthaloyl moieties.
This strategy came with two problems: First, a sufficient solubility of the cyclization products in dichloromethane could not be achieved. The second - and even worse - problem is the selective formation of octalactam macrocycles instead of the tetralactam analoga, if the 4,6-dimethoxy-substituted extended diamine building block is reacted with 4,6-dimethoxy isophthaloyl dichloride.
This rather surprising result will be discussed in detail in chapter 4.2.

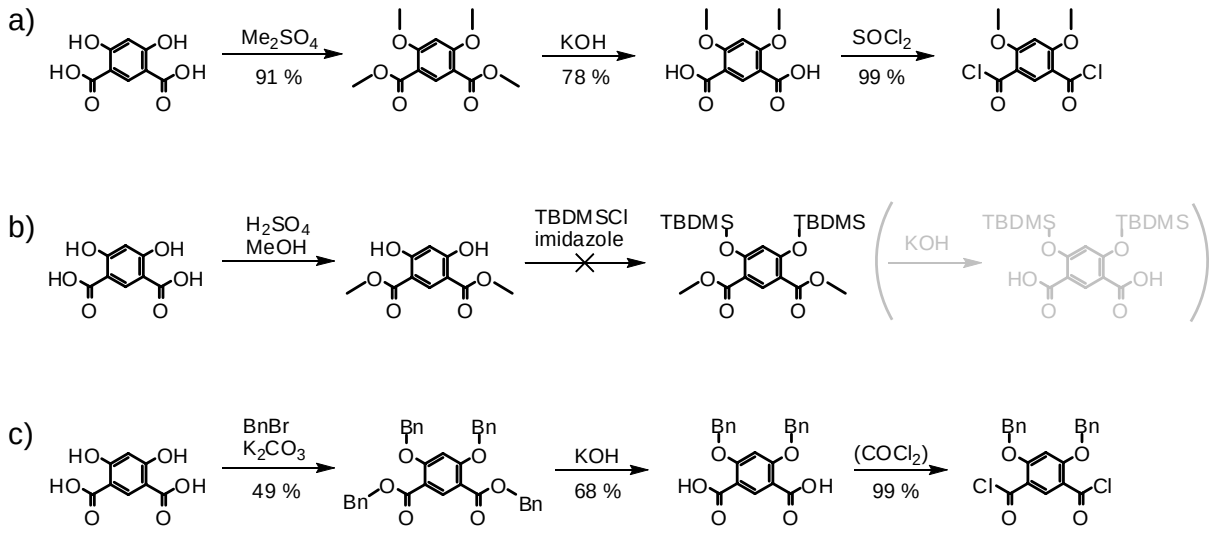

Figure 4.1.4 *Overview of the three possibilities of protecting the phenolic OH groups of 4,6-dihydroxyisophthalic acid as discussed below: a) Methyl protection: three steps from starting material to the corresponding acid chloride with an overall yield of 71 %. b) Protection with the tert-butyl-dimethylsilyl group after prior methyl protection of the carboxyl groups: this strategy would require in total four steps from starting material to the corresponding acid chloride. As no uniform product could be isolated after introduction of the TBDMS groups, this strategy was abandoned. c) Benzyl protection of the hydroxyl groups: three steps from starting material to the corresponding acid chloride with an overall yield of 33 %. Even if this approach provides an overall yield way below the methyl protection strategy, it offers essential advantages in terms of solubility of the macrocylization products as well as ease of deprotection. Furthermore, toxic methylating agents such as dimethylsulfate or methyl iodide can be avoided.*

A simplified approach invokes the use of only mono-methoxy-substituted 4-methoxyisophthalic acid, which would yield a tetralactam macrocycle with one hydroxy group for conformation switching if reacted with an unsubstituted extended diamine building block and deprotection.

Reaction of 4-methoxy-isophthaloyl dichloride with the 5-*tert*-butyl-extended diamine building block results in the formation of the octalactam macrocycle as the only cyclization product, again. Therefore, this will be discussed in chapter 4.2, too.

Reaction with the preorganized dipicolinyl extended diamine building block, however, results in the formation of the corresponding tetralactam macrocycle with a yield of 64 %, whereas the corresponding octalactam macrocycle was only observed in traces (< 1 %). Unfortunately, this macrocycle proved to be rather insoluble in common organic solvents once it is eluted

from the silica column after purification, which made it impossible to prepare any rotaxanes from it. Any attempts to solubilize the macrocycle by complexing it to an axle component failed.

b) The *tert*-butyl-dimethylsilyl protective group (TBDMS) can be introduced by reaction of the alcohol to pretect with *tert*-butyl-dimethylsilyl chloride after deprotonation with imidazole. Suitable stability of TBDMS ethers is given under basic and slightly acidic contitions. Solubility in dichloromethane should be even better as compared to the methyl protected species. Also, there exists a convenient way for deprotection, namely the reaction with tetra-*n*-butylammonium fluoride.[68]

Nevertheless, this strategy comes with a certain inconvenience: First, the carbonic acid groups should be protected prior to introducing the TBDMS groups, which still is rather easily done by esterification of 4,6-dihydroxyisophthalic acid with methanol in the presence of sulfuric acid. After protection of the phenolic hydroxyl groups, the methyl esters have to be cleaved again by reaction with potassium hydroxide, which still is not an overly complicated procedure, but nevertheless raises the number of necessary additional steps to two.

Unfortunately, this pathway did not even lead that far, because already the introduction of the TBDMS group did not work as expected and the protection could not be achieved with a quantitative conversion of both hydroxyl groups.

Therefore, the focus was shifted towards another possibility:

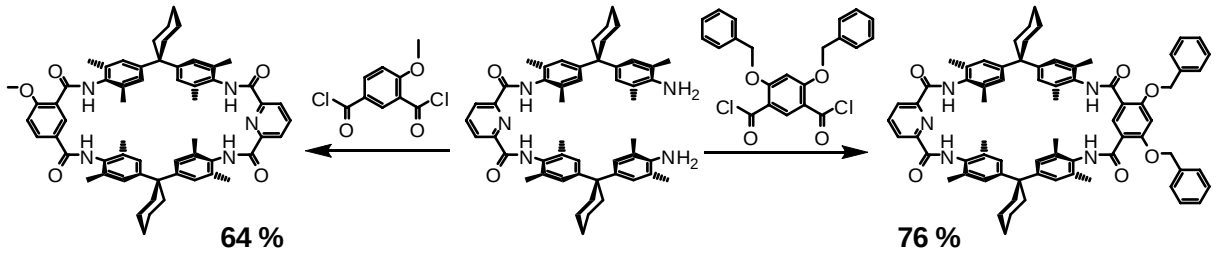

Figure 4.1.5 *Preparation of two different tetralactam macrocycles with protected hydroxyl functions in position 2 or 2 and 6 on the isophthaloyl moiety allowing for pH-dependent conformation change by deprotonation of the phenolic OH.*

c) For the introduction of the benzyl protective group, two different pathways are possible: Either the carboxyl groups can be methyl protected prior to benzyl protection of the hydroxyl groups as described above for the TBDMS protection or the 4,6-dihydroxyisophthalic acid is directly reacted with benzyl bromide under basic conditions, which leads to a quadruple substitution of the isophthaloyl moiety on the hydroxyl as well as on the carboxyl groups.
The latter approach works quite well, even if the reaction quenching produces a considerable amount of benzylic alcohol, which could not be removed directly after this step. However, after basic deprotection of the carboxyl groups, the 4,6-dibenzyloxyisophthalic acid can be purified without any problem resulting in a still acceptable yield of 34 % over these two steps.
After conversion to the corresponding acid chloride, reaction with the dipicolinyl extended diamine building block under high dilution conditions gives a macrocycle with the desired substitution pattern in a relatively high yield of 76 %.
This macrocycle (Py-di-OBn-tetralactam macrocycle) finally provides a good solubility to allow for rotaxane formation in a nonpolar solvent like dichloromethane.

4.1.3 Design of the Axle

The axle component of a rotaxane-based molecular shuttle has to fulfill certain requirements:
a) First, both ends of the axle should be terminated by large stopper groups to prevent the macrocycle from deslipping. Triphenylmethyl groups are known to work well for the tetralactam macrocycles used in this work. They can be attached to an amine-terminated axle center piece by reaction of the amine with triphenylacetic acid (Figure 4.1.6a).
b) The axle has to incorporate two binding stations with the ability to work as a hydrogen bond acceptor towards the amide hydrogens pointing inwards the macrocyclic cavity. For this purpose, diamides with a 1,6-distance between the carbonyl groups were found to be a promising alternative in earlier works. [22,23,69]
c) Finally, the axle should feature a spacer between the two diamide stations that has to be longer than the distance between the carbonyl groups of a unique diamide station. This avoids the formation of an unwanted third diamide station in the middle of the complete axle, which would interfere with the shuttling motion of the macrocycle.

Based on these basic ideas, several possibilities arise to construct a suitable axle that fulfills the requirements discussed above. All of the axle center pieces presented in the following subsection are amine terminated, which would allow for a stoppering reaction with triphenylacetyl chloride during rotaxane formation:
Figure 4.1.6b shows the initially planned axle center piece: An adipoyl moiety forms the central spacer whereas two *N*,*N*'-dimethyl-ethylene diamine moieties preform the diamide stations that are to be completed by the stoppering reaction during rotaxane formation. Methylation of the axle's amide nitrogens might enhance the binding strength, because this should force all of the macrocycle's amide hydrogens to point into the cavity and be involved in binding to the axle, which finally would lead to a higher rotaxane yield. Attachment of mono-Boc-protected *N*,*N*'-dimethyl-ethylene diamine to adipoyl dichloride works quite well, but deprotection of the di-Boc-protected axle center piece with trifluoroacetic acid causes severe problems, because the desired center piece proved to be almost insoluble in common organic solvents, which makes it absolutely unsuitable for the intended purpose.

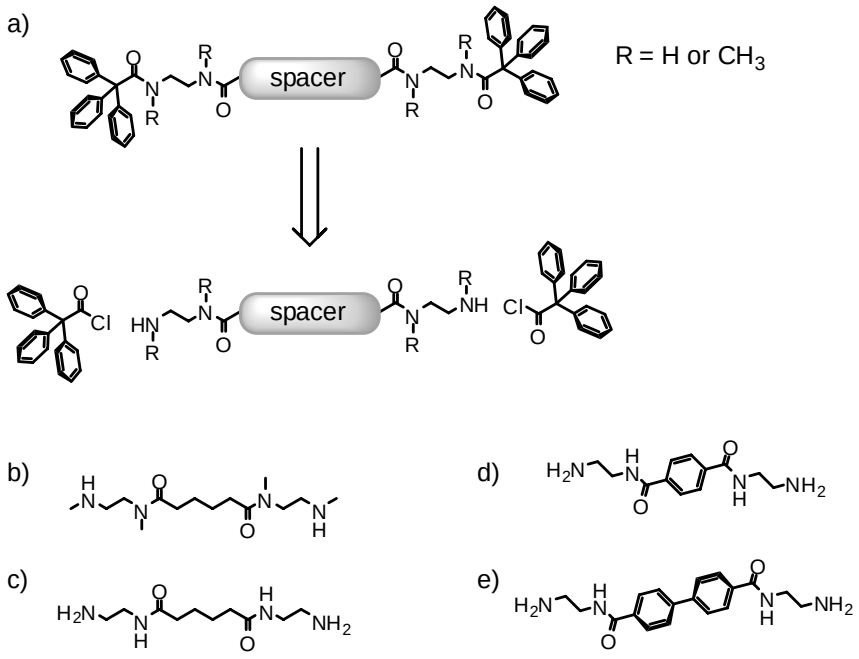

Figure 4.1.6 *a) General idea about preparation of the axle component for the construction of a molecular shuttle rotaxane. b) Axle center piece with central adipoyl spacer and two N-methylated ethylene diamine moieties that would form two diamide stations after stoppering during rotaxane synthesis. This compound proved to be almost completely insoluble in organic solvents in the deprotonated state and therefore could not be used for rotaxane synthesis. c) Analogous axle center piece with central adipoyl spacer and two ethylene diamine moieties as binding station precursors. It could not be isolated and apparently decomposes during deprotection of the Boc-protected precursor. d) Axle center piece with central terephthaloyl spacer and two ethylene diamine moieties. It could not be isolated either and also apparently decomposes during deprotection of the Boc-protected precursor. e) Axle center piece with central 4,4'-biphenyl spacer and two ethylene diamine moieties. It can be isolated, but the extremely poor solubility makes a proper analysis complicated and excludes this compound from application for the construction of the rotaxane molecular shuttle.*

The preparation of the corresponding di-Boc-protected non-methylated analogue (Figure 4.1.6c) again does not represent a problem, however, after the deprotection with trifluoroacetic acid, no product at all could be isolated. The most likely explanation was thought to be an intramolecular attack of the deprotected primary amine to a carbonyl group causing decomposition of the product resulting in only volatile alternative products that would be evaporated together with the solvent (dichloromethane).

Therefore, the focus was shifted towards rigid aromatic spacers between the ethylene diamine moieties like a 1,4-phenylene and a 4,4'-biphenylene moiety that would inhibit such an intramolecular nucleophilic attack of a primary amine.
Also, in both of these cases, reaction of *N*-Boc-ethylene diamine with the corresponding aromatic di-acid chloride can be achieved with fairly high yields. The decisive difference between the two aromatic spacers becomes evident after cleavage of the Boc protecting groups by reaction with trifluoroacetic acid: Whereas the terephthaloyl axle center piece (Figure 4.1.6d) could only be observed in traces, the analogous axle center piece with biphenyl spacer (Figure 4.1.6e) could be obtained in satisfactory yields. The reason for this very different behaviour could not be clarified. However, both of them again proved to be insoluble in common organic solvents, which did not allow NMR analysis and also excludes these compounds from any application for rotaxane formation.

As the previous attempts to find a suitable way of constructing the axle of the planned molecular shuttle rotaxane failed – mainly due to serious solubility problems – attaching the ethylene diamine moiety to the trityl stopper semmed to be a very promising alternative. Indeed, the reaction of triphenylacetyl chloride with *N*-Boc-ethylene diamine and subsequent deprotection with trifluoroacetic acid yields an extended stopper building block with excellent solubility properties (Figure 4.1.7a). Furthermore, the workup does not require any time-consuming steps liks chromatography. The extended trityl stopper can be prepared in larger quantities (gram scale); purification of all intermediate products as well as of the extended stopper can be performed by extraction and/or recrystallization techniques.

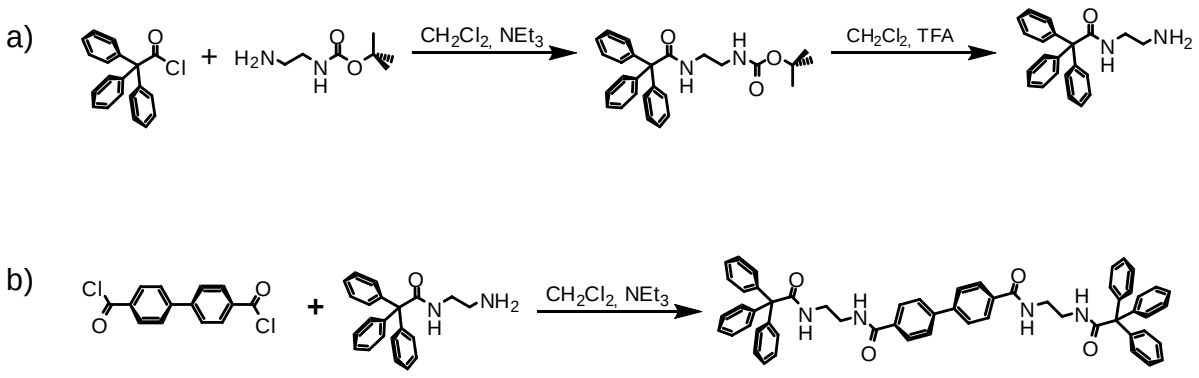

Figure 4.1.7 *a) Preparation of an elongated stopper by attaching N-Boc-ethylene diamine to the triphenylacetyl moiety followed by deprotection of the terminal amine. b)Preparation of the corresponding free axle from the elongated trityl stopper by reaction with 4,4'-biphenyl-dicarbonyl dichloride. This compound is further required for NMR comparison with rotaxanes.*

4.1.4 Construction of the Rotaxane Shuttles

Using to the optimized macrocycle and axle building blocks as described in the previous chapters (4.1.1 and 4.1.2), a series of [2]rotaxanes with bistationary axles could be prepared: All of the rotaxanes are prepared from the di-benzyloxy-substituted tetralactam macrocycle described in chapter 4.1.1, because it shows much better solubility as compared to the mono-methoxy-substituted macrocycle.

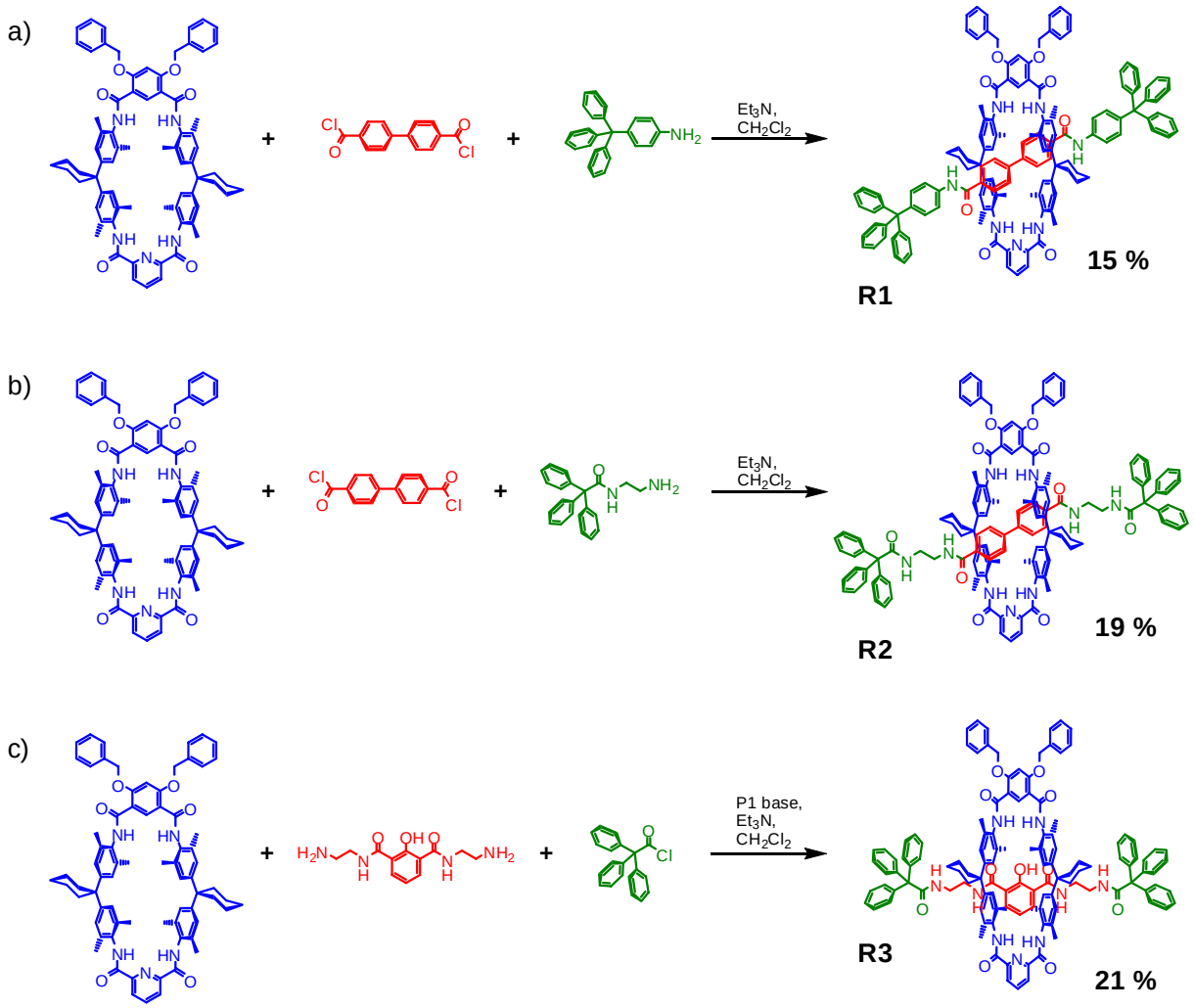

Figure 4.1.8 *Preparation of different molecular shuttle rotaxanes from the pyridine-di-OBn-macrocycles: a) Rotaxane synthesis through amide template with axle constructed from 4,4'-biphenyl-dicarbonyl dichloride as axle center piece and triphenylmethyl aniline as the stopper. b) Same approach as for a) with N-(2-aminoethyl)-2,2,2-triphenylacetamide as stopper. c) Rotxane synthesis through a phenolate anion template.*

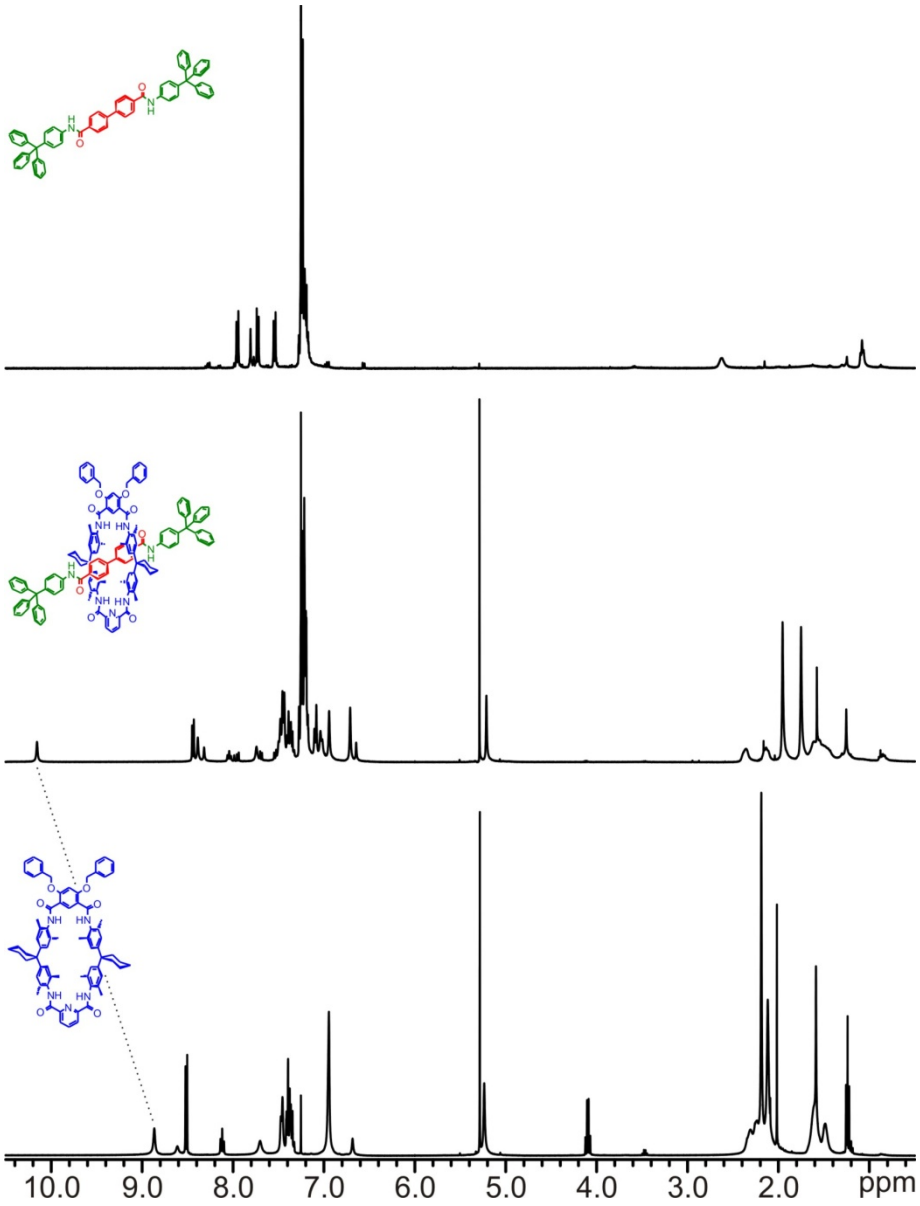

Figure 4.1.9 *Comparison of the ^{1}H NMR spectra of the short axle constructed out of 4,4'-biphenyl-dicarbonyl dichloride and triphenylmethyl aniline (top), the di-benzyloxy-tetralactam macrocycle (bottom) and the [2]rotaxane* ***R1*** *prepared from these two building blocks (middle).*
The most evident sign indicating successful rotaxane formation is the low-field shift of the macrocycle's amide protons as indicated by the dotted line (pyridine side, δ = 10.2 ppm).

Figure 4.1.8a shows the first test reaction, which should verify that the di-OBn-macrocycle is able to form rotaxanes if reacted with a di-acid chloride axle center piece and an amine terminated stopper unit. As the success of this strategy was unclear, the extended trityl stopper described above was substituted by the commercially available triphenylmethylaniline. In this reaction, the separate building blocks of the axle were added in an excess of two equivalents

to raise the rotaxane yield. This reaction resulted in the formation of the expected rotaxane **R1** with an isolated yield of 15 % proving the applicability of the three-component synthetic pathway for this system.

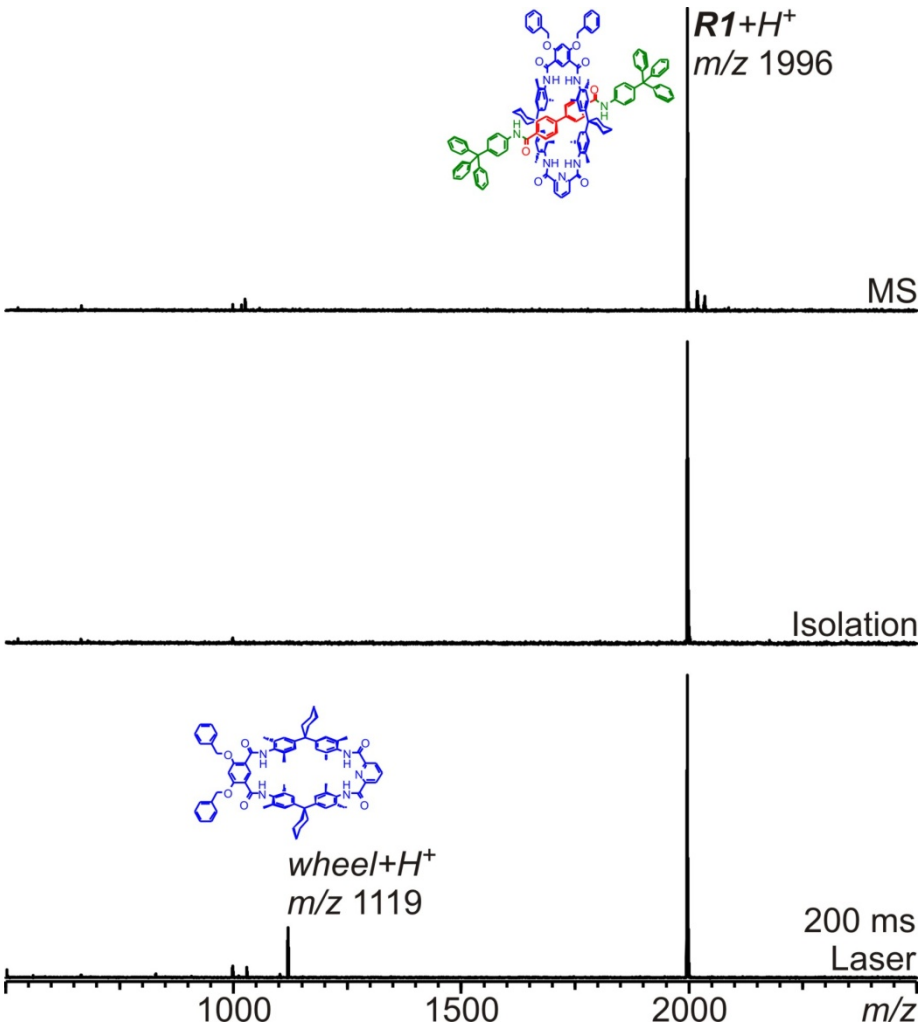

Figure 4.1.10 *ESI mass spectrum of the rotaxane constructed out of the di-benzyloxy-tetralactam macrocycle, 4,4'-biphenyl-dicarbonyl dichloride, and triphenylmethylaniline; the major peak corresponds to the protonated rotaxane* ***R1*** *(top), the spectrum after gas-phase isolation of the rotaxane (middle), and finally the spectrum after irradiation with an IR laser showing the loss (and therefore also the disruption) of the axle.*

The successful construction of the rotaxane out of the di-benzyloxy-tetralactam macrocycle, 4,4'-biphenyl-dicarbonyl dichloride, and triphenylmethylaniline can be observed by ^{1}H NMR spectroscopy, when the spectrum of the rotaxane is compared to those of the macrocyle and of the free axle (Figure 4.1.9). For the rotaxane, the signal for the macrocyle's amide protons on

the pyridine side is shifted to lower field (δ = 10.2 ppm) indicating that they are involved into hydrogen binding. The expected high-field shift of the aromatic axle protons, however, cannot be observed due to a severe overlap of the signals in the aromatic region.

The unambiguous identity of the rotaxane could furthermore be proven by ESI-FTICR mass spectrometry and tandem-MS experiments (Figure 4.1.10). The ESI mass spectrum only shows the proton, sodium, and potassium adducts of the rotaxane **R1**. After gas-phase isolation of the protonated rotaxane and irradiation with an IR laser, the axle is disrupted and therefore lost from the not anymore mechanically linked complex. What remains is the protonated macrocycle.
Another reasonable explanation for the found fragmentation behaviour is represented by the formation of a non-covalently bound proton-bridged complex of free axle and free macrocycle, which would also most likely fragment as observed during the previously described experiment with the rotaxane. This alternative can be ruled out by mixing the two components - axle and macrocycle - and performing the same MS experiment. Under exactly the same conditions, such a complex could not be generated thus ruling out this option and confirming the rotaxane structure for the first sample.

These results suggest that rotaxane formation should also be possible with the elongated stopper described in chapter 4.1.2. Indeed, the reaction of the di-benzyloxy-tetralactam macrocycle, 4,4'-biphenyl-dicarbonyl dichloride, and the elongated trityl stopper leads to the formation of the desired [2]rotaxane **R2** (Figure 4.1.8b) with an isolated yield of 19 %.
Figure 4.1.11 shows the corresponding ^{1}H NMR spectra of free axle, free macrocycle and the rotaxane **R2**. These spectra clearly indicate the formation of the rotaxane. For the rotaxane, the signal for the macrocycle's amide protons on the pyridine side is shifted to lower field (δ = 10.2 ppm) indicating that they are involved into hydrogen binding as already observed for the rotaxane with the shorter biphenyl axle (see above). Furthermore, also the axle's ethylene protons experience a considerable shift to higher field (Δδ = 0.5 ppm) indicating that they are influenced by the anisotropic cones of the macrocycle's aromatic rings perpendicular to the macrocycle plane. The shift is rather small as compared to other rotaxanes with this kind of macrocycle, which is due to an averaging of the signals for the two sides of the axles (covered and uncovered of the macrocycle). The averaging already indicates a shuttling movement fast on the NMR timescale

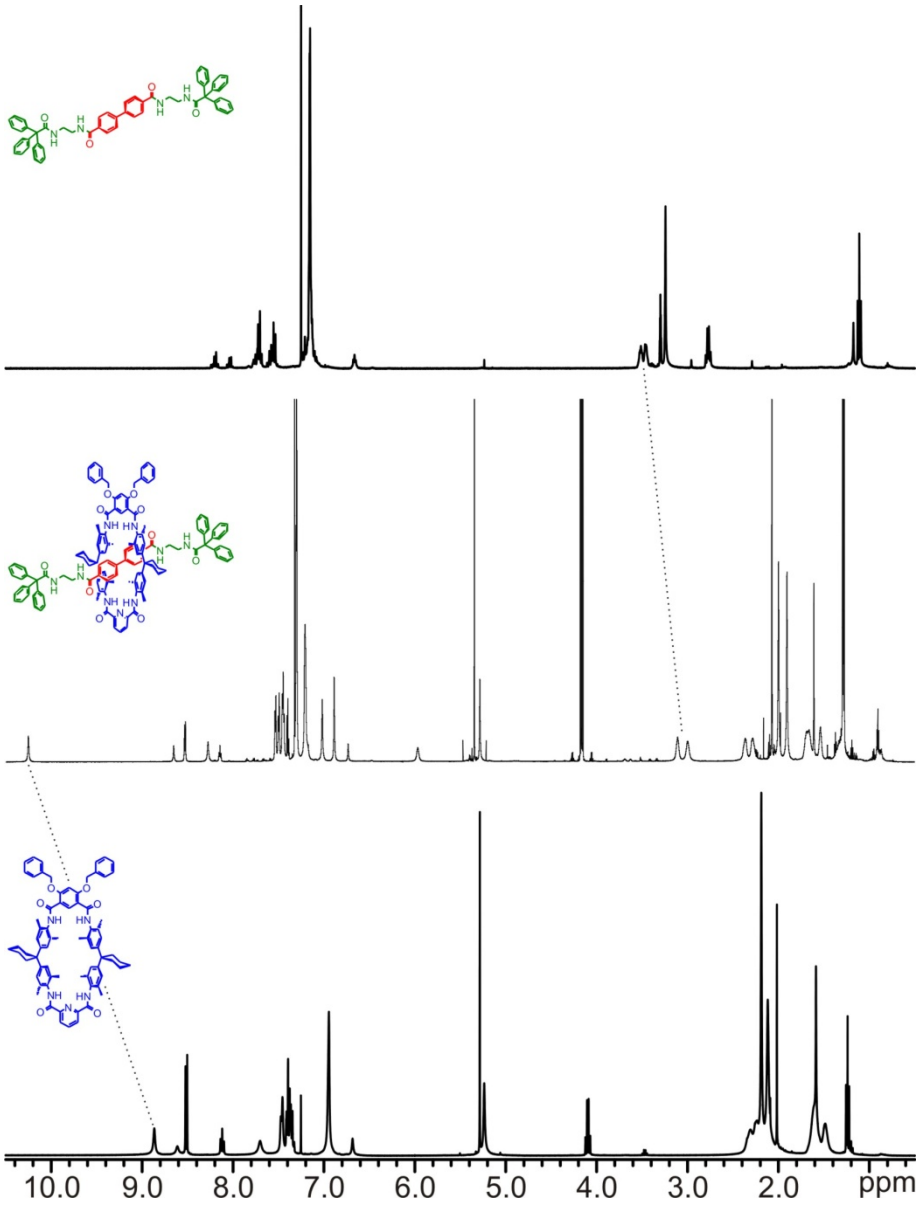

Figure 4.1.11 *Comparison of the ^{1}H NMR spectra of the bistationary axle constructed out of 4,4'-biphenyl-dicarbonyl dichloride and the elongated trityl stopper (top), the di-benzyloxy-tetralactam macrocycle (bottom) and the [2]rotaxane* ***R2*** *prepared from these two building blocks (middle).*
The most evident signs indicating successful rotaxane formation are the low-field shift of the macrocycle's amide protons (pyridine side, δ = 10.2 ppm) as well as the high-field shift of the axle's ethylene protons (δ = 2.95 and 3.06 *ppm in the rotaxane). Both are indicated by dotted lines.*

The ESI mass spectrum of rotaxane **R2** shows the protonated rotaxane as the major peak (Figure 4.1.12). Additionally, signals for a Fe(II) adduct as well as for a [**R2**+Fe(III)+NO_3] complex are observed in the spectrum, which originate from impurities in the ion source from earlier experiments.

After gas-phase isolation of the protonated rotaxane and irradiation with an IR laser for 200 ms, the axle is disrupted and therefore lost from the not anymore mechanically linked complex. What remains is the protonated macrocycle.

As already observed for rotaxane **R1**, a proton-bridged complex consisting of free axle and macrocycle could not be generated under the same ionization conditions thus confirming the rotaxane structure.

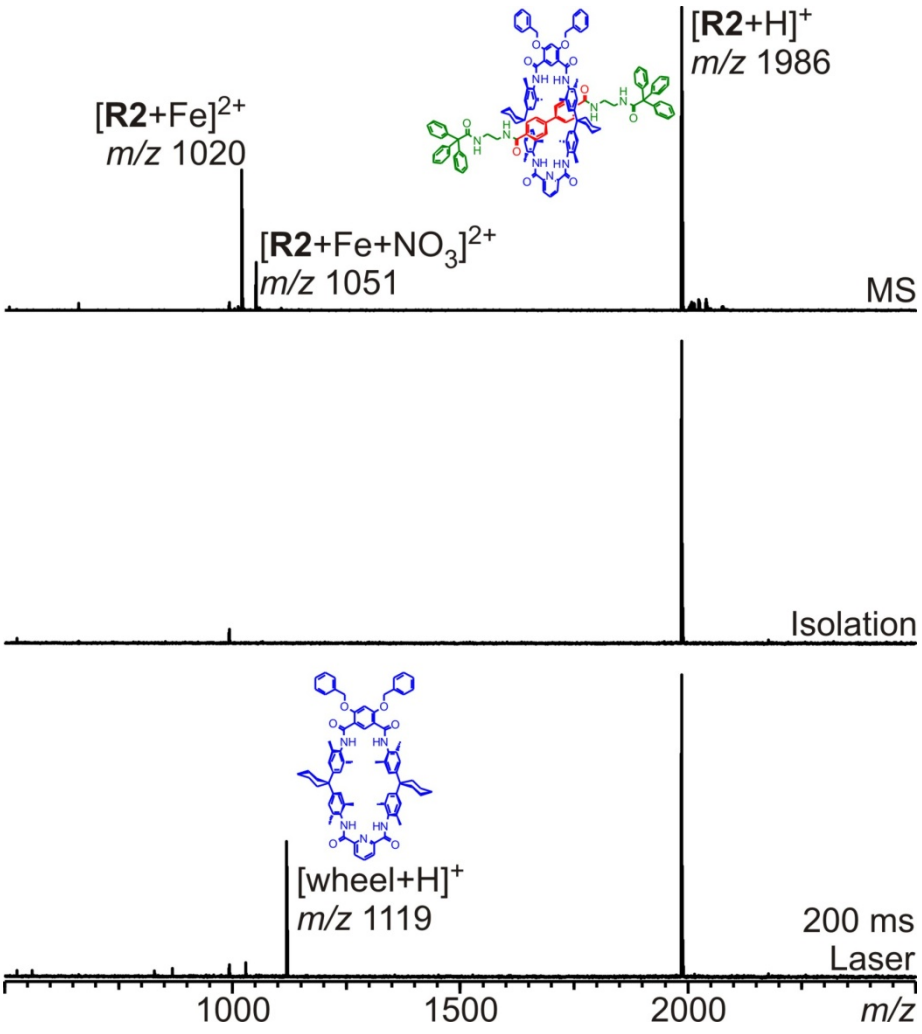

Figure 4.1.12 Top: *ESI mass spectrum of the rotaxane constructed out of the di-benzyloxy-tetralactam macrocycle, 4,4'-biphenyl-dicarbonyl dichloride, and the elongated trityl stopper (rotaxane **R2**); the major peak corresponds to the protonated rotaxane.* ***Middle:*** *The spectrum after gas-phase isolation of the rotaxane.* ***Bottom:*** *The spectrum after irradiation with an IR laser showing the loss (and therefore also the disruption) of the axle.*

The third rotaxane shown in Figure 4.1.8c (**R3**) can be prepared applying the phenolate template effect using the previously designed axle center piece N^1,N^3-bis(2-aminoethyl)-2-hydroxyisophthalamide.[22,23] The synthesis was performed analogous to the published procedure (see above) with the significant change that twice the amount of axle precursors (center piece and stoppers) was used to raise the rotaxane yield.

Unlike the previously discussed spectra of the rotaxanes **R1** and **R2**, the ^{1}H NMR spectrum of rotaxane **R3** does not give an unambiguous evidence for the formation of the desired rotaxane. Surprisingly, a signal for the axle's ethylene CH_2 protons is not observed in the spectrum in the expected region around 3 ppm (see Figure 4.1.13). Nevertheless, the macrocycle's amide protons on the pyridine side are shifted to lower field as already observed for **R1** and **R2**. Furthermore, the signal at 15.0 ppm indicates the presence of the phenol spacer in the axle.

In combination with TLC, this can already be regarded as a fairly good indication for rotaxane formation.

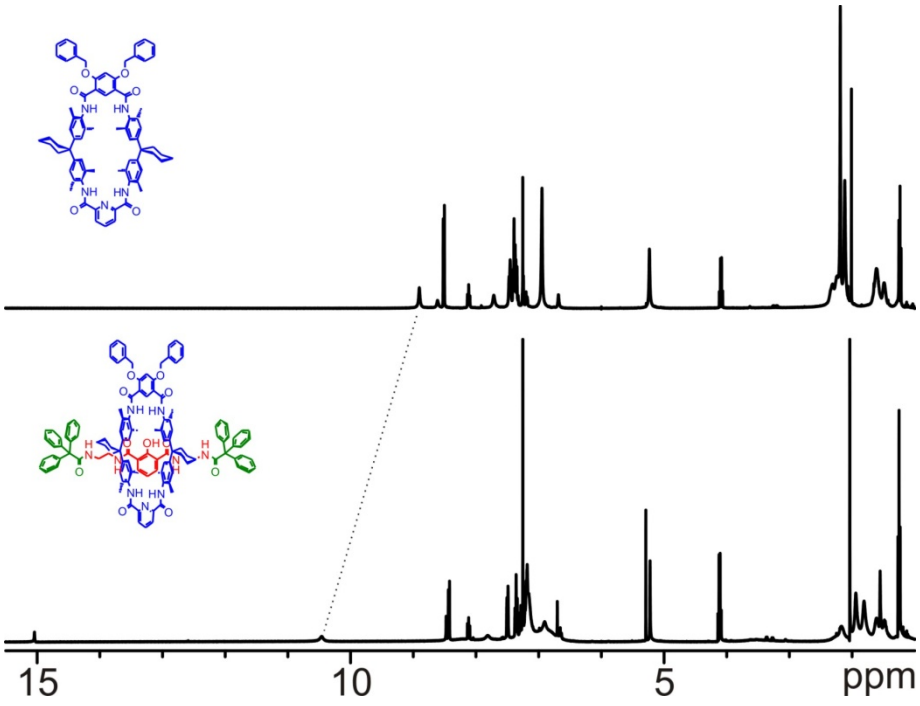

Figure 4.1.13 *Comparison of the ^{1}H NMR spectra of the di-benzyloxy-tetralactam macrocycle (top) and the [2]rotaxane* ***R3*** *prepared through phenolate template (bottom).*

The most evident sign for successful rotaxane formation is the low-field shift of the macrocycle's amide protons (pyridine side, δ = 10.2 ppm) shown by a dotted line.

However, a detailed (tandem) mass spectrometric analysis is definitely required to explicitly prove the formation of rotaxane **R3**.

The negative-mode ESI-FTICR mass spectrum shows the deprotonated rotaxane as the major peak. Gas-phase isolation and fragmentation by irradiation with an IR laser lead to disruption of the macrocycle, while the deprotonated axle remains (Figure 4.1.14) proving the interlocked structure of **R3**.

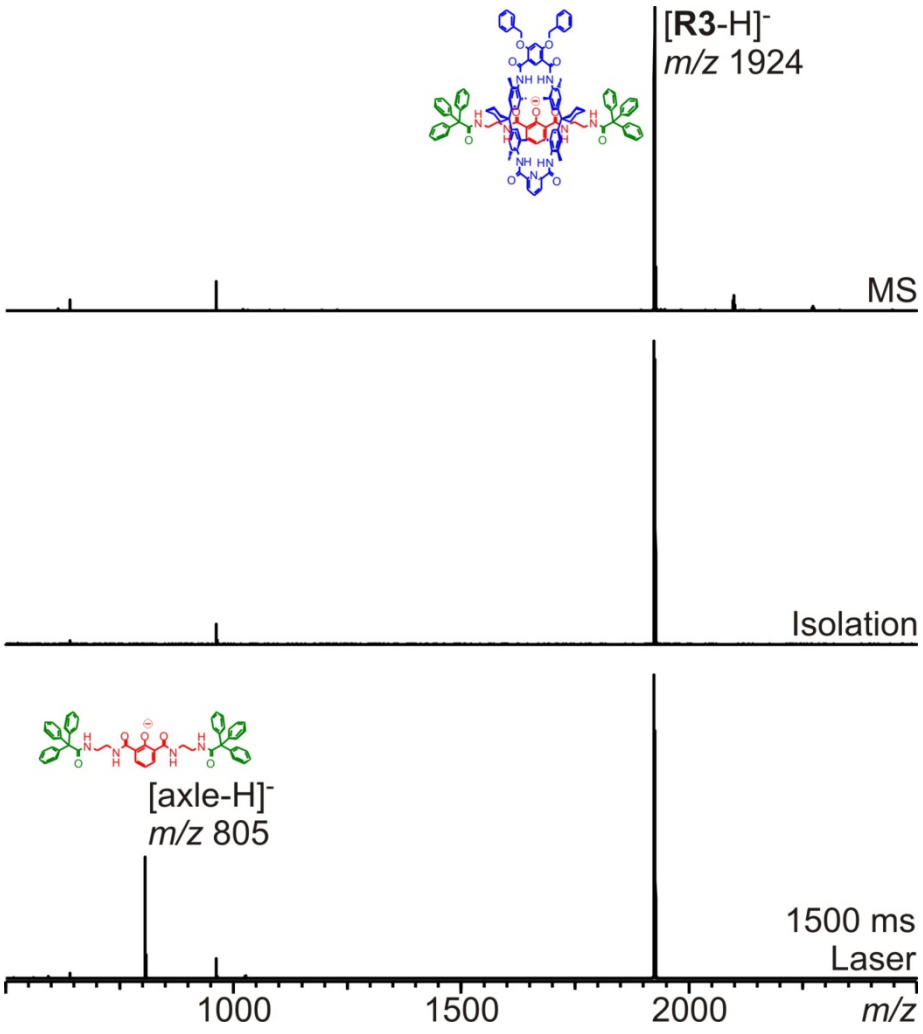

Figure 4.1.14 Top: *Negative-mode ESI mass spectrum of the rotaxane* ***R3*** *constructed out of the di-benzyloxy-tetralactam macrocycle, the phenolate axle center piece, and triphenylacetyl chloride as stopper (rotaxane* ***R2****); the major peak corresponds to the deprotonated rotaxane.* ***Middle:*** *The spectrum after gas-phase isolation of the rotaxane.* ***Bottom:*** *The spectrum after irradiation with an IR laser showing the loss (and therefore also the disruption) of the axle.*

Having now several – still protected – molecular shuttle rotaxanes in hand, the pH-controllable shuttles can be obtained by deprotection of the macrocycle's phenol functional groups, which are to be utilized to change the conformation of the macrocycle in the rotaxane and thereby also the speed of the shuttling motion of the ring along the axle.

The benzyl protecting groups can easily be cleaved by catalytic hydrogenation with palladium on charcoal as the catalyst. Starting from the benzyl-protected rotaxanes rotaxanes **R2** and **R3**, the deprotected rotaxanes **R4** and **R5** are obtained in high yields of 88 and 92 % (Figure 4.1.15).

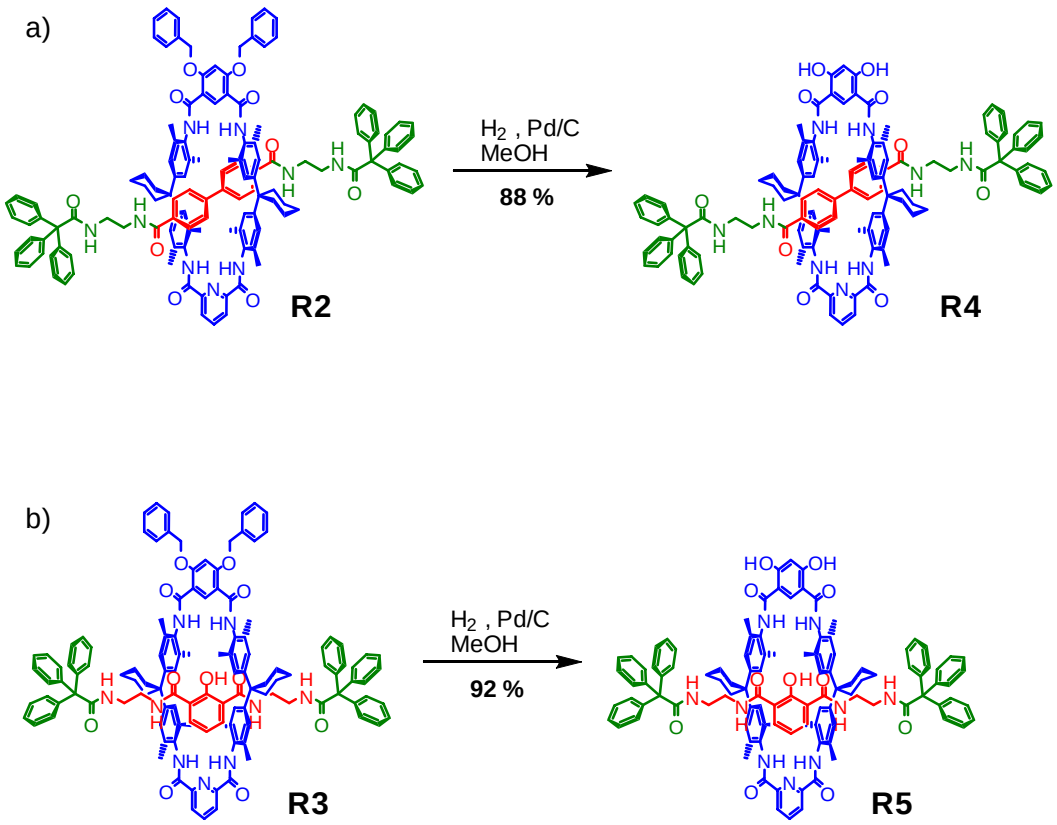

Figure 4.1.15 *Deprotection of the phenol groups of the tetralactam macrocycle in the molecular shuttle rotaxanes* ***R2*** *and* ***R3*** *by palladium catalyzed hydrogenation yielding the deprotected rotaxanes* ***R4*** *and* ***R5****.*

The successful deprotection of **R2** yielding **R4** is proven by ^{1}H NMR spectroscopy: The spectrum after deprotection (Figure 4.1.16 bottom) does not show the signal for the benzyl-CH_2 groups anymore (δ = 5.2 ppm). Instead, a new signal for the macrocycle's free OH groups is observed at δ = 11.9 ppm.

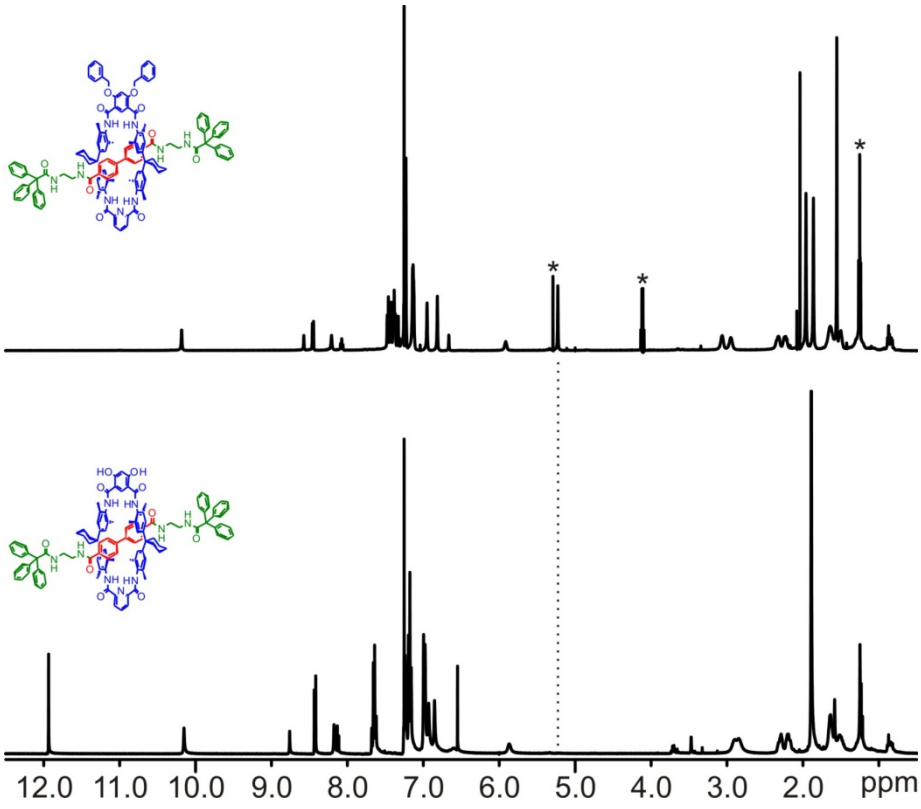

Figure 4.1.16 *Comparison of the ^{1}H NMR spectra of rotaxane **R2** (top) and the deprotected rotaxane **R4** obtained by catalytic hydrogenation of **R2** (bottom). The most evident sign for successful deprotection is disappearance of the signal for the benzyl-CH_2 protons (δ = 5.2 ppm) indicated by a dotted line. The asterisks denote signals originating from small remains of ethyl acetate.*

Further proof for the deprotection is given by tandem mass spectrometry: The negative mode ESI-FTICR mass sprectrum shows the deprotonated rotaxane as the major peak (Figure 4.1.17 top) and additionally a signal for a chloride adduct of rotaxane **R4**, whereas no signal for benzyl-protected rotaxane **R2** is observed.

Gas-phase isolation and fragmentation by irradiation with an IR laser lead to disruption of the macrocycle, while the deprotonated axle remains (Figure 4.1.17 middle and bottom) proving the interlocked structure of **R4**.

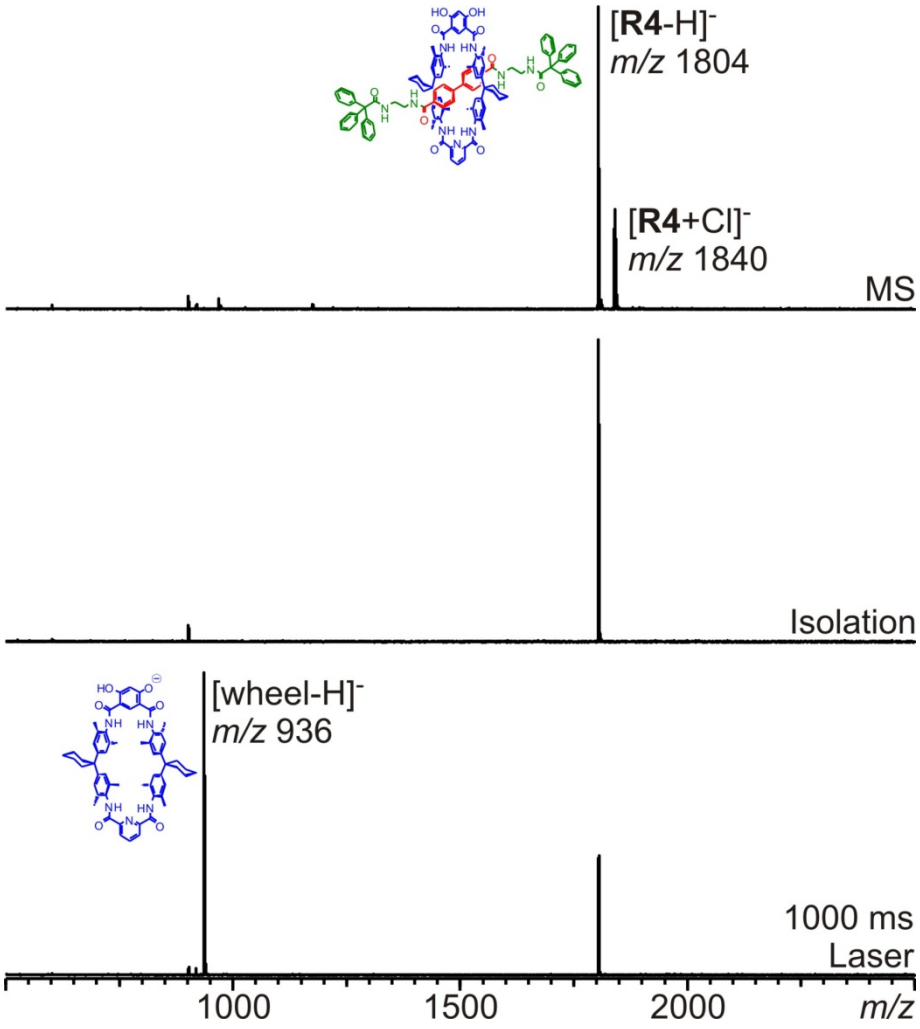

Figure 4.1.17 *Negative-mode ESI mass spectrum of rotaxane* ***R4*** *(top) , the spectrum after gas-phase isolation of the rotaxane (middle), and finally the spectrum after irradiation with an IR laser (bottom) showing the loss (and therefore also the disruption) of the axle.. The major peak in the original spectrum (*m/z *1804) corresponds to the deprotonated rotaxane; furthermore,* ***R4*** *is observed as chloride adduct (*m/z *1840).*

The ultimate proof for the interlocked structure of rotaxane **R4** could be obtained by crystallization of the rotaxane by slow evaporation of a chloroform solution and single crystal X-ray analysis. The solid state structure of **R4** is shown in Figure 4.1.18. It clearly shows the axle is threaded through the tetralactam macrocycle. The macrocycle itself is bound to one of the axle's diamide stations by four hydrogen bonds from axle N-H towards macrocycle C=O. Furthermore, the macrocle is found in two different orientations differing in a 180° rotation around the C_2 axis perpendicular to the macrocycle plane, which is also the reason that the

phenolic OH groups appear on both isophthaloyl moieties in the graphic representation of the structure. The ratio of these two orientations is approximately 3:1.

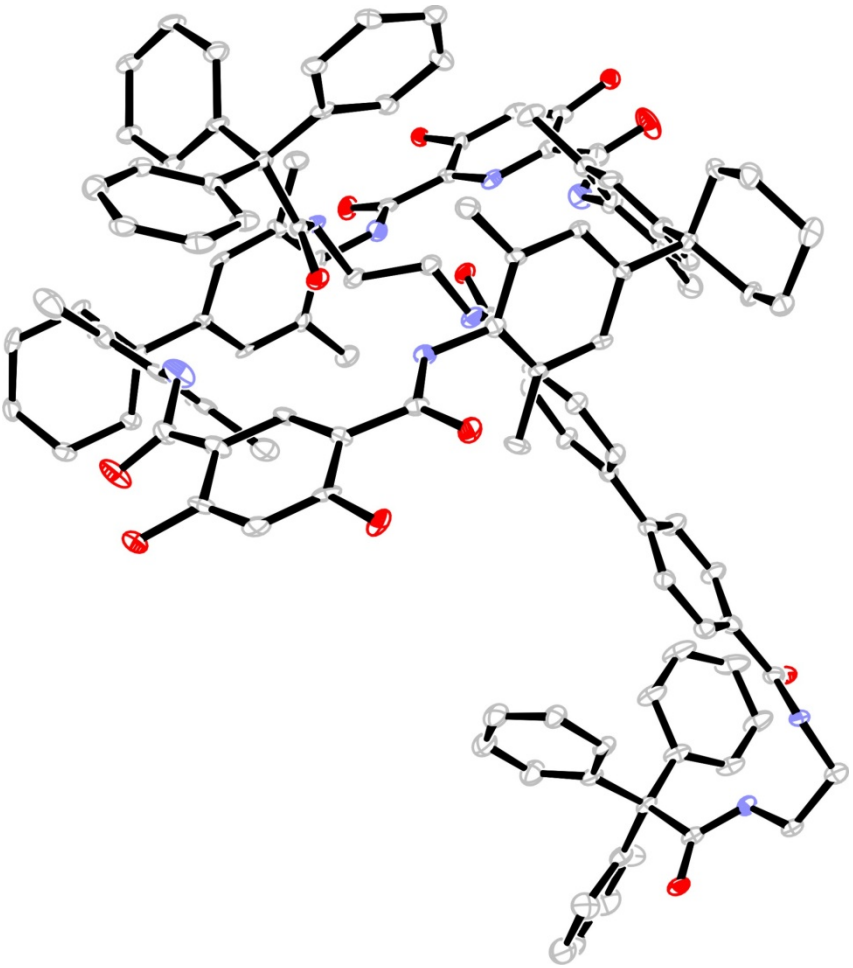

Figure 4.1.18 *Solid state structure of rotaxane* ***R4****. Solvent molecules (six chloroform molecules per asymmetric unit) as well as hydrogen atoms are omitted for clarity.*

The successful deprotection of rotaxane **R3** yielding rotaxane **R5** following the same experimental protocol can be verified by the same methods:

As described above for the transformation of **R2** to **R4**, the signal for the benzyl-CH_2 (δ = 5.2 ppm) is not observed in the ^{1}H NMR spectrum of **R5** (Figure 4.1.19 bottom). Together with the new signal for the macrocycle's free OH at δ = 12.0 ppm, this provides evidence for successful deprotection.

It should be noted that the shuttling movement is significantly slowed down in the deprotected rotaxane, as for **R5**, two separate sets of signals are observed for the two ethylene moieties in

the axle (δ = 2.06 ppm for the covered binding station and 3.56 & 3.69 ppm for the non-covered binding station), which is not observed for **R3**.

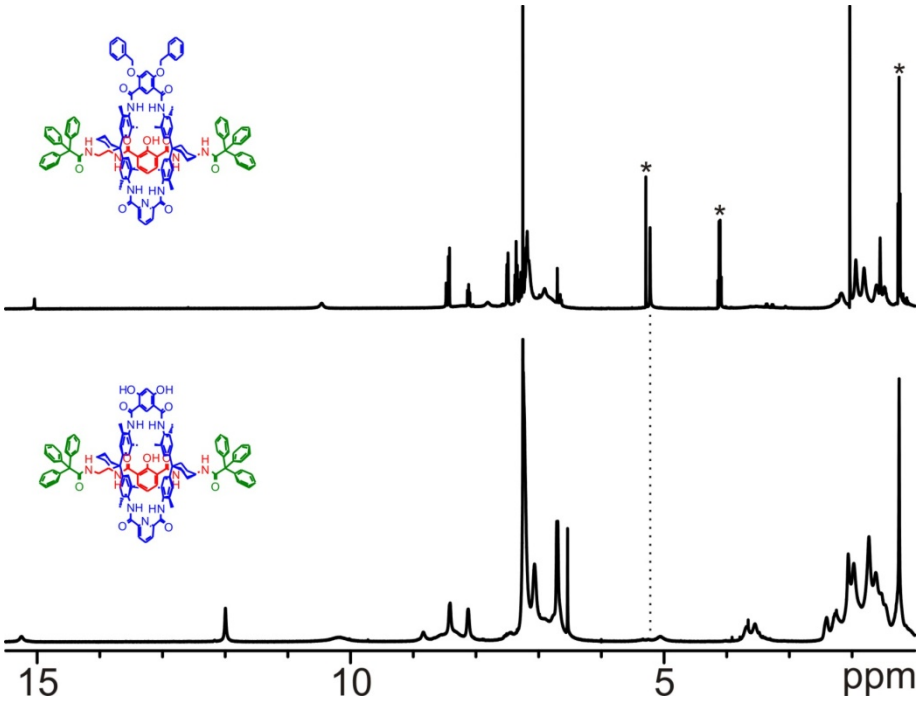

Figure 4.1.19 *Comparison of the ^{1}H NMR spectra of rotaxane **R3** (top) and the deprotected rotaxane **R5** obtained by catalytic hydrogenation of **R3** (bottom). The most evident sign for successful deprotection is disappearance of the signal for the benzyl-CH_2 protons (δ = 5.2 ppm) indicatd by a dotted line. The asterisks denote signals originating from small remains of ethyl acetate.*

The negative mode ESI-FTICR mass sprectrum of deprotected rotaxane **R5** shows the deprotonated rotaxane as the major peak (Figure 4.1.20 top) and additionally a very minor signal for a chloride adduct of the rotaxane**,** whereas no signal for benzyl protected rotaxane **R3** is observed.

Gas-phase isolation and fragmentation by irradiation with an IR laser break the macrocycle after what the deprotonated axle remains (Figure 4.1.20 middle and bottom) proving the interlocked structure of **R5**.

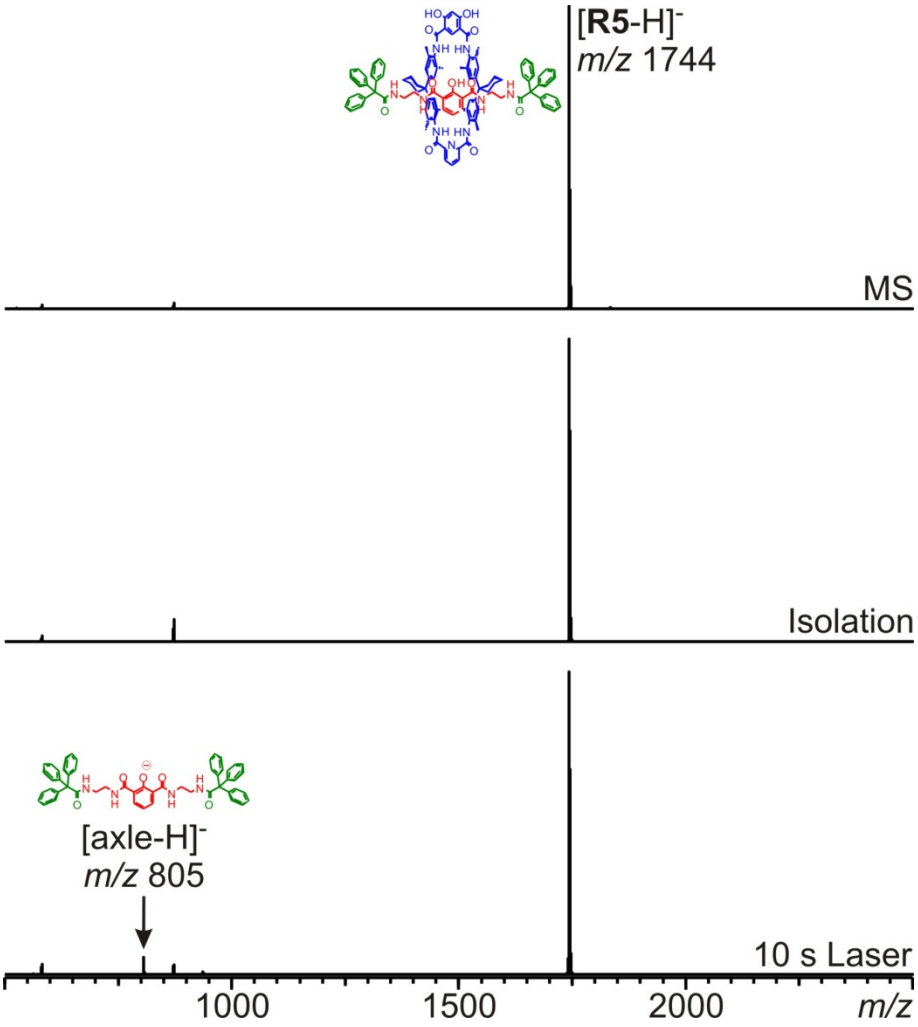

Figure 4.1.20 *Negative mode ESI mass spectrum of rotaxane* ***R5*** *(top), the spectrum after gas-phase isolation of the rotaxane (middle), and finally the spectrum after irradiation with an IR laser (bottom) showing the loss (and therefore also the disruption) of the macrocycle. The major peak in the original spectrum (*m/z *1744) corresponds to the deprotonated rotaxane.*

4.1.5 Analysis and Control of the Shuttling Dynamics in the Rotaxane Shuttles

Before the analysis and control of the shuttling dynamics in the rotaxane shuttles are dicussed, it should be considered, how deprotonation of the macrocycle's pheonolic OH groups influences its conformation.

The deprotonation of one OH group is expected to cause the amide proton to turn outwards of the macrocyclic cavity and forming a strong hydrogen bond to the phenolate.[70] Deprotonation of the second OH group is not expected to cause the second amide bond of the 4,6.dihydroxy isophthaloyl moiety to turn outwards, too, as this would cause a quite high ring strain. Rather, it should be questioned, whether only one amide N-H will be turned outwards (right illustration in Figure 4.1.21) or whether turning the first amide bond will cause the opposite one to turn otwards, too (left illustration in Figure 4.1.21). The density functional calculations discussed above (see chapter 4.1.1, Figure 4.1.1) suggest the "two-in-two-out" structure to be energetically more favorable than the "three-in-one-out" structure due to lower ring strain for a macrocycle without the pyridine nitrogen.[64] However, the strong NH•••N_{py} hydrogen bond (~25 kJ/mol) is expected to overcompensate the ring strain and lock the dipicoline amide in the syn conformation, which should therefore favor the "three-in-one-out" conformation.

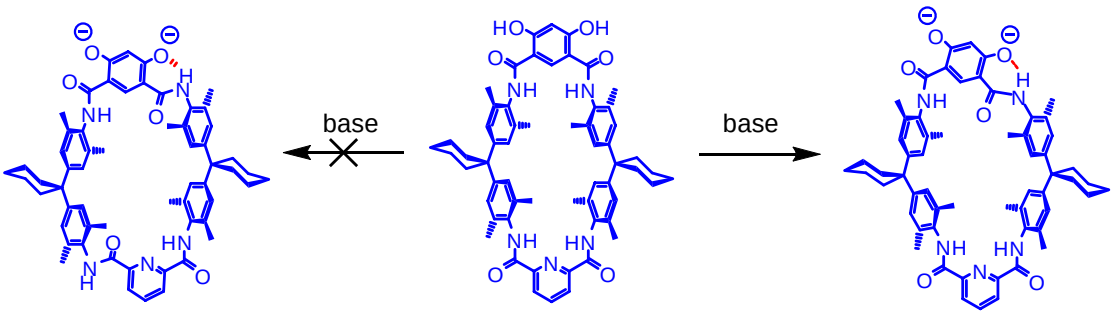

Figure 4.1.21 *Two possible alternatives for the conformation shift induced by deprotonation of the macrocycle's phenolic OH groups: Density functional calculations (see also Figure 4.1.1) suggest the "two-in-two-out" structure (left) to be energetically more favorable than the "three-in-one-out" structure (right) for a macrocycle without the pyridine nitrogen. However, the strong NH•••N_{py} hydrogen bond (~25 kJ/mol) should lock the dipicoline amide in the syn conformation and therefore favor the "three-in-one-out" conformation.*

The intramolecular dynamics of the degenerate shuttling motion of the macrocycle between the two ethylene diamide stations of the axle can be analyzed by different techniques in NMR

spectroscopy. For these investigations described in the following, the signals for the ethylene-CH_2 protons in the axle were employed, as they can be observed without severe overlap with other signals and furthermore since the macrocycle's shuttling motion causes the largest chemical shift difference for these protons between wheel-covered and non-covered shuttling position ($\Delta\delta \approx 1.5$ ppm).

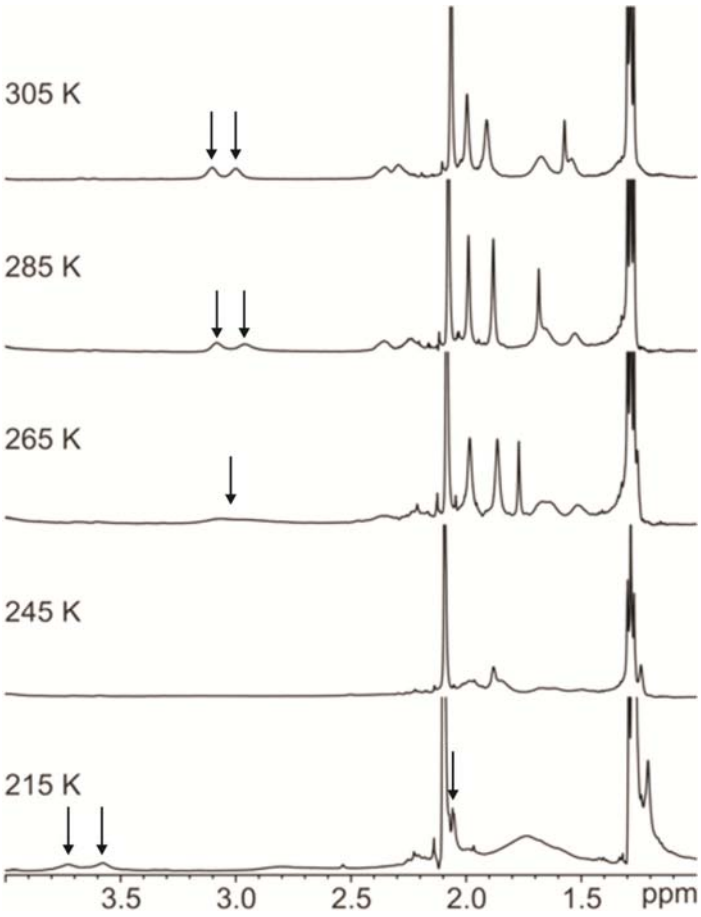

Figure 4.1.22 *High field region of several temperature dependent ^{1}H NMR spectra of rotaxane* ***R5****. From this experiment, one can obtain the shuttling rate at the coalescence temperature (T_c = 250 ± 5 K) as well as the energetic barrier of the shuttling motion. The signals for the axle's ethylene-CH_2 protons split into two sets of signals at 215 K (averaged signals at approx. 3.0 ppm; free axle site at approx. 3.6 ppm, axle site covered by the macrocycle at approx. 2 ppm overlayed by other signals; both sets of signals are indicated by vertical arrows).*

Temperature-dependent ^{1}H NMR spectra of rotaxane **R5** show the signals for the axle's ethylene-CH_2 protons to split into two sets of signals at low temperature (Figure 4.1.22). At 215 K, instead of the averaged signals at approx. 3.0 ppm, the signals for the free axle site appear at approx. 3.6 ppm, whereas the signal for the axle site covered by the macrocycle

appears at approx. 2 ppm. In the latter case, the two signals collapse into one, which is overlayed by other signals, e.g. the CH_3 signal of an ethyl acetate impurity. However, the unambiguous indentity and exact location of these signals could be confirmed by EXSY experiments as described later in this chapter.

From these temperature dependent experiments, it is possible to determine the shuttling rate at the coalescence tempereature of $T_c = 250 \pm 5$ K. At the coalescence tempereature, the shuttling rate can be approximated as

$$k \approx \frac{\pi}{\sqrt{2}} |\delta(uncovered\ axle\ side) - \delta(covered\ axle\ side)| \qquad [4.1]$$

with the δ values given in Hz.[71] This approximation gives for rotaxane **R5** a shuttling rate of $k \approx 1584\ s^{-1}$ at T = 250 ± 5 K in $CDCl_3$.
According to the Eyring equation (equation [4.2]),[71]

$$k = \frac{k_B T}{h} e^{-\frac{\Delta G^{\ddagger}}{RT}} \qquad [4.2]$$

this allows the calculation of the energetic barrier for the shuttling motion:

$$\Delta G^{\ddagger} = -RT\ ln\frac{kh}{k_B T} \qquad [4.3]$$

For rotaxane **R5**, one gets

$$\Delta G^{\ddagger} = 45.5 \pm 1.2\ kJ/mol$$

The influence of a change of the pH value and therefore deprotonation of the macrocycle inducing a conformation shift on the shuttling rate k can be determined by two-dimensional NMR exchange spectroscopy (EXSY).[72]

In contrast to the temperature dependent approach, which only gives the rate at the coalescence temperature, EXSY experiments allow the determination of the shuttling rate for protonated and deprotonated rotaxane at the same temperature given the shuttling motion is slow as compared to the NMR timescale at this temperature. From the mixing time (t_m) and the intensities of the diagonal and the cross peaks (I_D and I_C), the shuttling rate (k) can be determined according to equation [4.4]:[73]

$$k \approx \frac{1}{t_m\left(\frac{I_D}{I_C+1}\right)} \qquad [4.4]$$

For rotaxane **R5**, the EXSY experiments were performed at a temperature of 215 K, whereas for rotaxane **R4**, a temperature of 225 K was sufficient to obtain separated signal sets for the two different sides of the axle (ethylene-CH_2 covered and non-covered by macrocycle). In both cases, a mixing time of 10 ms was applied. For **R4**, the rates were determined by 2D-EXSY experiments, whereas for **R5**, the rate was obtained from more easy to evaluate 1D-GOESY measurements.

In both cases, the conformational switch of the macrocycle was induced by adding an appropriate amount of P1 base through an Eppendorf pipette. The exact rotaxane/P1 base ratio was determined from the integrals in the corresponding 1H NMR spectra and was found to be 6 eq. P1 base for **R4** and 9 eq. P1 base for **R5** resulting in 3 equivalents of P1 base per OH group for both rotaxanes. This can be attributed to the rather inaccurate measureability of extremely small volumes with Eppendorf pipettes. Therefore, it should be noted that the 3 eq. of P1 base added per OH group might additionally deprotonate the axle's amides, which could influence the shuttling rate. However, the comparison of the ^{1}H NMR spectra of rotaxane **R4** with and without P1 base clearly shows this not to be the case (Figure 4.1.23). Although the resolution of the correspondent spectrum of the deprotonated rotaxane **R5** is too low to unambiguously verify this for **R5**, one may assume the axle's amides not to be deprotonated in **R5** either.

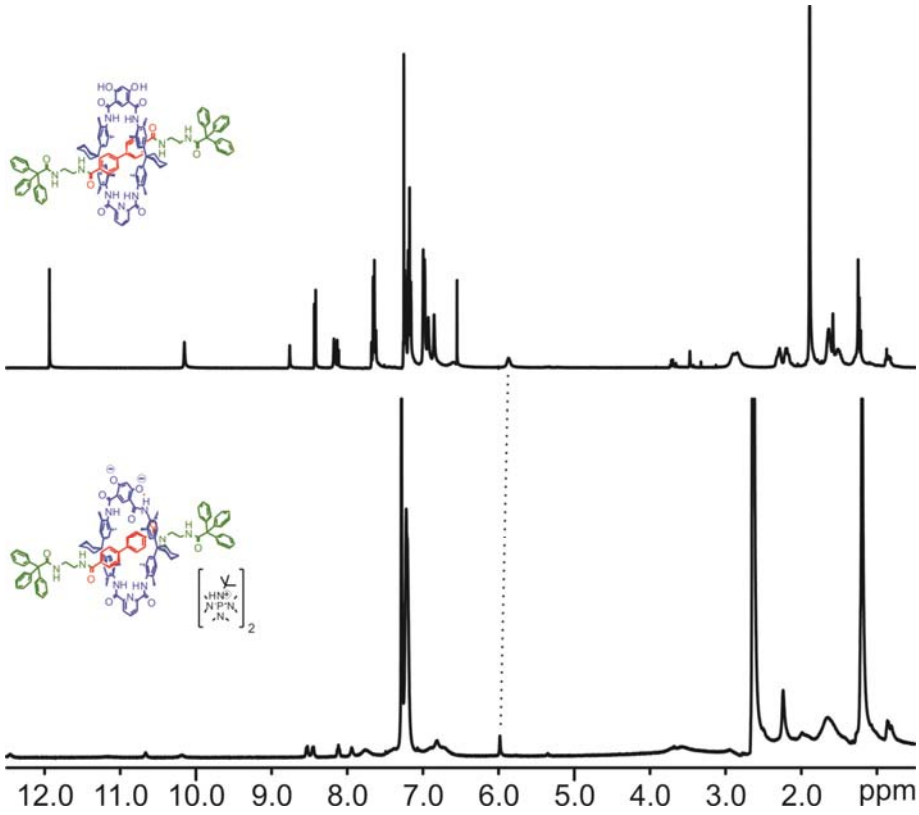

Figure 4.1.23 *Comparison of the ^{1}H NMR spectra of rotaxane* ***R4*** *(top) and the deprotonated rotaxane* ***R4*** *(bottom) – both recorded in $CDCl_3$. The dotted line indicates the axle's amides not to be deprotonated by the excess P1 base.*

In case of **R4**, the shuttling rate is slowed down from 27.5 s^{-1} to 14.6 s^{-1} upon deprotonation (Figure 4.1.24 top) corresponding to a raise of the energetic barrier from 48.8 kJ/mol to 49.6 kJ/mol.

In case of **R5**, the shuttling rate is accelerated from 6.5 s^{-1} to 16.9 s^{-1} upon deprotonation (Figure 4.1.24 bottom), which corresponds to a lowering of the energetic barrier from 48.7 kJ/mol to 47.0 kJ/mol.

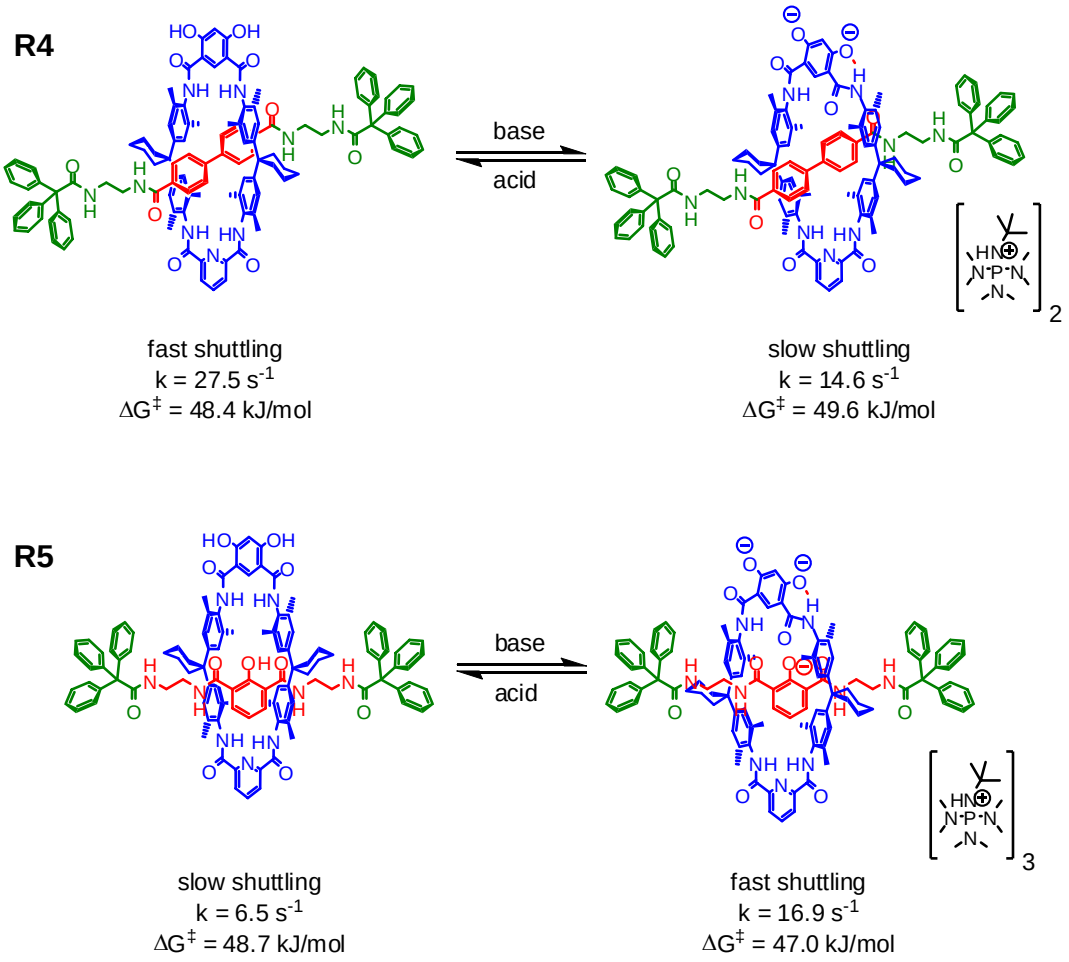

Figure 4.1.24 *Influence of deprotonation-induced conformation shift in the macrocycle on the shuttling rate of rotaxanes* ***R4*** *and* ***R5****: The shuttling motion in* ***R4*** *(determined at 225 K) is slowed down by deprotonation, whereas the shuttling in* ***R5*** *(determined at 215 K) is accelerated by deprotonation.*

These very surprising results indicate that two different effects have to be taken into account to explain the observed effects:

The density functional calculations discussed in chapter 4.1.1 (Figure 4.1.1) as well as a close analysis of the crystal structure of a related tetralactam macrocycle in the "3-in-1-out" conformation[74] show that the deprotonation-induced conformation shift leads to a significant contraction of the macrocyclic cavity. So the reduction of the shuttling rate in rotaxane **R4** upon deprotonation-induced macrocycle contraction can be explained by steric reasons: due to the smaller cavity, it is harder for the macrocycle to slip along the axle from one ethylene diamide binding station to the other one, which finally results in a lower rate.

Obviously, the acceleration of the shuttling rate for rotaxane **R5** must be caused by a different effect. From previous studies with a similar rotaxane consisting of the same axle and a non-switchable macrocycle[23] (see chapter 3.1.3.3), it is known that deprotonation of the axle's phenol group leads to a reduction of the shuttling rate, because the P1 cation acts as a brake for the shuttling motion of the macrocycle by forming a strong ion pair with the phenolate in the axle. This effect is stronger, the less polar the solvent is, so it should also take place in the case of **R5**. However, the expected reduction of the shuttling rate is not observed here.
The cation brake scenario might be ruled out by invoking coordination of the P1 cations to the phenolates of the macrocycle rather than to the axle. Still, the shuttling rate is expected to be lower in the deprotonated state due to the macrocycle contraction as suggested for **R4**. However, the switched macrocycle as shown in Figure 4.1.21 with only three amide N-H protons pointing inwards the macrocyclic cavity forms fewer hydrogen bods to the axle's phenolate, which has to be passed during the movement of the macrocycle from one ethylene diamide station to the other one. Consequently, turning one amide N-H bond outwards of the macrocyclic cavity lowers the barrier for the suttling motion, overcomes the rate-reducing effect of the macrocycle contraction and finally leads to an acceleration of the shuttling rate.

From the analysis of the two rotaxane-based molecular shuttles **R4** and **R5**, one could learn that the shuttling rate can be controlled by two different effects, which are both triggered by deprotonation of the 4,6-dihydroxy isophthaloyl moiety in the macrocycle (Figure 4.1.25):
a) In rotaxane **R4** with a long biphenyl spacer in the middle of the axle, the shuttling rate is mostly controlled by steric effects. Deprotonation of the macrocycle leads to contraction of the macrocyclic cavity, which causes a reduction of the shuttling rate.
b) In rotaxane **R5** with a shorter phenol spacer in the middle of the axle, the shuttling rate depends more on the strength of the hydrogen-bonding interactions between macrocycle and axle phenol/phenolate. In the deprotonated case, the macrocycle is able to form only three hydrogen bonds towards the axle, which therefore simplifies it to slip over the central phenolate in the axle. Consequently, deprotonation increases the shuttling rate in rotaxane **R5**.

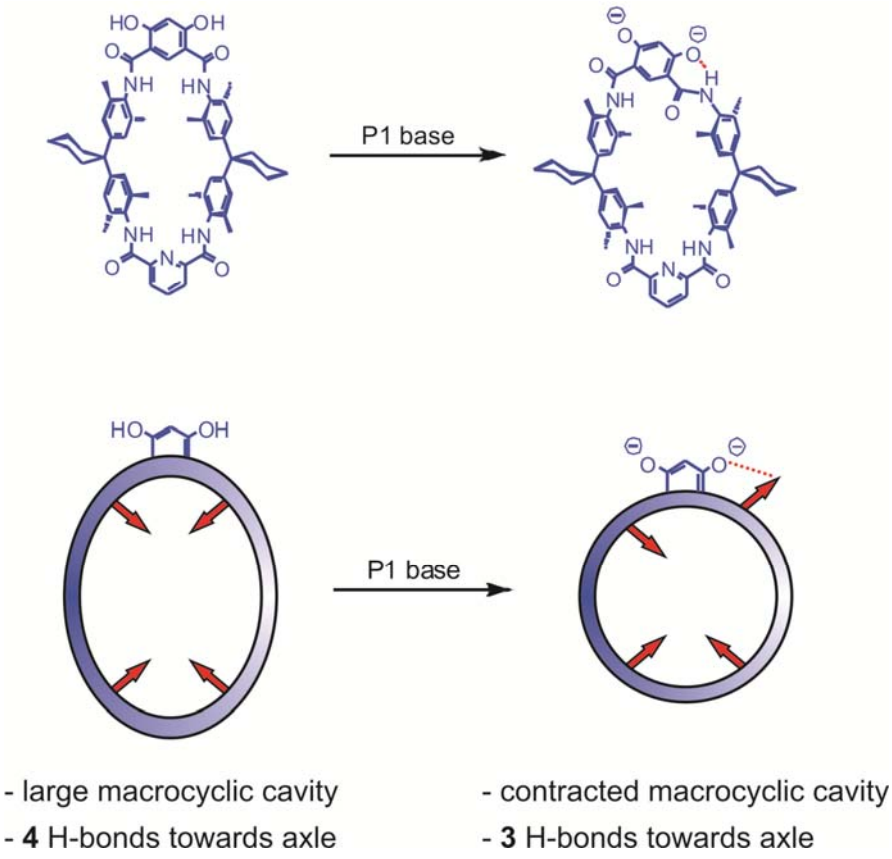

Figure 4.1.25 *Schematic illustration of the effects caused by deprotonation of the 4,6-dihydroxy isophthaloyl moiety in the macrocycle of rotaxanes* ***R4*** *and* ***R5****: a) contraction of the macrocyclic cavity, which causes a reduction of the shuttling rate in* ***R4*** *and b) one of the four amide N-H bonds is turned outwards of the macrocyclic cavity, which causes an acceleration of the shuttling rate in* ***R5****. The nature of the axle – particularly the nature of the spacer between the two ethylene diamide stations – determines which one of these two effects is predominant.*

4.1.6 Fluocescence Properties of the Rotaxane Shuttles R3 and R5

The rotaxanes **R3** and **R5** do not only work as pH-controllable molecular shuttles, but also show very interesting light absorbtion and emission properties: Both rotaxanes – the benzyl-protected **R3** as well as the deprotected **R5** – emit at a wavelength of $\lambda = 433$ nm when irradiated at their absorbance maximum, which lies at $\lambda = 317$ nm for **R3** and at $\lambda = 313$ nm for **R5**.

This behavior is rather surprising, as very similar rotaxanes do not show fluorescence (see Figure 4.1.26). Substituting the phenol spacer in the axle by a 4,4'-biphenyl moiety gives non-fluorescent rotaxanes, as well as replacing the macrocycle by different ones that have been prepared and examined in earlier studies on molecular shuttles.

This indicates the fluorescent properties to be caused by an interaction of the phenol spacer in the axle with the 4,6-dihydroxy isophthaloyl moiety in the macrocycle. One might imagine a kind of charge transfer complex as observed for the 1,4-benzoquinone/hydroquinone complex.

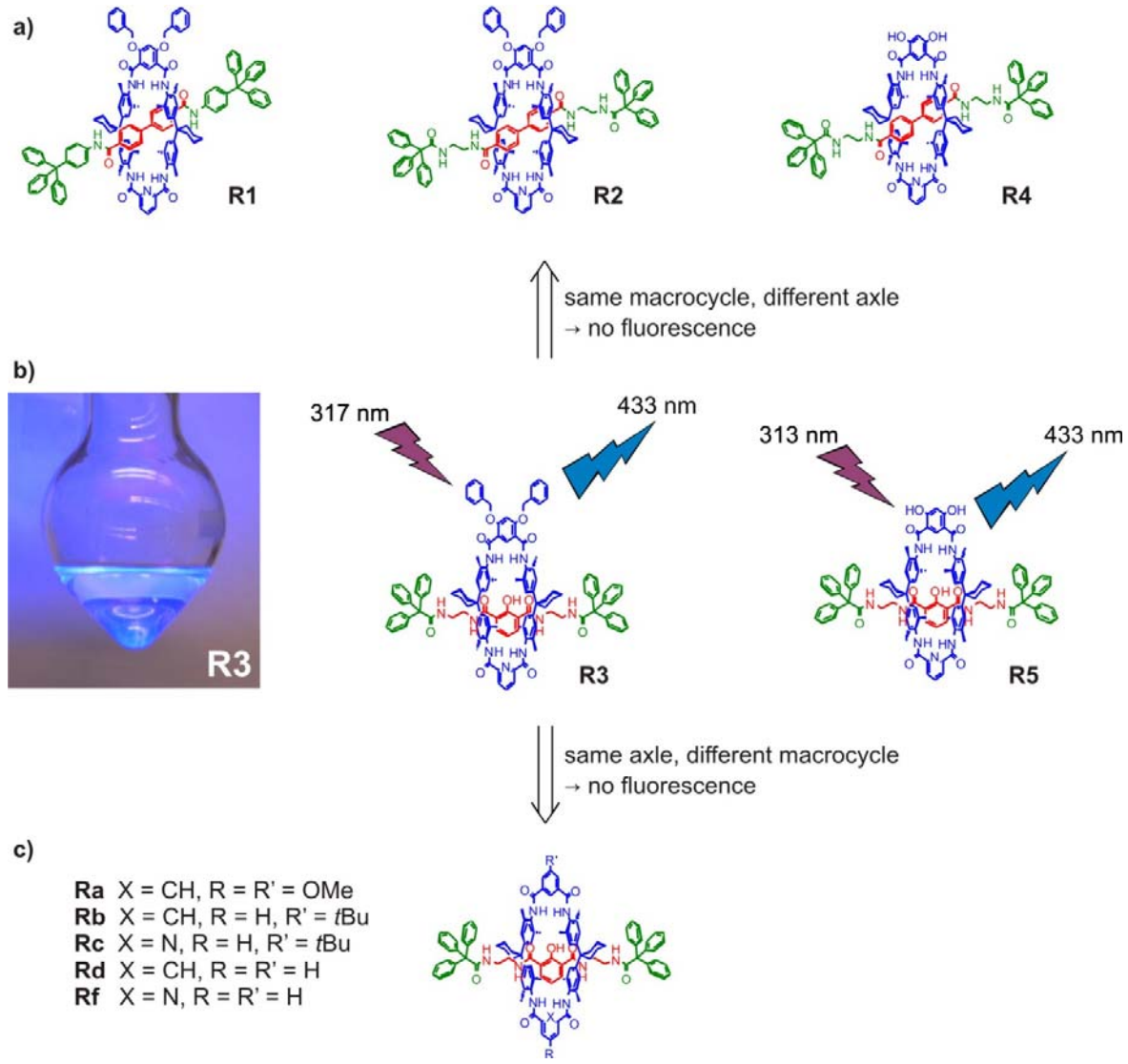

Figure 4.1.26 *Schematic illustration of the light-absorbing and emitting properties of the molecular shuttle rotaxanes* ***R3*** *and* ***R5****. The photography shows a solution of* ***R3*** *in chloroform irradiated with UV light (λ = 336 nm). The photography of an* ***R5*** *solution is not shown, as it looks exactly the same. As shown in* ***a)*** *and* ***c)****, exclusively this combination of macrocycle and axle results in the formation of a fluorescent rotaxane. This indicates the fluorescent properties to be related to the combination of the phenol spacer in the axle with the 4,6-dihydroxy isophthaloyl moiety in the macrocycle.*

4.1.7 Conclusion

In conclusion, the evaluation of several different ways for the synthesis of a bistationary switchable [2]rotaxane-based molecular shuttle finally resulted in a three-component reaction combining an amine-terminated stopper with one incorporated amide for templation, a dicarbonyl chloride center piece, and a conformation-switchable tetralactam macrocycle. The second amide of both diamide stations in the axle is formed through the stoppering reaction. Furthermore, attaching the ethylene diamine spacer to the stopper instead of the center piece keeps all components of the axle in all preliminary steps well soluble and easy to isolate in high yields.

The desired switchability of the tetralactam macrocycle is achieved by substitution of one of the isophthaloyl moieties with hydroxyl groups in position 4 and 6, whereas sufficient solubility of the macrocycle in non-polar solvents is provided by large benzyl protective groups that can be cleaved easily after rotaxane formation.
In the first switchable rotaxane **R4**, deprotonation of the macrocycle's OH groups leads to a contraction of the macrocycle caused by one of the macrocycle's amide protons to coordinate to the isophthaloyl-O^- resulting in a decrease of the shuttling rate, because the contracted inner cavity of the macrocycle obstructs it to slip over the central biphenyl spacer between the two diamide stations.

In the second switchable rotaxane **R5** – prepared according to a well-known anion template[22,23] – another effect influences the shuttling rate: Upon deprotonation and switching of the macrocycle's conformation – from "all in" regarding the amide protons towards "3-in-1-out" – leads to an increase of the shuttling rate. In this case, the contraction of the macrocycle is not the dominant process. The shuttling rate is rather determined by the strength of the interactions between the macrocycle and the phenol spacer in the middle of the axle. Obviously, this interaction should become stronger, if the phenol is deprotonated. However, the fact that one of the amide protons is turned outwards of the macrocyclic cavity and consequently only the three other amide protons are able to interact with the axle's central phenolate leads to an increase of the shuttling rate.

Overall, two molecular shuttle rotaxanes could be prepared based on the same tetralactam macrocycle with integrated pH-controllable conformation switchability. Depending on the nature of the axle, the same external trigger – namely change of the pH from neutral towards strongly basic – influences the shuttling rate in two completely opposing ways due to two different effects that are caused by the switching – either the contraction of the macrocycle or the partial "switching off" of the interactions between macrocycle and axle.

4.2 Influence of Alkoxy-Substitution of the Isophthalic Acid Moiety on Macrocycle Formation – Tetra- vs. Octalactam Macrocyle

As already mentioned in chapter 4.1.1, the reaction of the 4,6-dimethoxy-extended diamine building block (N^1,N^3-bis(4-(1-(4-amino-3,5-dimethylphenyl)cyclohexyl)-2,6-dimethyl-phenyl)-4,6-dimethoxyisophthal-amide) with 4,6-dimethoxy-isophthaloyl dichloride does not result in the formation of the expected tetralactam macrocycle. Instead, a mixture of octalactam macrocycle and octalactam catenane is obtained (Figure 4.2.1).[75-80]

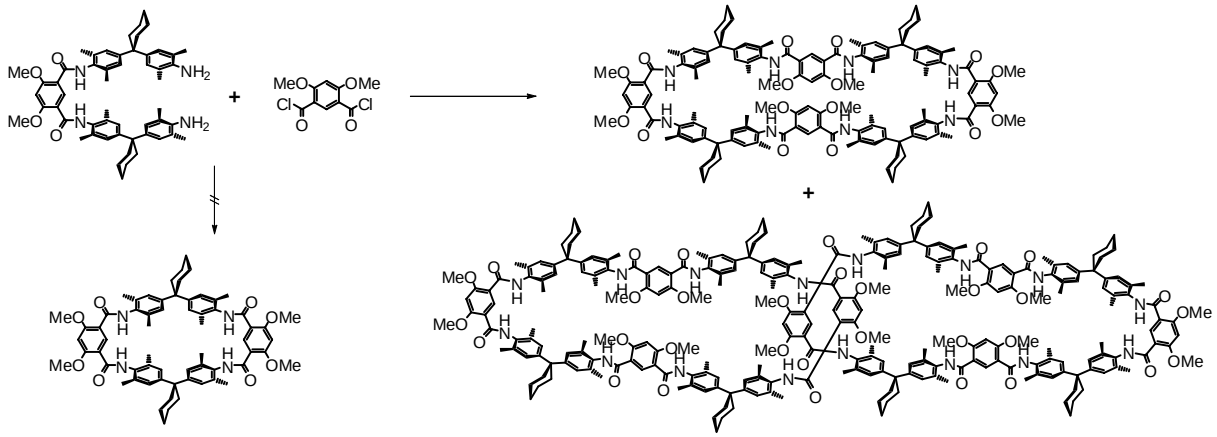

Figure 4.2.1 *Preparation of octa-methoxy-substituted octalactam macrocycle and the corresponding catenane.*

A separation of octalactam macrocycle and octalactam catenane was not possible due to the poor solubility in non-polar solvents, which caused both products either to stick to the column material in case of less polar eluents or to elute in the same fraction in case of more polar eluents, regardless of whether standard column chromatography or high performance liquid chromatography (HPLC) was applied.

However, the identidy of the products in the mixture could be ensured by the combination of NMR spectroscopy and mass spectrometry: While the ^{1}H NMR spectrum only shows signals that could be interpreted as tetralactam macrocycle, octalactam macrocycle or octalactam catenane, the ESI-FTICR mass spectrum indicates the presence of two species with the mass of two and four times the mass of a tetralactam macrocycle, respectively. Tandem-MS experiments then revealed the structure of octalactam macrocycle and di-octalactam catenane.

This obviously very different macrocyclization behaviour as compared to differently substituted isophthaloyl units might be explained by a preferred “anti”-orientation of the two diamine subunits in the extended diamine building blocks due to intramolecular hydrogen bonding (see Figure 4.2.2) which would obstruct the formation of the smaller tetralactam macrocycle.

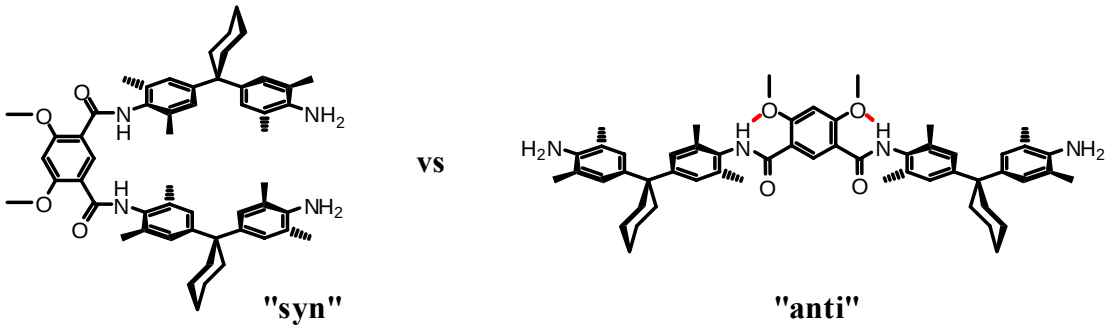

Figure 4.2.2 *Probable stabilization of “anti”-orientation in the 4,6-di-OMe-extended diamine building block by intramolecular hydrogen bonding.*

The preferred formation of larger macrocycles has been observed earlier in case of a terephthaloyl spacer in the extended diamine building block instead of an isophthaloyl spacer.[81] Whereas in the terephthaloyl case, mostly steric reasons favor the octalactam over the tetralactam macrocycle, here, an intramolecular template effect preorganizes the 4,6-di-OMe-extended diamine building block in a way that only allows for the formation of the octalactam macrocycle.

To overcome this effect, the addition of lithium ions (as LiOTf) to the solution during cyclization was regarded as an appropriate way to fix the “syn”-orientation of the extended diamine by coordination of the Li^+ cation to one methoxy- and one carbonyl group (Figure 4.2.3a). Unfortunately, this did not affect the reaction at all and again only the octalactam macrocycle and the corresponding catenane (Figure 4.2.1) were formed.

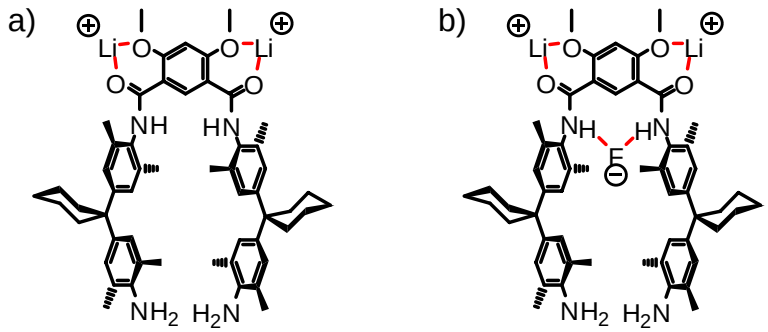

Figure 4.2.3 *Proposed stabilization of "syn"-orientation in the di-OMe-extended diamine building block by (a) cationic and (b) proposed combined cationic-anionic template.*

A further improvement of this strategy could involve the usage of LiF (or other halogen) to generate a combined cationic-anionic template to fix the "syn"-orientation of the extended diamine building block at two different positions (Figure 4.2.3b), as it is known that Hunter-type tetralactam macrocycles bind halogenides in dichloromethane solution (e.g. the binding constant for fluoride is $k_a(F^-) = 200\ M^{-1}$).[82]

However, also the addition of Li^+ and F^- to the macrocyclization reaction did not change the result and again, the mixture of octalactam macrocycle and the corresponding catenane was formed.

Due to these problems – low solubility and the formation of octalactam instead of tetralactam macrocycles – the symmetric synthetic approach with methoxy groups in position 4 and 6 on the extended diamine building block as well as on the isophthaloyl dichloride was abandoned.

Therefore, the synthetic route was simplified by reducing the number of methoxy groups to one (Figure 4.2.4). This tetralactam macrocycle would still allow – after deprotection – to switch at least *one* of the amide bonds in the macrocycle for an application in a molecular shuttle rotaxane (see chapter 4.1).

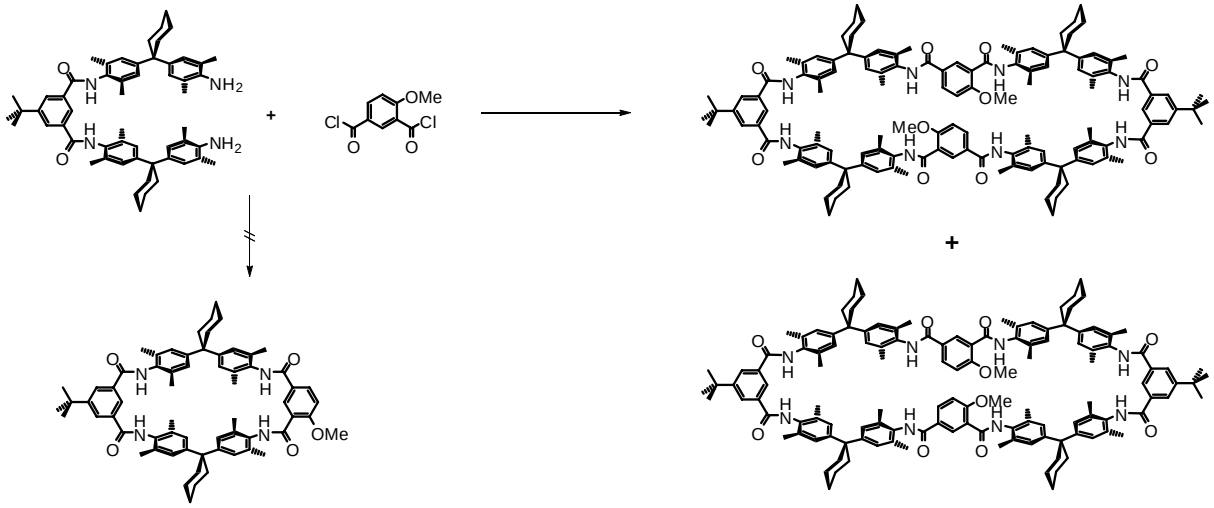

Figure 4.2.4 *The reaction of the 5-^{t}Bu-extended diamine building block with 4-methoxy-isophthaloyl dichloride does not result in the formation of the corresponding tetralactam macrocycle; instead, two isomers of di-OMe-di-^{t}Bu-substituted octalactam macrocycle are formed as the only macrocyclization products with a combined yield of 4 %.*

However, also this approach did not result in formation of a mono-methoxy substituted tetralactam macrocycle, but rather in the formation of a compound with an extremely crowded ^{1}H NMR spectrum similar to the expected one, but just showing way too many signals, especially in the aromatic region (Figure 4.2.5). The possible formation of two different isomers of the octalactam macrocycle might explain this observation.

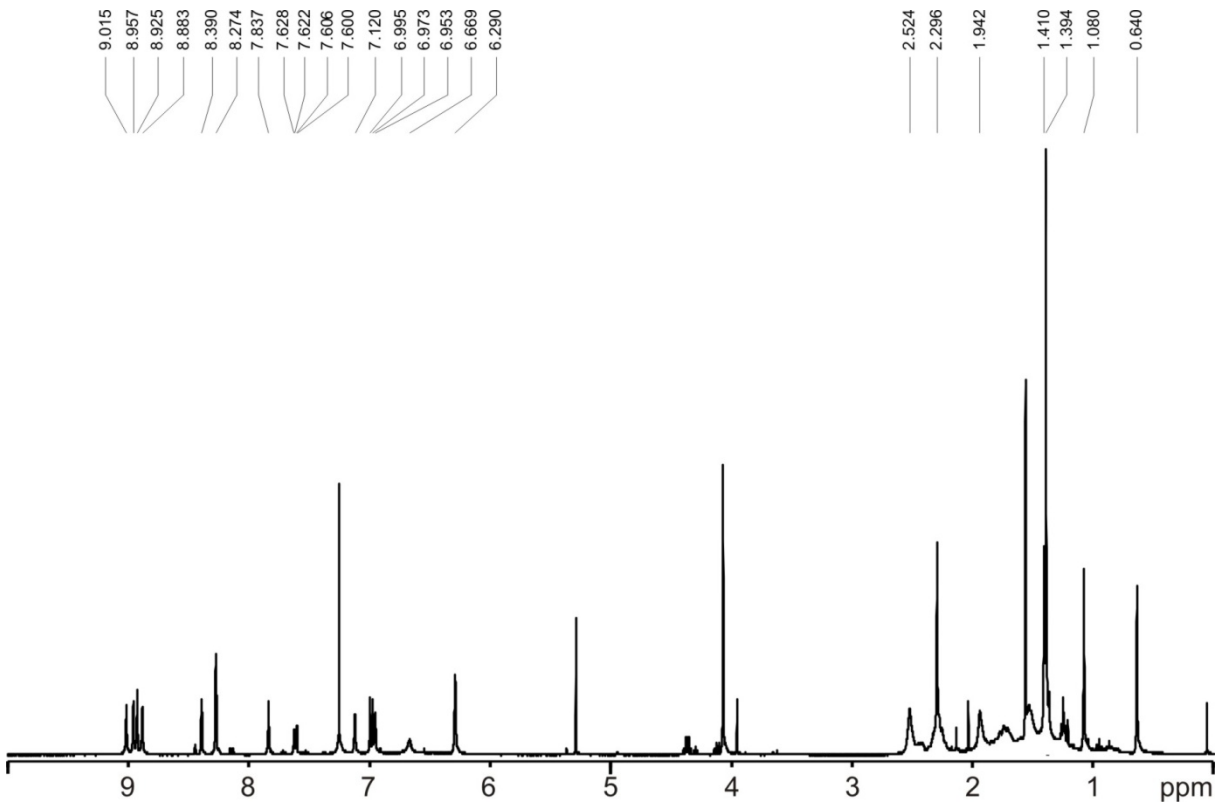

Figure 4.2.5 *^{1}H NMR spectrum of the product obtained from the reaction of the 5-^{t}Bu-extended diamine building block with 4-methoxy isophthaloyl dichloride.*

Finally, ESI-FTICR mass spectrometry and laser induced fragmentation experiments (Figure 4.2.6) suggest formation of an octalactam macrocycle, because the observed unsymmetric fragmentation into two fragments with different *m/z* ($992^{2+} \rightarrow 974^{+} + 1010^{+}$) would not be expected for a catenated structure. The additional peak at *m/z* 983^{2+} can be attributed to the loss of one water molecule from the parent ion, which is very common among this kind of macrocycles.

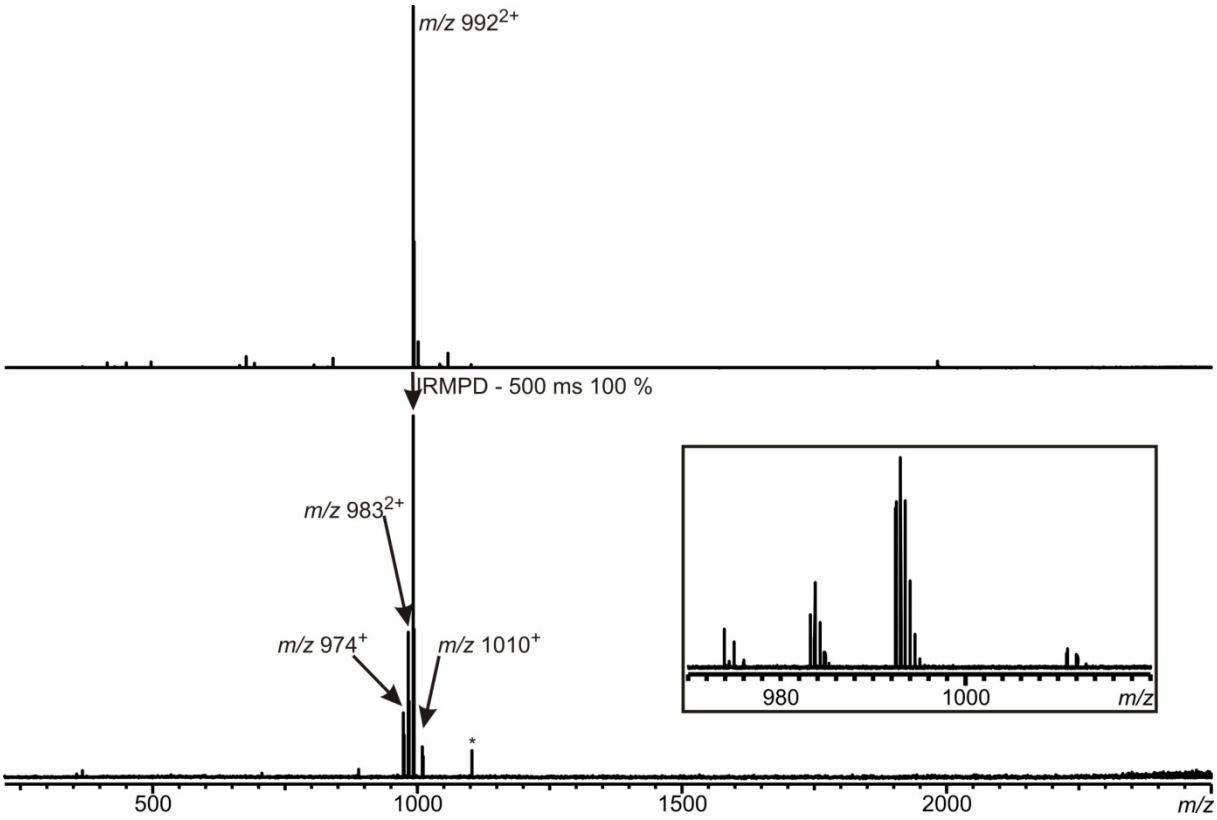

Figure 4.2.6 *ESI-FTICR mass spectrum and laser-induced fragmentation of di-methoxy-di-^{t}Bu-substituted octalactam macrocycle. The asterisk denotes a signal originating from stray radiation.*

The fragments at *m/z* 974^+ and *m/z* 1010^+ are corresponding fragments: After ring opening of the doubly protonated octalactam macrocycle releasing an amine and an acylium ion, the free amine attacks one of the carbonyl groups at the central isophthaloyl moiety forming one closed and one open-chain tetralactam macrocycle. The the next step is a tautomeric rearrangement, which involves the transfer of on water molecule to the acylium ion. This is followed by proton transfer from the closed macrocyclic part to the open part and cleavage of the C-N bond between these two parts releasing two fragments with *m/z* values corresponding to those observed in the mass spectrum after laser-induced fragmentation (*m/z* 974^+ and *m/z* 1010^+). The first one is a nitrilium analogue of a tetralactam macrocycle, which lost one water molecule. The second one is a related open-chained structure terminated by one protonated carboxylic acid and one amine, which would finally undergo a proton transfer to the free amine (Figure 4.1.8). This fragementation pathway would also be applicable for the other isomer of this macrocycle.

The fragementation processes described above have been observed previously during the examination of the fragementation patterns of oligolactam macrocyles and catenanes.[83] Also

the loss of up to four water molecules from one tetralactam macrocycle has been observed before.

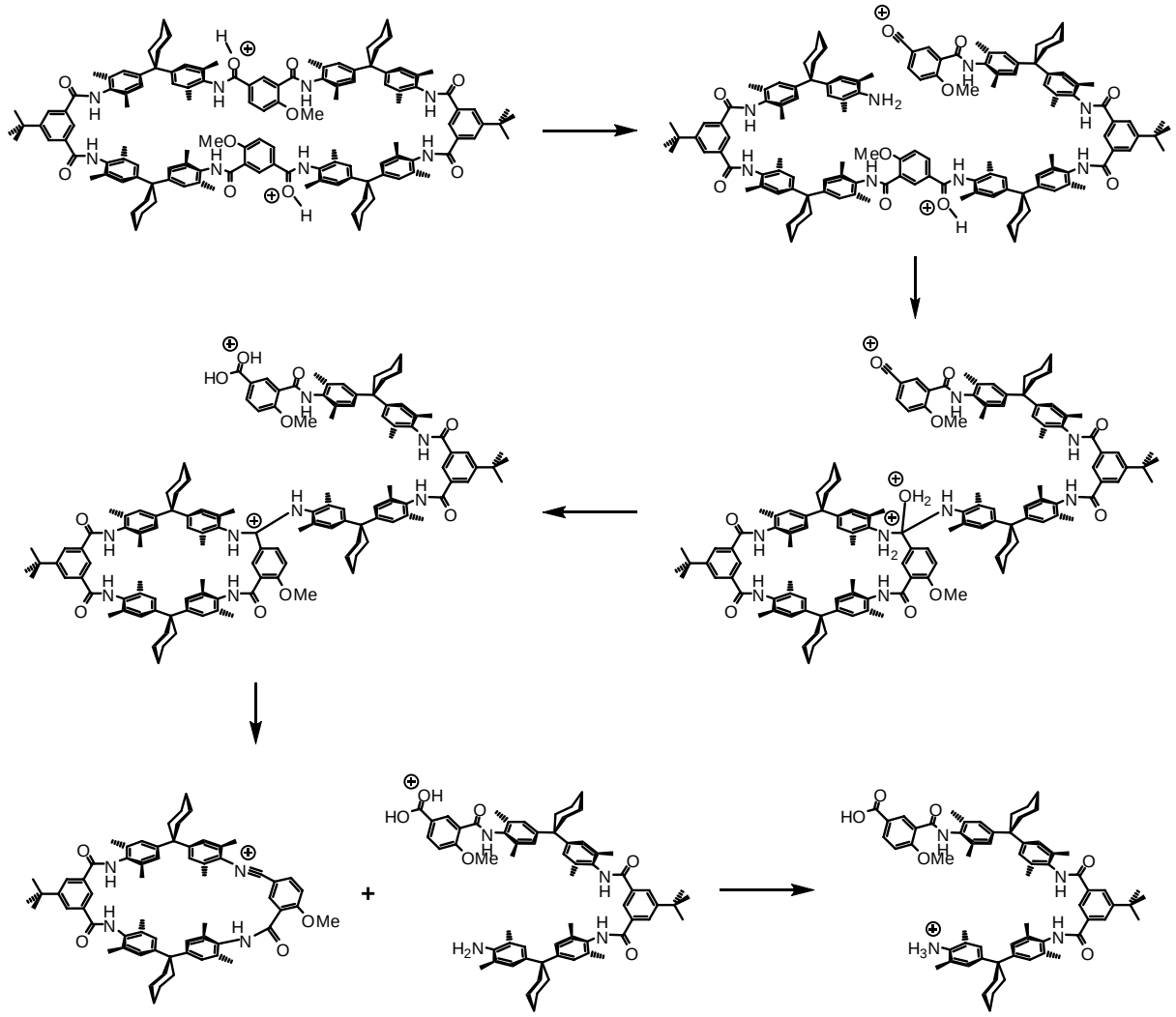

Figure 4.2.7 *Suggested structures of the fragments of the di-methoxy-di-^{t}Bu-substituted octalactam macrocycle according to the MS^2 experiment shown in Figure 4.2.6: after ring opening of the doubly protonated octalactam macrocycle, the macrocycle breaks between amide-N and one of the m-xylylene rings in radical process. The displayed fragmentation pathway also fits for the second possible isomer.*

It should also be noted that the similar reaction of the 4-OMe-extended diamine building block with 5-tert-butyl-isophthaloyl dichloride does not result in the formation of the octalactam macrocycle described above but rather in uncontrolled polymerization.

After the previous attempts to prepare and successfully isolate a multiply substituted octalactam macrocycle failed, the influence of the benzyl protecting group for the hydroxyl functions was examined.

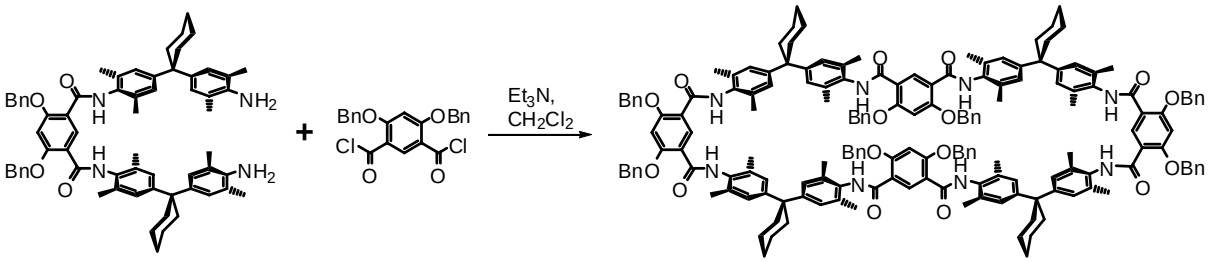

Figure 4.2.8 *Preparation of an octa-benzyloxy-substituted octalactam macrocycle.*

The synthetic pathway towards oligolactam macrocycles with 4,6-dibenzyloxy-substituted isophthaloyl moieties follows in close analogy the pathway described above for the methoxy-substituted macrocycles (Figure 4.2.1): Tetra-benzylation of 4,6-dihydroxyisophthalic acid is followed by selective deprotection of the carboxyl groups and conversion to the acid dichloride. Reaction of the acid chloride with diamine 4,4'-(cyclohexane-1,1-diyl)bis(2,6-dimethylaniline) gives the corresponding di-benzyloxy substituted extended diamine building block (di-Bn-EDA). The macrocyclization reaction of di-OBn-extended diamine building block with 4,6-dibenzyloxy-isophthaloyl dichloride finally results in the selective formation of the well soluble octalactam macrocycle, whereupon neither tetralactam macrocycle nor di-octalactam catenane are observed (Figure 4.2.8).

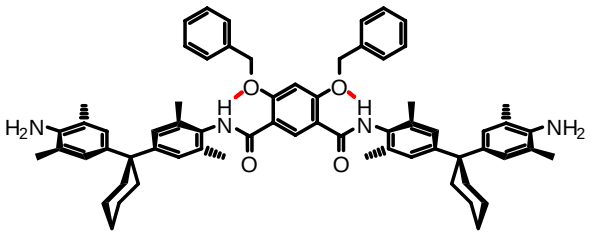

Figure 4.2.9 *Preferred conformation ("anti") of the di-benzyloxy-substituted extended diamine building block determined by intramolecular hydrogen bonding.*

The selective formation of the octalactam macrocycle is most probably caused by intramolecular hydrogen bonds forcing the di-benzyloxy-substituted extended diamine

building block to adopt a conformation, which does not allow the formation of the tetralactam macrocycle (Figure 4.2.9). The formation of a di-octalactam catenane might be suppressed because of the steric demand of the benzyl groups preventing the macrocycle precursor to thread through the other macrocycle.

As already discussed in chapter 4.1.1, the use of an extended diamine building block with pyridine-2,6-dicarbonyl moiety in a macrocyclization reaction with either 4-methoxy-isophthaloyl dichloride or 4,6-dibenzyloxy-isophthaloyl dichloride leads to the preferable formation of the tetra- and not the octalactam macrocycle (Figure 4.1.5). Apparently, the hydrogen bonding interactions between pyridine nitrogen and the amide protons help to overcompensate the template effect of the N-H•••O-R hydrogen bridge (Figure 4.2.10).

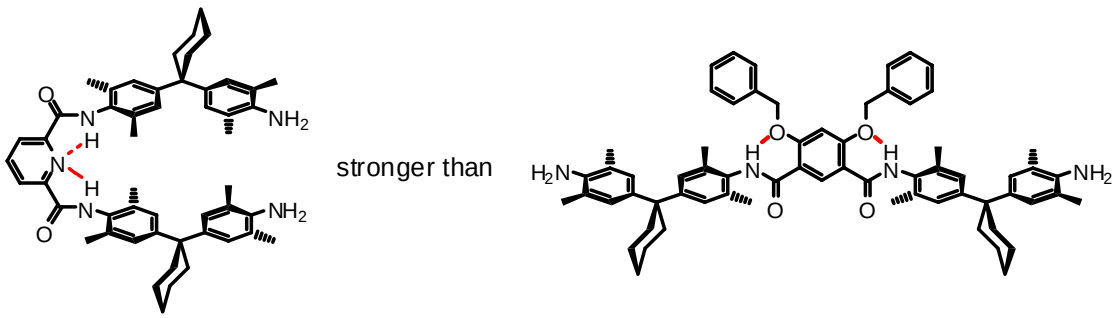

Figure 4.2.10 *Comparison of different intramolecular hydrogen bonding patterns templating the preorganization of the extended diamine building block prior to macrocyclization.*

Study of the conformation of the $(OBn)_8$-octalactam macrocycle – is it possible through NOESY NMR?

The ^1H NOESY spectrum of the octa-benzyloxy substituted octalactam macrocycle (Figure 4.2.11) does unfortunately not give too much information about the macrocycle's conformation. All cross peaks reasonably fit to the octalactam structure, but do not give any information about the spatial orientation. For example, a coupling between amide proton and isophthal-H2 can be observed. This is a hint that the amide protons preferably point inwards the macrocyclic cavity.

A detailed analysis of the conformation is not possible, as the amide protons cannot even be distinguished from each other in low temperature NMR experiments, at least not at the lowest temperature possible with the applied spectrometer (~ 215 K).

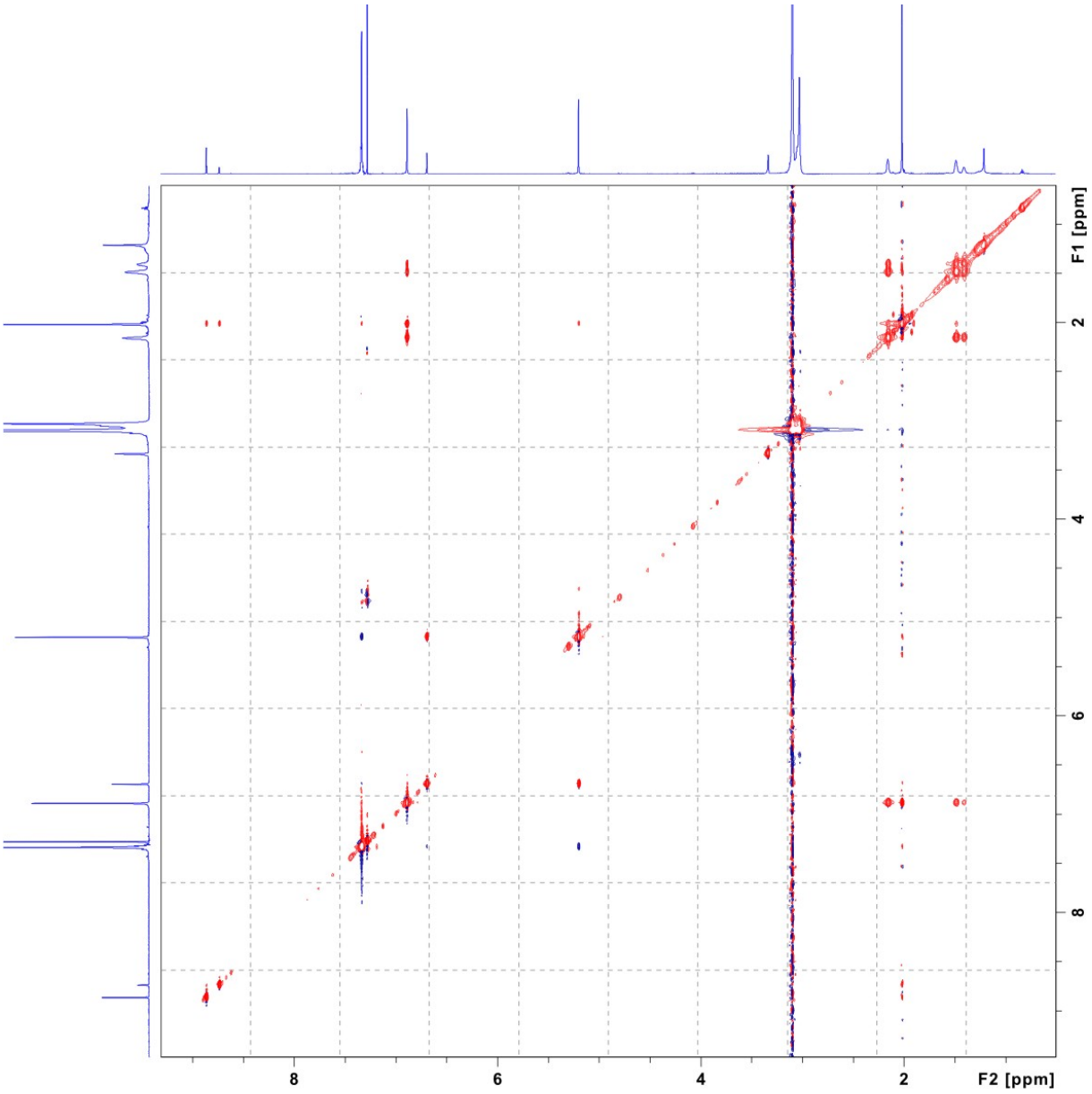

Figure 4.2.11 *^{1}H NOESY spectrum of octa-benzyloxy substituted octalactam macrocycle in $CDCl_3$. The coupling between amide proton and isophthal-H2 indicates the amide protons preferably to point inwards the macrocyclic cavity.*

The octa-benzyloxy-substituted octalactam macrocycle can be deprotected by palladium-catalyzed hydrogenation yielding the corresponding octa-hydroxy-substituted octalactam macrocycle (Figure 4.2.12).

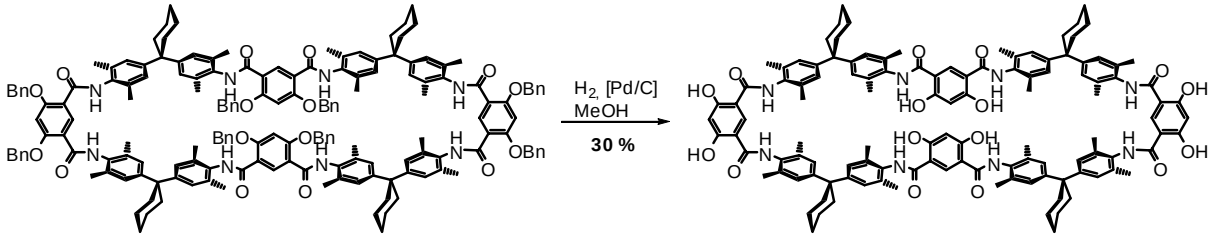

Figure 4.2.12 *Preparation of an octa-hydroxy-substituted octalactam macrocycle by palladium-catalyzed hydrogenation of the corresponding octa-benzyloxy-substituted octalactam macrocycle.*

In conclusion, the integrated template effect directing the 4,6-dimethoxy extended diamine building block into a "anti" orientation and therefore avoiding formation of the corresponding tetralactam macrocycle during a cyclization reaction causes the octalactam macrocycle to be the only cyclization product.

However, the methoxy groups are small enough to allow for threading of an open macrocyclization intermediate through another $(OMe)_8$-octalactam macrocycle leading to the formation of the corresponding di-octalactam catenane.

In case of 4,6-benzyloxy substitution of the isophthalic moieties, the corresponding macrocyclization intermediates are too sterically demanding to be threaded through another $(OBn)_8$-octalactam macrocycle thus leading to the exclusive formation of $(OBn)_8$-octalactam macrocycles and no catenanes.

So finally, a method was found to guide the macrocyclization reaction of Hunter-type oligo-lactam macrocycles towards the exclusive formation of octalactam macrocycles as the only cyclization product. Furthermore, this strategy comes with the possibility of later eightfold functionalization of the macrocycle after cleavage of the benzyl protective groups.

4.3 A "Spacewalk" on the Molecular Scale - Highly Dynamic Motion of Crown-Ethers in Non-Covalent Complexes[†]

4.3.1 The Idea of the "Spacewalk"

Brownian motion, the rotation of molecules, and vibrations within molecules are typical forms of thermal motion. Fast chemical equilibria such as the inversion at the ammonia nitrogen, the interconversion of conformers in alkanes, or highly dynamic association/dissociation processes in weakly bound non-covalent complexes are also thermally induced.

Non-covalent interactions control almost all biological processes just because of their reversible formation and dynamic nature. During peptide (re-)folding, structural elements move relative to each other exploring part of the available conformational space and thus optimizing their mutual interactions. The dynamics of non-covalent complexes is also the basis for the geometry changes mediating induced-fit binding, cooperativity and effector-controlled allosteric interactions.

It is therefore of prime importance to investigate the molecular motions occurring within non-covalent complexes and how mobile their constituents are. Here, the investigation of whether crown ethers are able to move along an oligolysine scaffold or on the periphery of **G1** to **G5** polyamino propylene amine (POPAM) dendrimers by *directly* hopping from binding site to binding site *without* intermediate dissociation/reassociation is decribed (Figure 4.3.1). The examination of such well-defined artificial supramolecular models contributes to unravelling the underlying concepts and to developing a more profound understanding of the dynamics of non-covalent interactions in more complex artificial as well as natural systems.

[†] The results presented in this chapter have been published in:

a) H. D. F. Winkler, D. P. Weimann, A. Springer, C. A. Schalley, *Angew. Chem.* **2009**, *121*, 7382-7386

b) D. P. Weimann, H. D. F. Winkler, J. A. Falenski, B. Koksch, C. A. Schalley, *Nature Chem.* **2009**, *1*, 573-577

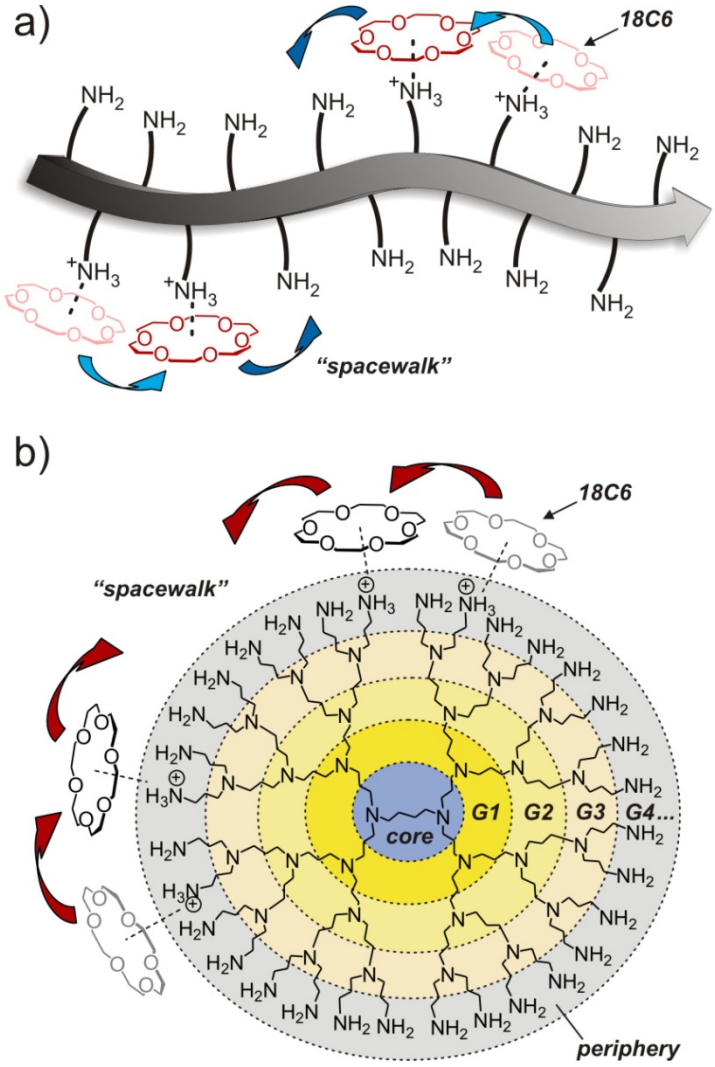

Figure 4.3.1 a) *Schematic representation of crown ethers' movement along a* Lys_{15} *peptide. The work presented in chapter 4.3 addresses the question whether 18-crown-6 molecules are positionally fixed at their respective ammonium binding site or whether they can move from binding site to binding site without intermediate dissociation from the peptide (indicated by the blue arrows). As this process proceeds in the high vacuum inside a mass spectrometer, it is referred to as a molecular "spacewalk".* ***b)*** *Schematic representation of the movement of 18-crown-6 on a generation 4 (**G4**) POPAM dendrimer (symbolized by the red arrows). Starting with a 1,4-diaminobutane core, the nth shell of branches is divergently grown on the (n-1)th generation dendrimer by two Michael additions of acrylnitrile to each branch followed by hydrogenolytic reduction of the nitrile groups.* ***G1 - G5*** *POPAM dendrimers have been used in the present study.*

4.3.2 Gas-Phase H/D Exchange as the Method of Choice to Track Molecular Motion in 18-Crown-6/Ammonium Complexes

In solution, any direct *intra*-complex binding-site hopping would be indistinguishable from *inter*-complex dissociation/reassociation equilibria. A straightforward analysis is thus not feasible in the condensed phase. However, isolating the crown ether/oligolysine or crown ether/dendrimer complexes, respectively, eliminates any possibility of crown exchange between them. The high vacuum inside a mass spectrometer provides the ideal means to efficiently isolate the ions from each other and from their free components. A direct exchange between two complexes can be ruled out, because they are all positively charged and thus repel each other. Also, the exchange of neutral crown ethers through dissociation/ reassociation can be excluded. The only source for neutral crown ethers in the hexapole region of the mass spectrometer would be dissociation from one of the complexes, after which they are quickly pumped away and thus not available for reassociation anymore.
Since the molecular mass does not change when a crown ether moves within its complex, a simple mass analysis is not able to provide direct evidence for its motion. A gas-phase reaction is therefore essential to probe the crowns' motion, which must (a) proceed energetically below the complex dissociation energy (ca. 180 kJ mol^{-1}),[84] (b) cause a change in molecular mass, and (c) be coupled to the crown ether's motion along the oligolysine backbone. Gas-phase H/D exchange reactions[85] exactly fulfil these criteria and have been used earlier to provide evidence for hydrogen bonding interactions in supramolecular host/guest complexes.[86,87,88] In this context, one report is particularly interesting:[89] H/D exchanges have been applied to uncover a tumbling motion of ammonium guests bound inside the cavity of resorcinarene hosts. Gas-phase isotope exchange reactions are not only a valuable tool for supramolecular chemistry. They can also provide valuable information on protein conformation in the gas phase. Cytochrome c,[90] for example, exists – depending on the charge state – in six different conformations. Gas-phase folding and unfolding of the protein can be monitored by H/D exchange reactions.

In the presence of suitable functional groups, H/D exchanges preferentially proceed through "relay" mechanisms[91] such as that shown in Figure 4.3.2 for protonated ethylenediamine (ED),[92] which quickly exchanges all its five nitrogen-centred hydrogen atoms. If no functional group is available to mediate the exchange, H/D exchanges are postulated[93] to proceed through proton/deuteron transfer steps as indicated in Figure 4.3.2c. The energy demand of

these reactions correlates with the differences in proton affinity of the amine and the CH_3OD exchange reagent.

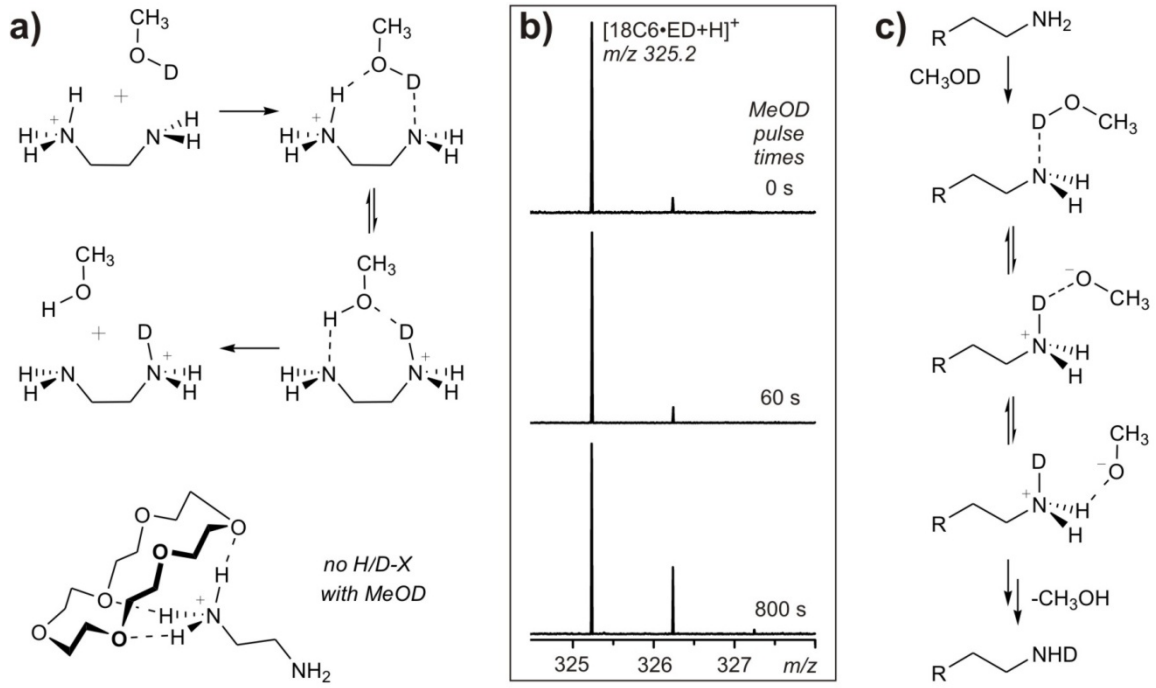

Figure 4.3.2 a) *The relay mechanism for H/D exchange on singly protonated ethylenediamine (ED) involves both functional groups and cannot efficiently operate, when a crown ether is complexed to the ammonium group.* ***b****) H/D exchange experiment performed with the protonated 1:1 complex of 18-crown-6 and ED. The spectrum remains more or less unchanged for the first 60 s. Only after much longer reaction times, the extremely slow exchange of the amine hydrogen atoms becomes detectable by the increase of the signal at m/z 326.2.* ***c)*** *Alternative mechanism: If no relay mechanism is feasible, hydrogen/deuterium-transfer intermediates rather high in energy must be involved. This mechanism explains the slow H/D exchange within the 18-crown-6/ED complex.*

18-crown-6 and other crown ethers bind to primary ammonium ions in solution[94,95] as well as in the gas phase.[96-101] Gas-phase H/D exchange experiments with the 18-crown-6 complex of protonated ED revealed the crown to prohibit the relay mechanism and thus to protect *all five* labile hydrogen atoms against isotopic exchange (Figure 4.3.2) - even including the two amine hydrogens.[92] Since crown ether/oligolysine peptide complexes[102,103] as well as crown ether/ POPAM dendrimer complexes bear more than two functional groups, a relay mechanism may still operate, even when some of them are involved in crown ether binding.

Nevertheless, one expects at least the three ammonium hydrogens per complexed crown to be protected against exchange when the crown ethers are immobilized at their initial positions. Instead, *all* labile hydrogen atoms should exchange, if the crowns can freely move between lysine side chains or dendrimer arms, respectively.

4.3.3 Molecular Motion of 18-Crown-6 on Oligolysine Peptides

Complexes of Lys_5 and Lys_{15} with 18-crown-6 were generated from a slightly acidified solution of the peptide in methanol ($c \approx 50\ \mu M$) by electrospray ionization (ESI).[104] In terms of the longer Lys_{15} peptide and its crown complexes, a broad range of charge states (z = +2 to +10) of the complexes appears in the spectra - each one with a variety of stoichiometries (up to n = 8 crown ethers attached to the peptide's +10 charge state). The ions generated in the ion source were trapped and subjected to H/D exchange with deuterated methanol (CH_3OD) for well-defined reaction time intervals in the collision hexapole of our Fourier-transform ion-cyclotron-resonance (FTICR)[53] mass spectrometer. The exchange reaction in the hexapole proceeds with high efficiency[105,106] and permits all charge states and complex stoichiometries to be reacted simultaneously under the same conditions so that they can be directly compared with each other with respect to the deuterium incorporation rates.

Figure 4.3.3 shows the pulse program used for the H/D experiments. After ion accumulation in the hexapole collision cell (orange bar), the entrance of new ions into the hexapole was blocked by switching off the radio frequency of the quadrupole in front of the hexapole ("Q1/Q2 RF level" in Figure 4.3.3). To conduct the isotopic exchange, CH_3OD was then introduced into the collision cell after a short delay. The reaction time was controlled with the help of a pulse valve ("Valve #1-Sourc" in Figure 4.3.3; green bar). After the H/D exchange reaction, the product ions were transferred into the instrument's FTICR analyzer cell and detected by a standard excitation and detection sequence (blue bar) with resolutions high enough for baseline-separated isotope patterns even of the higher charge states.

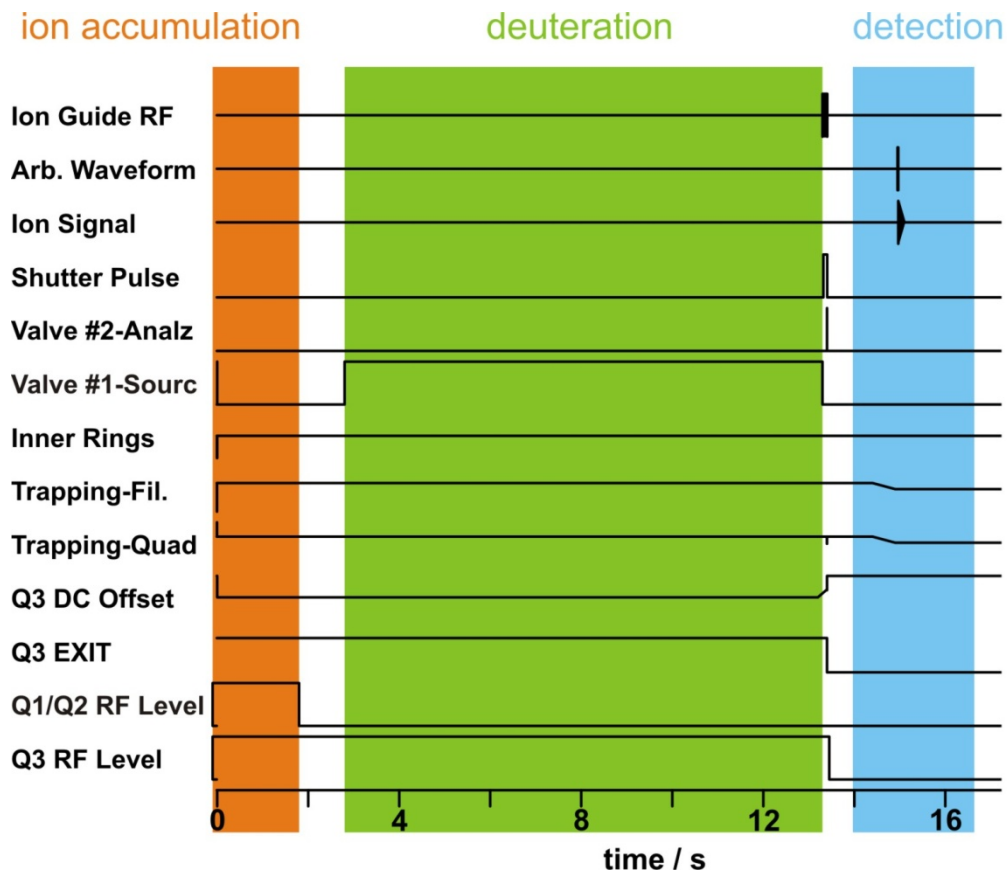

Figure 4.3.3 *Pulse program for the H/D exchange in the mass spectrometer's hexapole.*

When Lys_{15} alone is subjected to gas-phase H/D exchange, all exchangeable hydrogens are quickly replaced by deuterium atoms. This is true for all charge states; the quadruply protonated Lys_{15} with its 51 labile hydrogen atoms (30 side-chain amine hydrogens, 14 amide NHs, 3 H atoms from the N- and C-termini, and 4 protons providing the charges), is shown in Figure 4.3.4a as a representative example. The progress of the exchange can easily be monitored by systematically varying the reaction time. These two findings – the exchangeability of all labile H atoms and the independence from the charge state – also indicate all exchangeable hydrogen atoms to be exposed to the exchange reagent. Consequently, the Lys_{15} chain likely does not adopt any stable, well-defined secondary structure in the gas phase.

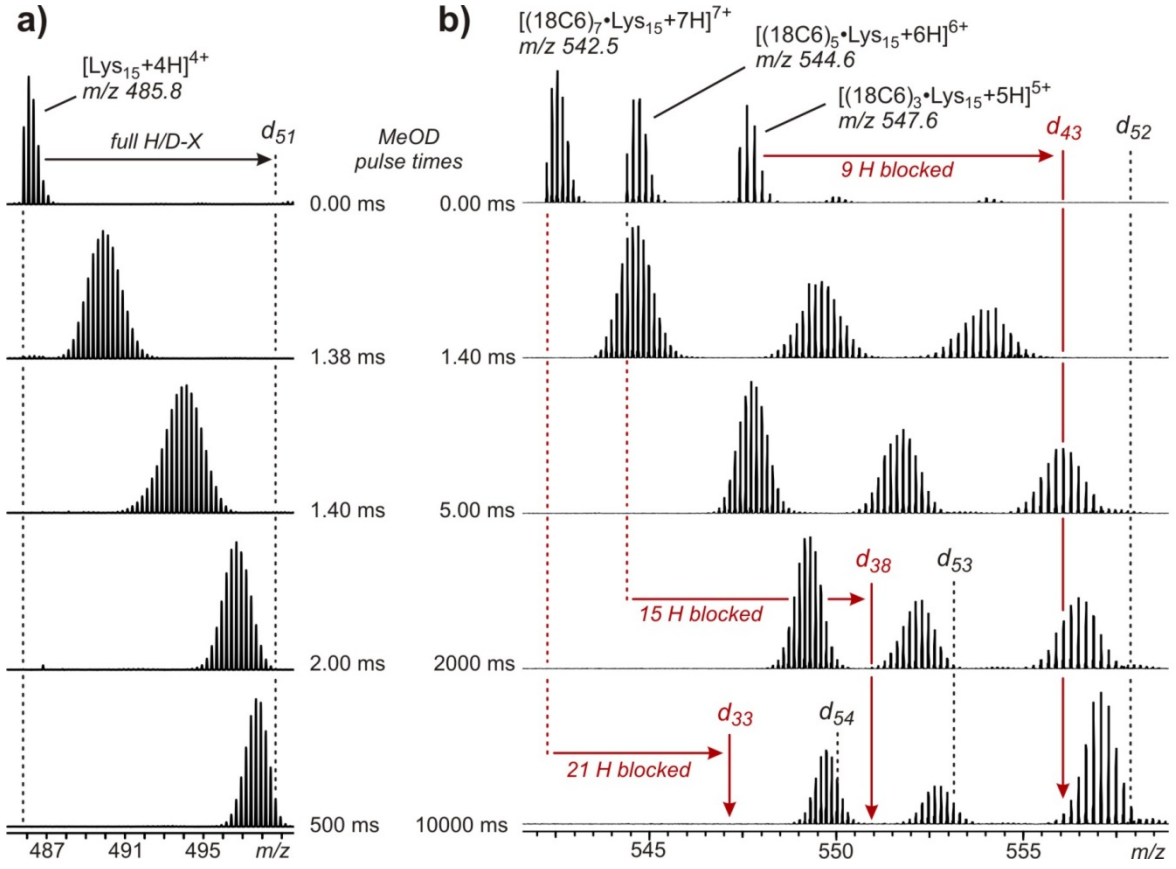

Figure 4.3.4 a) *H/D exchange experiment with quadruply protonated Lys_{15}.* ***b)*** *Sections of ESI mass spectra showing the H/D exchange on 18C6/Lys_{15} complexes with different charge states and stoichiometries. Dotted lines indicate the signal position before and after complete exchange. Red vertical arrows indicate, where the exchange reaction should terminate, when each crown ether protected the three NH hydrogens of one ammonium group against H/D exchange. Clearly, the exchange proceeds far beyond these thresholds.*

When the same experiment is performed with a 1:2 mixture of Lys_{15} and 18-crown-6 (Figure 4.3.4b), all ions undergo almost complete H/D exchange irrespective of charge state and stoichiometry. Most intriguingly, significantly more hydrogens are exchanged than expected for complexes with immobile crown ethers. For example, the $[(18C6)_7•Lys_{15}+7H]^{7+}$ complex (m/z = 542.5) bears a total of 54 labile H atoms. If each of the seven crown ethers protected three of them, one would expect to observe the exchange to terminate after the exchange of 33 hydrogens. Already after a reaction time of just 5 ms, far more than these have been exchanged. The signals for $[(18C6)_5•Lys_{15}+6H]^{6+}$ (m/z = 544.6) and $[(18C6)_3•Lys_{15}+5H]^{5+}$ (m/z = 547.6) in Figure 4.3.4b exhibit a similarly fast H/D exchange which again proceeds clearly beyond the expected threshold for 15 and 9 protected hydrogen atoms, respectively.

Interestingly, the exchange on crown ether complexes is not much slower than that on the free oligolysine ions (Figure 4.3.4 – 4.3.9). These findings provide unambiguous evidence for a motion of the crown along the peptide backbone.

To illustrate that that the H/D exchange can simultaneously be followed for complexes of all observed charge states and stoichiometries in one experiment, the ESI mass spectra of a 1:1 mixture of 18-crown-6 and Lys_{15} after different H/D exchange intervals are shown as a representative example (Figure 4.3.5 – 4.3.9). For the sake of clarity, the whole spectra have been subdivided in five mass ranges. Clearly, the relative signal intensities do not change much during the exchange reaction. This indicates dissociation of the complexes not to efficiently compete neither with the exchange reaction nor with the crown ethers' motion.

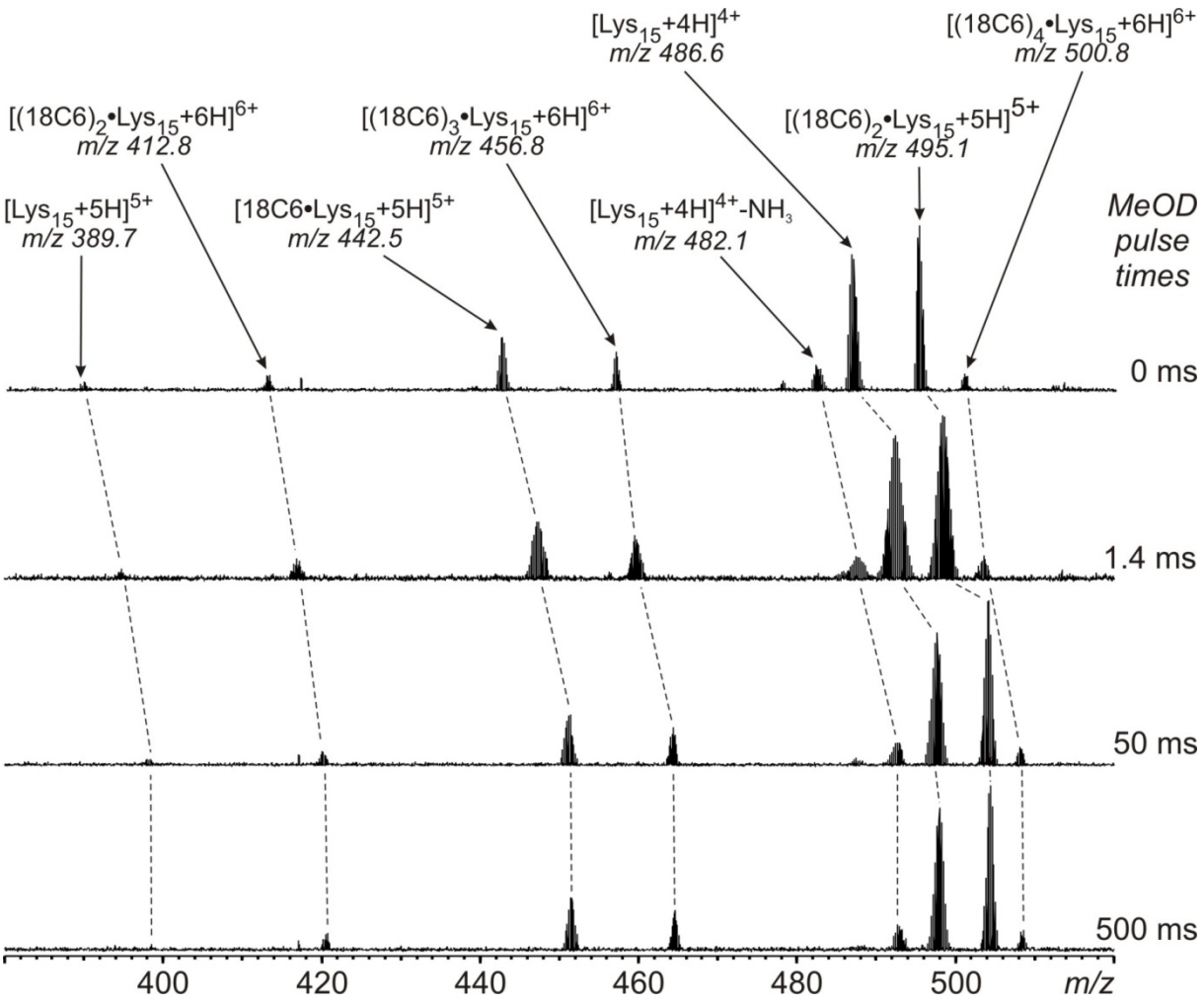

Figure 4.3.5 *H/D exchange on different charge states and stoichiometries of 18C6/Lys_{15} complexes – part 1: m/z 380 - 520.*

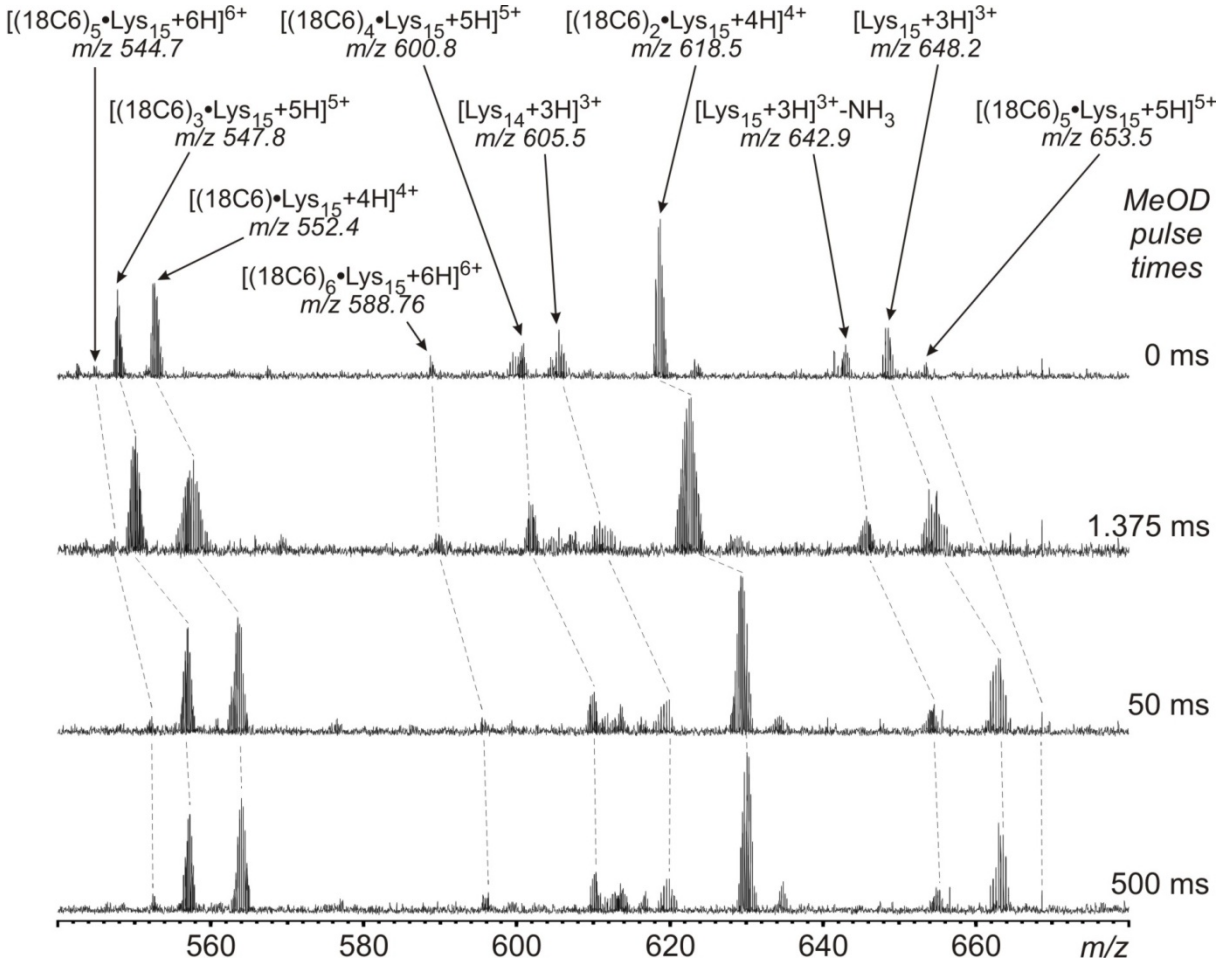

Figure 4.3.6 *H/D exchange on different charge states and stoichiometries of 18C6/Lys$_{15}$ complexes – part 2: m/z 540 - 680.*

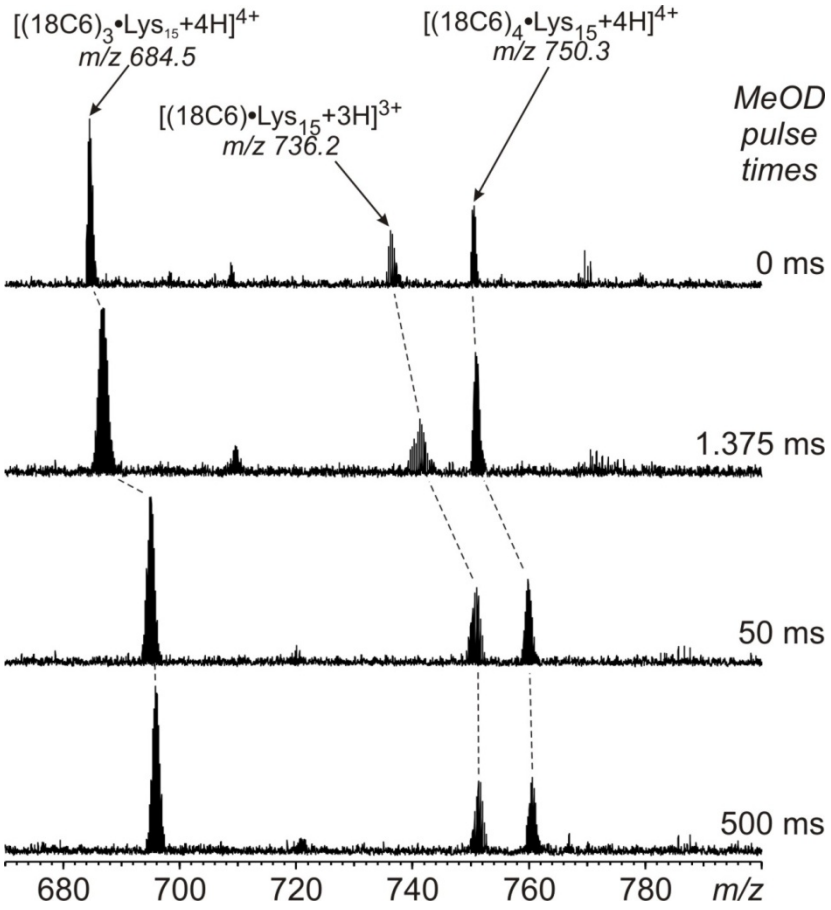

Figure 4.3.7 *H/D exchange on different charge states and stoichiometries of 18C6/Lys$_{15}$ complexes – part 3: m/z 670 - 800.*

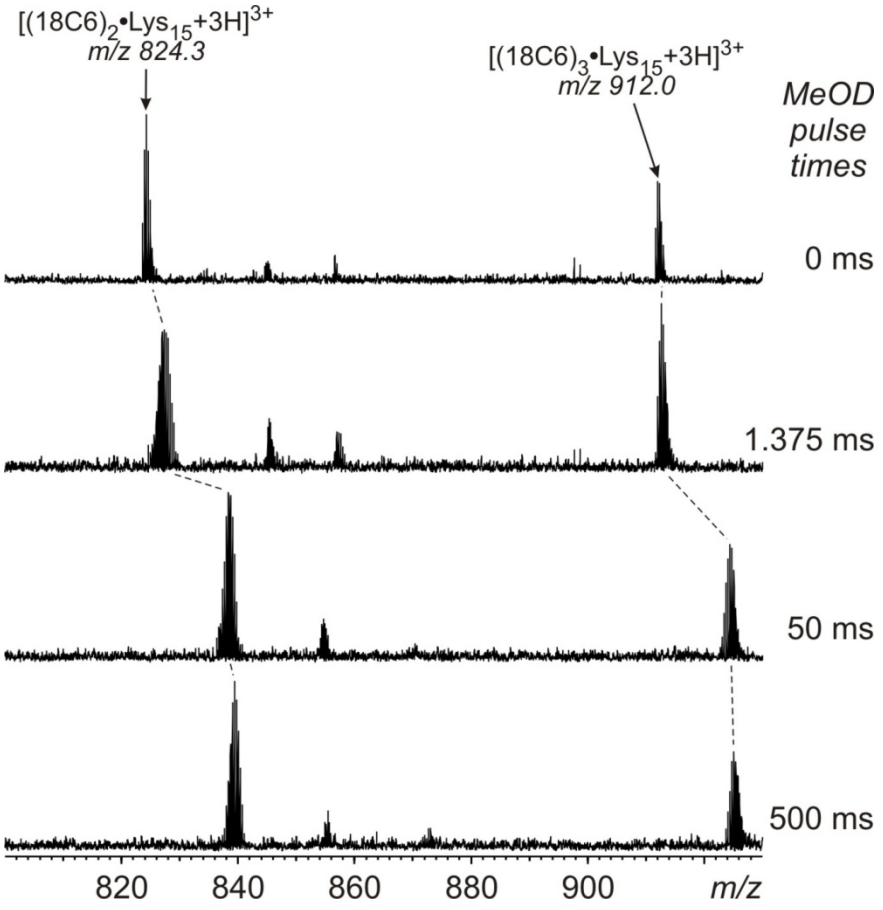

Figure 4.3.8 *H/D exchange on different charge states and stoichiometries of 18C6/Lys$_{15}$ complexes – part 4: m/z 800 - 930.*

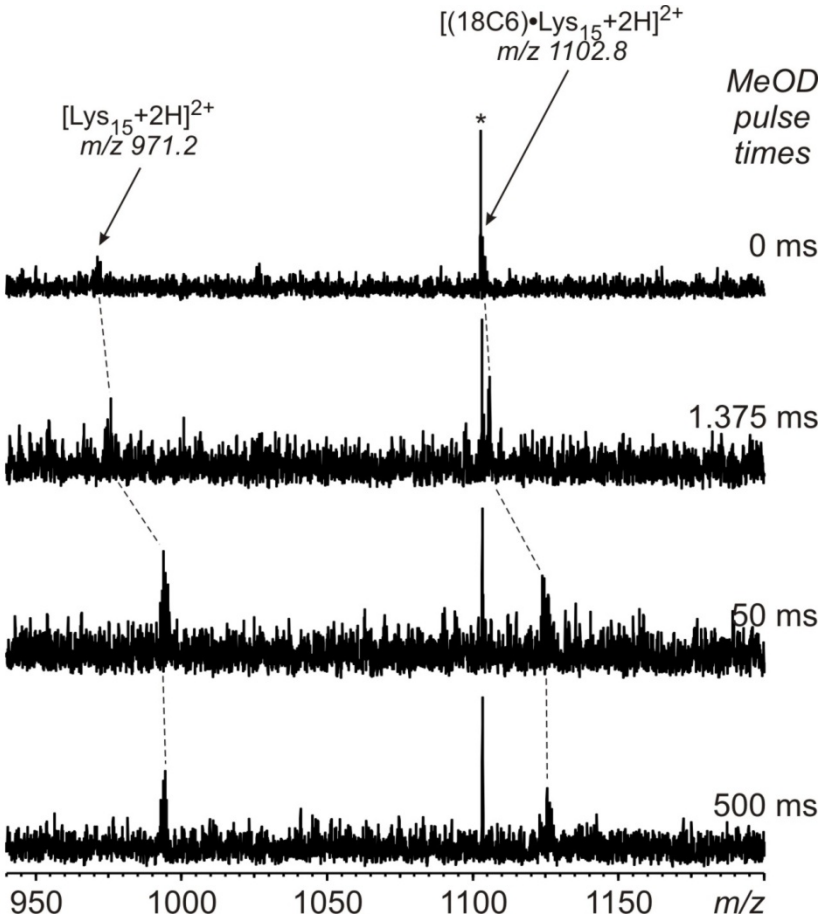

Figure 4.3.9 *H/D exchange on different charge states and stoichiometries of 18C6/Lys_{15} complexes – part 5: m/z 940 - 1200. The asterisk denotes a signal originating from stray radiation.*

In addition to the experiments described above for Lys_{15}, the crown ether movement can also be followed on smaller oligolysine peptides such as Lys_5. As shown before for Lys_{15}, also singly protonated Lys_5 is able to quickly exchange all 18 protons for deuterons when reacted with CH_3OD in the gas phase (Figure 4.3.10). Also in complexes of doubly protonated Lys_5 with one (Figure 4.3.11) or two crown ethers (Figure 4.3.12), still all protons are exchangeable thus confirming the crown ethers' movements along shorter oligolysine peptides to follow the same principles as deduced for the longer Lys_{15} peptide and its complexes.

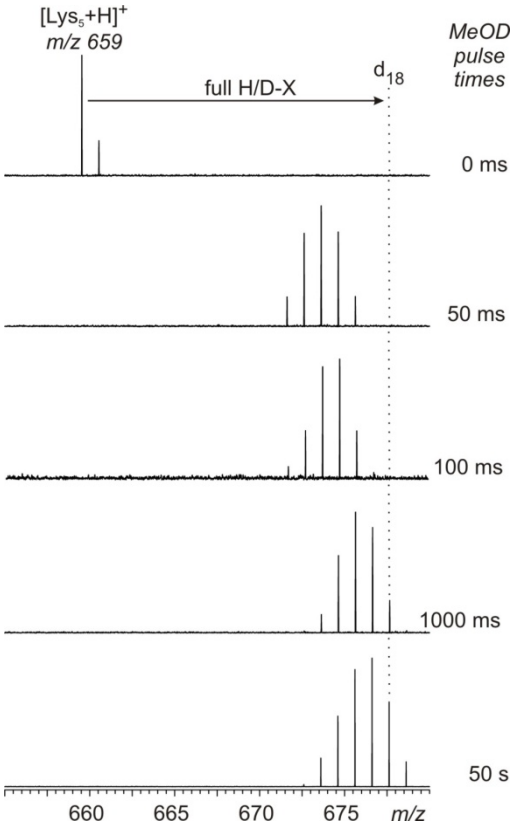

Figure 4.3.10 *Gas-phase H/D exchange on singly protonated Lys_5.*

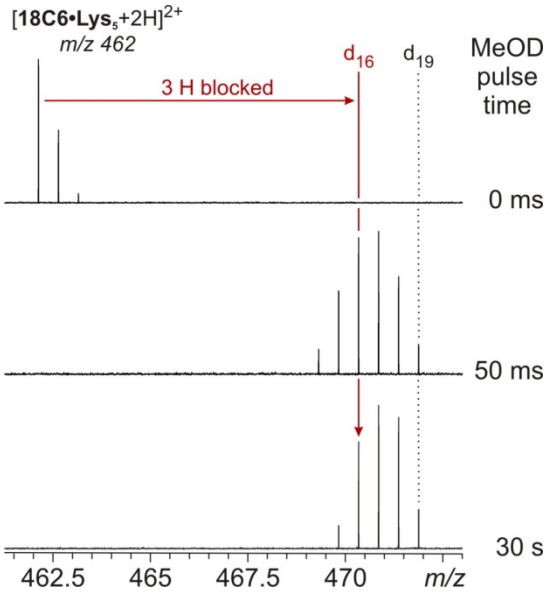

Figure 4.3.11 *Gas-phase H/D exchange on $[18C6•Lys_5+2H]^{2+}$.*

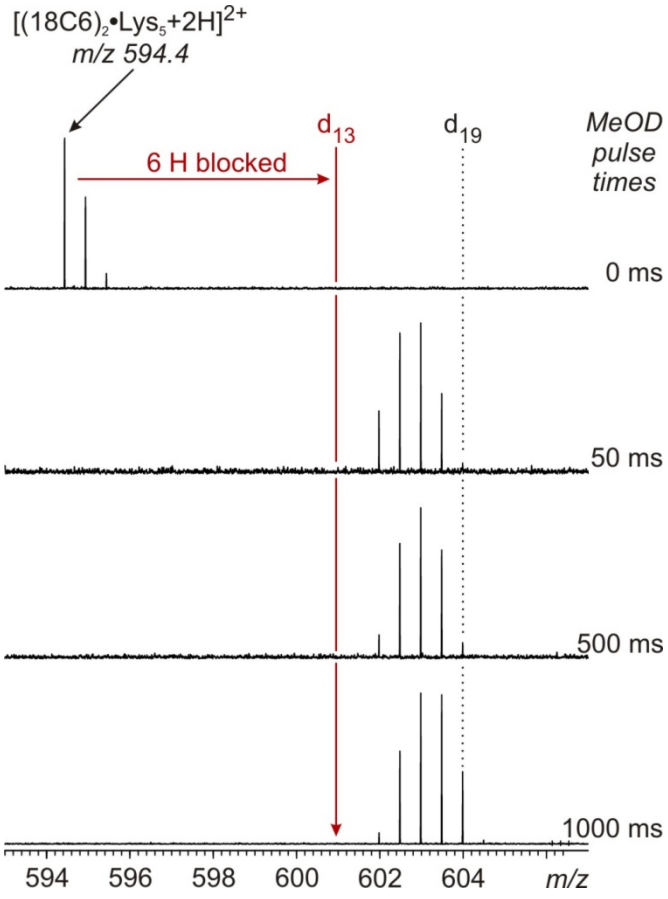

Figure 4.3.12 *Gas-phase H/D exchange on* $[(18C6)_2 \bullet Lys_5+2H]^{2+}$.

4.3.4 Molecular Motion of 18-Crown-6 on POPAM Dendrimers

The methodology described above for oligolysine peptides was then applied to polyamino propylene amine (POPAM) dendrimers as the multitopic scaffold. These dendrimers have highly branched onion-layer-type structures (Figure 4.3.1b). From each generation (**G*n***) to the next, the number of peripheral amino groups doubles from four in the **G1** dendrimer to 64 in **G5**. Their gas-phase chemistry has been studied quite well.[107] In the absence of a solvating agent, protonation is likely to occur at interior tertiary amines rather than the peripheral primary NH_2 groups.[108] Only a few examples exist so far.[109] Also here, 18-crown-6 serves as the guest, which is known to bind to primary ammonium ions in solution,[110] and in the gas phase.[111] Dendritic crown ether/ammonium complexes are already charged and can easily be transferred into the gas phase as positively charged ions by electrospray ionization (ESI)[112] from slightly acidic solutions of the corresponding dendrimer and 18-crown-6 in methanol. A broad distribution of charge states (up to z = +8 for **G5**) with various stoichiometries (up to n = 5 **18C6** molecules bound to **G5**) is observed in the ESI mass spectra. Since crown ethers bind more strongly to primary (ca. 200 kJ mol^{-1}) than to tertiary ammonium ions (ca. 170 kJ mol^{-1}),[113] they provide solvation to the primary ammonium ions and thus contribute to shifting the charges to the peripheral amines.

Based on these considerations, the question can be addressed, whether the crown ethers are able to move from binding site to binding site at the periphery of a POPAM dendrimer. As 18-crown-6 efficiently blocks the gas-phase exchange of the ammonium protons against deuterons in its 1:1 complex with protonated ethylene diamine[92] (chapter 4.3.2), the H/D exchange reaction[114] is the reaction of choice to probe the crown ether's mobility on the dendrimer periphery: If it is unable to walk from binding site to binding site, the corresponding ammonium protons (i.e. three protons per crown ether) cannot be exchanged. In contrast, an exchange of all acidic protons on the dendrimer would be expected, when the crown ether moves.

The gas-phase H/D exchange experiments for the POPAM/crown ether complexes were performed as described above for the corresponding oligolysine complexes (for experimental details, see chapter 5.1.3).

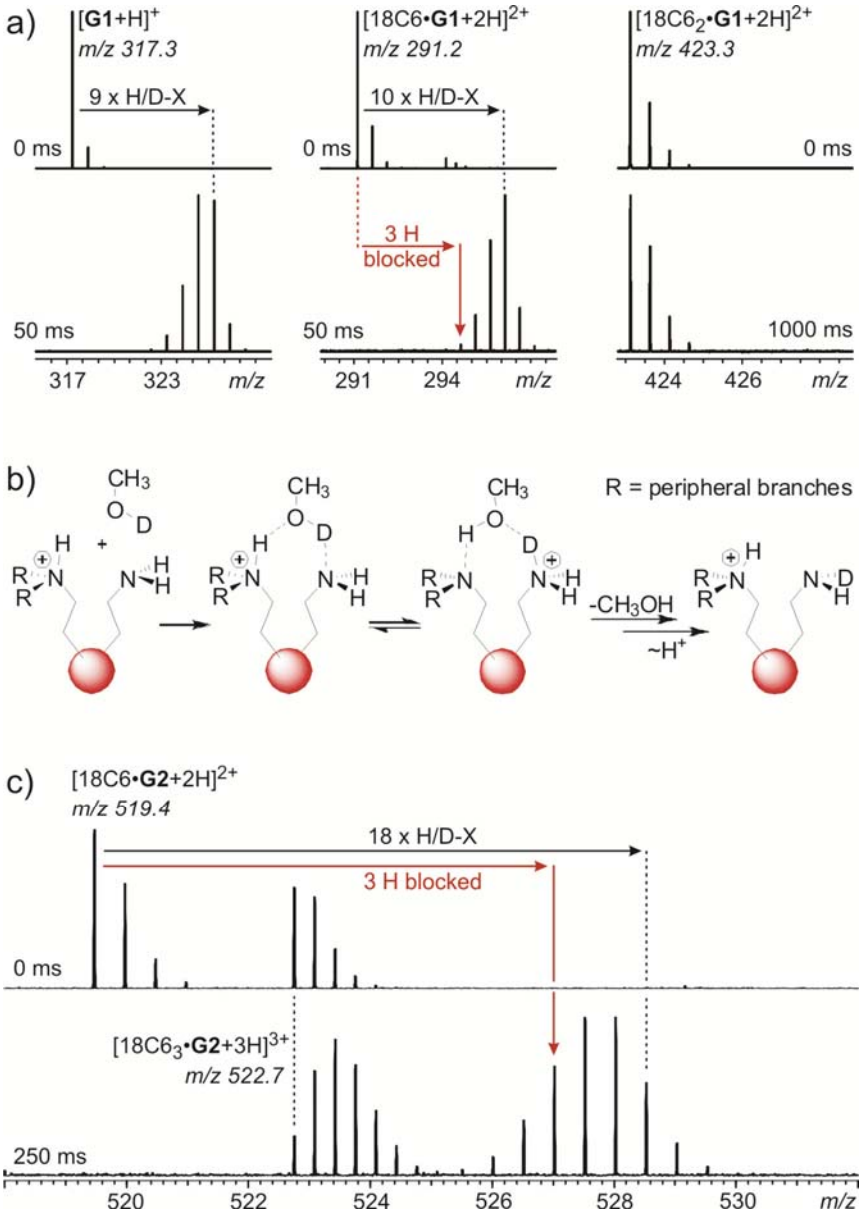

Figure 4.3.13 a) *Left: H/D exchange experiment with singly protonated* ***G1*** *(0 and 50 ms reaction time). Fast exchange of all nine NH protons is observed. Center: H/D exchange of all ten NH protons of the doubly protonated 1:1 18-crown-6/****G1*** *complex (0 and 50 ms). The red vertical arrow marks the endpoint of the H/D exchange expected in case of a positionally fixed crown ether blocking three protons against isotope exchange. Right: An extremely slow H/D exchange is observed for the doubly charged 2:1 18-crown-6/****G1*** *complex (0 and 1000 ms).* ***b)*** *A "relay" mechanism*[92,115] *for the gas-phase H/D exchange at protonated POPAM dendrimers explains why the exchange is so slow in* $[18C6_2@\mathbf{G1}+2H]^{2+}$*: No excess charge is available that mediates the exchange reactions with* CH_3OD*.* ***c)*** *The same scenario is observed for higher generation dendrimers: While the exchange is fast for the* ***G2*** *complex* $[18C6\bullet\mathbf{G2}+2H]^{2+}$ *bearing more charges than crown ethers, it is very slow when all charges are involved in crown ether binding as in* $[18C6_3\bullet\mathbf{G2}+3H]^{3+}$*.*

As shown in Figure 4.3.1a, all nine N-centered protons of singly protonated **G1** can be quickly exchanged for deuterons. When a crown ether is bound to **G1**, one would expect three protons to be protected against the isotope exchange. In marked contrast to expectation, $[18C6•\mathbf{G1}+2H]^{2+}$ exchanges all its ten NH protons, which only is possible, if the crown ether has moved from one binding site to another during the exchange reaction. After 50 ms, the progress of the H/D exchange on the complex is more or less the same as that of free **G1**. Consequently, the crown ether movement proceeds with a rate more or less comparable to that of the isotope exchange. Remarkably, hardly any exchange is observed in the 2:1 complex $[18C6_2•\mathbf{G1}+2H]^{2+}$, which bears the same number of crown ethers and charges ($n = z$). This finding can be explained by a "relay" mechanism (Figure 4.3.13b) which has been postulated earlier for crown ether complexes of ethylene diamine[91] and other small (bio-) molecules.[115] As long as at least one ammonium group remains uncomplexed and thus freely accessible ($n < z$), the exchange reaction can operate efficiently according to the relay mechanism. When all charge sites are involved in crown ether binding instead ($n = z$), no ammonium group is available anymore to mediate the exchange.

The exchange behavior observed for **G1** is confirmed in analogous experiments with higher generation dendrimers. For example, the isotope exchange on $[18C6•\mathbf{G2}+2H]^{2+}$ ($n < z$) is fast, while $[18C6_3•\mathbf{G1}+3H]^{3+}$ ($n = z$) proceeds at a much slower pace (Figure 4.3.13c).

For **G3**, **G4**, and **G5** dendrimer/crown complexes with their 16, 32, and 64 peripheral NH_2 groups, respectively, the number of signals in the mass spectra increases significantly. On the one hand, the number of different charge states and complex stoichiometries increases. On the other hand, defects in the dendrimer structure unavoidably accumulate due to the divergent synthesis of POPAM dendrimers. Nevertheless, an unambiguous correlation of the signals *after* H/D exchange to those *prior* to the experiment is easily possible by gradually increasing the reaction times. Each isotope pattern is then shifted step by step to higher m/z values so that the progress can be directly followed. Figure 4.3.14 depicts selected results for **G3** and **G4** with charge states up to $z = +7$ and $n = 5$ crown ethers: For all ($n < z$) complexes, the H/D exchange clearly proceeds beyond the endpoint expected for complexes of non-moving crown ethers. Even the complexes of **G4** and **G5** (see Figure 4.3.15), which bear up to 71 and 136 exchangeable protons depending on their charge states, reach this threshold within less than 50 ms reaction time. Therefore, one can conclude the crown ethers to travel quickly on the dendrimer peripheries independent of the dendrimer size.

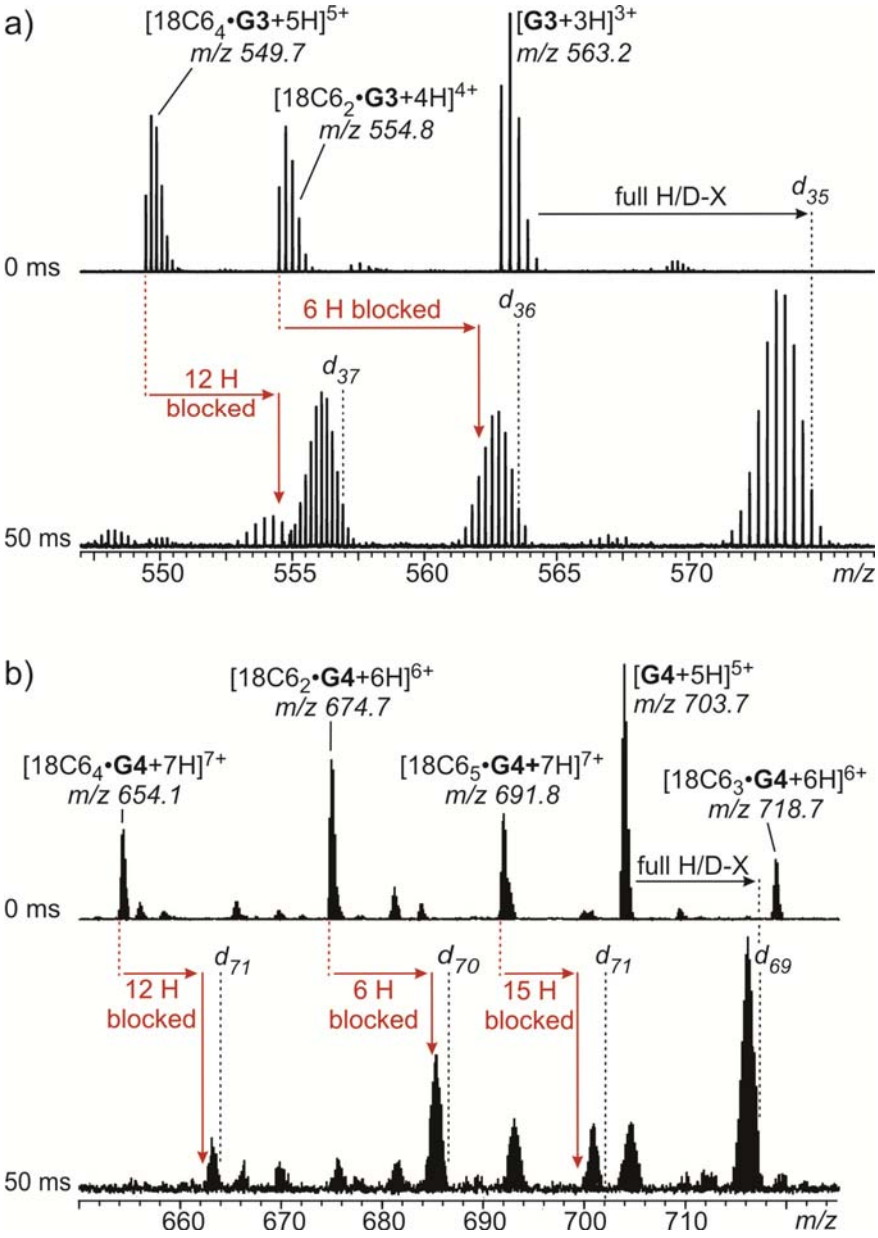

Figure 4.3.14 *H/D exchange experiments conducted with 18-crown-6 complexes of a)* ***G3*** *and b)* ***G4*** *POPAM dendrimers. Already after 50 ms, the exchange has proceeded beyond the positions at which it would be expected to stop, if the crown ethers would protect the ammonium protons against exchange (red vertical arrows). Minor signals in the spectra are due to the typical defects in the dendrimer structure which unavoidably accumulate in the higher generations.*

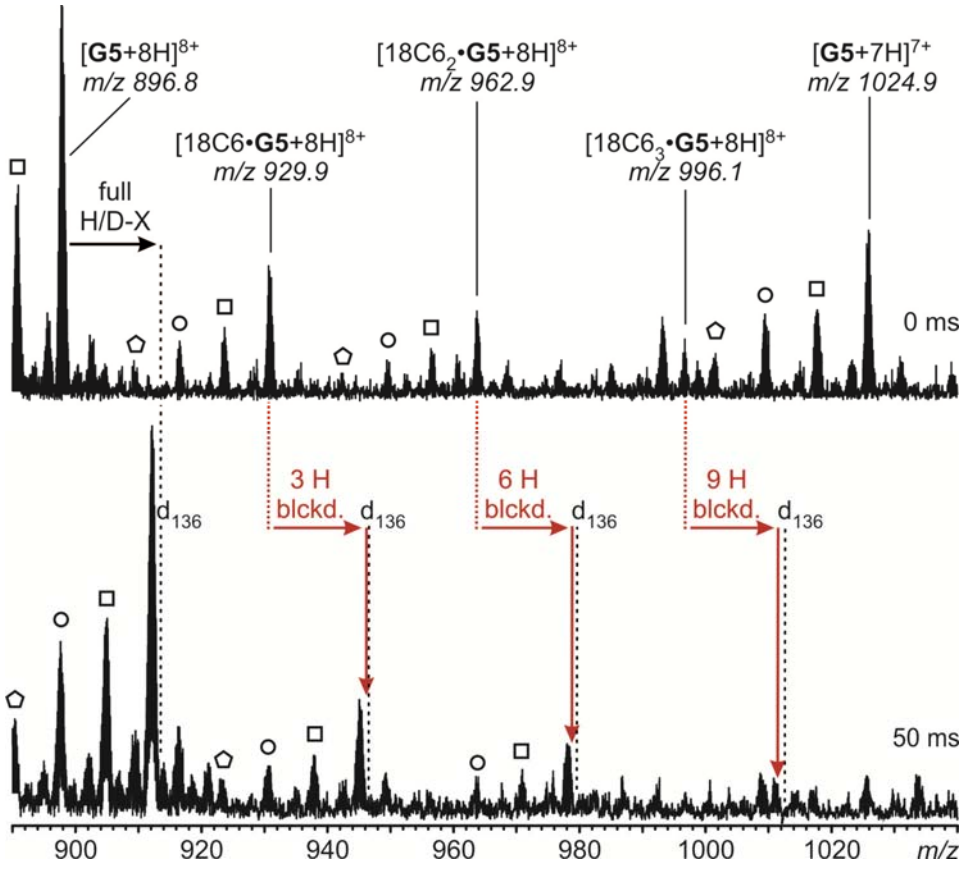

Figure 4.3.15 *H/D exchange on POPAM-G5/18-crown-6 complexes of different stoichiometries. Squares, circles, and pentagons indicate signals for defect structures with one, two, and three missing terminal branches. As the large dendrimers reach the technical detection limit of the QFT-7 FTICR mass spectrometer, the signal-to-noise-ratio is comparably low and a clean baseline separation of all isotopic patterns is not possible anymore. Nevertheless is, as shown in the case of the eightfold protonated* ***G5*** *POPAM, an almost complete exchange of 136 N-acidic protons observable, independent of the number of attached crown ethers, therefore providing evidence for the "spacewalk" of crown ethers on the POPAM periphery.*

4.3.5 Mechanism of the Crown-Ether Transfer

The fact that the crown ethers indeed move between the different binding sites in oligolysine peptides and POPAM dendrimers raises the question, how this process proceeds mechanistically. In principle, two scenarios are imaginable (Figure 4.3.16): a) A *neutral* crown ether may be transferred from one ammonium group to another or b) it moves *together with a proton* from its ammonium binding site to a non-protonated amine. Both mechanisms must proceed stepwise by replacing one hydrogen bond after the other through new ones because otherwise the dissociation of the crown ether should be observed to compete with the exchange reaction. With 1,12-diaminododecane (DAD), a suitable model exists, in which the two amino groups have the same distance as the amino groups of two adjacent oligolysine side chains as well as two amino groups in POPAM **G1**.

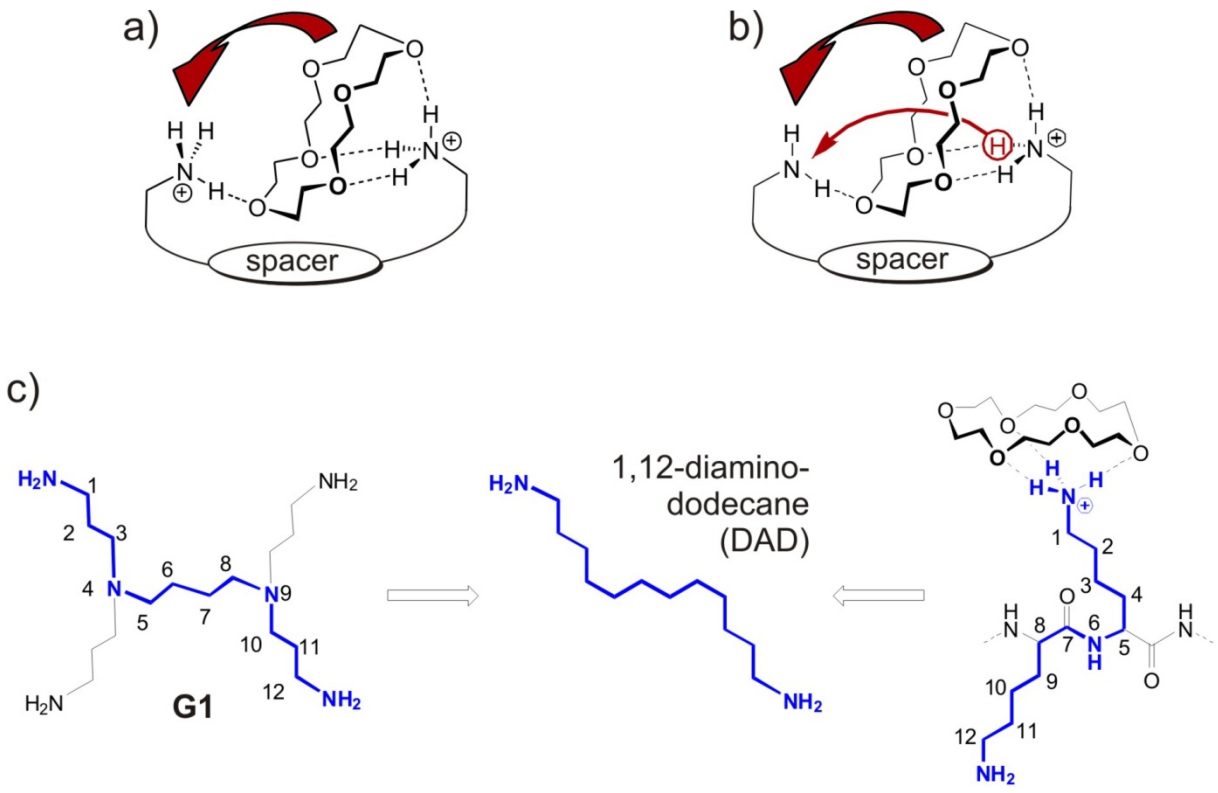

Figure 4.3.16 a) *Schematic representation of spacewalk mechanism 1: A neutral crown ether moves from its ammonium binding site to another one.* ***b)*** *Schematic representation of spacewalk mechanism 2: The crown ether is transferred from its ammonium binding site to a nearby amino group together with a proton.* ***c)*** *1,12-diaminododecane (DAD) is a suitable model compound to experimentally examine the mechanism.*

A crown transfer within the doubly protonated 1:1 18-crown-6/DAD complex would only be possible, when the ammonium-to-ammonium scenario is feasible. Instead, the singly protonated analogue would only allow the crown to move together with one of the protons from the ammonium to the amine site.

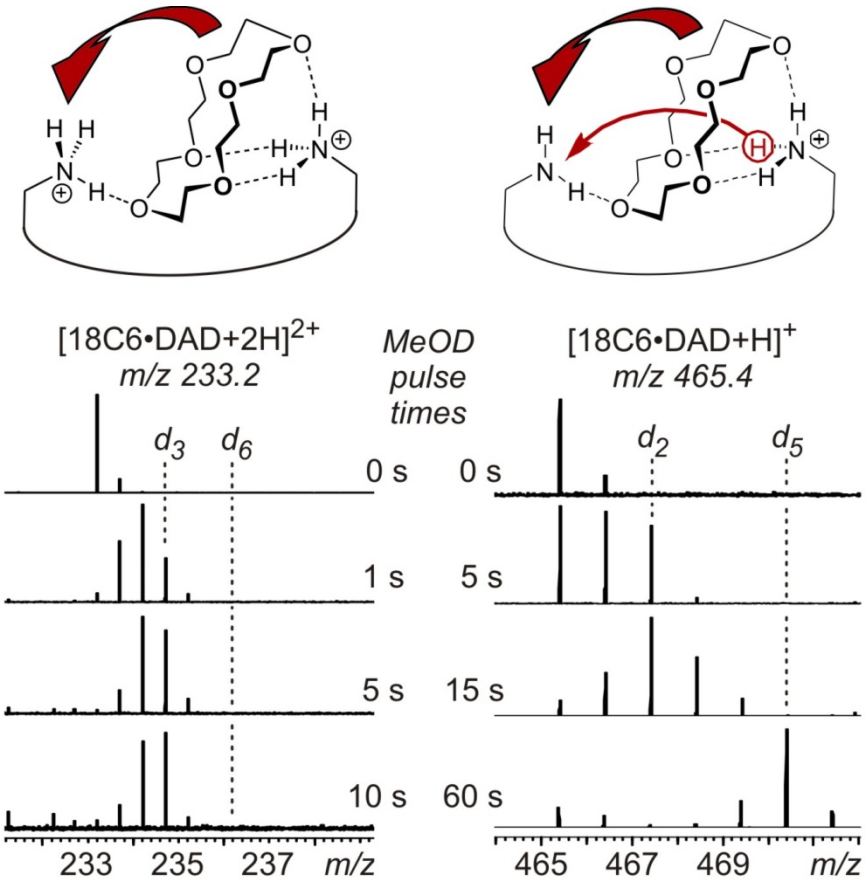

Figure 4.3.17 Top left: *Mechanistic scenario 1: Transfer of a neutral crown ether from ammonium to ammonium.* ***Top right:*** *Mechanistic scenario 2: Transfer from ammonium to amine together with a proton.* ***Bottom left:*** *Exchange experiments with the doubly protonated 18-crown-6•1,12-diaminododecane (DAD) complex rule out the first scenario. The crown ether prevents three H atoms from being exchanged.* ***Bottom right:*** *All five labile hydrogen atoms can instead be exchanged in the singly charged 18C6/DAD complex providing evidence that the crown transfer follows the second mechanistic pathway.*

The mass spectra in Figure 4.3.17 clearly rule out the ammonium-to-ammonium transfer: In the doubly protonated complex, only the three free ammonium hydrogens are exchanged, while the three protons mediating crown binding remain unaffected. Thus, no crown transfer

occurs here - most likely because of the strong repulsion between the two repellent positive charges. This repulsion hampers the approach of the second ammonium site to the crown ether and thus prevents the crown ether movement. At the same time, the exchange of the three H atoms at the free ammonium site is slow (Figure 4.3.17, bottom left), because no relay mechanism is possible. In marked contrast, all five N-centred H atoms can be exchanged in the singly protonated complex - even if this reaction is also comparably slow in the absence of an additional free ammonium site permitting the relay mechanism. This clearly indicates the crown to move between both ends of the diamine. This clearly indicates the crown to move together with one proton from its ammonium binding site to an adjacent amine. For a full exchange of all labile hydrogens, at least two transfer steps of each crown ether are thus necessary: In the first step, the crown ether can move together with a H^+ to an already deuterated $-ND_2$ site. It would consequently be bound there by an $-ND_2H^+$ group. The exchange of the last hydrogen is only possible, when the crown ether moves on to yet another lysine side chain together with a D^+ in a second step thus exposing the remaining H atom to the exchange reagent.

Figure 4.3.18 depicts an alternative mechanistic scenario explaining the observed exchange of all labile hydrogen atoms without invoking crown ether transfers between binding sites. An adjacent terminal ammonium group or protonated tertiary amine in the dendrimer scaffold might form a proton bridge to one of the crown ether oxygens. The binding energy gained helps to break an ammonium-crown proton bridge exposing a proton to exchange. However, two reasons speak against such a scenario: First of all, the generation of doubly charged complexes is possible with longer spacers like the C_{12} chain in DAD - although quite some effort is required to optimize ionization conditions. As the above results show, no complete exchange is observed in this complex ruling out the operation of the alternative mechanism at least for longer spacers. Secondly, all attempts to generate doubly charged model complexes with shorter spacers such as $[18C6•1,3\text{-diaminopropane}+2H]^{2+}$ failed. This points to the significance of charge repulsion which will not only affect ion generation, but also prevent the approach of the two charges in the gaseous complexes. For these reasons, the crown ether transfer can be regarded to be the more convincing mechanism.

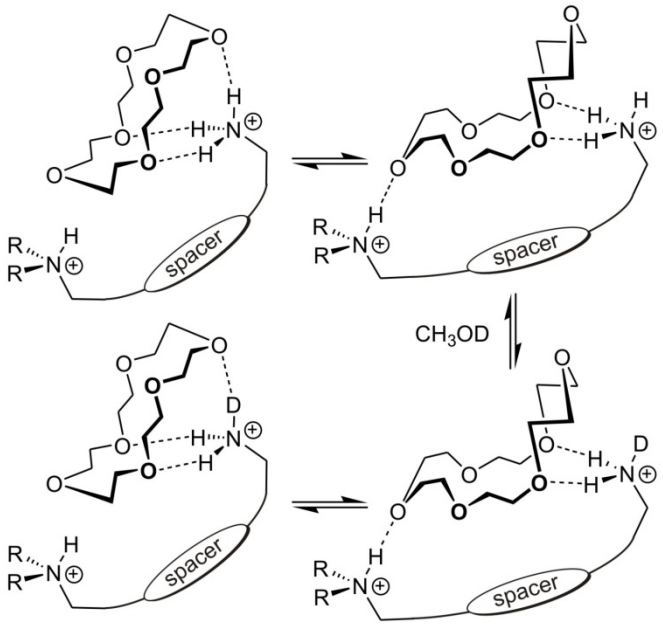

Figure 4.3.18 *A conceivable alternative exchange mechanism, in which a nearby second charged site supports the release of an N-H•••O hydrogen bond. A sequence of such steps would also lead to a complete exchange of all labile hydrogens without involving the motion of the crown between binding sites.*

4.3.6 Are Oligolysine Peptides Zwitterions in the Gas Phase?

When comparing the H/D exchange experiments with 18C6/oligolysine complexes to those with the corresponding POPAM dendrimers, a crucial difference becomes apparent:
Whereas for the 18C6•POPAM+nH$^+$ complexes, the H/D exchange is significantly slowed down, when the number of crown ethers equals the number of charges ($n = z$), in the H/D exchange experiments with the corresponding crown ether complexes of Lys_{15}, a quick exchange of all N-centred hydrogen atoms is observed even when the number of crowns equals that of the charges ($n = z$). In this case, all ammonium sites are expected to be occupied by crown ethers. The singly protonated 1:1 complexes of 18-crown-6 and ED or DAD also belong to the ($n = z$) class. Also here, hardly any or much slower exchanges, respectively, were observed for them because of the inhibition of the relay mechanism (Figure 4.3.2c) caused by the presence of the crown.

This discrepancy in the exchange behaviour suggests the presence of an additional ammonium group in the crown ether/peptide complexes that would again enable the relay mechanism. Since the overall charge state of the ions remains unchanged, the only convincing explanation is the formation of zwitterions through proton transfer from the C-terminal carboxylic acid to one of the amino groups. In contrast to amino acids and peptides in aqueous solution, the formation of zwitterions is much less frequently observed in the gas phase[116] because of the energetically disfavoured charge separation. To verify this assumption, the ($n = z$) complexes of acid-terminated $Lys_{15}COOH$ (which can form a zwitterion) have been compared to the analogous complexes of amide-terminated $Lys_{15}CONH_2$ (which is much less acidic at the C-terminus and thus cannot form a zwitterion).

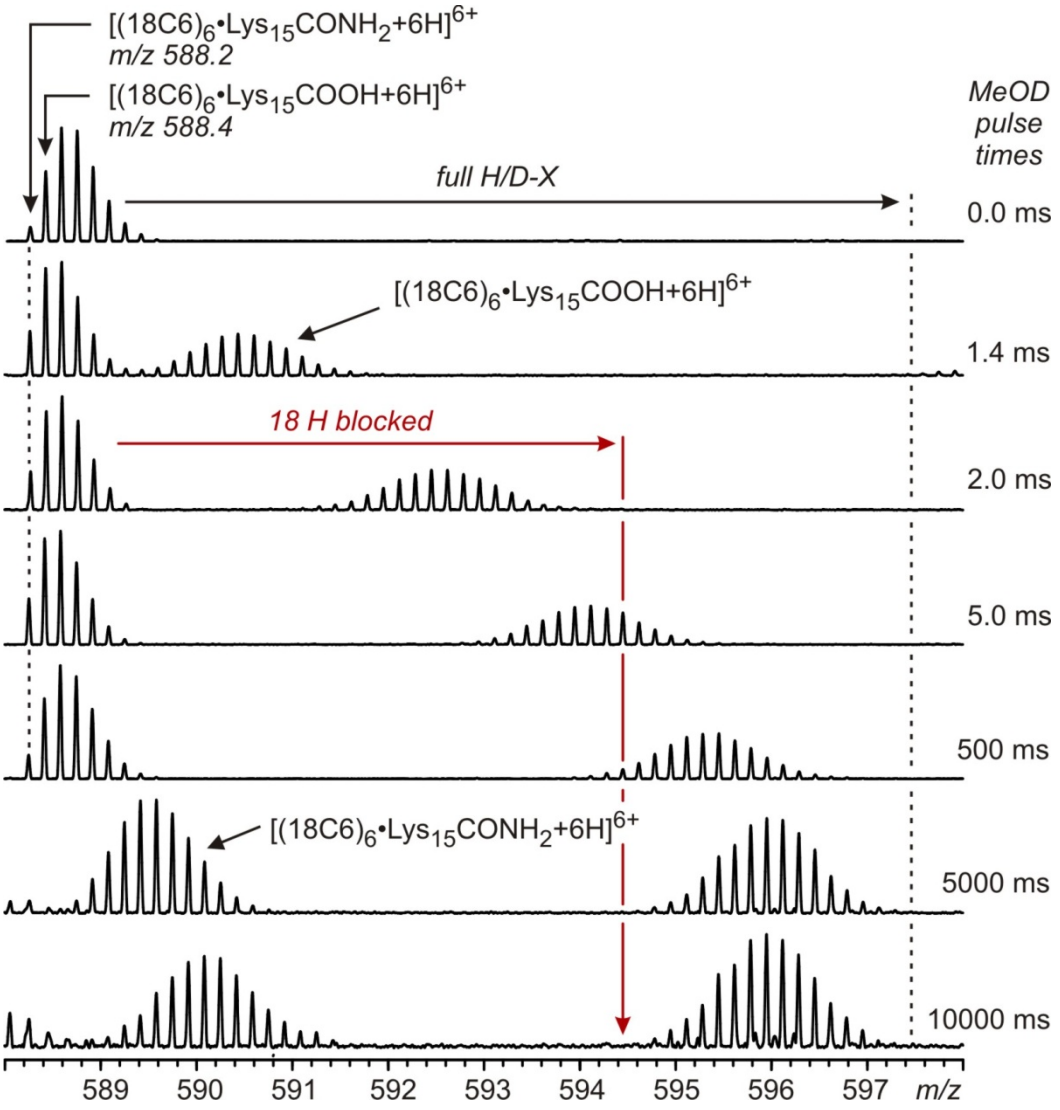

Figure 4.3.19 *A direct comparison of the exchange rates of acid- and amide-terminated crown/Lys$_{15}$ complexes is possible, since both complexes are subjected to the same experiments simultaneously as shown here. In both complexes, the number of crown ethers and charges is identical ($n = z = 6$). Depending on the C-terminal functional group, two very different exchange rates are observed. The vertical arrow indicates, where the exchange reaction should terminate, when 18 hydrogen atoms are protected against H/D exchange by the six crown ethers. The assignment of the two populations is based on the very first peak in the isotope pattern, which corresponds exclusively to the amide-terminated peptide/crown ether complex.*

Figure 4.3.19 shows the simultaneous H/D exchange of $[(18C6)_6•Lys_{15}COOH+6H]^{6+}$ and $[(18C6)_6•Lys_{15}CONH_2+6H]^{6+}$ as a representative example. Both complexes differ in molecular mass by one Da and therefore initially appear with overlapping isotope patterns ($\Delta m/z = 1/6$). Clearly, the acid-terminated $[(18C6)_6•Lys_{15}COOH+6H]^{6+}$ complex ($n = z = 6$)

undergoes a significantly faster H/D exchange as compared to its amide-terminated $[(18C6)_6 \bullet Lys_{15}CONH_2+6H]^{6+}$ analogue. Similar results are obtained for other charge states of the ($n = z$) complexes. This is strong evidence for the zwitterionic nature of $[(18C6)_n \bullet Lys_{15}COOH+nH]^{n+}$. It is important to note that the slow exchange on the amide-terminated $[(18C6)_n \bullet Lys_{15}CONH_2+nH]^{n+}$ complexes does not imply the crown movement to be slow. Only the H/D exchange reaction does not proceed efficiently anymore, while the crown ethers' transfer from an ammonium to a free amino group is likely proceeding with undiminished rate.

4.3.7 Conclusion

In conclusion, intriguingly simple H/D exchange experiments conducted under the well-defined conditions in the high vacuum inside a mass spectrometer provide evidence for the ability of 18-crown-6 to quickly move along oligolysine peptide chains and over the periphery of POPAM dendrimers – in what could be called a "spacewalk" on the molecular level. In addition, mechanistic conclusions can be drawn from the examination of suitable model compounds: The crown ethers move together with a proton from an ammonium to an amino group. Finally, the zwitterionic structure of crown complexes of acid-terminated oligolysine peptides is expressed in the isotope exchange behaviour. Only the unique environment-free conditions of the highly diluted gas phase inside a mass spectrometer provide the ideal means required to investigate the dynamics within non-covalent complexes. Since the investigation of such reactions is difficult, if not impossible in the condensed phase, gas-phase chemistry provides insight into a completely new reactivity of weakly bound supramolecular complexes. The experiments discussed above document the crown ether/oligolysine and crown ether/POPAM dendrimer complexes to be highly dynamic and suggest that many synthetic as well as biological non-covalent complexes may exhibit a more pronounced dynamic behaviour than commonly recognized. Unravelling the dynamics in non-covalent complexes will contribute significantly to the analysis of biomolecular function. The H/D exchange discussed above for the particular example of crown ether/oligolysine and crown ether/POPAM dendrimer complexes establishes a novel and remarkably simple approach to address this mobility phenomenon. From a methodological point of view, the experiments discussed here extend the scope of H/D exchange experiments to the question of large-scale molecular motion, but also point to a potential limitation: An exchange of more hydrogen atoms than expected from a postulated hydrogen-bonded structure of a supramolecular complex or folded biomolecule does not necessarily imply a structural change upon transfer into the gas phase. Dynamic processes may also well contribute to this additional exchange, although the overall structure is indeed the expected one.

4.4 Mass Spectrometric Studies of the Binding Properties of a Resorcinarene-based Anion Receptor[‡]

The resorcin[4]arene based anion receptor (**RAR**) shown in Figure 4.4.1 was constructed by attaching four amine-functionalized side arms to tetramethoxy-resorcinarene. These amine groups (primary and secondary) combined with the possibility of the resorcinarene scaffold to reorganize its conformation to a certain extent might provide a means to bind two guest anions by directional hydrogen bonds as indicated in Figure 4.4.1.

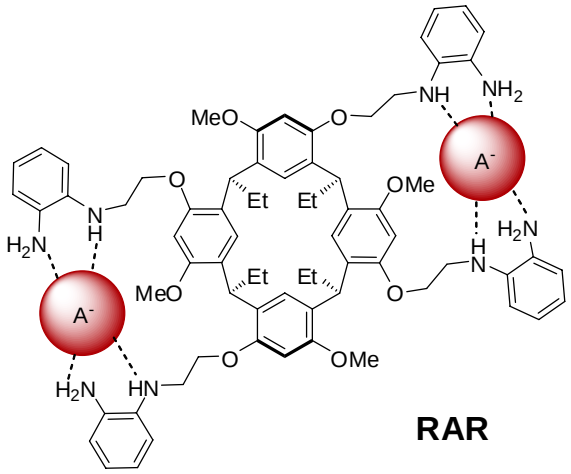

Figure 4.4.1 *Chemical structure of resorcianrene based anion receptor* ***RAR*** *and suggested binding mode for the simultaneous binding of two anions.*

^{1}H NMR experiments with several tetrabutylammonium salts show no interaction of **RAR** towards Cl^-, Br^-, I^-, NO_3^-, PF_6^- and BF_4^-, whereas the addition of the fluoride and acetate salts caused significant changes in the spectra (large downfield shift of the NH and NH_2 protons, upfield shift of the aromatic protons of the resorcinarene core).

^{1}H NMR titration studies in d_6-DMSO revealed the F^- and CH_3COO^- anions to bind to **RAR** in 2:1 soichiometry (two anions + one **RAR**). In case of the fluoride, formation of the HF_2^- anion is observed upon addition of 2 eq. of TBAF.

[‡] The results presented in this chapter have been partially published in:

K. Salorinne, D. P. Weimann, C. A. Schalley, M. Nissinen, *Eur. J. Org. Chem.* **2009**, 6151-6159

These experiments were performed by cooperation partners and will therefore not be disussed here further.

In order to provide additional evidence for the binding of anions to the *neutral* receptor and to gain insight into similarities or solvation-induced differences between the situation in solution and the gas-phase, negative-mode electrospray-ionization mass spectrometric (ESI-MS) experiments were performed. For this purpose, an equimolar solution of **RAR** and each anion (or a combination of two different anions in the case of fluoride and acetate, respectively) was electrosprayed, and the formation of complexes was monitored by high-resolution fourier-transform ion-cyclotron-resonance (FTICR) mass spectra.

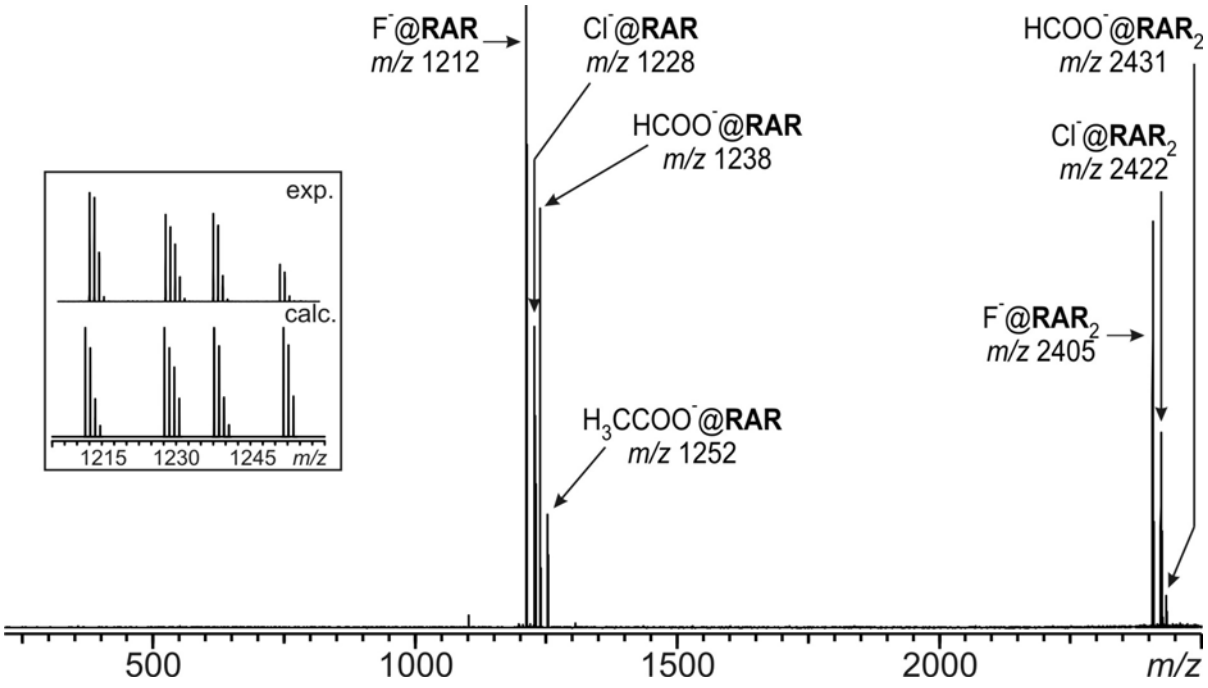

Figure 4.4.2 *Negative mode ESI-FTICR mass spectrum of an equimolar solution of* ***RAR****,* NBu_4F*, and AgOAc in acetonitrile (50 μM). The small signal at m/z 1100 originates from stray radiation.*

Figure 4.4.2 shows the ESI-FTICR mass spectrum obtained from a 50 μM solution of **RAR**, acetate, and fluoride in acetonitrile. In addition to the expected complexes of **RAR** with fluoride and acetate, the complexes with chloride and formate are also formed from background anions. Chloride is almost omnipresent in the negative mode and the formate anion is due to a hard-to-remove memory effect from previous experiments in the positive

mode, in which formic acid was used. It is advantageous to use AgOAc to generate the acetate complexes, because the silver ions help to scavenge background chloride, which however is not possible completely.

Irrespective of the ionization conditions, 1:2 complexes of the receptor and the anion (two anions + one **RAR**) have not been observed – a finding which can be attributed to the significantly stronger repulsion between the two charges in the desolvated complex. Instead, 2:1 complexes are observed, which however are likely due to "unspecific" binding.

An HF_2^- complex of receptor **RAR** is not observed in the gas phase. This is not unexpected, because it would easily lose HF during the ionization/desolvation process, even when initially formed in solution. Consequently, these findings already show that there are differences between the solution situation and that in the gas-phase.

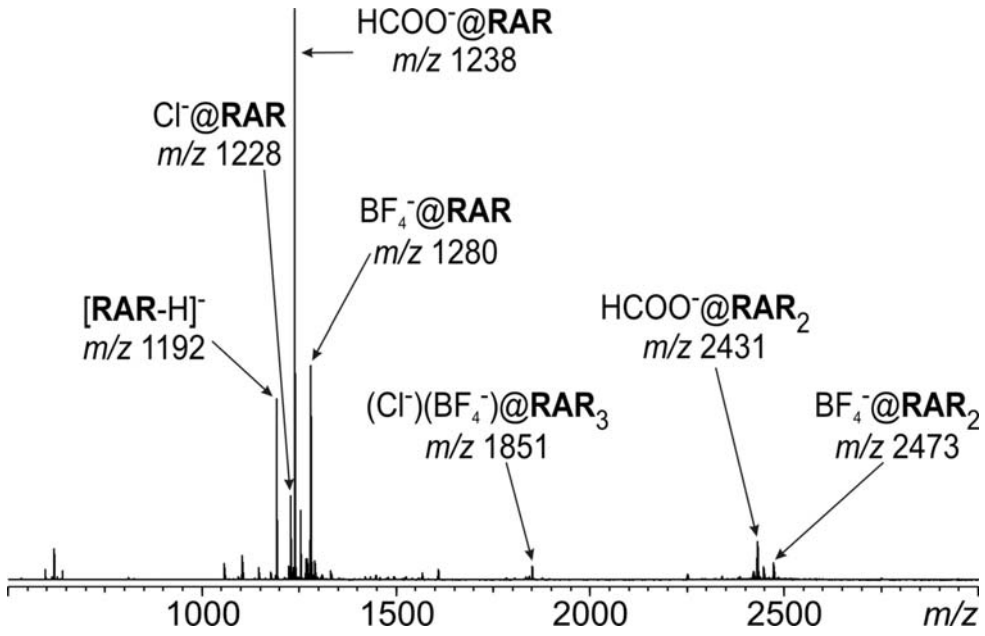

Figure 4.4.3 *Negative mode ESI-FTICR mass spectrum of an equimolar solution of* ***RAR*** *and* $TBABF_4$ *in acetonitrile (50 μM).*

The most remarkable difference between solution and gas-phase binding behavior of **RAR** is that not only fluoride and acetate complexes are observed in the mass spectra. The gas-phase experiments furthermore provide evidence for chloride, nitrate, tetrafluoroborate, and formate to form 1:1 complexes. Likewise, many other anions will certainly bind. Consequently, a number of anions – among them even the weakly binding ones such as BF_4^- (Figure 4.4.3) –

experience attractive interactions with the receptor, although no binding is observed in solution.

This finding can be easily traced back to the competition with the solvent. In the solution studies, DMSO was used, which is a rather strong hydrogenbond acceptor and present in large excess. Consequently, weakly hydrogen-bonding anions cannot compete with the solvent. In the gas phase, however, this competition does not exist and the intrinsic attractive forces are seen that hold the complex together.

It should be briefly noted the mass spectrometric data is not used to monitor solution concentrations of the complexes, but simply refers to the fact that the mere existence of a complex in the gas phase provides evidence for an attractive binding interaction. In that sense, the spray solvent (acetonitrile or methanol in the presented experiments) does not play a role. Furthermore, electrostatic interactions are significantly increased in the gas phase as compared to solution due to the change in permittivity of the medium as expressed in the dielectric constants. The vacuum dielectric constant is 1 by definition, while that of DMSO is 48. Consequently, any electrostatic interaction between the anion and the dipoles of the receptor should increase in strength by a factor of approximately 48 upon the transition into the gas phase. In a tandem mass spectrometric experiment, the complex ions of interest can be mass-selected and subjected to pure gas-phase experiments. After isolation of the parent ions, a 25 W CO_2 laser ($\lambda = 10.6\ \mu m$) was used to fragment the ions in the FTICR cell in an infrared radiative multiphoton dissociation (IRMPD) experiment. The corresponding spectra for three selected anions, i.e. the formate, chloride, and fluoride complexes of **RAR**, are shown in Figure 4.4.4.

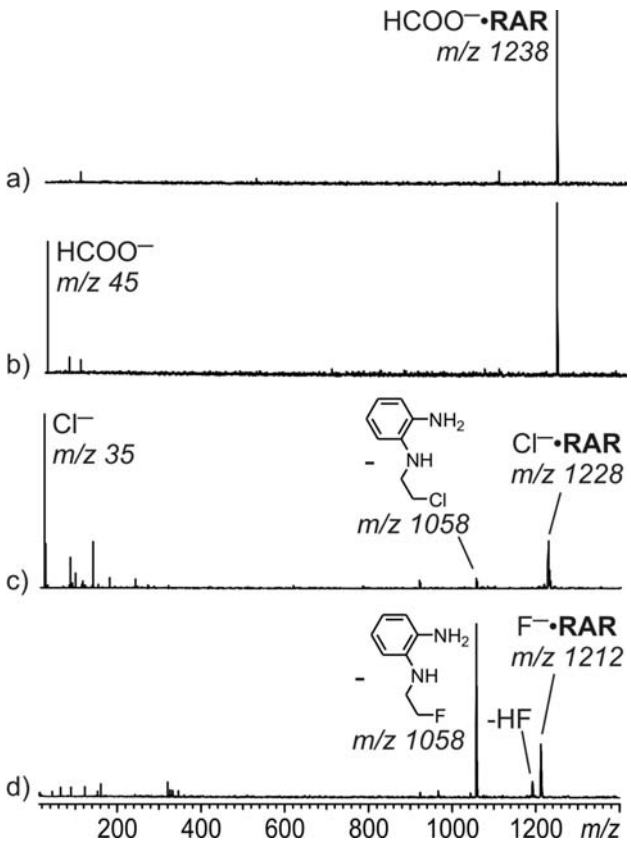

Figure 4.4.4 a) *ESI-FTICR mass spectrum of $HCOO^-$·**RAR** after mass selection. The small signal at m/z 1102 corresponds to stray radiation.* ***b)*** *IRMPD experiment with 500 ms irradiation time of a 25 W IR laser.* ***c)*** *IRMPD experiment conducted with Cl^-·**RAR** under the same conditions.* ***d)*** *Analogous IRMPD experiment with F^-·**RAR**.*

These complexes show interesting differences in their fragmentation behavior (Figure 4.4.5):

(a) The fragmentation spectrum of the formate complex is very simple. The only dominating fragmentation channel is the loss of the complete neutral receptor (Figure 4.4.5, channel A).

(b) For the chloride complex, the complete receptor loss is again by far the most abundant fragmentation channel, but in addition a quite low-intensity fragment is observed at *m*/*z* 1057. It can be attributed to a nucleophilic attack of the almost naked chloride at the spacer connecting one of the branches to the resorcinarene scaffold (Figure 4.4.5, channel B).

(c) For the fluoride complex, no loss of the complete receptor is observed anymore. Instead, the anion is so nucleophilic in the absence of a solvent that channel B becomes by far the major one.

The fact that the fragment (*m*/*z* 1057) appears at the same *m*/*z* as that observed in the MS/MS spectrum of the chloride complex also confirms that the halide is incorporated in the neutral fragment in both cases. This reaction is already quite remarkable in that a reaction involving covalent bonds smoothly proceeds as the major reaction pathway within a noncovalent complex.[117] Noncovalent bond fragmentation cannot efficiently compete, which indicates how strongly bound the fluoride indeed is. But a second aspect is also important to note: As a minor fragment, a loss of HF is observed at *m*/*z* 1191. In view of the proton affinities of fluoride (1529 kJ/mol)[118] and anilide (1502 kJ/mol)[119] as a model compound for the receptor for which the gas-phase thermochemical data is known, fluoride is capable of deprotonating the receptor in the gas phase. This aspect nicely closes the cycle back to the above discussed solution-phase binding of the HF_2^- anion. These fragmentation spectra clearly reflect the properties of the different anions, for example the much higher nucleophilicity and basicity of fluoride in the gas phase.

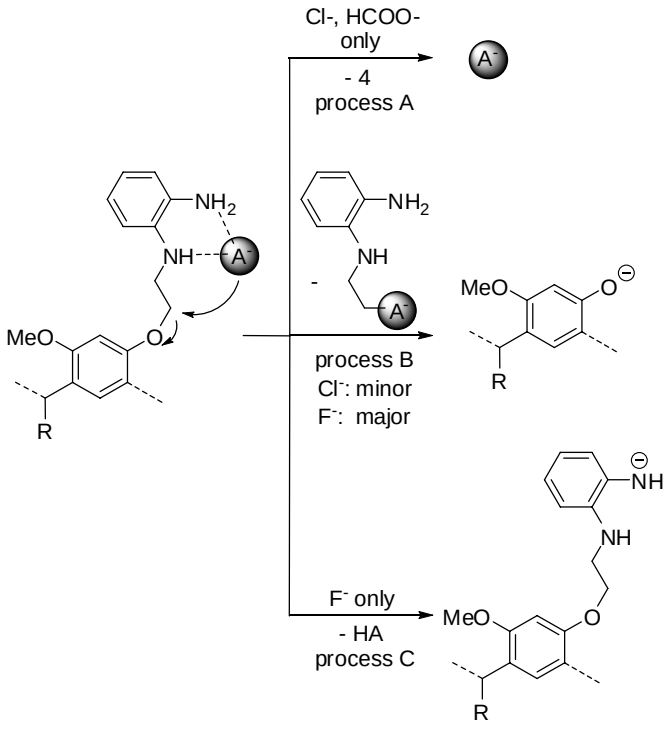

Figure 4.4.5 *Fragmentation reactions observed in the tandem MS spectra shown in Figure 4.4.4.*

To gain more insight into the anion binding mode of **RAR**, gas-phase H/D exchange experiments were performed according to the experimental protocol described in chapter 4.3.
It is known from previous works that hydrogen atoms involved in hydrogen binding of guest molecules might be protected against such an exchange.[87,88,89,92] Therefore, this method has been previously applied to macrocyclic oligourea anion receptors.[120]
As shown in Figure 4.4.6, a maximum of nine of the twelve N-centered protons in the chloride and formate complexes of **RAR** can be exchanged for deuterium, even after very long reaction times of 10 minutes. In the control experiment with deprotonated [**RAR**-H]$^-$, it is possible to exchange ten of the eleven protons for deuterons (spectra not shown), which most probably is due to the reaching of a saturation limit that should be the same for the 1:1 complexes with Cl^- and $HCOO^-$, making these experiments comparable.
The difference of **two** exchanged protons between deprotonated receptor and anion complex suggests the anions to be bound by two hydrogen bonds in the gas phase.

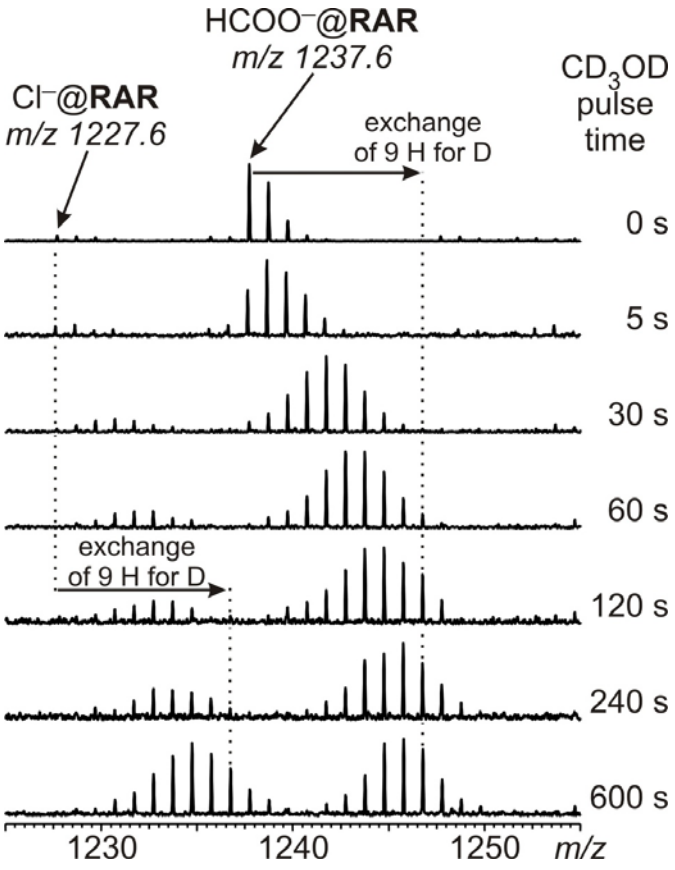

Figure 4.4.6 *Fragmentation Gas-phase H/D exchange reaction performed with the chloride and formate complex of resorcinarene based anion receptor* ***RAR.***

In conclusion, it could be shown that mass spectrometry is perfectly suited to examine weak non-covalent interactions such as anion binding through hydrogen bonding, so that the gas-phase experiments described above were able to deliver the proof for the binding of additional anions by the resorcinarene-based anion receptor under study, which could not be seen in the solution studies.

Gas-phase IRMPD experiments reflect the relative gas-phase nucleophilicity of the bound anions: the stonger nucleophlic ones (F^- > Cl^- >> $HCOO^-$) are able to nucleophilicly attack the receptor upon laser irradiation instead of simply dissociating from the neutral receptor.

Finally, gas-phase H/D exchange experiments according to the same experimental protocol as described above (see chapter 4.3) could give a basic understanding of the binding mode of the anions: Most probably, they are simply bound by a single hydrogen bond.

4.5 Gas-Phase Studies of Anion Binding to Naphthalene Diimide Systems[§]

Although anion-π interactions have been confirmed in theory to exist, they have never really been observed at work.[121] To catch them in action, a series of monomeric and cyclic naphthalenediimide (**NDI** and **NDIM**) transporters was prepared with a systematic variation of π-acidity, active-site confinement and supramolecular organizability (Figure 4.5.1 and 4.5.2).[122-126] Their ability to exert anion-π interactions was investigated by ESI-FTICR mass spectrometry. Tandem-MS experiments were performed to qualitatively evaluate the binding ability of the different host molecules.

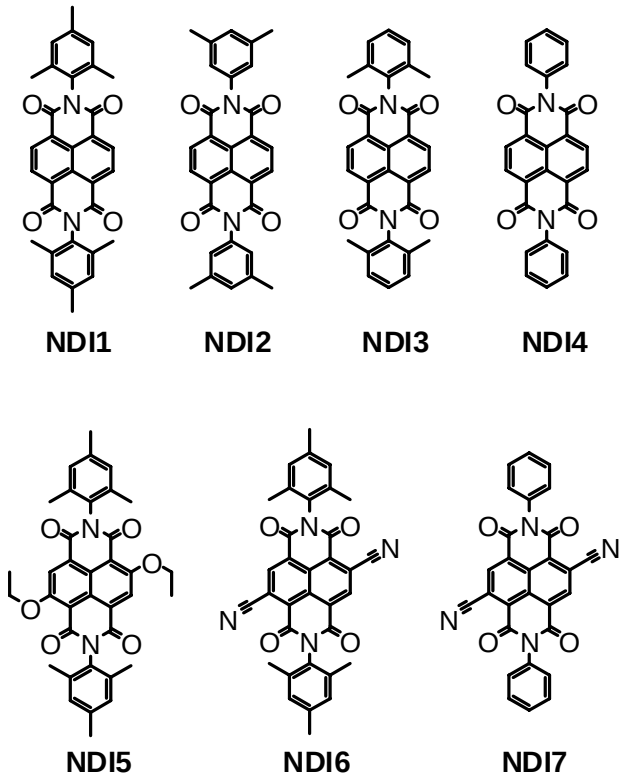

Figure 4.5.1 Chemical structures of the different monomeric naphthalene diimide systems (**NDI**) investigated with respect to their anion-binding behavior.

[§] The results presented in this chapter have been partially published in:

R. E. Dawson, A. Hennig, D. P. Weimann, D. Emery, V. Ravikumar, J. Montenegro, T. Takeuchi, S. Gabutti, M. Mayor, J. Mareda, C. A. Schalley, S. Matile, *Nature Chem.* **2010**, *2*, 533-538

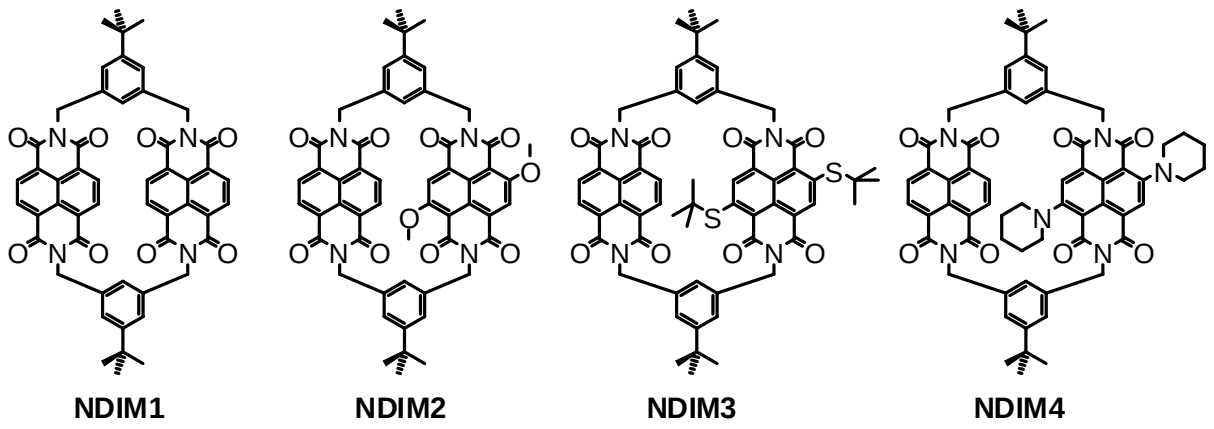

Figure 4.5.2 Chemical structures of the different macrocyclic naphthalene diimide dimers (**NDIM**) investigated for their anion-binding behavior.

Whereas the detection of anion-π interactions via NMR and ITC experiments was not possible with NDI monomers, because anion binding is too weak and solvent interactions are too competitive, ESI-MS and ESI-MS/MS experiments should be able to deliver the desired direct experimental evidence for anion-π interactions. Gas-phase studies offer the additional advantage that non-solvated complexes are monitored, which can be compared more easily to quantum chemical calculations than the corresponding complexes in solution.

4.5.1 Basic Mass Spectrometric Studies of the Anion Binding to Monomeric and Dimeric Naphthalene Diimide Hosts

In a first step, equimolar, 50 μM solutions of **NDI1** or **NDIM1** and salts of different anions were electrosprayed from acetonitrile (methanol gives the same results) under as mild as possible ionization conditions, to examine, whether ESI mass spectrometry can be applied to monitor anion binding to NDI systems. Quite fragile 1:1 complexes of **NDI1** and anion were observed for Cl^-, Br^- and NO_3^- (see figure 4.5.3 for an example of a typical ESI-FTICR mass spectrum). For chloride and bromide, also 2:1 complexes are formed.

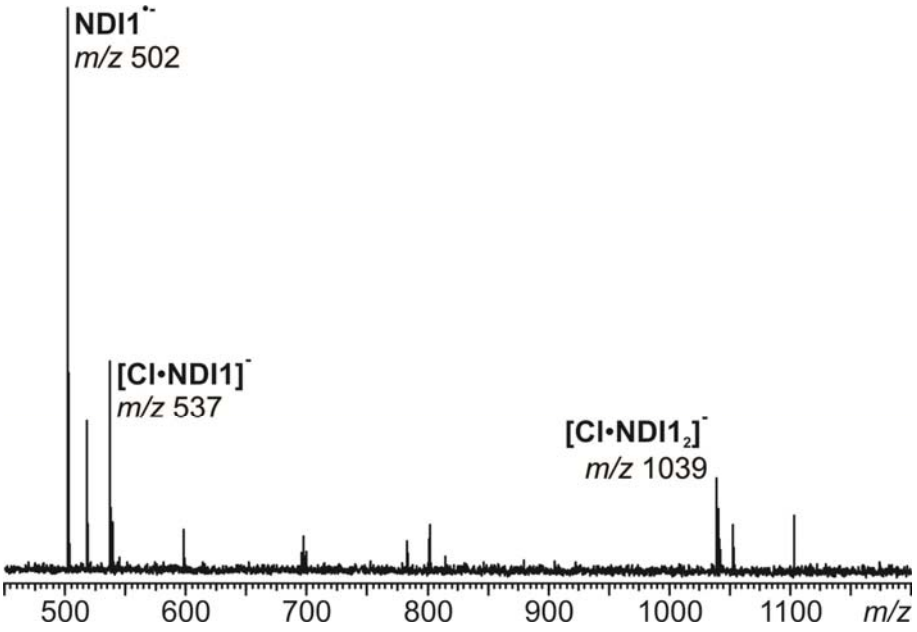

Figure 4.5.3 *ESI-FTICR mass spectrum of an equimolar 50 μM solution of* ***NDI1*** *and NEt_4Cl in acetonitrile: besides the radical anion of* ***NDI1****, which is formed by reduction on the spray capillary, 1:1 and 2:1 complexes of* ***NDI1*** *and chloride are observed. The signal at m/z 518 corresponds to oxidized* ***NDI1****, which most probably also is formed during the electrospray process.*

Furthermore, these simple MS experiments unraveled a much higher ability to bind anions for the macrocyclic NDI cyclophane **NDIM1**. Because of the apparently stronger binding to dimer **NDIM1**, an additional series of anions was observed to bind: Adduct detectability decreased with $NO_3^- \sim Cl^- \sim Br^-$ (1:1 and 2:1 adducts) > $I^- \sim H_2PO_4^- \sim OTf^- \sim ClO_4^-$ (1:1 adducts) > $OAc^- \sim BF_4^-$ (weak 1:1 adducts) >> $PF_6^- \sim BPh_4^- \sim SO_4^{2-} \sim MnO_4^-$ (not detected). Figure 4.5.4 shows an example of this series.

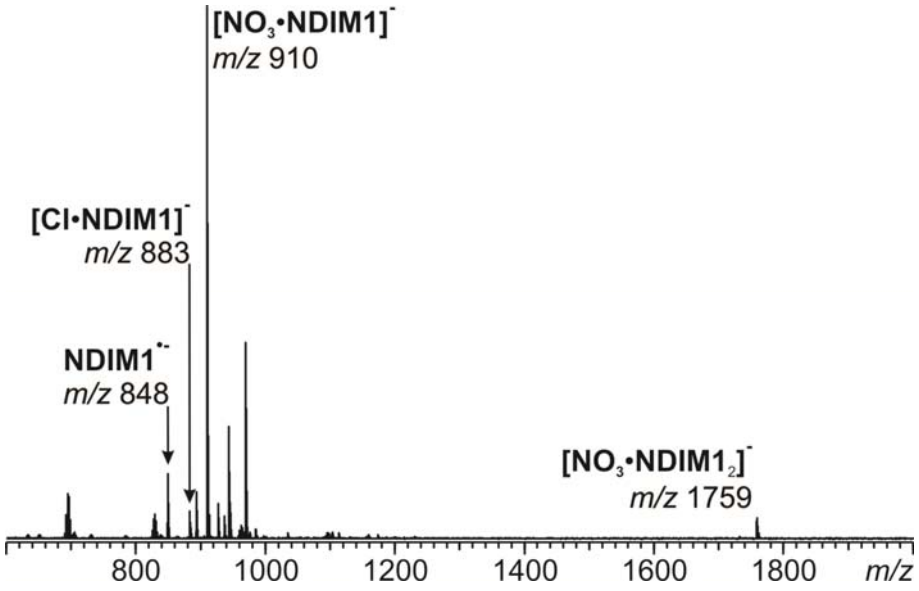

Figure 4.5.4 *ESI-FTICR mass spectrum of an equimolar 50 μM solution of* ***NDI1*** *and $AgNO_3$ in acetonitrile: besides the radical anion of* ***NDIM1****, which is formed by reduction on the spray capillary, 1:1 and 2:1 complexes of* ***NDI1*** *and nitrate are observed. The use of $AgNO_3$ is advantageous to generate the nitrate complexes, because the silver ions help to scavenge background chloride, which however is not possible completely.*

The much higher anion binding ability of the macrocyclic NDI cyclophane **NDIM1** might be explained by binding simultaneously to two NDI faces. This however, would force the NDIM to adopt kind of a "bowl" shape as opposed to parallel NDI planes that would not provide enough space for the incorporation of an anion. The optimal binding distance between the chloride anion and the NDI plane was found to be approximately 3 Å according to DFT calculations.[127] Parallel NDI planes are observed in the solid state structure of **NDIM3** with a distance of 4.3 – 4.8 Å,[131] whereas the more bowl-like shape is found in the solid state structure of **NDIM1**.[128] This shows that both conformations are reasonable and most probably do not differ too much in energy.

The unambiguous identity of the NDI-anion complexes can be assured by the determination of exact mass-to-charge ratios. As an additional proof, the 1:1 complex of **NDIM1** and chloride was isolated in the gas phase and fragmented by irradiation with a 25 W IR laser (λ = 10.6 μm). Upon excitation, the complex releases neutral **NDIM1** and "naked" chloride ions are left (Figure 4.5.5).

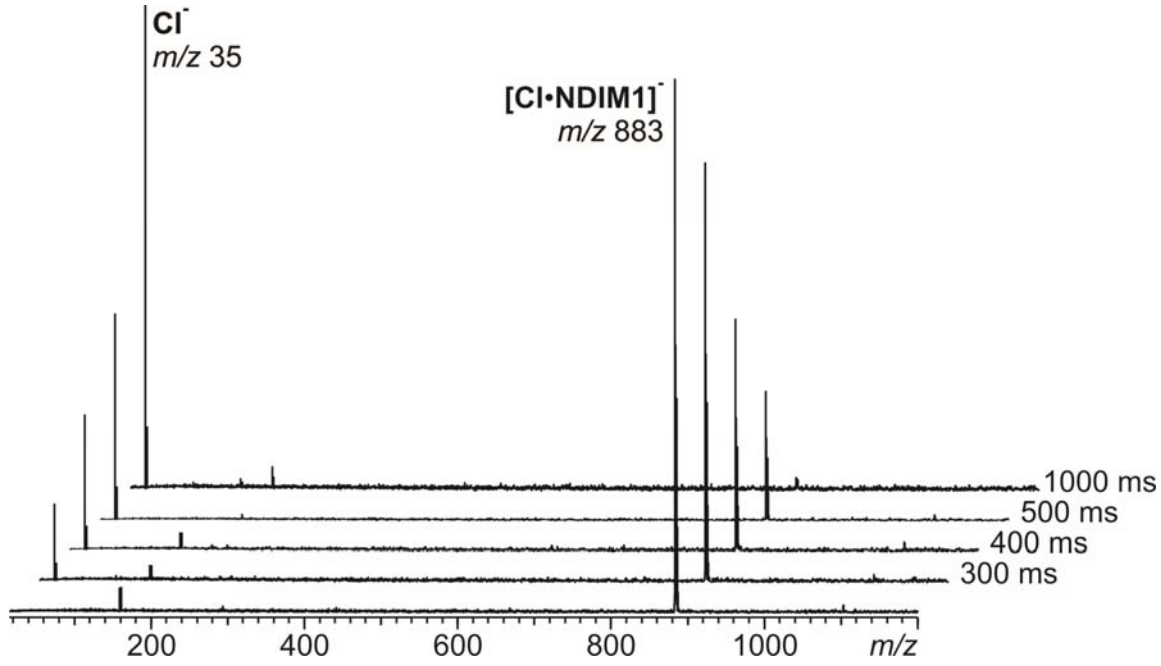

Figure 4.5.5 *Gas-phase isolation and laser induced fragmentation of the 1:1 complex of* ***NDIM1*** *chloride. The laser irradiation time is given on the right side of each spectrum.*

Although very qualitative as long as no ESI response factors are known,[129] in the basic ESI-MS studies, an apparent preference for chloride among halides and nitrate among oxyanions can be seen (see Table 4.5.1 for an overview on the anions binding to monomeric and macrocyclic NDIs). In this context, it should also be noted that chloride complexes appear in almost every spectrum originating from the NDI hosts strongly binding background chloride.

Anion	NDI1	NDIM1
Cl^-	[Cl^-•**NDI1**] + [Cl^-•**NDI1**$_2$]	[Cl^-•**NDIM1**] + [Cl^-•**NDIM1**$_2$]
Br^-	[Br^-•**NDI1**] + [Br^-•**NDI1**$_2$] + [Cl^-•**NDI1**] + [Cl^-•**NDI1**$_2$]	[Br^-•**NDIM1**] + [Br^-•**NDIM1**$_2$]
I^-	X	[I^-•**NDIM1**]
OTf^-	X	[OTf^-•**NDIM1**]
$H_2PO_4^-$	X	[$H_2PO_4^-$•**NDIM1**]
BF_4^-	X	[BF_4^-•**NDIM1**] (very weak)
BPh_4^-	-	X
PF_6^-	X	X
CH_3COO^-	X	[CH_3COO^-•**NDIM1**] (very weak)
NO_3^-	[NO_3^-•**NDI1**]	[NO_3^-•**NDIM1**] + [NO_3^-•**NDIM1**$_2$]
MnO_4^-	-	X
ClO_4^-	-	[ClO_4^-•**NDIM1**]
SO_4^{2-}	-	X
Cl^- & I^-	-	[Cl^-•**NDIM1**] + [I^-•**NDIM1**] (~ 10:1) (+ [Cl^-•**NDIM1**$_2$])

Table 4.5.1 *Overview on the anion binding to naphthalene diimide systems from ESI-FTICR mass spectrometric experiments with different salts (X = no complex observed; - = experiment not performed).*

4.5.2 Gas-Phase Competition Experiments with Monomeric Naphthalene Diimide Systems

While the mere formation of NDI/anion complexes already clearly indicates the operation of attractive interactions between both, the formation of dimers was used for true gas-phase competition experiments with the differently substituted NDI monomers **NDI1** - **NDI7** and chloride as the preferred anion.

For these studies, an equimolar mixture of each two NDIs was electrosprayed together with one equivalent of NEt_4Cl, and the corresponding heterodimer **NDIa**+**NDIb**+Cl^- was mass-selected in the FTICR analyzer cell. Fragmentation of the heterodimer was then induced by irradiation with a 25 W IR laser (Infrared Multiphoton Dissociation; IRMPD experiment).

Figure 4.5.6 shows the gas-phase isolation and laser-induced fragmentation of the heterodimeric NDI complex [Cl•**NDI1**•**NDI2**]$^-$. After 100 ms irradiation, the original peak for the heterodimer nearly disappeared and a two new peaks for [Cl•**NDI1**]$^-$ and [Cl•**NDI2**]$^-$ appeared with approximately equal intensities (Figure 4.5.6 bottom). This observation demonstrates chloride to bind just as strongly to **NDI1** as to **NDI2**.

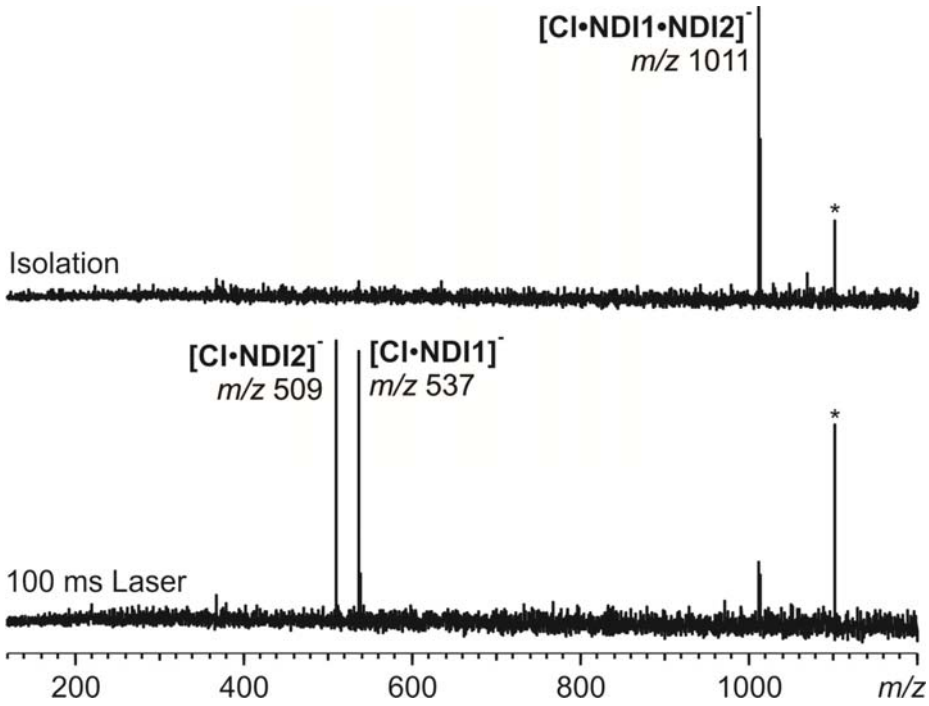

Figure 4.5.6 *Gas-phase isolation of the heterodimeric complex* ***NDI1•NDI2*** *with one chloride (top) and laser-induced fragmentation induced by a 100 ms laser pulse (bottom). The asterisk denotes a signal originating from stray radiation.*

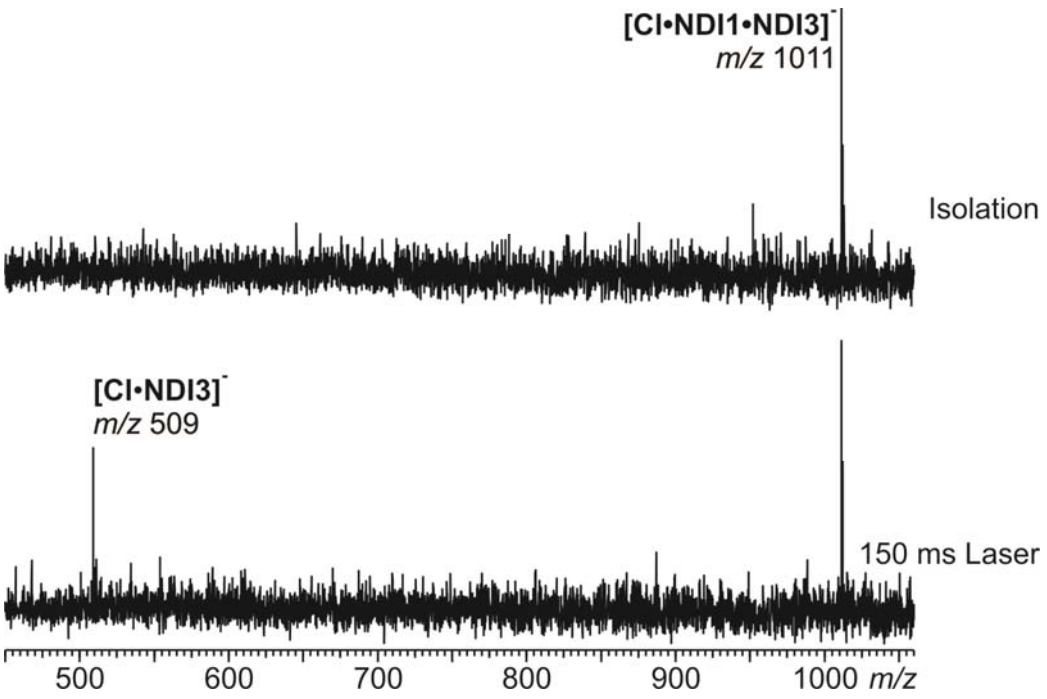

Figure 4.5.7 *Gas-phase isolation of the heterodimeric complex* ***NDI1•NDI3*** *with one chloride (top) and laser-induced fragmentation induced by a 150 ms laser pulse (bottom).*

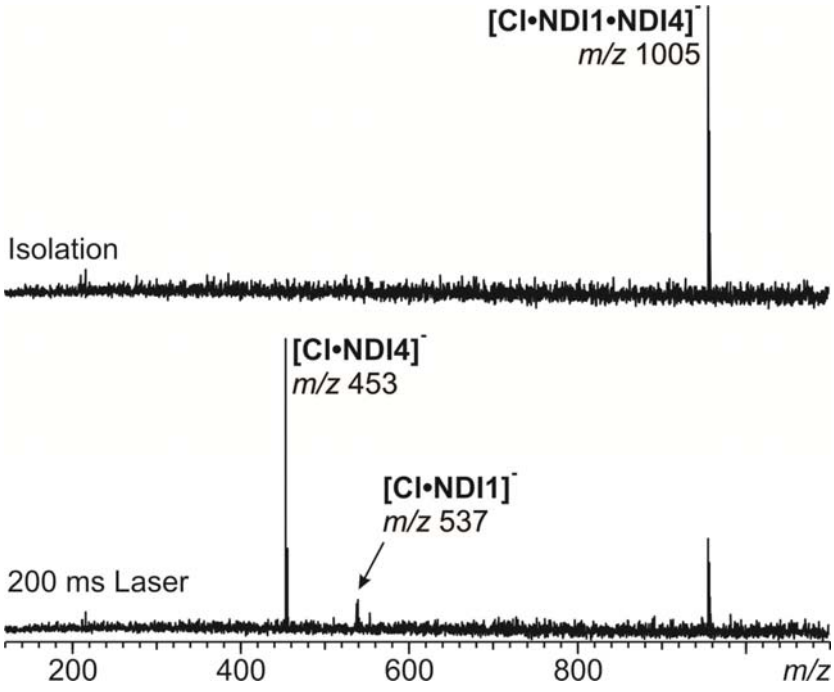

Figure 4.5.8 *Gas-phase isolation of the heterodimeric complex* ***NDI1•NDI4*** *with one chloride (top) and laser-induced fragmentation induced by a 200 ms laser pulse (bottom).*

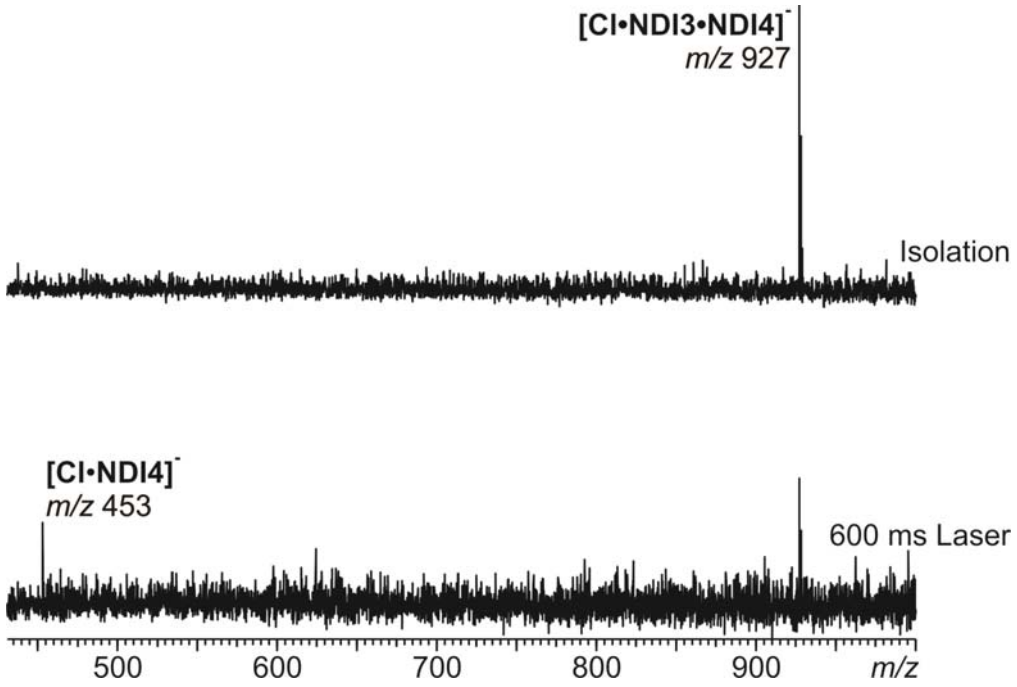

Figure 4.5.9 *Gas-phase isolation of the heterodimeric complex* ***NDI3•NDI4*** *with one chloride (top) and laser-induced fragmentation induced by a 600 ms laser pulse (bottom).*

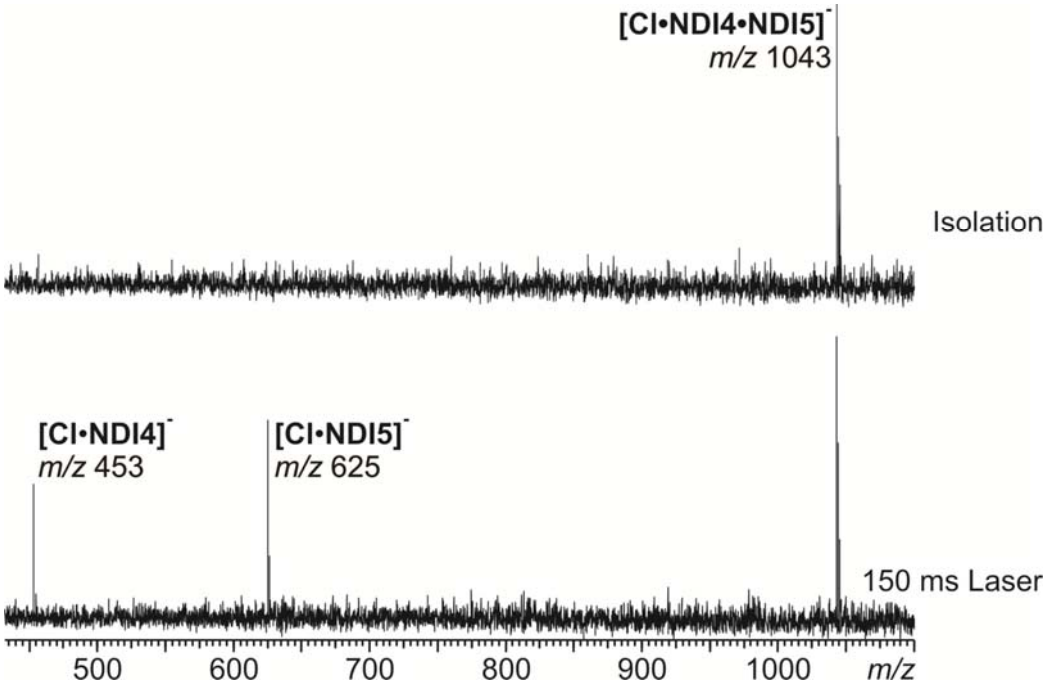

Figure 4.5.10 *Gas-phase isolation of the heterodimeric complex* ***NDI4•NDI5*** *with one chloride (top) and laser-induced fragmentation induced by a 150 ms laser pulse (bottom).*

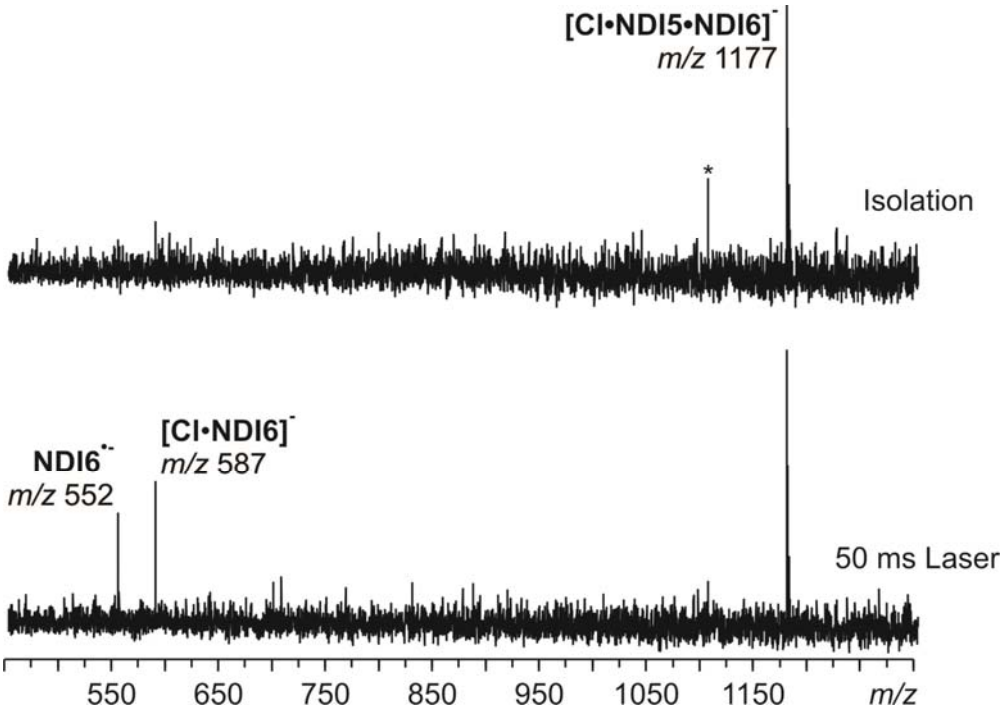

Figure 4.5.11 *Gas-phase isolation of the heterodimeric complex* ***NDI5•NDI6*** *with one chloride (top) and laser-induced fragmentation induced by a 50 ms laser pulse (bottom). The asterisk denotes a signal originating from stray radiation.*

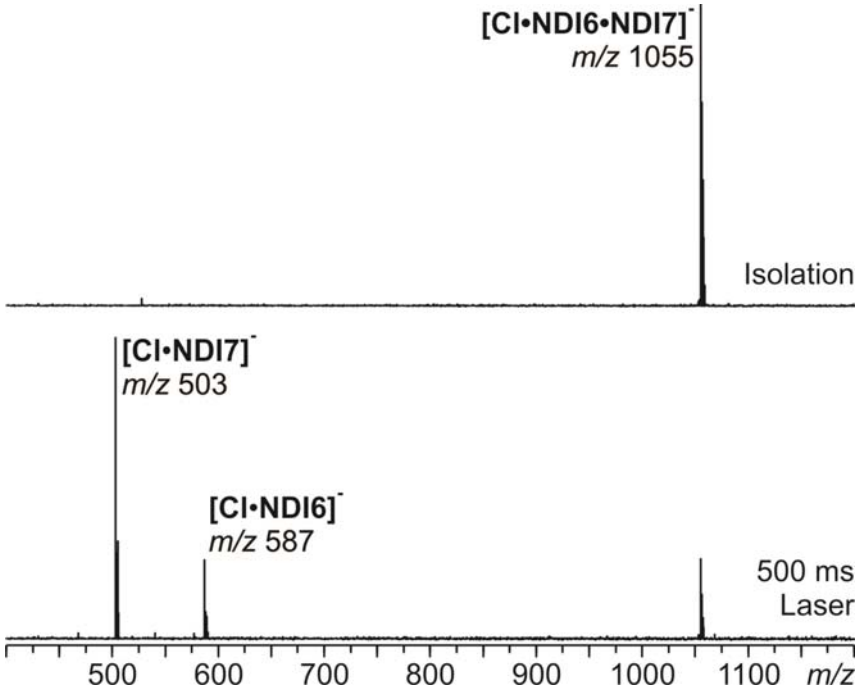

Figure 4.5.12 *Gas-phase isolation of the heterodimeric complex* ***NDI6•NDI7*** *with one chloride (top) and laser-induced fragmentation induced by a 500 ms laser pulse (bottom).*

The same tandem ESI-MS experiment revealed that chloride prefers **NDI3** over **NDI1** (Figure 4.5.7), **NDI4** over **NDI1** (Figure 4.5.8), **NDI4** over **NDI3** (Figure 4.5.9), **NDI5** over **NDI4** (Figure 4.5.10), **NDI6** over **NDI5** (Figure 4.5.11), and **NDI7** over **NDI6** (Figure 4.5.12).
In case of the heterodimer [Cl•**NDI5**•**NDI6**]$^-$, apparently a charge transfer from chloride to **NDI6** takes place upon irradiation with the IR laser causing the release of an **NDI6**$^{\bullet -}$ radical anion from the heterodimer (Figure 4.5.11 bottom).
In contrast to the more qualitative results from routine ESI-MS measurements, intensities found in ESI-FTICR-MS/MS experiments relate to true gas phase experiments and can be used to determine anion affinity sequences quantitatively.[129]

The selectivity sequence found is **NDI7** > **NDI6** >> **NDI5** > **NDI4** > **NDI3** > **NDI2** ≈ **NDI1** and demonstrates increasing anion affinity with increasing π-acidity and decrowding of the anion-π binding site (Figure 4.5.13). The π-acidity mainly relates to the electron withdrawing properties of the substituents on the NDI core. Furthermore, polarizability seems to play an additional role: ethoxy substituted **NDI5** shows an unexpectedly high anion binding behavior, which can only be explained by invoking the increased polarizability of the NDI receptor by the OEt substituents.
From the fragmentation of the complex [Cl•**NDI1**•**NDI2**]$^-$ (Figure 4.5.6), one can clearly see that C-H-anion interactions (between the CH_3 groups in position 2 and/or 6 and the anion) apparently do not play a role for the anion recognition, as the chloride anion does not preferably stick to one of the two receptors after fragmentation.

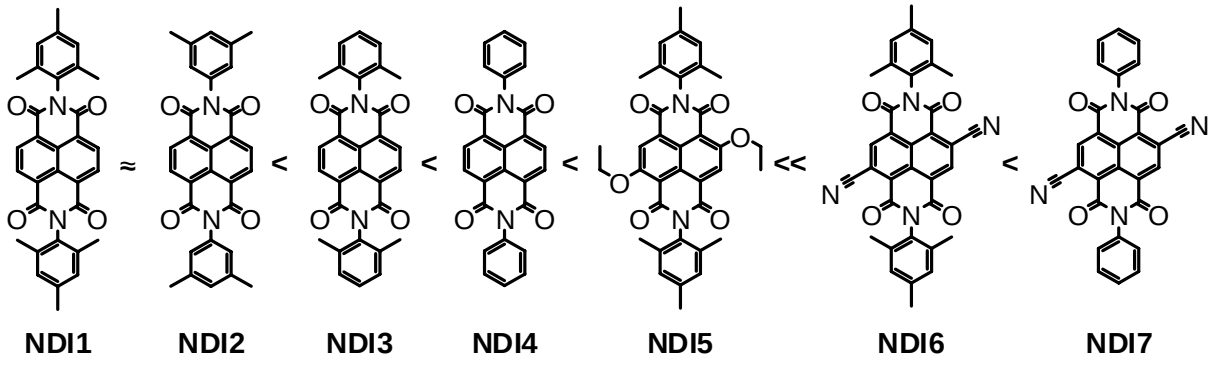

Figure 4.5.13 *Structures of differently substituted NDI monomers and their order of binding strength towards chloride as obtained from gas-phase fragmentation experiments.*

The results described above provide direct experimental evidence for anion binding to minimalist NDI models that contain nothing else to bind to than a π-acidic surface.

Furthermore, the observed chloride binding behavior is perfectly in line with the results obtained from solution phase transport experiments (performed by Andreas Hennig, group of Prof. S. Matile, University of Geneva) that showed the NDIs to work as anion transporters able to transport chloride into large unilamellar vesicles composed of egg yolk phosphatidylcholine loaded with the chloride-sensitive fluorophore lucigenin.[130] These experiments revealed the highest anion binding capability for phenyl substituted **NDI4** and di-cyano-substituted **NDI6**, however, they were not able to provide direct evidence for the binding of anions to the NDIs.

4.5.3 The Unexpected Formation of Heptameric Complexes with Monomeric Naphthalene Diimides ($[NDI_7 \bullet Cl]^-$)

During the basic binding studies (chapter 4.5.1) as well as during the competition experiments (chapter 4.5.2), some of the NDI systems showed a remarkably high preference for the formation of heptameric complexes of the form $[Cl \bullet \mathbf{NDI}_m \bullet \mathbf{NDI'}_n]^-$ (m + n = 7).

Figure 4.5.14 shows the ESI-FTICR mass spectrum of an equimolar 50 μM solution of **NDI1** and NEt_4Cl in acetonitrile with optimized ionization conditions, ion-transfer and detection parameters for maximum appearance of large ions. The spectrum shows the $[Cl \bullet \mathbf{NDI1}_7]^-$ complex as the by far most prominent signal.

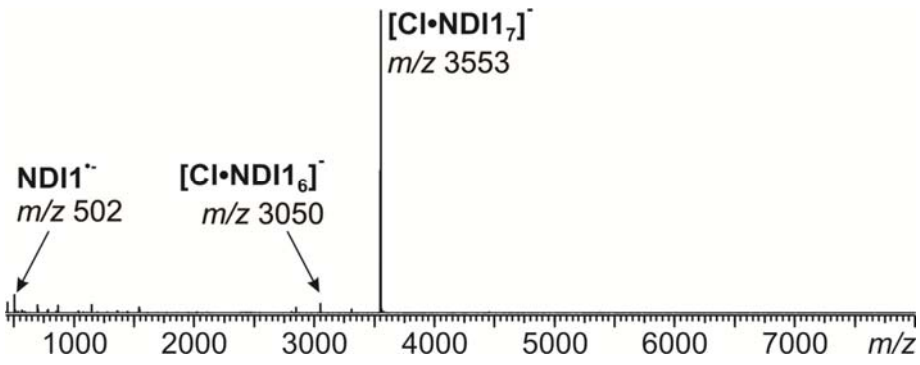

Figure 4.5.14 *ESI-FTICR mass spectrum of an equimolar 50 μM solution of* ***NDI1*** *and NEt_4Cl in acetonitrile. Ionization conditions as well as ion-transfer and detection parameters were optimized towards high molecular masses. Besides the radical anion of* ***NDI1****, which is formed by reduction on the spray capillary, 6:1 and intense signals for the 7:1 complexes of* ***NDI1*** *and chloride are observed.*

It should be noted that homo-heptamers are only formed with mesityl substituted **NDI1**, whereas other NDIs only form hetero-heptamers in combination with **NDI1 (**Figures 4.5.14 - 4.5.18).

Figure 4.5.15 shows the ESI-FTICR mass spectrum of an equimolar 50 μM solution of **NDI1**, **NDI2**, and NEt_4Cl in acetonitrile. The spectrum shows considerably intense signals for the heptameric complexes $[Cl \bullet \mathbf{NDI1}_7]^-$ and $[Cl \bullet \mathbf{NDI1}_6 \bullet \mathbf{NDI2}]^-$ (and also several 1:1, 2:1, and 3:1 complexes of NDIs and chloride).

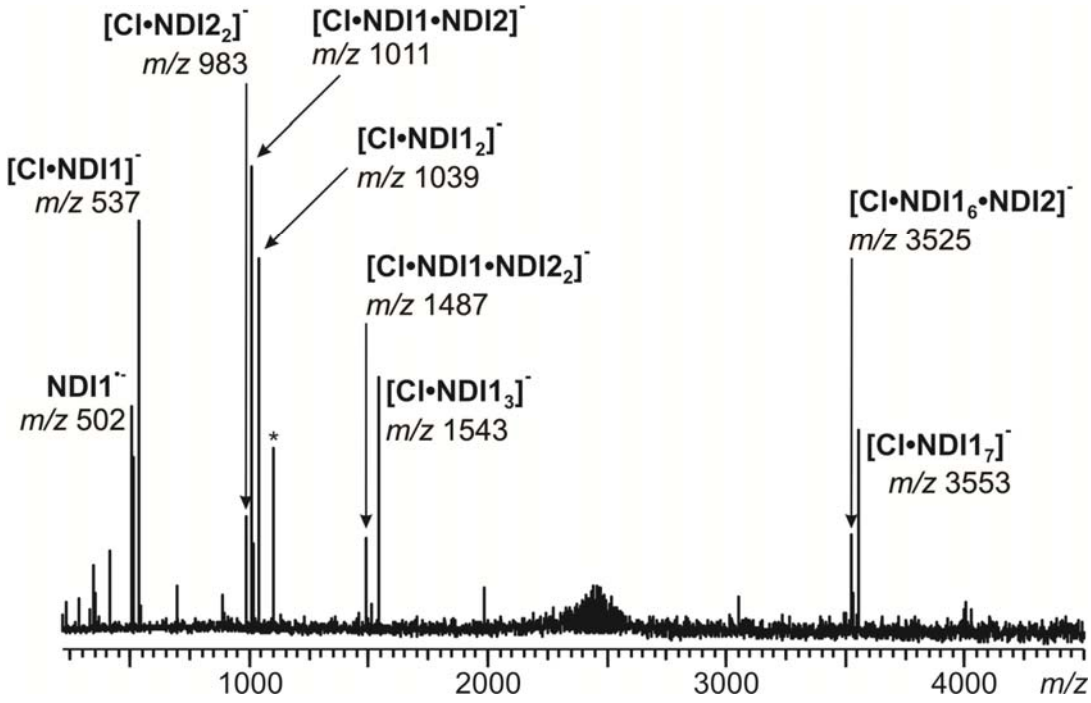

Figure 4.5.15 *ESI-FTICR mass spectrum of an equimolar 50 μM solution of* ***NDI1***, ***NDI2***, *and NEt_4Cl in acetonitrile. Ionization conditions as well as ion-transfer and detection parameters were chosen similar to the experiment with only* ***NDI1***. *Besides the radical anion of* ***NDI1***, *several NDI dimers and trimers of different composition can be found. Furthermore, two different NDI heptamers are observed with considerably high intensity. The asterisk denotes a signal originating from stray radiation.*

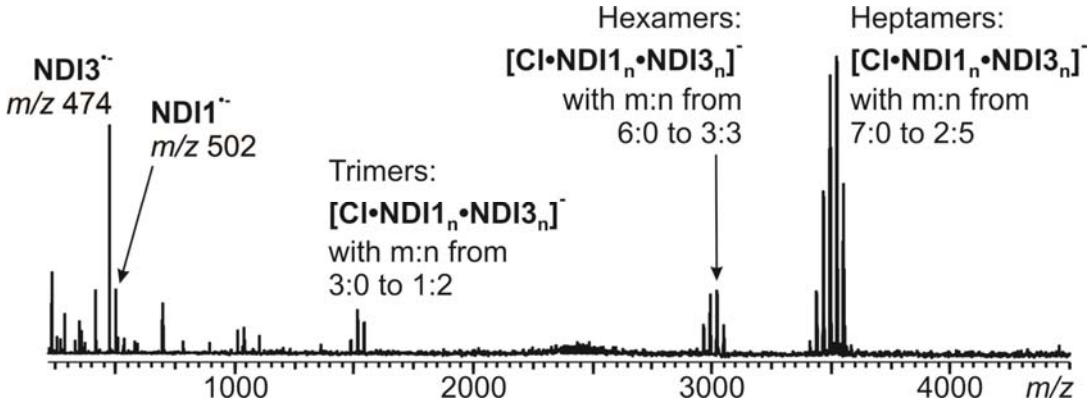

Figure 4.5.16 *ESI-FTICR mass spectrum of an equimolar 50 μM solution of* ***NDI1***, ***NDI3***, *and NEt_4Cl in acetonitrile. Ionization conditions as well as ion-transfer and detection parameters were chosen similar to the experiment with only* ***NDI1***. *Besides the radical anions of* ***NDI1*** *and* ***NDI3***, *several NDI trimers of different composition can be found. Furthermore, a broad distribution of NDI hexamers and heptamers is observed with considerably high intensity.*

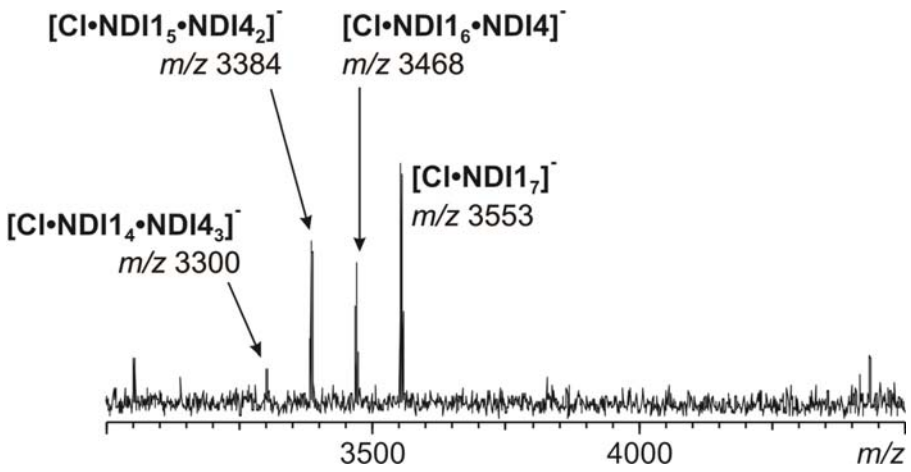

Figure 4.5.17 *High-mass region of the ESI-FTICR mass spectrum of an equimolar 50 μM solution of* ***NDI1***, ***NDI4***, *and NEt_4Cl in acetonitrile. Ionization conditions as well as ion-transfer and detection parameters were chosen similar to the experiment with only* ***NDI1***. *As observed for* ***NDI1*** *and* ***NDI3***, *a broad distribution of NDI heptamers is found with considerably high intensity.*

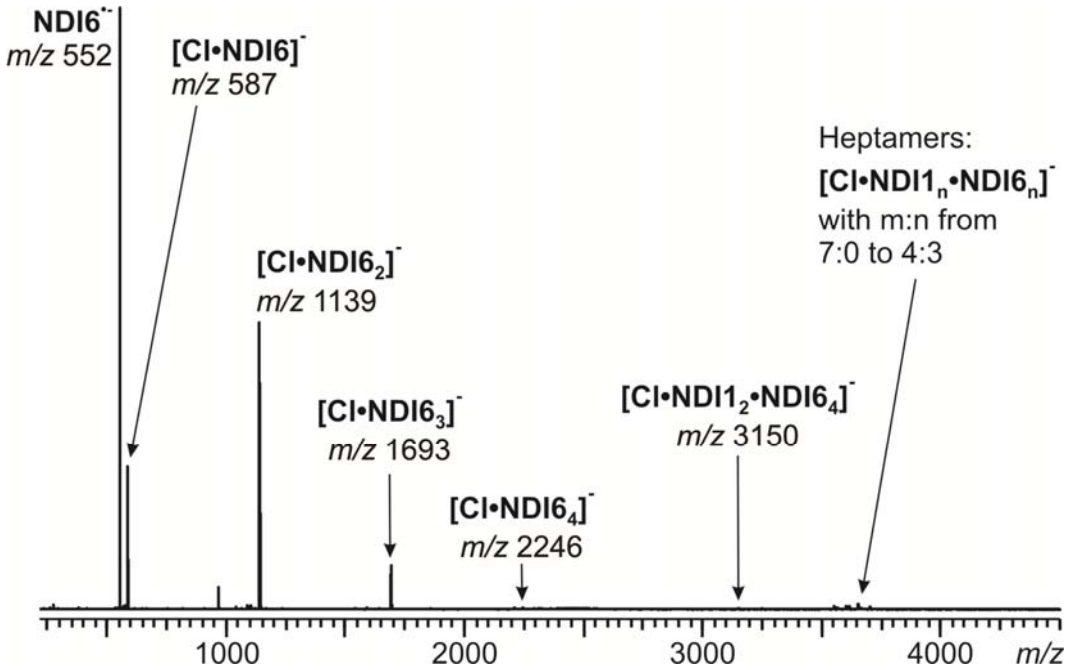

Figure 4.5.18 *ESI-FTICR mass spectrum of an equimolar 50 μM solution of* ***NDI1***, ***NDI6***, *and NEt_4Cl in acetonitrile. Besides the radical anion of* ***NDI6*** *and several 1:1, 2:1, 3:1, and 4:1 complexes of* ***NDI6*** *and chloride, a broad distribution of NDI heptamers is observed with rather low intensity.*

For the combination of **NDI1** and **NDI3** as well as for **NDI1** and **NDI4**, broad distributions of heptamers are observed besides smaller oligomers. These range from [Cl•**NDI1**$_7$]$^-$ to [Cl•**NDI1**$_2$•**NDI3**$_5$]$^-$ and from [Cl•**NDI1**$_7$]$^-$ to [Cl•**NDI1**$_4$•**NDI3**$_3$]$^-$ **(**Figures 4.5.16 & 4.5.17).

If **NDI1** and **NDI6** are combined, smaller complexes in the range of monomer to tetramer are observed for **NDI6** exclusively – owing to the much higher anion binding capability of **NDI6** as compared to **NDI1** – whereas **NDI1** only appears in heptameric complexes of the composition [Cl•**NDI1**$_7$]$^-$ to [Cl•**NDI1**$_4$•**NDI6**$_3$]$^-$ **(**Figure 4.5.18).

The different behavior of NDIs with and without methyl groups in position 2 and 6 of the N-phenyl substituents – NDIs without these methyl groups cannot be incorporated into the heptamer by more than three subunits – indicates a significant influence of these methyl groups. One possible explanation could involve C-H•••O=C hydrogen bonds bridging different NDIs in the heptamer.

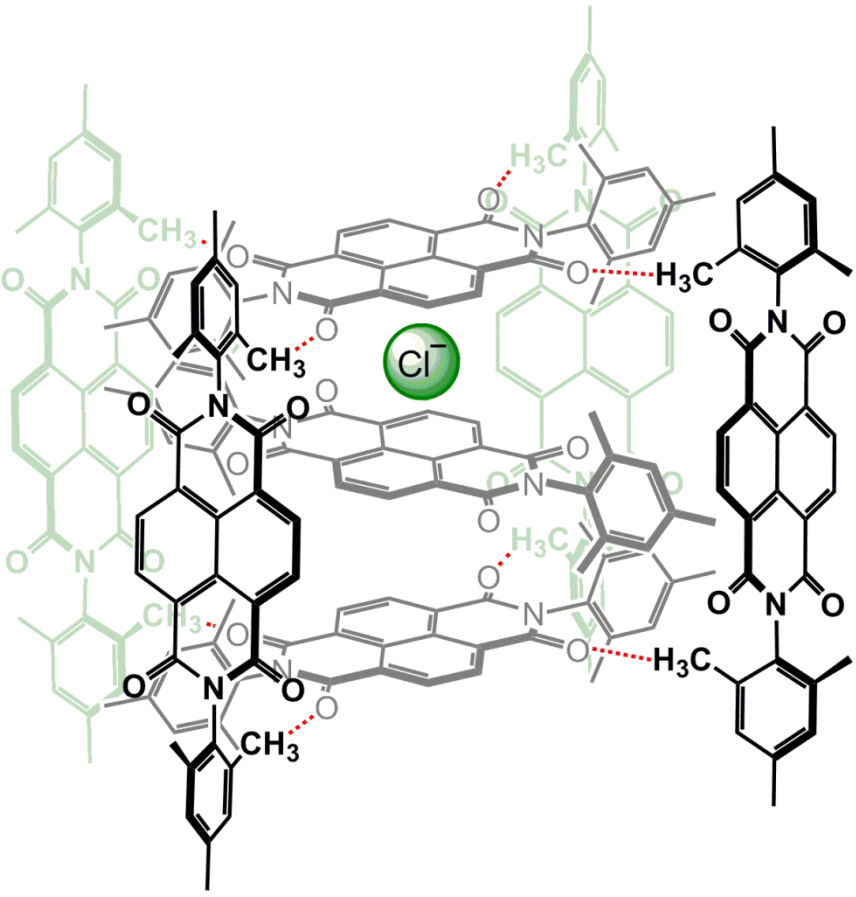

Figure 4.5.19 *Possible structre of an NDI heptamer: Two parallel NDIs coordinate to the chloride anion, which renders them more electron-rich and making them more susceptible to coordinate another electron-poor NDI through π-π -interactions. This stack of tree NDI subunits (grey) might then be bridged by four additional NDIs through C-H•••O=C hydrogen bonds.*

Figure 4.5.19 shows a suggestion for a structure with such C-H•••O=C hydrogen bonds. In this structure, two parallel NDIs coordinate to the chloride anion rendering them more electron-rich and therefore more susceptible to coordinate another electron-poor NDI through π-π-interactions. This stack of tree NDI subunits (grey NDIs in Figure 4.5.19) might then be bridged by four additional NDIs through C-H•••O=C hydrogen bonds. This would require at least four NDIs with mesityl or 2,6-phenyl substituents, which explains that not more than three subunits of **NDI2** and **NDI4** are incorporated into the heptamer.
This structural model could provide a decent explanation for the unexpectedly outstanding stability of naphthalene diimide heptamers.

To gain more insight into the structure of the $[Cl•\mathbf{NDI1}_7]^-$ heptamer, it was fragmented in tandem-MS experiments: These experiments indicated that the heptamer consists of two trimers and one monomer.

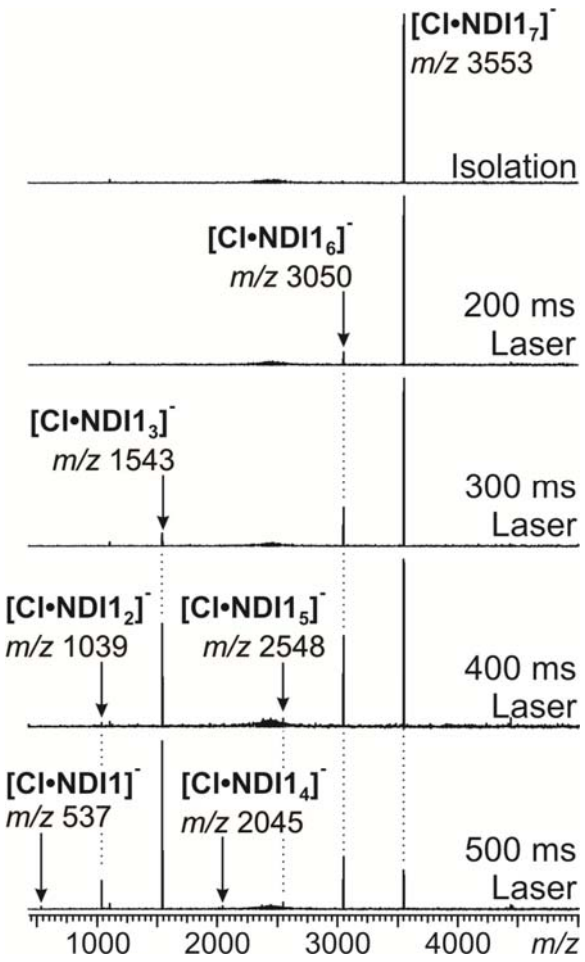

Figure 4.5.20 *Laser induced fragmentation of mass selected* $[Cl•\mathbf{NDI1}_7]^-$.

Gas-phase isolated $[Cl•\mathbf{NDI1}_7]^-$ first loses one molecule of **NDI1** upon laser irradiation (Figure 4.5.20). With increasing laser irradiation time, a signal for the trimer $[Cl•\mathbf{NDI1}_3]^-$ appears in the spectrum. Signal for the corresponding 1:1, 2:1, 4:1, and 5:1 complexes of **NDI1** and chloride appear later at longer laser irradiation times. This already indicates the subsequent loss of a monomer and a trimer from the NDI heptamer followed by the loss of further monomers from the trimer $[Cl•\mathbf{NDI1}_3]^-$ (generating the 2:1 and 1:1 complexes). The 5:1 and 4:1 complexes are generated by monomer loss from the hexamer through a minor fragmentation pathway.

To confirm this hypothesis, the $[Cl•\mathbf{NDI1}_6]^-$ hexamer originating from the fragmentation of the heptamer was again mass-selected and fragmented by laser irradiation. This MS^3 experiment confirmed the previous results, although the resolution and signal intensity drastically decrease after the second fragmentation step.

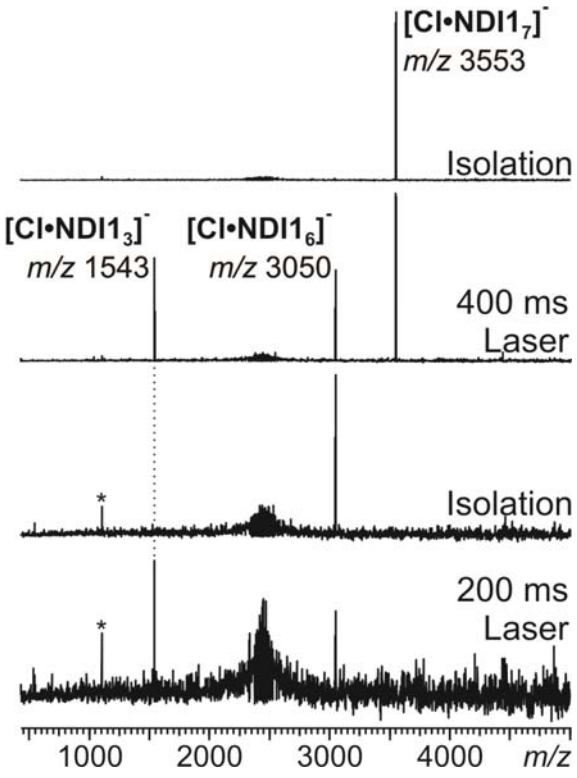

Figure 4.5.21 *Laser induced fragmentation of mass selected* $[Cl•\mathbf{NDI1}_7]^-$ *followed by gas-phase isolation and fragmentation of* $[Cl•\mathbf{NDI1}_6]^-$*. The asterisk denotes a signal originating from stray radiation, which also causes the broad signal around m/z 2500.*

The MS^2 and MS^3 experiments with the NDI heptamer leave two possible explanations for the structure:

a) The heptamer actually consists of two trimers and one monomer, which, however, would rule out the suggested structure shown in Figure 4.5.19.

b) The heptamer – with the supramolecular structure shown in Figure 4.5.19 – loses an NDI monomer in the first fragmentation step, as this is the exit channel with the lowest energetic barrier. The remaining hexamer then might rearrange into some kind of 3+3+chloride superstructure, whereas it is unclear, how this looks like, where the anion sits, and especially why exactly a subunit of *three* NDIs is so stable.
This cannot be further clarified by mass-spectrometric experiments.

4.5.4 Anion Binding to Substituted Dimeric Naphthalene Diimide Systems

Di-methoxy substituted **NDIM2**, di-tert-butylthio substituted **NDIM3**, and di-piperidin-1-yl substituted **NDIM4** have been investigated earlier with respect to their fluorescence resonance energy transfer (FRET) properties.[131]
After rather simple ESI-MS experiments (see chapter 4.5.1) revealed a high ability to bind a large variety of anions for the cyclic naphthalene diimide dimer **NDIM1**, this raised the question, how different substituents on one of the NDI cores influence the binding behavior.

First ESI-MS experiments with the substituted NDIMs revealed them to bind to chloride just as **NDIM1** (see Figure 4.5.22 and 4.5.23 for exemplary spectra). However, ionization conditions had to be adjusted much more carefully in case of the substituted NDIMs as compared to **NDIM1** to generate the chloride complexes. Also, a lot more scans had to be recorded to obtain similar signal-to-noise ratios as previously for **NDIM1**. This could be regarded as a hint that **NDIM2**, **NDIM3**, and **NDIM4** bind less strongly to anions than **NDIM1**.

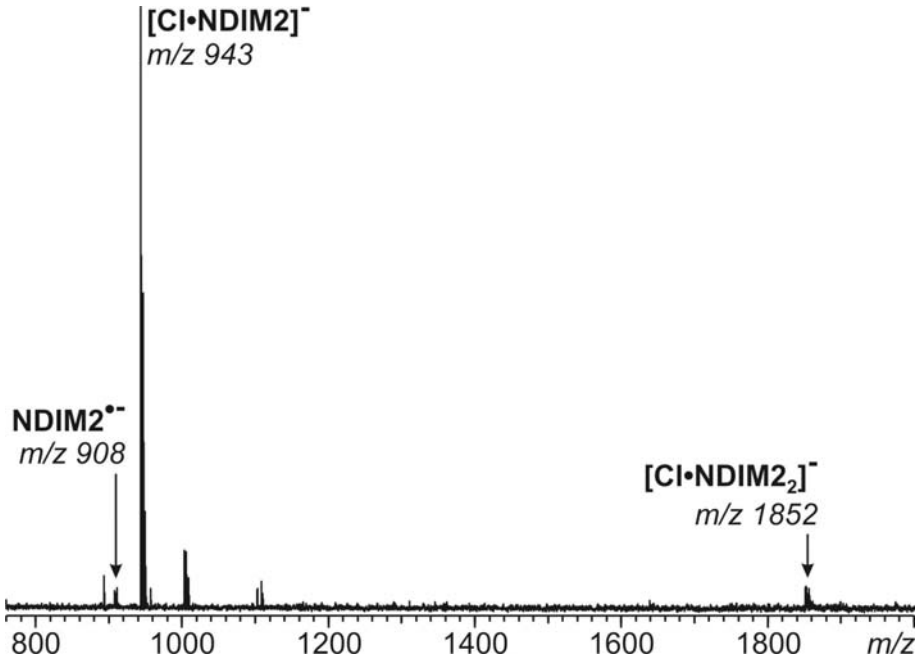

Figure 4.5.22 *ESI-FTICR mass spectrum of an equimolar 50 μM solution of* ***NDIM2*** *and NEt_4Cl in acetonitrile. Besides the radical anion of* ***NDIM2****, which is formed by reduction on the spray capillary, 1:1 and 2:1 complexes of* ***NDIM2*** *and chloride are observed.*

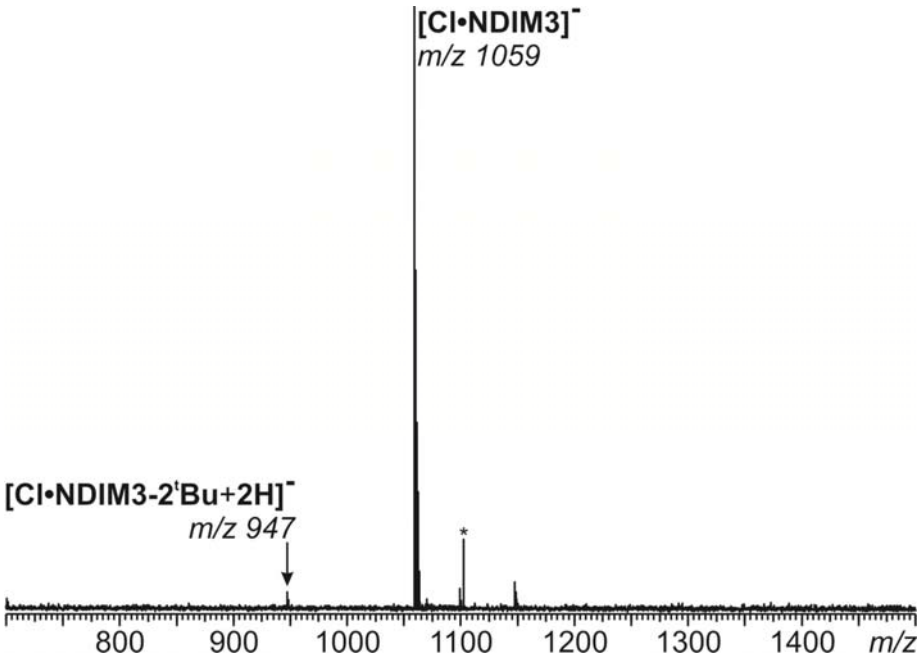

Figure 4.5.23 *ESI-FTICR mass spectrum of an equimolar 50 μM solution of* ***NDIM3*** *and NEt_4Cl in acetonitrile. The main signal corresponds to the 1:1 complex of* ***NDIM3*** *and chloride. The small signal at m/z 947 corresponds to the choride complex of a minor side product of the synthesis without tert-butyl groups. The asterisk denotes a signal originating from stray radiation.*

Although for **NDIM1** and **NDIM2** at least small signals for $[Cl•\mathbf{NDIM_2}]^-$ complexes are observed, these are not really expected to be suitable for the comparison of the anion binding ability of the four NDIMs, as the binding of both NDIMs to the chloride anion is rather unlikely due to steric reasons, if the anion is bound to a bowl-shaped conformation of the NDIM. Also, the formation of heterodimers could not be observed with chloride as the anion so that a determination of relative binding strength of the NDIMs towards chloride through tandem-MS experiments is not possible.

This problem might be solved by using an elongated dication such as indigocarmine (**IC**), which offers two possible binding sites for anion receptors (two sulfonate groups) and has already been applied for the comparison of the anion binding ability of resorcinarene-based cavitands in previous studies.[132]

An ESI-MS experiment with di-*tert*-butylthio-substituted **NDIM3** with the addition of 10 eq. of **IC** showed no binding of the dianion to the NDIM (Figure 4.5.24). The main signal in this spectrum corresponds to the 1:1 complex of **NDIM3** and chloride, which was only present in traces as a common ubiquitous impurity.

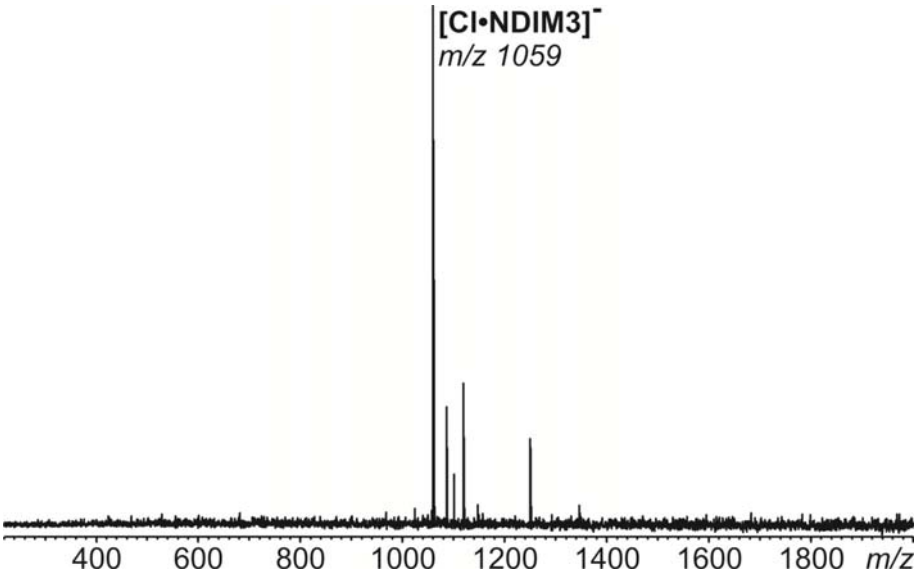

Figure 4.5.24 *ESI-FTICR mass spectrum of a solution of* ***NDIM3*** *(50 μM) and indigocarmine (****IC****, disodium salt, 500 μM) in acetonitrile. Surprisingly, no signal for an indigocarmine complex is observed; instead, the main signal corresponds to the 1:1 complex of* ***NDIM3*** *and chloride.*

In contrast to this, di-piperidin-1-yl substituted **NDIM4** does indeed bind to indigocarmine, even if this is only observed, if the indigocarmine concentration is significantly lower than that of the NDI (Figure 4.5.25). To be precise, the **IC** complexes of **NDIM4** can only be observed, if the equimolar solution of **NDIM4** and NEt_4Cl is electrosprayed using the same transfer capillary and the same syringe that have right before been used for introducing an equimolar solution of **NDIM4** and Na_2**IC** into the ESI source without intermediate cleaning.
Strange as it seems, the minor traces of IC seem to be enough to generate **NDIM4**/**IC** complexes during the electrospray process with reasonable intensities. Even stranger, this apparently is the only way to generate these complexes. However, this approach does not work for the other NDIMs. Also, all attempts to generate heterodimeric complexes of two different NDIMs and **IC** failed.
This of course ceased the plans to determine an order of relative anion binding streghth. Therefore, this approach was not followed up any longer.

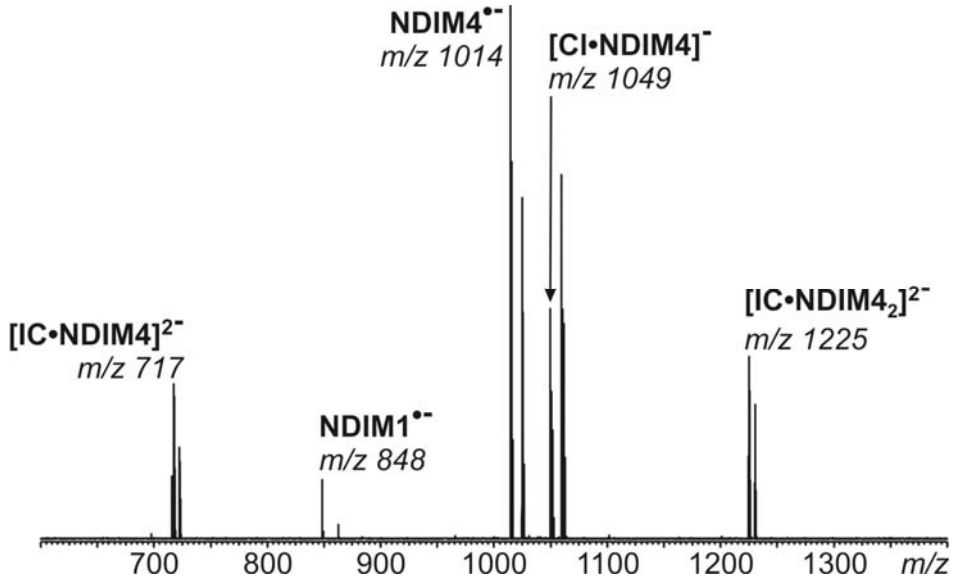

Figure 4.5.25 *ESI-FTICR mass spectrum of an equimolar 50 μM solution of* ***NDIM4*** *and NEt_4Cl in acetonitrile that contains traces of indigocarmine (***IC****, disodium salt). Surprisingly, indigocarmine complexes of* ***NDIM4*** *could not be generated at higher concentrations of* ***IC****. However, under these rather special conditions, complexes of* ***IC*** *with one and two molecules of* ***NDIM4*** *can be generated. Furthermore, the spectrum shows the radical anion and the 1:1 chloride complex of* ***NDIM4****. All of the complexes containing* ***NDIM4*** *are accompanied by an unknown impurity with an m/z that is by 10 Da larger than that of the original complex. The signal for the radical anion of* ***NDIM1*** *(m/z 848) most probably originates from a side product during the synthesis of* ***NDIM4****.*

However, as a proof of principle, both the 1:1 and 2:1 complexes of **NDIM4** and indigocarmine (**IC**) – the only ones that could actually be generated – were isolated in the FTICR cell and fragmented by irradiation with a 25 W IR laser in an IRMPD experiment (Figure 4.5.26 and 4.5.27). Both complexes show the expected loss of one or stepwise loss of two NDIMs, which at least shows the applicability of the method.

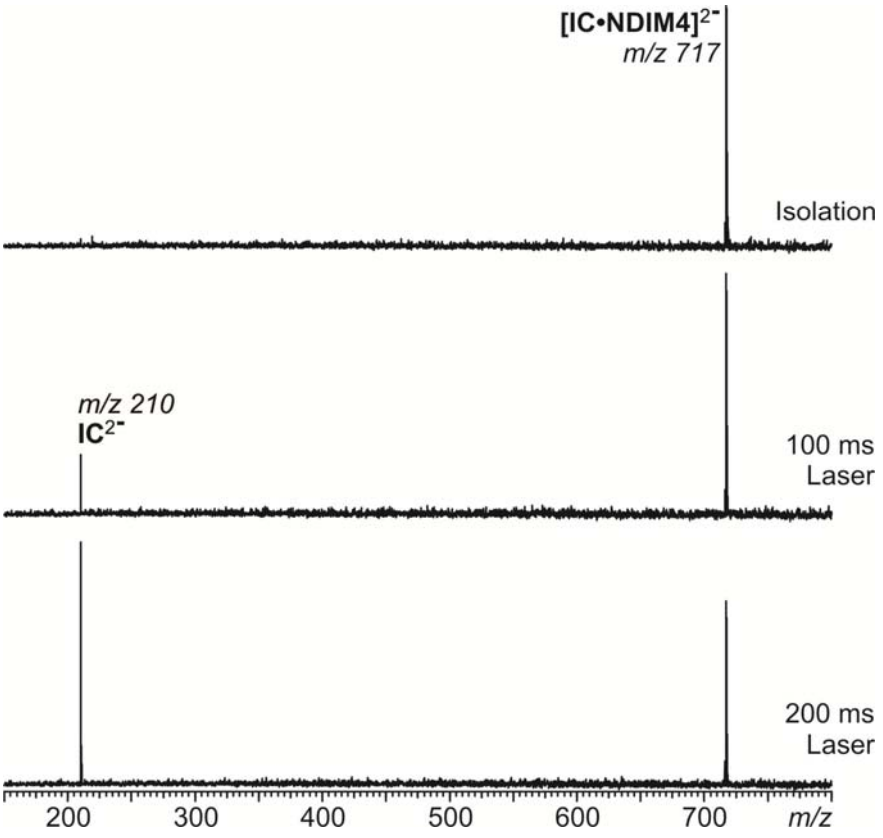

Figure 4.5.26 *Gas-phase isolation and laser induced fragmentation of mass selected [**IC•NDIM4**]$^{2-}$.*

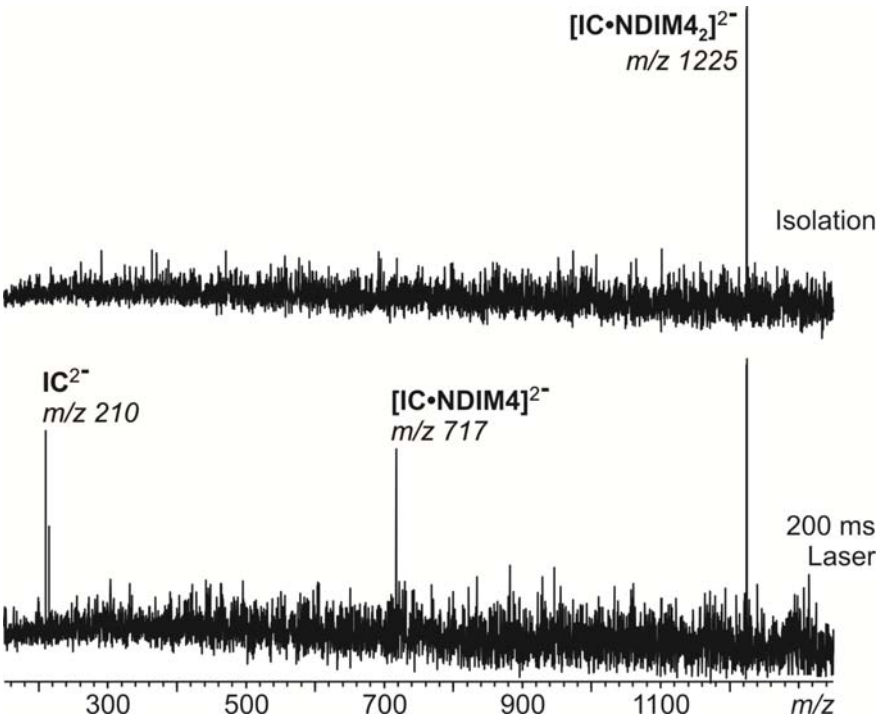

Figure 4.5.27 *Gas-phase isolation and laser induced fragmentation of mass selected [**IC•NDIM4**$_2$]$^{2-}$.*

4.5.5 Ion-Pair Binding to Crown Ether Substituted Naphthalene Diimides?

The successful experiments decribed above proving monomeric naphthalene diimides to bind several anions raise the question, whether a suitable functionalization of the NDI core might result in an ion-pair receptor. The structure of doubly [15]crown-5 substituted **NDI8** (Figure 4.5.28) exhibits besides the NDI core for anion binding also two crown ether moieties for the binding of cations such as alkaline metals. Two cations might bridge two NDI units forming a binding pocket for an anion between the two NDI faces. The resulting sandwich-type complex is schematically illustrated in Figure 4.5.29. Such a complex would be singly positively charged and therefore detectable by mass spectrometry.

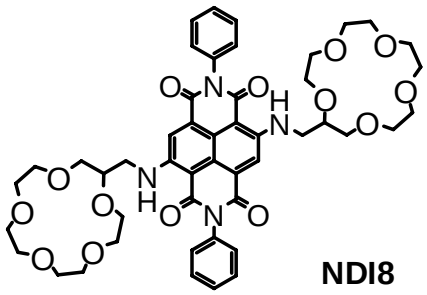

Figure 4.5.28 *Chemical structure of the doubly [15]crown-5 substituted monomeric naphthalene diimide system (**NDI8**) investigated for their ion pair binding behavior.*

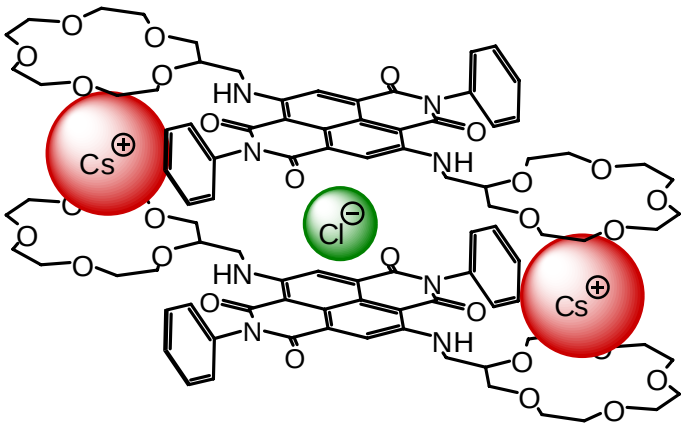

Figure 4.5.29 *Schematic illustration of the sandwich-type complex formed out of two **NDI8** subunits bridged by two alkaline cations (here: Cs^+) that might form a binding pocket for one anion surrounded by two NDI faces and two cations.*

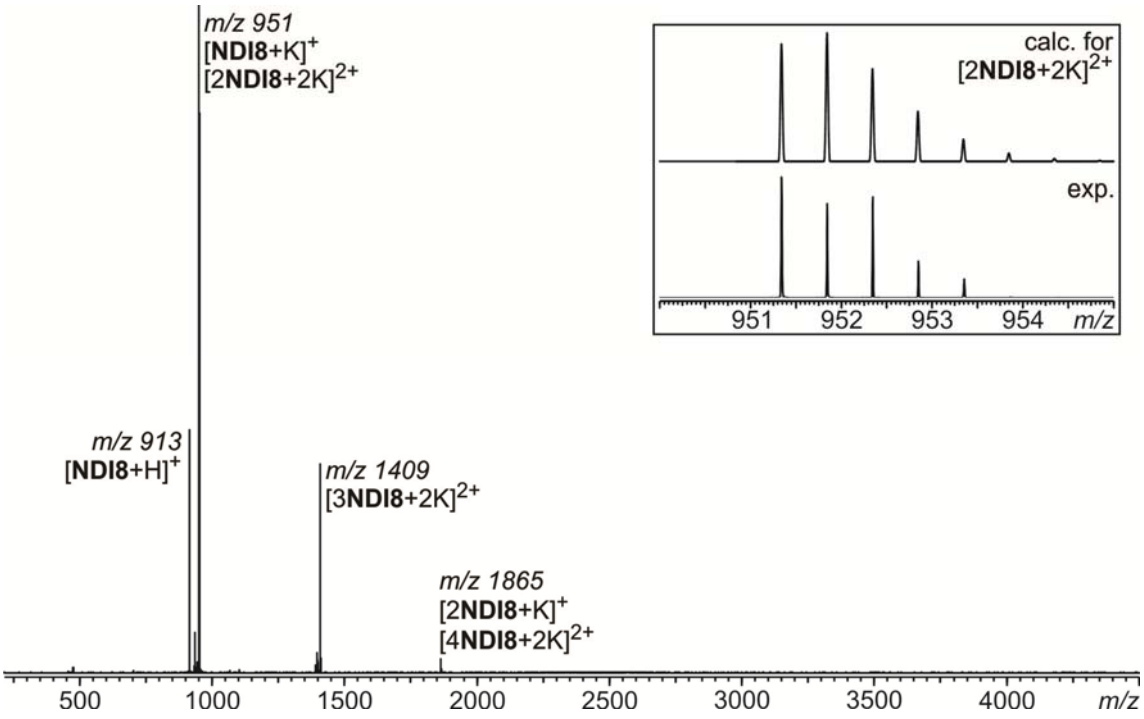

Figure 4.5.30 *Positive mode ESI-FTICR mass spectrum of an equimolar 50 μM solution of* ***NDI8*** *and KCl in acetonitrile. The spectrum shows a relatively wide range of complexes of* ***NDI8*** *and* K^+ *in various compositions. The inset shows the enlarged region from m/z 950 - 955 (bottom) and the calculated isotope pattern of the complex* $[2\mathbf{NDI8}+2K]^{2+}$ *(top). The comparison of the calculated and the experimental isotope pattern shows that the signal at m/z 951 does not only stand for the 2:1 (two* ***NDI8*** *+ one* K^+*) but also for the 1:1 complex.*

The positive mode ESI-FTICR mass spectrum of a 50 μM equimolar solution of crown-ether substituted **NDI8** and KCl does not show any signal that could be attributed to a sandwich-type structure such as the one shown in Figure 4.5.29. Nevertheless, a $[K_2 \bullet \mathbf{NDI8}_2]^{2+}$ complex, which would most probably exhibit a sandwich-like though anion-less structure, was observed as the main component among some larger (most probably unspecific and open-chain) oligomers (Figure 4.5.30). So one might assume that potassium ions are too small to form a pocket that is large enough to incorporate an additional chloride anion between the NDI-π-faces.

Therefore, the same experiment was performed with a solution of **NDI8**, CsF, and NEt_4Cl (Cs^+ as a larger cation and Cl^- as the most strongly binding anion as shown by previous experiments), to increase the spacing between the aromatic NDI faces.

The mixture of the two salts instead of CsCl was used in order to probably also observe a complex including Cs^+ and F^- ions in case chloride would still be too large.
First, a mass spectrum in the negative mode was recorded to verify anion binding indeed to take place. As can be seen from Figure 4.5.31, also the crown-ether substituted **NDI8** is able to bind to anions, namely chloride.

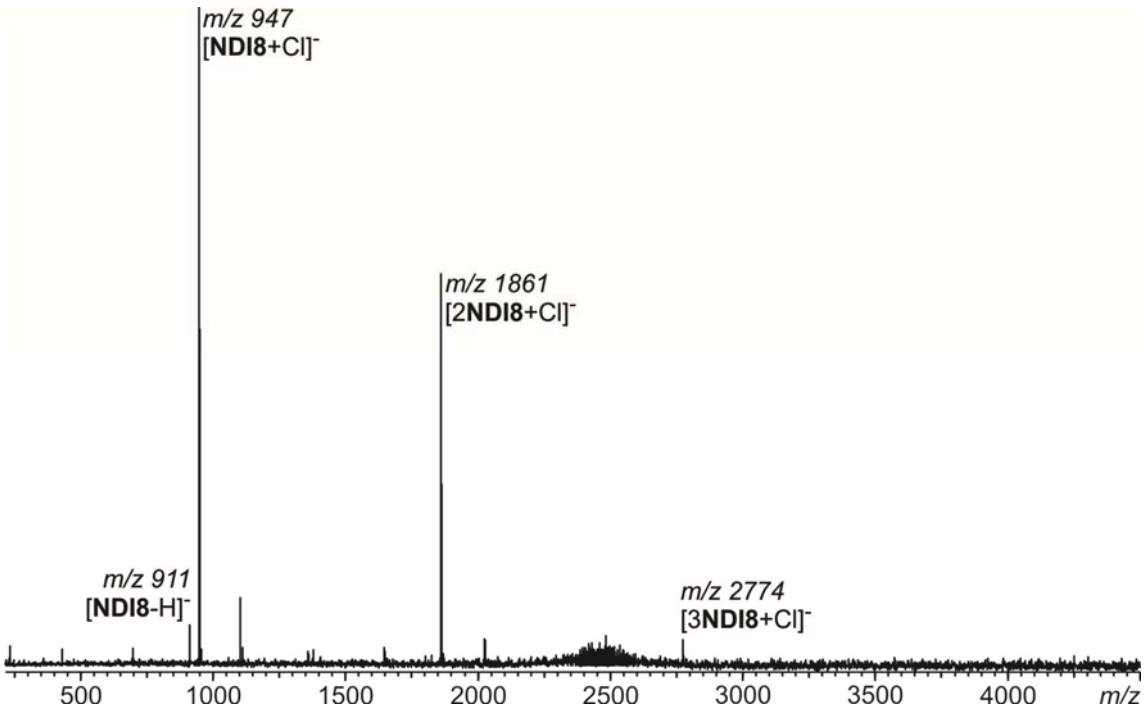

Figure 4.5.31 *Negative mode ESI-FTICR mass spectrum of an equimolar 50 μM solution of* ***NDI8****, CsF, and NEt_4Cl in acetonitrile. The spectrum shows 1:1, 2:1, and 3:1 complexes of* ***NDI8*** *and Cl^- as well as the deprotonated* ***NDI8****.*

Unfortunately, the corresponding spectrum recorded in the positive mode of the same sample only shows the same complexes for Cs^+ that are also observed for K^+ (Figure 4.5.32). As already observed for K^+, the signal for the 2:2 complex (*m/z* 1045) is superimposed by the signal of the corresponding 1:1 complex that appears at the same *m/z* value. The presence of both of these complexes is shown by higher intensities of the first and third peak of the isotope pattern of the signal at *m/z* 1045, which indicates the presence of the 1:1 complex.

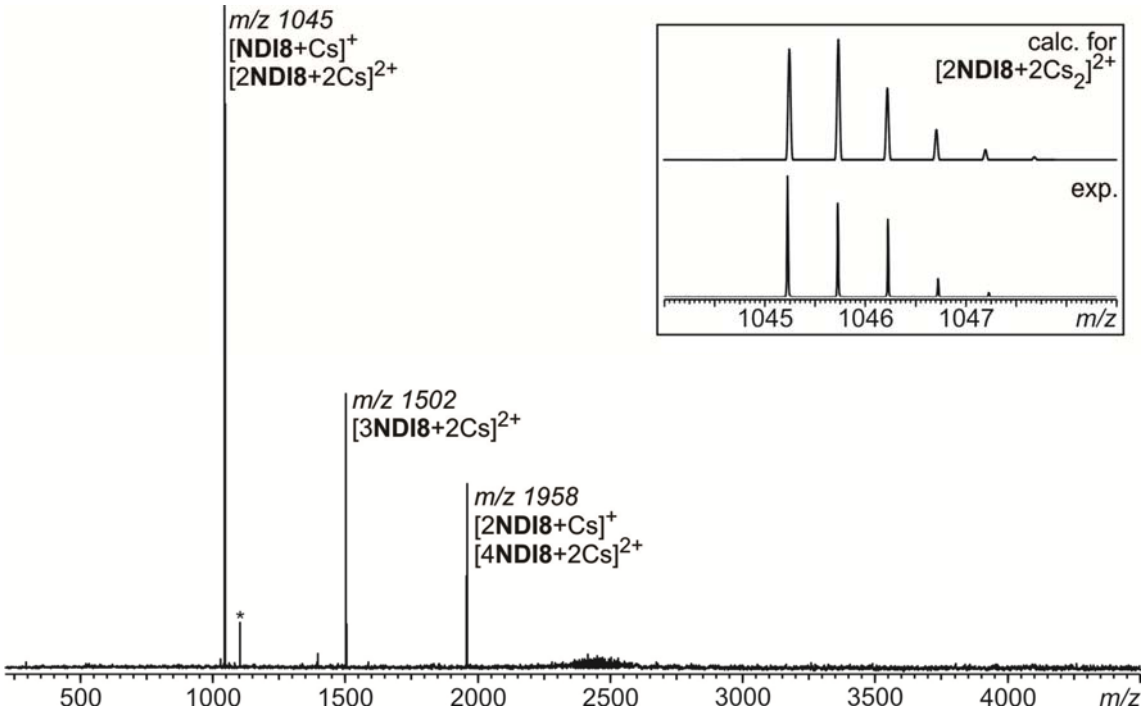

Figure 4.5.32 *Positive mode ESI-FTICR mass spectrum of an equimolar 50 μM solution of* ***NDI8****, CsF, and NEt_4Cl in acetonitrile. The spectrum shows a relatively wide range of complexes of* ***NDI8*** *and Cs^+ in various compositions. The inset shows the enlarged region from m/z 1044 – 1048.5 (bottom) and the calculated isotope pattern of the complex $[2$**NDI8**$+2Cs]^{2+}$ (top). The comparison of the calculated and the experimental isotope pattern shows that the signal at m/z 1045 does not only stand for the 2:1 (two* ***NDI8*** *+ one Cs^+) but also for the 1:1 complex. The asterisk denotes a signal originating from stray radiation.*

The results obtained from the positive mode ESI mass spectra (**NDI8** + either K^+ or Cs^+) can be reproduced in a concentration range from 1.25 μM to 50 μM, whereas at lower concentrations the predominance of 1:1 complexes increases.

A possible solution for this problem could be the use of protonated 1,n-diaminoalkanes (n = 2, 3, 4, 5, 6) as spacers between the two NDI systems. However, the corresponding ESI-MS experiments showed that in total four positive charges on two short-chain diaminoalkanes can apparently not effectively be solvated by two crown ether substituted **NDI8**, as no complexes of protonated 1,n-diaminoalkanes and **NDI8** could be observed. The acid (formic or hydrochloric acid) that had to be added to protonate the 1,n-diaminoalkanes rather leads to protonation of **NDI8**, therefore **NDI8**$+H^+$ is the only signal observed.

Therefore, other organic dications that do not require protonation were examined with respect to providing an appropriate distance between the aromatic NDI planes. An efficient binding between the NDI faces would require at least a distance of 6 Å, whereas molecular modelling indicates a distance of only 4 Å with caesium as the bridging cation.
N,N'-dimethylated DABCO (1,4-diazabicyclo[2.2.2]octane) might fulfill the necessary requirements, however, complexes of N,N'-dimethyl-1,4-diazabicyclo[2.2.2]octane could not be generated.

A possible alternative is shown in Figure 4.5.33: Suggested that methylpyridinium cations are bound by [15]crown-5 through cation-dipole interactions, the paraquat dication (1,1'-dimethyl-4,4'-bipyridine-1,1'-diium, **PQ**) would provide a spacing of around 11 Å between the NDI faces as suggested by molecular modelling (Figure 4.5.34), which might be to large to efficiently bind to an anion to both NDI faces.

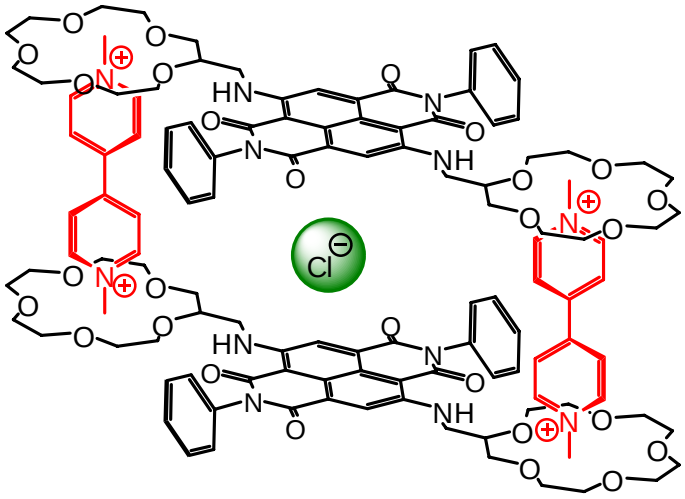

Figure 4.5.33 *Suggested complex of di-[15]crown-5-substituted* ***NDI8****, two paraquat dications (****PQ****), and one chloride anion sitting between the NDI faces.*

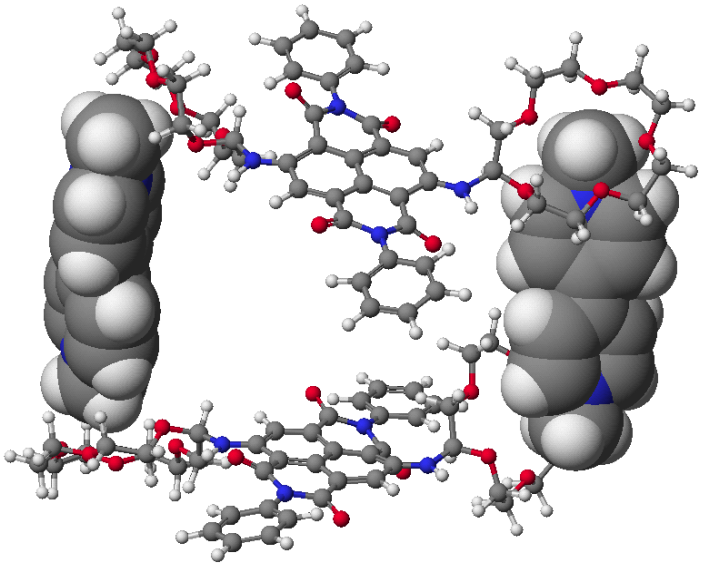

Figure 4.5.34 *MM2 energy minimized structure of the complex of two doubly [15]crown-5-substituted* ***NDI8*** *and two paraquat dications (***PQ***). This arrangement would provide an average distance of 11 Å between the aromatic NDI planes.*

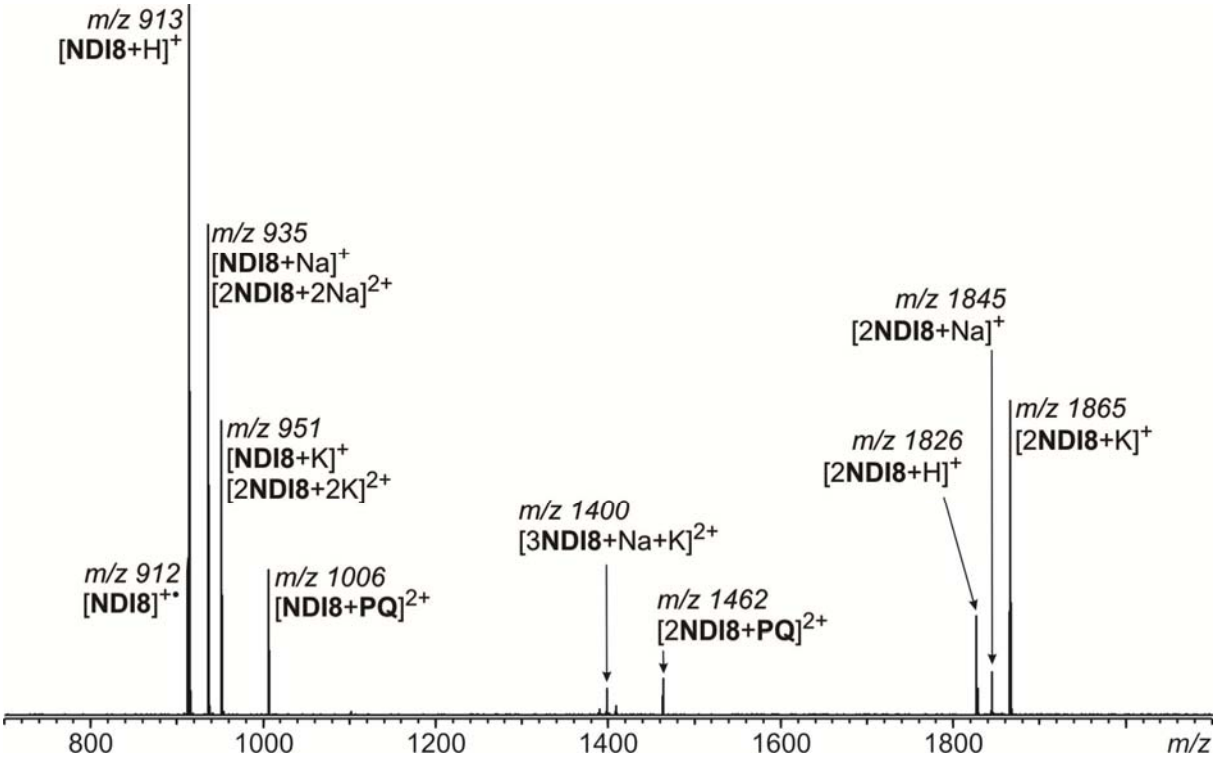

Figure 4.5.35 *ESI mass spectrum of a solution of* ***NDI8*** *(5 μM) and paraquat (55 μM, as* ***PQ****I_2) in acetonitrile.*

The ESI mass spectrum of a solution of doubly [15]crown-5 substituted **NDI8** containing 11 eq. of paraquat dication (**PQ**) shows the expected signals for the NDI radical cation and the proton, sodium, and potassium adducts as well as some higher oligomers, which is in line with previous measurements with NDI systems (Figure 4.5.35).
Furthermore, the spectrum also shows signals for paraquat complexes ([**NDI8**+**PQ**]$^{2+}$ and [**NDI8**$_2$+**PQ**]$^{2+}$) of **NDI8** of which the 1:1 complex is the more prominent one (Figure 4.5.35).

An extremely small signal at m/z 1134 corresponds to a 2:2:2 complex of each two crown ether substituted NDIs, two paraquat dications, and two chloride anions. The chloride anions originate from ubiquitous background chloride. Despite the low intensity, this complex could be isolated in the FTICR cell. The laser induced fragmentation confirmed the expected complex stoichiometry (Figure 4.5.36). The complex breaks symmetrically into two idendical halves.

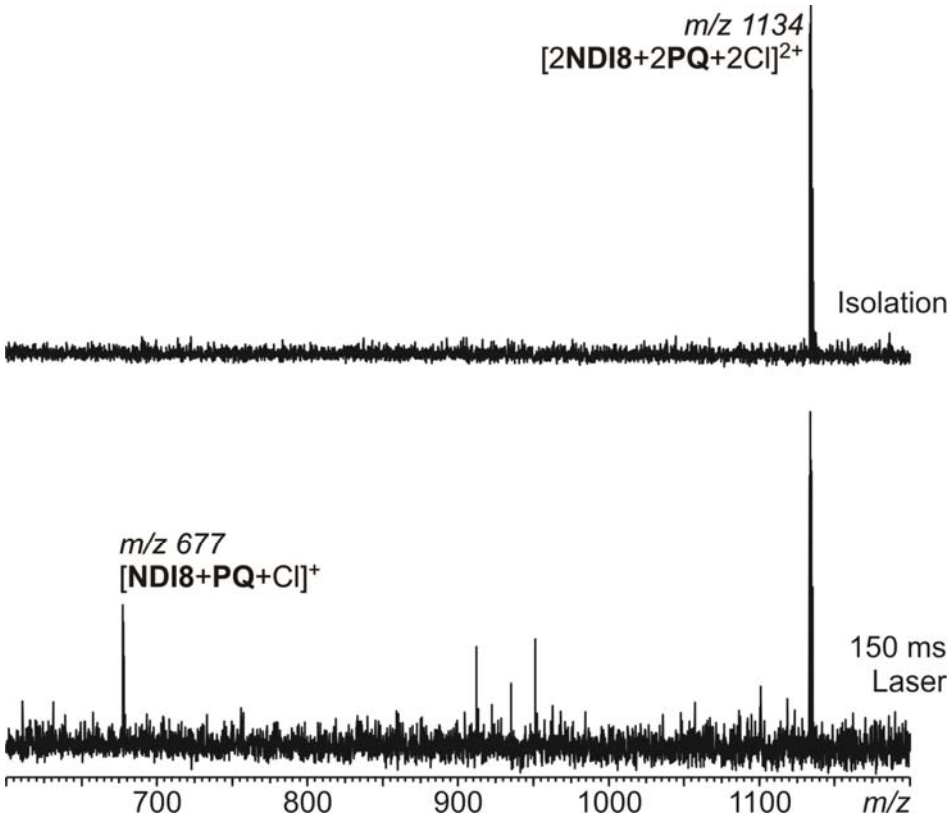

Figure 4.5.36 *Gas-phase isolation and laser induced fragmentation of a 2:2:2 complex of each two* ***NDI8****, two paraquat dications (****PQ****), and two chloride anions. The chloride anions originate from ubiquitous background chloride. Upon laser irradiation, the complex breaks into two identical halves.*

However, this does only prove the basic possibility that cations *and* anions can be bound simultaneously by **NDI8**. Furthermore, the mere existence of this complex still does not mean that the anions – or at least one of them – is indeed bount to the NDI faces. They might as well be bound somehow to the **PQ** cations, which is supported by the fact that actually only the complex with *two* anions is observed.

Nevertheless, this does not seem to be the most preferred composition of **NDI8**-**PQ** complexes; The complex with the highest intensity in the mass spectrum ([**NDI8**+**PQ**]$^{2+}$) might experience additional stabilization by binding of both cationic parts by the two crown ethers, which however would still leave the opposite NDI face open for anion binding.

Finally, the question, whether doubly [15]crown-5 substituted **NDI8** is able to simultaneously bind cations and anions most probably has to be answered with ‘no’, whereas the reason for this behavior remains unclear.

4.5.6 Conclusion

In conclusion, the mass spectrometric experiments performed with different monomeric and dimeric NDI systems proved to be successful to provide evidence for anion binding to the π-faces of the NDIs, which would not have been possible in solution due to the weakness of the anion-π interactions, similar to the experiments described for the resorcinarene-based anion receptor in chapter 4.4.

Furthermore, gas-phase IRMPD experiments with dimeric NDI complexes of the type $[Cl•\mathbf{NDI}^{a}•\mathbf{NDI}^{b}]^-$ were able to unravel the ranking of relative binding strength of the seven monomeric NDIs towards chloride anions, which overall is in line with the electronic effects of the substituents at the NDI core (more electron-withdrawing substituents lead to stronger binding) and also depends on the steric demand of the phenyl group attached to the NDI nitrogen atoms (less crowded active site leads to stronger binding). Consequently, **NDI7** with two cyano substituents on the NDI core and to simple phenyl groups on the NDI nitrogen atoms proved to be the strongest anion binder among the monomeric NDI systems.

Similar experiments with differently substituted cyclic NDI dimers (NDIMs) did unfortunately not give satisfactory results, as probably the binding to the substituted NDIM analoga is too weak. Also, indigocarmine – a disulfonate – might not be the ideal anion to form $[IC•\mathbf{NDIM}^{a}•\mathbf{NDIM}^{b}]^{2-}$ complexes, because sulfate binding to the unsubstituted **NDIM1** did not turn out to be successful. However, a "proof-of-principle" experiment with an $[IC•\mathbf{NDIM2_2}]^{2-}$ complex could prove the basic concept of laser-induced fragmentation experiments to be applicable to the NDI dimers, too. However, finding a suitable strongly binding dianion – required to bind to each one **NDIM** – might be impossible, as the strongly binding monoanions (halogenides and nitrate; see chapter 4.5.1) do not have any dianionic analoga.

The same applies to the crown-ether substituted NDI (**NDI8**): In fact, dimeric sandwich complexes with each one cation between two crown ethers could be observed In the gas phase. However, an additional anion – that would be expected to bind to one or even both of the NDI faces – is not observed, even when paraquat as a dication is used. Due to the limitations of the method and also because these anion-π interaction are too weak to be studied by other methods in solution, the reason for this behavior will most probably remain unclear.

Besides the basic proof of anion binding, the rather simple binding experiments with **NDI1** (unsubstituted NDI core + mesityl-substituted nitrogen atoms) resulted in a fairly unexpected additional result: this special NDI appears to preferably form heptameric $[Cl•\mathbf{NDI1}_7]^-$ aggregates, which can only be observed with exactly this NDI. However, up to 5 **NDI1** can be exchanged for other NDIs, even if these mixed hetero-heptamers appear in much lower intensity as compared to the corresponding 1:1 complexes. Gas-phase tandem-MS experiments suggest kind of an $[anion•(NDI_3)_2•NDI]^-$ structure. However, a detailed structural analysis of the heptamer is not possible by mass spectrometric techniques and might require high-level theoretical calculations.

4.6 Encapsulation Complexes of Resorcinarene Hexamers

4.6.1 Basic Idea of the Project

Resorcinarenes (and pyrogallarenes) have been shown to form hexameric structures in solution,[133,134] in the solid state,[135] and in the gas phase. In the gas phase, the hexamer formation requires the addition of a suitable template that fits the interior of the hexamer in size and shape (Figure 4.6.1).[136]

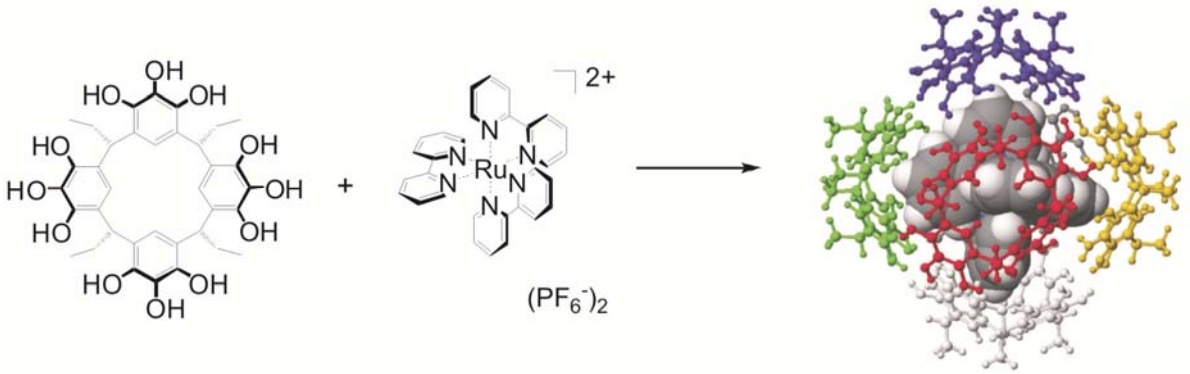

Figure 4.6.1 *Formation of a pyrogallarene hexamer in the gas phase after electrospray ionization from chloroform/acetone (7:3) with* $Ru(bpy)_3^{2+}$ *as templating guest.*

Several studies have shown that smaller guest molecules like chloroform, benzene or cobaltocenium can be included into the hexamer in solution.[137,138,139] Also, the exchange of neutral against positively charged guests can be followed (e.g. exchange of chloroform for tetrahexylammonium).[140]

These results raised the question, whether the hexameric capsule including a peudooctahedral complex such as $Ru(bpy)_3^{2+}$ could also be created in solution. First NMR experiments with $Ru(bpy)_3PF_6$ showed no signals for an encapsulated complex in $CDCl_3/d_6$-acetone.[141]

This could be caused by two different effects:

a) The acetone that has to be added to provide solubility of the ruthenium complex might be competing to strongly for hydrogen bonding to the resorcinarene OHs preventing the formation of the hydrogen-bridged hexameric structure.

b) The cation-anion separation energy might be too high, even with the relatively weakly coordinating hexafluorophosphate anion. As the $Ru(bpy)_3^{2+}$ complex would perfectly fill the hexamer's cavity, the complex *plus* the two hexafluorophosphate anions would be too large to fit inside, thus preventing the inclusion of the complex into the hexamer.

Alternative b) might be ruled out either by using the analogous neutral $Ir(ppy)_3$ complex or by substitution of the anion by an extremely weakly coordinating anion, namely the tetrakis(perfluoro-*tert*-butyloxy)aluminate (**pftb**).[142]

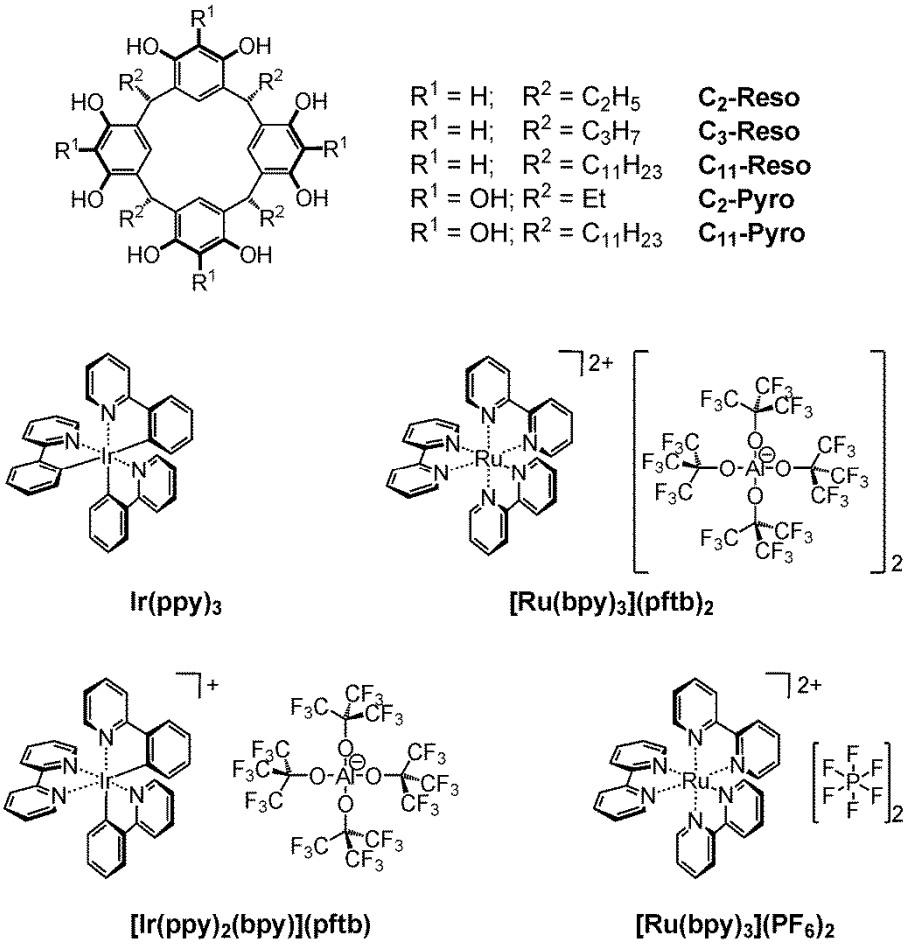

Figure 4.6.2 *Chemical Structures of the resorcinarenes, pyrogallarenes, and different pseudooctahedral Ir and Ru complexes with charge state 0, +I, and +II and different counter anions used in this study.*

Alternative a) could of course be ruled out by working in pure wet chloroform as described in references 137, 138, and 139. The small amount of water (solubility of water in chloroform:

0.056 % at 20°C [143]) would then help to build the seam of hydrogen bonds, which was initially expected for acetone, too, but apparently proved to be not true.

Figure 4.6.2 shows the chemical structures of the resorcin[4]arenes, pyrogallol[4]arenes, as well as the different neutral, singly and doubly charged iridium and ruthenium complexes used in this study to test the two hypotheses presented above.

4.6.2 Solution Studies on Resorcinarene Hexamer Formation

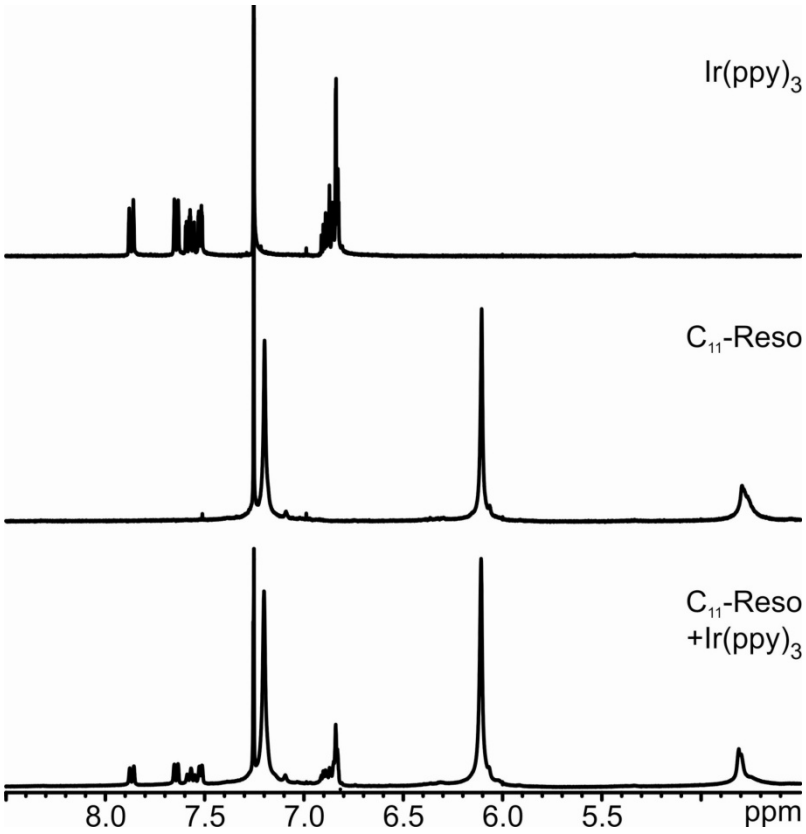

Figure 4.6.3 *^{1}H NMR spectra of top: Ir(ppy)$_3$, middle: C_{11}-resorcinarene, and bottom: a 6:1 mixture of C_{11}-resorcinarene and Ir(ppy)$_3$. All spectra were recorded in water-saturated $CDCl_3$. Obviously, no complexation occurs, as the chemical shift of the Ir complex' protons does not change at all. The signal at 4.8 ppm corresponds to chloroform encapsulated in the resorcinarene hexamer.*

The ^{1}H NMR spectra in Figure 4.6.3 do not show any shift for the aromatic protons of the neutral Ir(ppy)$_3$ complex upon addition of 6 eq. of C_{11}-resorcinarene in water-saturated $CDCl_3$. However, the resorcinarene hexamer is formed. This is shown by the signal at 4.8 ppm corresponding to encapsulated chloroform as previously reported by Rebek et al.[133] This signal is also observed in the mixture of resorcinarene and Ir(ppy)$_3$, which indicates chloroform to occupy the hexamer's interior cavity more likely than the Ir complex.

The same behaviour is observed for the mixture of C_{11}-pyrogallarene and Ir(ppy)$_3$ (Figure 4.6.4): No change is observed in the ^{1}H NMR spectrum of Ir(ppy)$_3$ upon addition of 6 eq. of C_{11}-pyrogallarene (solvent: water-saturated $CDCl_3$).

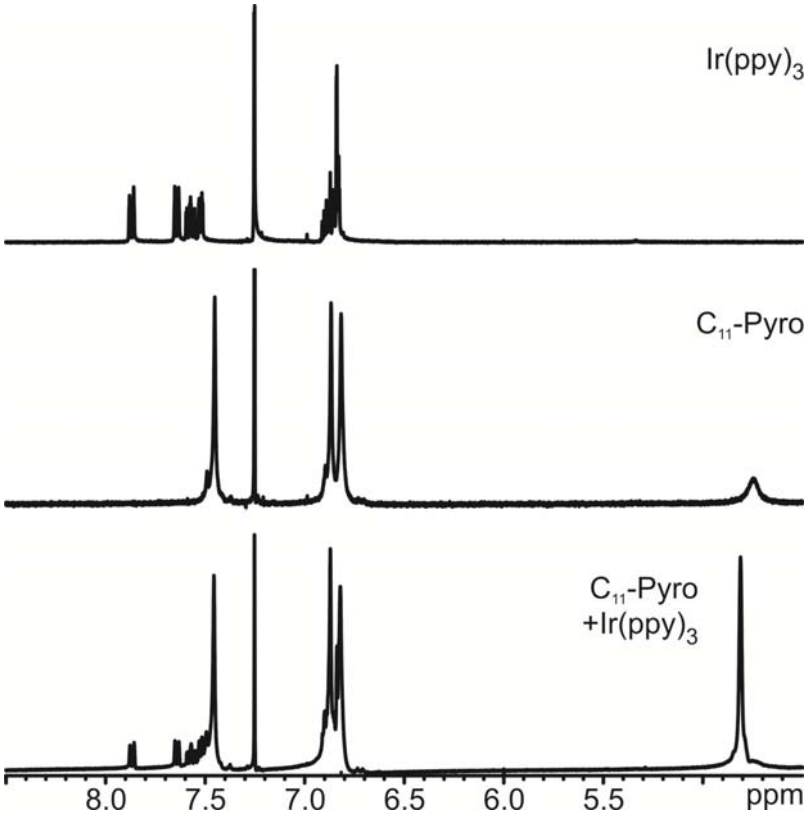

Figure 4.6.4 *^{1}H NMR spectra of top: $Ir(ppy)_3$, middle: C_{11}-pyrogallarene, and bottom: a 6:1 mixture of C_{11}-pyrogallarene and $Ir(ppy)_3$. All spectra were recorded in water-saturated $CDCl_3$. Again, no complexation occurs, as the chemical shift of the Ir complex' protons does not change at all. The signal at 4.8 ppm corresponds to chloroform encapsulated in the pyrogallarene hexamer.*

In case of a mixture of C_{11}-resorcinarene and $[Ir(ppy)_2(bpy)][Al(OC(CF_3)_3)_4]$ in water-saturated $CDCl_3$, again no change of the chemical shift of the iridium complex' protons could be observed (Figure 4.6.5b).

Also addition of some acetone for breaking the seam of hydrogen bonds holding together the resorcinarenes did not lead to a significant change (Figure 4.6.5c), which indicates the complex not to be included in a resorcinarene hexamer in both cases.

It should be noted that the analogous experiments with the doubly charged $Ru(bpy)_3^{2+}$ complexes in water-saturated $CDCl_3$ were not possible due to the poor solubility of the complexes in this solvent.

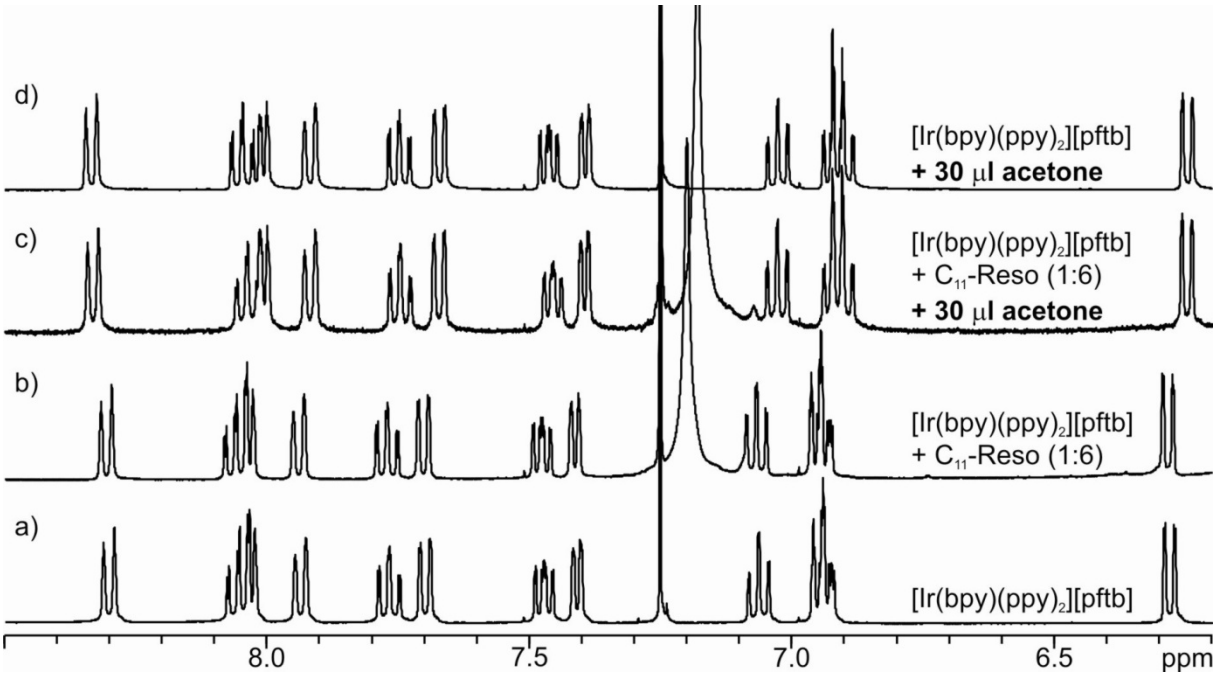

Figure 4.6.5 a) *^{1}H NMR spectrum of $[Ir(ppy)_2(bpy)][Al(OC(CF_3)_3)_4]$ in water-saturated $CDCl_3$.* ***b)*** *^{1}H NMR spectrum of a mixture of* ***C_{11}-Reso*** *(30 mM) and $[Ir(ppy)_2(bpy)][Al(OC(CF_3)_3)_4]$ (4.2 mM) in water-saturated $CDCl_3$.* ***c)*** *^{1}H NMR spectrum of the same mixture of* ***C_{11}-Reso*** *(30 mM) and $[Ir(ppy)_2(bpy)][Al(OC(CF_3)_3)_4]$ (4.2 mM) in water-saturated $CDCl_3$ after the addition of 30 µl of acetone.* ***d)*** *^{1}H NMR spectrum of $[Ir(ppy)_2(bpy)][Al(OC(CF_3)_3)_4]$ in water-saturated $CDCl_3$ + 30 µl of acetone for comparison with c).*

After previous experiments in water-saturated $CDCl_3$ did not give any reason for the assumption that the complexes are incorporated into resorcinarene hexamers, a solvent mixture of chloroform and acetone was assumed to provide the appropriate conditions for the inclusion of pseudooctahedral metal complexes into resorcinarene hexamers in solution.

Unfortunately, the addition of C_{11}-resorcinarene to a solution of $Ir(ppy)_3$. in a solvent mixture of $CDCl_3$ and [D_6]-acetone (7:3) causes just a minor shift of the signals of the aromatic protons of the Ir complex (Figure 4.6.6).
Also the ^{1}H NOESY NMR spectrum does not show any coupling interactions between resorcinarene and $Ir(ppy)_3$, which makes an inclusion of the complex in a resorcinarene hexamer very improbable.

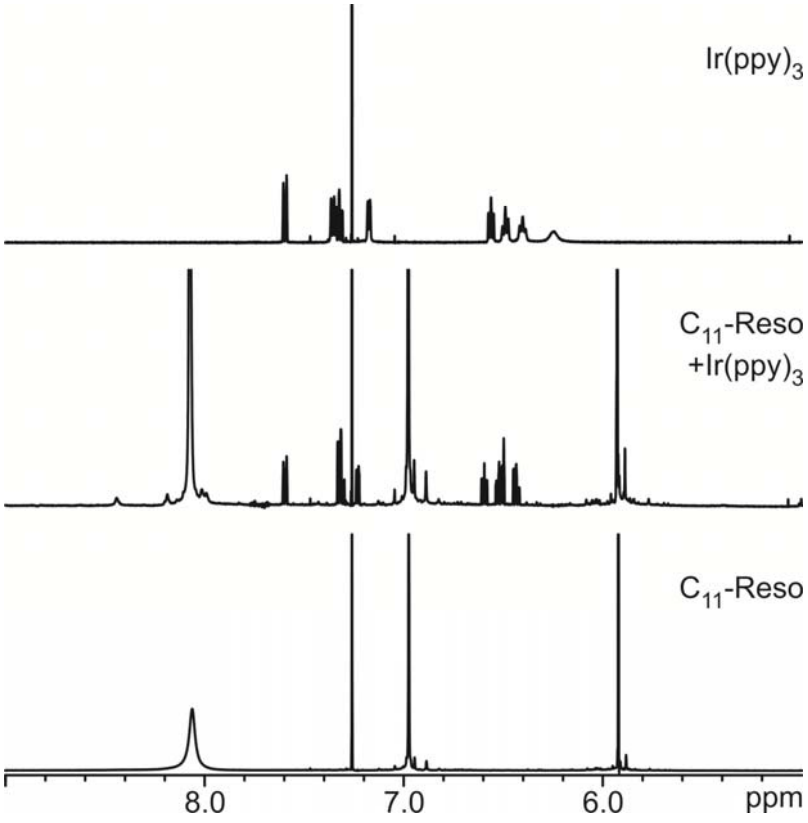

Figure 4.6.6 *^{1}H NMR spectra of top: $Ir(ppy)_3$, bottom: C_{11}-resorcinarene, and middle: a 6:1 mixture of C_{11}-resorcinarene and $Ir(ppy)_3$. All spectra were recorded in a solvent mixture of $CDCl_3$ and* [D_6]*-acetone (7:3). Apparently, no complexation occurs, as the signals of the Ir complex' protons just experience a very minor change upon addition of the resorcinarene.*

Also in case of the combination of C_{11}-pyrogallarene and $Ir(ppy)_3$ in a solvent mixture of $CDCl_3$ and $[D_6]$-acetone (7:3), the addition of C_{11}-Pyro does not affect the signals of the Ir complex. However, the ^1H NMR spectrum of the mixture shows several sets of signals for the pyrogallarene's OH groups (Figure 4.6.7), which indicates the formation of some stable aggregates, though without involving the $Ir(ppy)_3$ complex.

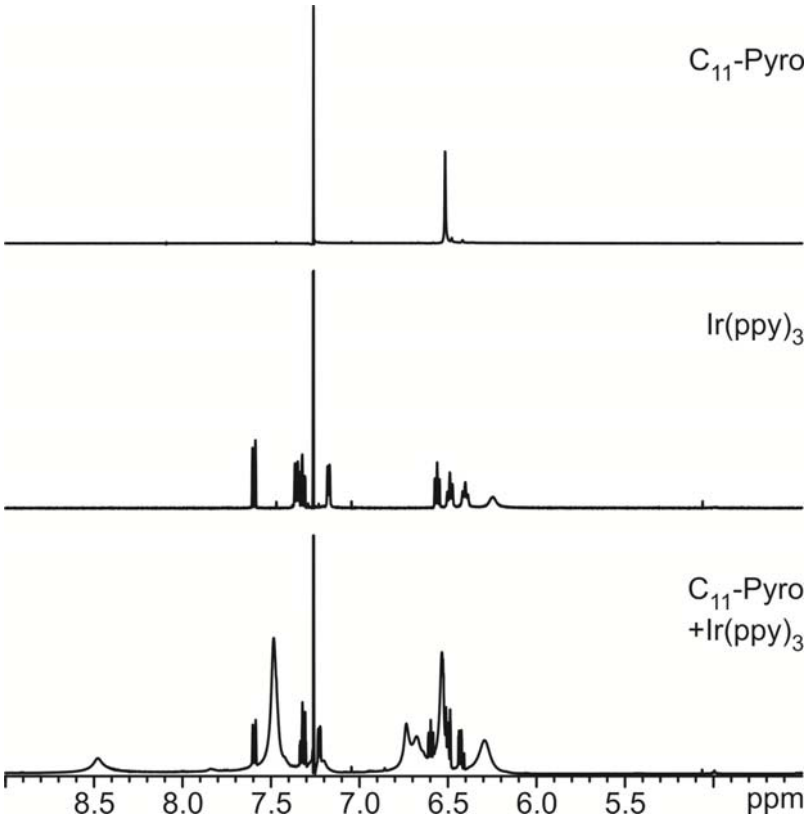

Figure 4.6.7 *^1H NMR spectra of top: C_{11}-pyrogallarene, middle: $Ir(ppy)_3$, and bottom: a 6:1 mixture of C_{11}-pyrogallarene and $Ir(ppy)_3$. All spectra were recorded in a solvent mixture of $CDCl_3$ and $[D_6]$-acetone (7:3). Whereas in the spectrum of* ***C_{11}-Pyro*** *alone, the signals for the phenol-OH protons are extremely broad, several sets of signals for these protons are observed in the mixture.*

In case of the combination of C_{11}-resorcinarene and the singly charged complex $[Ir(ppy)_2(bpy)]^+$ with the extremely weakly coordinating anion $[Al(OC(CF_3)_3)_4]^-$ in a solvent mixture of $CDCl_3$ and d_6-acetone (7:3), the addition of **C_{11}-Reso** slightly affects the signals of the Ir complex: Some of them are shifted upfield, some others are shifted downfield (Figure 4.6.8). However, for an inclusion of the complex in a resorcinarene hexamer, a large upfield shift would be expected for all of the signals.

Furthermore, the ^{1}H NOESY NMR spectrum does not show any coupling interactions between resorcinarene and $[Ir(bpy)_2(ppy)]^+$, which makes the formation of an encapsulation complex very improbable.

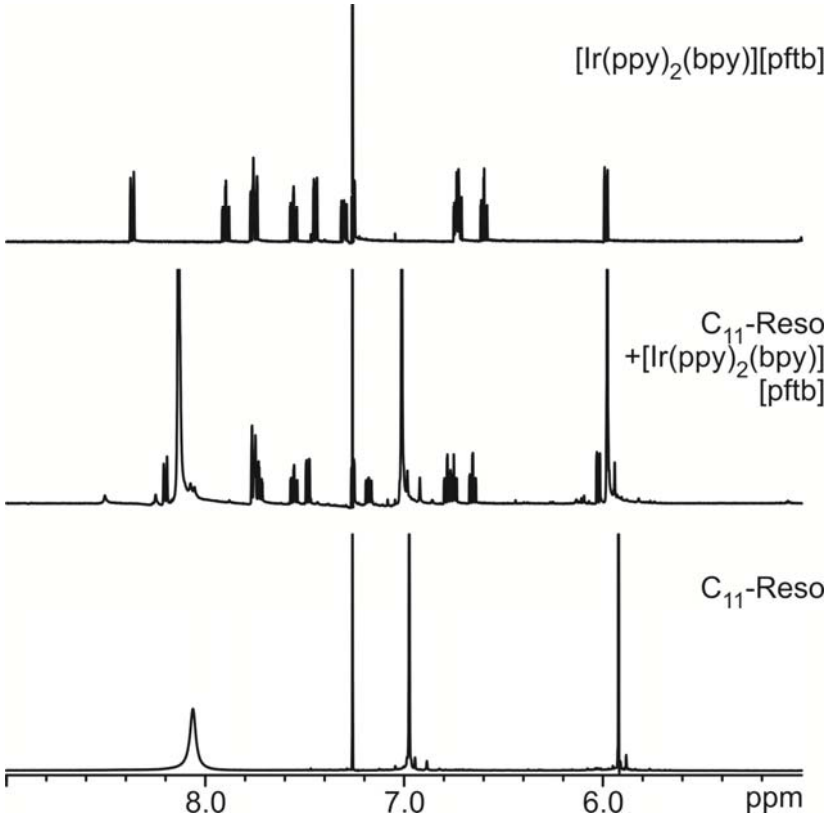

Figure 4.6.8 *^{1}H NMR spectra of top: $[Ir(ppy)_2(bpy)][Al(OC(CF_3)_3)_4]$, bottom: C_{11}-resorcinarene, and middle: a 6:1 mixture of resorcinarene and $[Ir(ppy)_2(bpy)][Al(OC(CF_3)_3)_4]$ complex. All spectra were recorded in a solvent mixture of $CDCl_3$ and $[D_6]$-acetone (7:3).*

In contrast to the three combinations of a singly charged or a neutral Iridium complex, respectively, with either C_{11}-resorcinarene or C_{11}-pyrogallarene (Figure 4.6.6 - 4.6.8), the combination of the doubly charged ruthenium complex $[Ru(bpy)_3][Al(OC(CF_3)_3)_4]_2$ with C_{11}-resorcinarene definitely shows some kind of interaction.

The ^1H NMR spectrum of a mixture of C_{11}-resorcinarene and $[Ru(bpy)_3][Al(OC(CF_3)_3)_4]_2$ shows clear upfield shifts for the aromatic protons of the bipyridine ligands as well as a small downfield shift for the upper-rim-resorcinarene protons (Figure 4.6.9). Although the shifts are smaller than expected – and also smaller than reported for the inclusion of chloroform – this is a good hint for encapsulation of the Ru complex by the resorcinarenes.

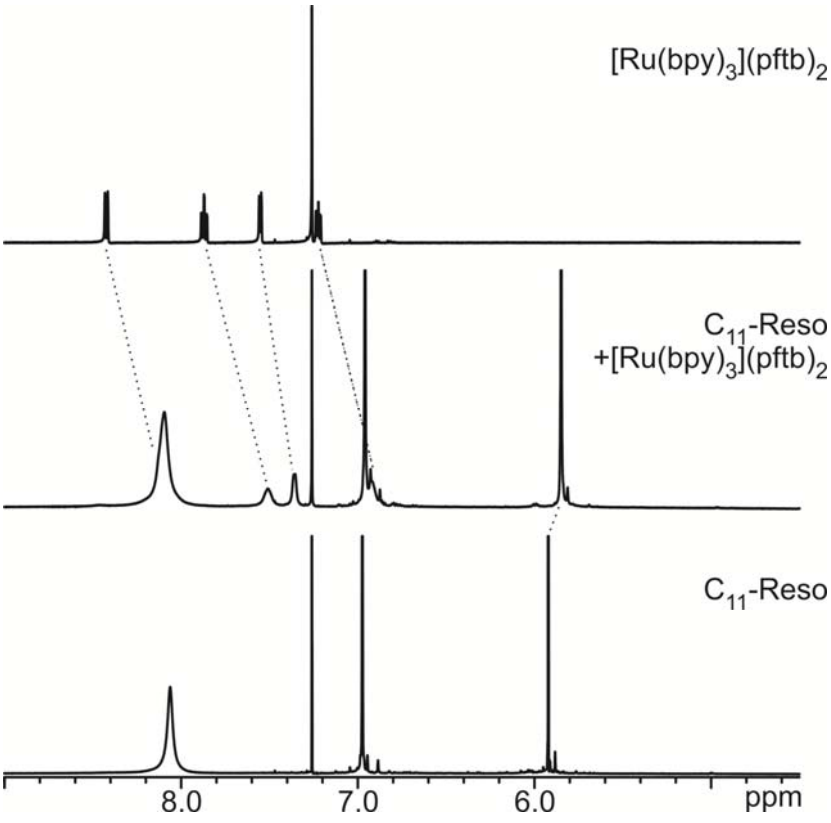

Figure 4.6.9 *^1H NMR spectra of top: $[Ru(bpy)_3][Al(OC(CF_3)_3)_4]_2$, bottom: C_{11}-resorcinarene, and middle: a 6:1 mixture of resorcinarene and $[Ru(bpy)_3][Al(OC(CF_3)_3)_4]_2$. All spectra were recorded in a solvent mixture of $CDCl_3$ and $[D_6]$-acetone (7:3).*

The ^{1}H NOESY NMR spectrum of the mixture of $[Ru(bpy)_3][Al(OC(CF_3)_3)_4]_2$ and C_{11}-resorcinarene gives additional hints for the formation of an inclusion complex: Coupling interactions can be observed between the resorcinarene-OH protons and two of the bipyridine protons (most probably H4 and H6) as well as between these bpy protons and the lower-rim-resorcinarene protons (Figure 4.6.10).

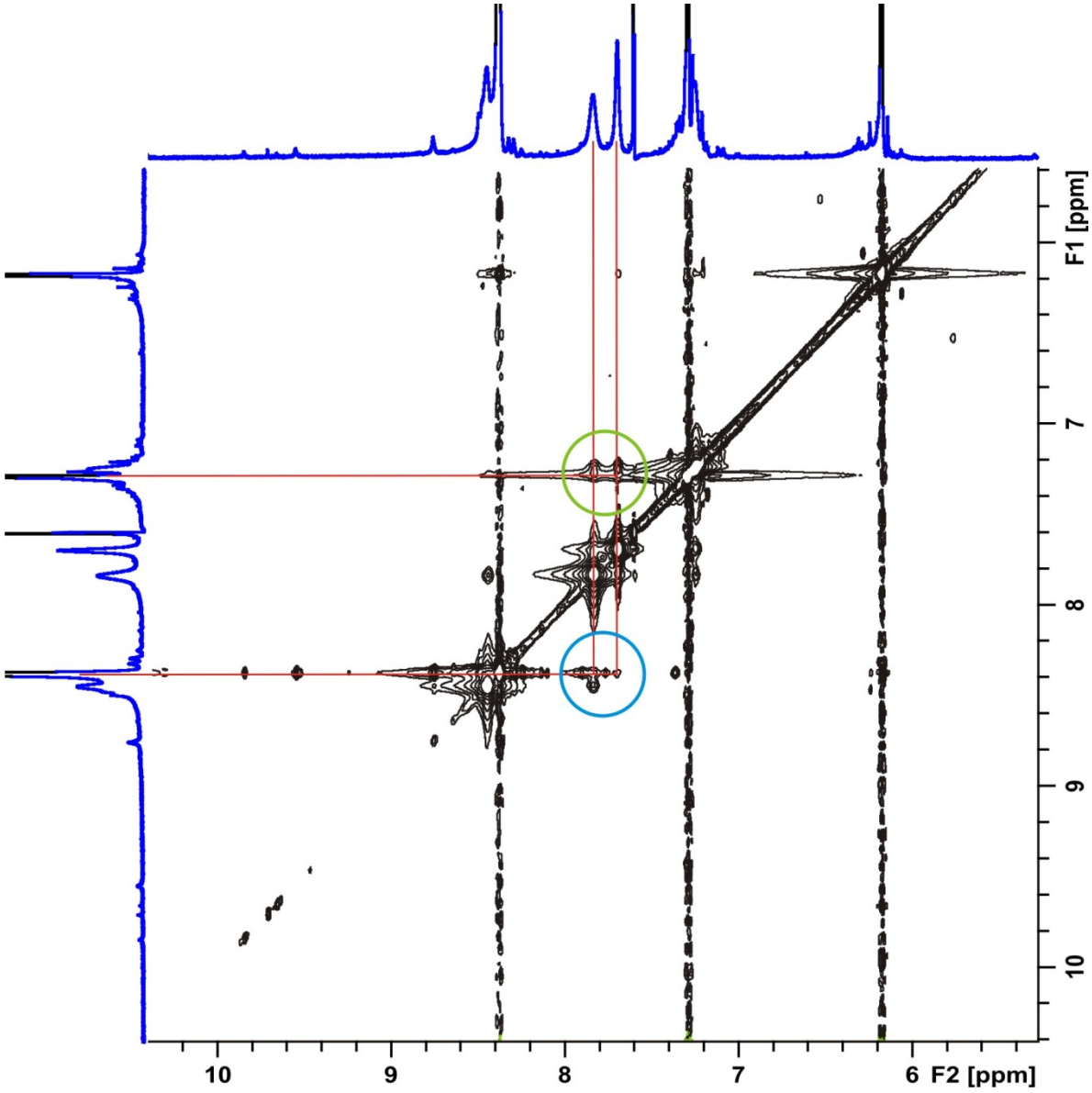

Figure 4.6.10 *^{1}H NOESY NMR spectrum of a mixture of $[Ru(bpy)_3][Al(OC(CF_3)_3)_4]_2$ and C_{11}-resorcinarene measured in a solvent mixture of $CDCl_3$ and d_6-acetone (7:3). Cross peaks are observed for couplings between two bpy-protons (most probably H4 and H6) and lower-rim-resorcinarene-H (green circle) as well as the two bpy protons and the resorcinarene-OHs (blue circle).*

As the experiments with the combination **C_{11}-Reso** + $[Ru(bpy)_3][Al(OC(CF_3)_3)_4]_2$ gave rather ambiguous results – upfield shift for the bpy protons, but no NOE contacts between bpy protons and upper-rim resorcinarene protons – these experiments were repeated in a mixture of tetrachloromethane and [D_6] -acetone (7:3), because CCl_4 was found to be less competitive for inclusion in resorcinarene capsules than $CHCl_3$.[144] As before, the addition of acetone is necessary to provide sufficient solubility of the ruthenium complex.

The ^{1}H NMR spectrum of a 6:1 mixture of C_{11}-resorcinarene and $[Ru(bpy)_3][Al(OC(CF_3)_3)_4]_2$ in CCl_4/[D_6]-acetone (7:3) shows larger upfield shifts for the aromatic protons of the bipyridine ligands (between 0.3 and 1.2 ppm) as well as a small downfield shift for the upper-rim-resorcinarene protons (Figure 4.6.11).

As the shifts are larger than in $CHCl_3$/[D_6]-acetone (7:3), the Ru complex seems to be complexed more strongly by the resorcinarenes or at least dive more deeply into the resorcinarenes' cavity.

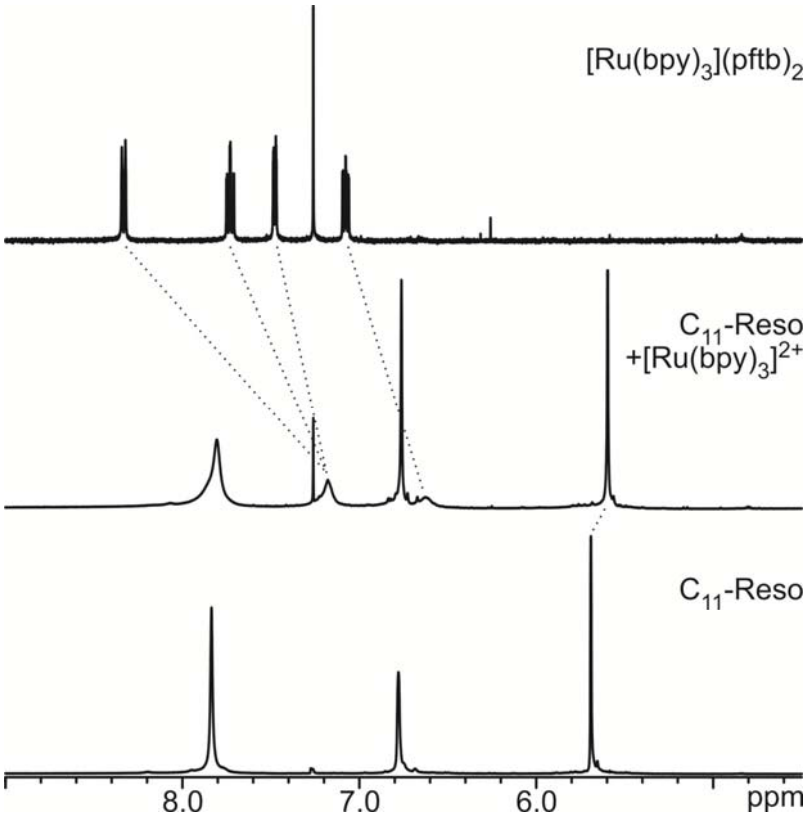

Figure 4.6.11 *^{1}H NMR spectra of top: $[Ru(bpy)_3][Al(OC(CF_3)_3)_4]_2$, bottom: C_{11}-resorcinarene, and middle: a 6:1 mixture of resorcinarene and $[Ru(bpy)_3][Al(OC(CF_3)_3)_4]_2$. All spectra were recorded in a solvent mixture of CCl_4 and [D_6]-acetone (7:3). The bpy protons experience an upfield shift between 0.3 and 1.2 ppm upon addition of the resorcinarene.*

The ^{1}H NOESY NMR spectrum of the mixture of $[Ru(bpy)_3][Al(OC(CF_3)_3)_4]_2$ and C_{11}-resorcinarene in CCl_4/[D_6]-acetone (7:3) shows NOE contacts between the resorcinarene-OH protons and the two signals for the bipyridine protons as well as between the bpy protons and the upper-rim-resorcinarene protons (Figure 4.6.12).

Particularly the latter speaks for the encapsulation of $[Ru(bpy)_3]^{2+}$ in a resorcinarene aggregate.

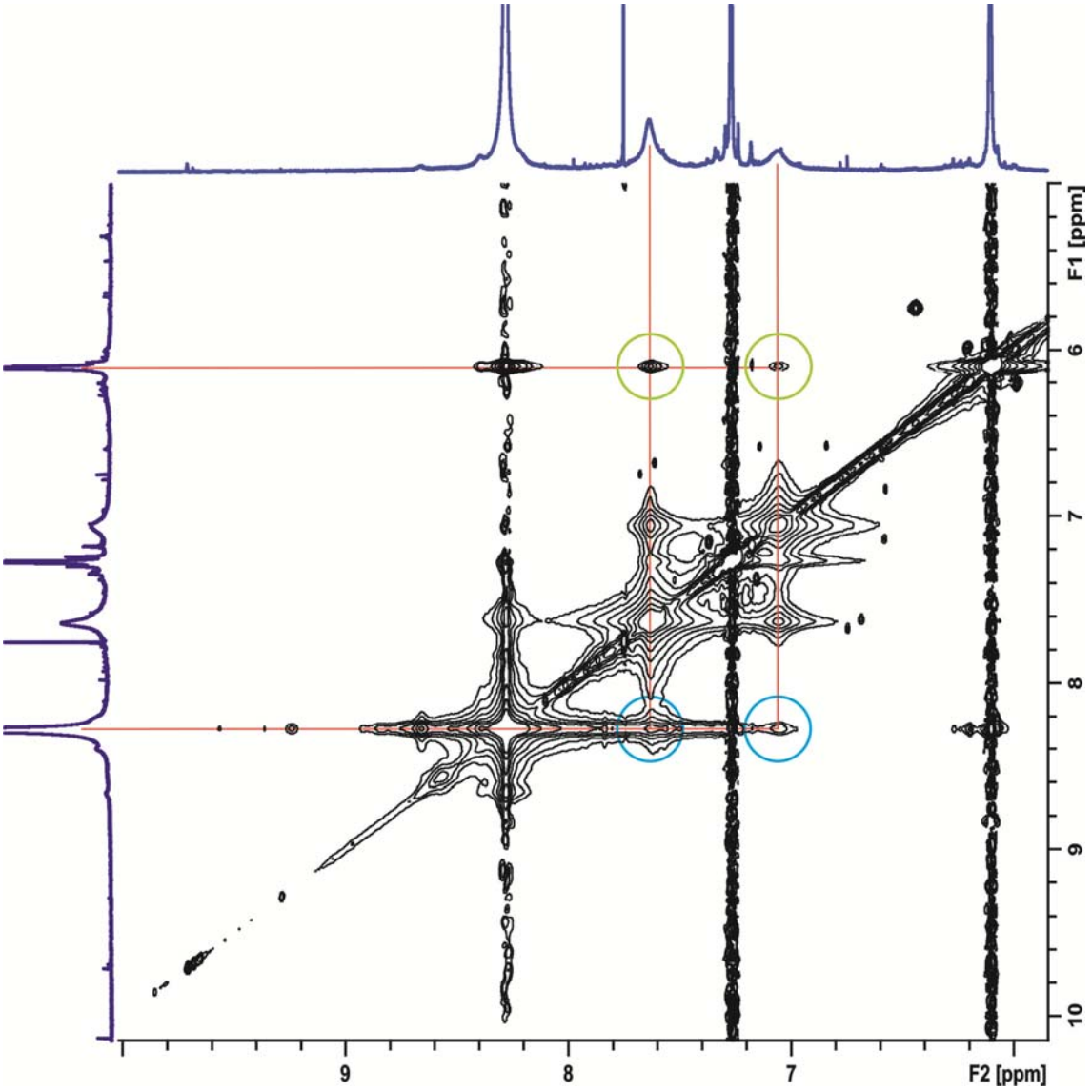

Figure 4.6.12 *^{1}H NOESY NMR spectrum of a 6:1 mixture of $[Ru(bpy)_3][Al(OC(CF_3)_3)_4]_2$ and C_{11}-resorcinarene measured in a solvent mixture of CCl_4 and [D_6]-acetone (7:3). Cross peaks are observed for couplings between the bpy-protons (unclear, which ones due to signal overlap) and upper-rim resorcinarene-H (green circles) as well as the bpy protons and the resorcinarene-OHs (blue circles).*

To finally assure for complex formation between resorcinarene and $Ru(bpy)_3^{2+}$, DOSY NMR experiments were performed.

The first experiment with **C_{11}-Reso** in pure $CDCl_3$ could confirm a diffusion coefficient of $0.25 \cdot 10^{-5}$ cm²/s corresponding to a hydrodynamic radius of 15.3 Å. Exactly the same value has been observed earlier by Cohen et al.[145] However, it should be noted that molecular modeling of a hexamer with six C_2-Resos according to the hydrogen bonding pattern found in the crystal structure results in an energetic minimum for the structure shown in Fig. 4.6.1 with an average diameter of approx. 20 Å.

The same experiment with $[Ru(bpy)_3][Al(OC(CF_3)_3)_4]_2$ and **C_{11}-Reso** measured in a solvent mixture of $CHCl_3$ and $[D_6]$-acetone (7:3) gives a diffusion coefficient of $0.47 \cdot 10^{-5}$ cm²/s for both, the Ru complex as well as for the resorcinarene. The dynamic viscosity of the mixture of chloroform and acetone can be estimated by the Refutas equation[146] and is approx. $\eta_{chloroform/acetone} = 0.48$ mPa•s. Given this, the hydrodynamic radius of the $[Ru(bpy)_3]^{2+}$/**C_{11}-Reso** complex corresponds to 4.5 Å, which clearly indicates the formed aggregate to be much smaller than expected for a hexamer. Most probably, this aggregate is a 1:1 complex.

However, the experiment with $[Ru(bpy)_3][Al(OC(CF_3)_3)_4]_2$ and **C_{11}-Reso** measured in a solvent mixture of CCl_4 and $[D_6]$-acetone (7:3) gives a diffusion coefficient of $0.28 \cdot 10^{-5}$ cm²/s for both, the Ru complex as well as for the resorcinarene (Figure 4.6.13). The dynamic viscosity of the mixture of tetrachloromethane and acetone is approx. $\eta_{tetrachloromethane/acetone} = 0.75$ mPa•s. The hydrodynamic radius of the $[Ru(bpy)_3]^{2+}$/**C_{11}-Reso** complex would then correspond to 10.5 Å, which clearly shows that the use of tetrachloromethane instead of chloroform helps to form larger aggregates. Nevertheless, one has to admit that the hydrodynamic radius observed for **C_{11}-Reso** in pure chloroform is not reached. The most likely explanation for this is the formation of an equilibrium of $[Ru(bpy)_3]^{2+}$/**C_{11}-Reso** aggregates of different sizes and stoichiometries.

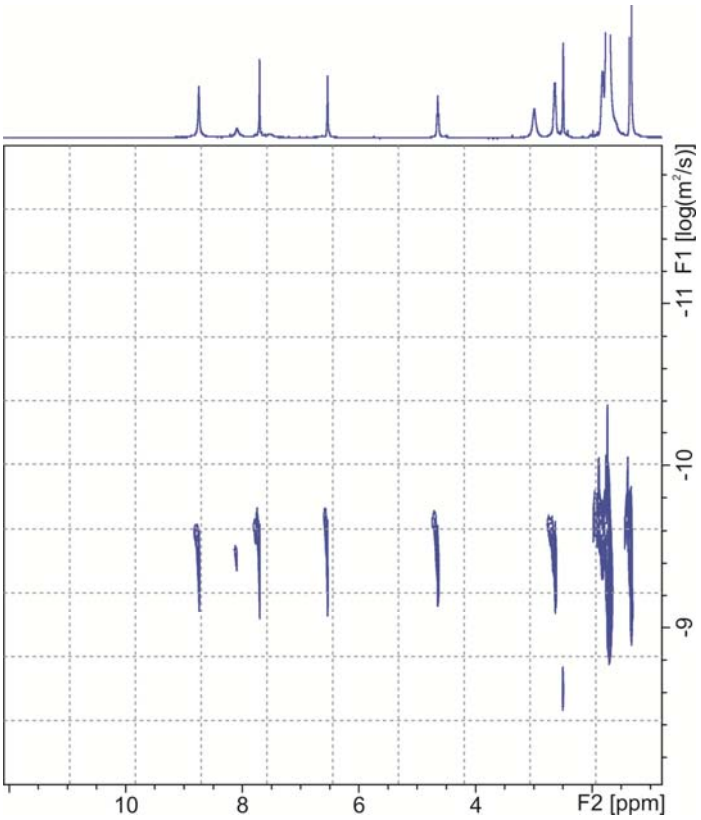

Figure 4.6.13 *^{1}H DOSY NMR spectrum of a mixture of $[Ru(bpy)_3][Al(OC(CF_3)_3)_4]_2$ and C_{11}-resorcinarene measured in a solvent mixture of CCl_4 and $[D_6]$-acetone (7:3).*

4.6.3 Gas-Phase Studies on Resorcinarene Hexamer Formation

ESI-MS experiments with mixtures of a) $[Ru(bpy)_3][Al(OC(CF_3)_3)_4]_2$ and C_2-resorcinarene sprayed from a solvent mixture of $CHCl_3$ and acetone (7:3) and b) $[Ir(ppy)_2(bpy)][Al(OC(CF_3)_3)_4]$ and C_2-resorcinarene sprayed from $CHCl_3$ showed the expected affinity for the formation of $[[Ru(bpy)_3]+\mathbf{C_2\text{-}Reso}]^{2+}$ hexamers (Figure 4.6.14) as already observed for the same mixture with the hexafluorophosphate anion.[136] For practical reasons, **C_2-Reso** is used for the gas phase experiments to keep the *m/z* values of the large hexamers in a lower and easier to measure region – especially in case of the singly charged guest complex.

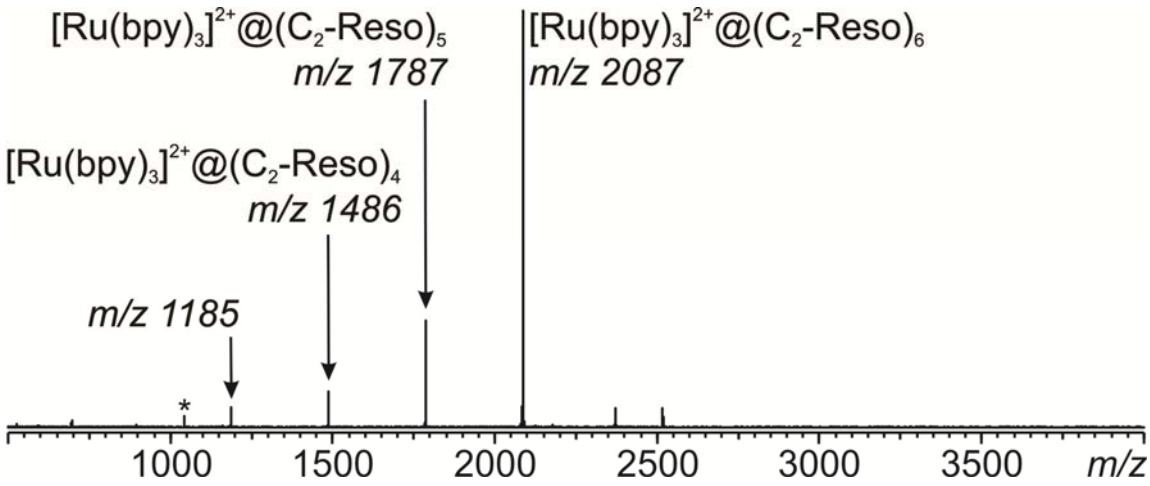

Figure 4.6.14 *ESI-FTICR mass spectrum of a mixture of $[Ru(bpy)_3][Al(OC(CF_3)_3)_4]_2$ and C_2-resorcinarene (1:6; concentration of* ***C_2-Reso*** *= 250 μM) sprayed from a solvent mixture of $CHCl_3$ and acetone (7:3). The signal for the 6:1 complex (m/z 2087) is by far the most intense. Furthermore, also smaller signals for the 5:1 (m/z 1787), 4:1 (m/z 1486), and 3:1 (m/z 1185) complexes are observed. The asterisk denotes the first overtone of the hexamer.*

In marked contrast, the use of the single charged complex $[Ir(ppy)_2(bpy)]^+$ with the $[Al(OC(CF_3)_3)_4]^-$ anion does not lead to the formation of resorcinarene hexamers. Instead, only smaller 1:1, 2:1, 3:1, 4:1, and 5:1 aggregates with an apparent preference for the 3:1 complex are observed (Figure 4.6.15).

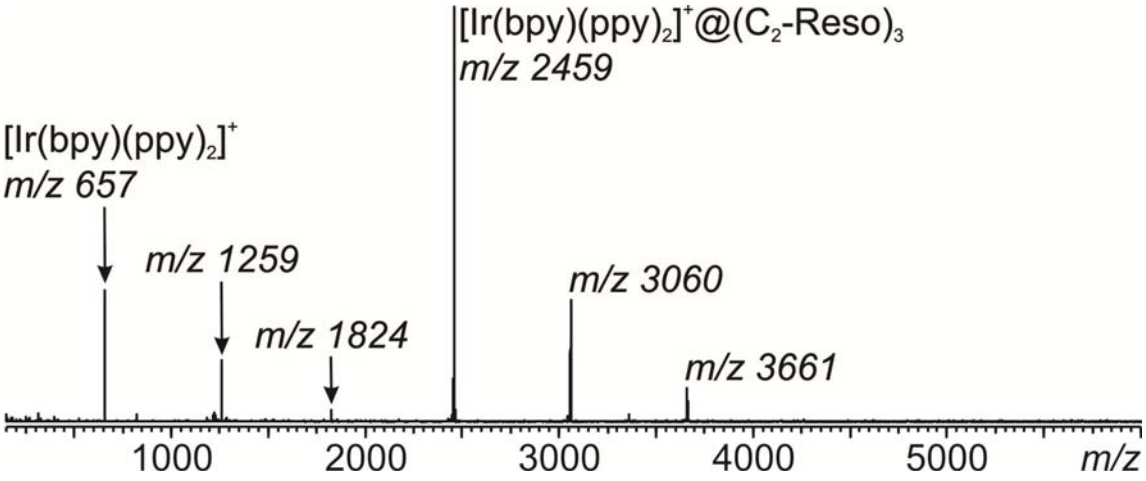

Figure 4.6.15 *ESI-FTICR mass spectrum of a mixture of $[Ir(ppy)_2(bpy)][Al(OC(CF_3)_3)_4]$ and C_2-resorcinarene (1:6; concentration of* ***C_2-Reso*** *= 250 μM) sprayed from $CHCl_3$. The spectrum shows signals for the 5:1 (m/z 3661), 4:1 (m/z 3060), 3:1 (m/z 2459), 2:1 (m/z 1824), and 1:1 (m/z 1259) complex as well as for the free iridium complex (m/z 657).*

In addition to these two experiments, a double syringe experiment was performed to gain more insight into the formation of and monomer exchange between resorcinarene hexamers. For this experiment, two solutions were prepared in two separate syringes: Solution 1 contained a mixture of $[Ru(bpy)_3][Al(OC(CF_3)_3)_4]_2$ and **C_2-Reso** in a ratio of 1:6 at a concentration of 250 μM for **C_2-Reso** in a solvent mixture of $CHCl_3$ and acetone (7:3). Solution 2 contained a mixture of $[Ru(bpy)_3][Al(OC(CF_3)_3)_4]_2$ and **C_3-Reso** in a ratio of 1:6 at a concentration of 250 μM for **C_3-Reso** in the same solvent mixture.

If the hexamers were already formed in solution and moderately stable, no or at least slow exchange of resorcinarene monomers might be observed at low mixing times – thus short transfer capillary – of two hexamers with different resorcinarenes.

However, after a reaction time of 10 s, the resulting mass spectrum (Figure 4.6.16) shows an almost perfect statistical distribution of mixed hexamers. This could be attributed to two possible reasons: a) If the hexamers are already formed in solution, the exchange of resorcinarene monomers is very fast, which is rather reasonable due to the 30 % of acetone in the solution. This competing solvent would help to disrupt the seam of hydrogen bond holding the hexamer together and therefore allow for a quick monomer exchange leading to the statistical distribution. b) If the hexamers are not already formed in solution but during the electrospray process, this would obviously lead to a statistical distribution as observed.

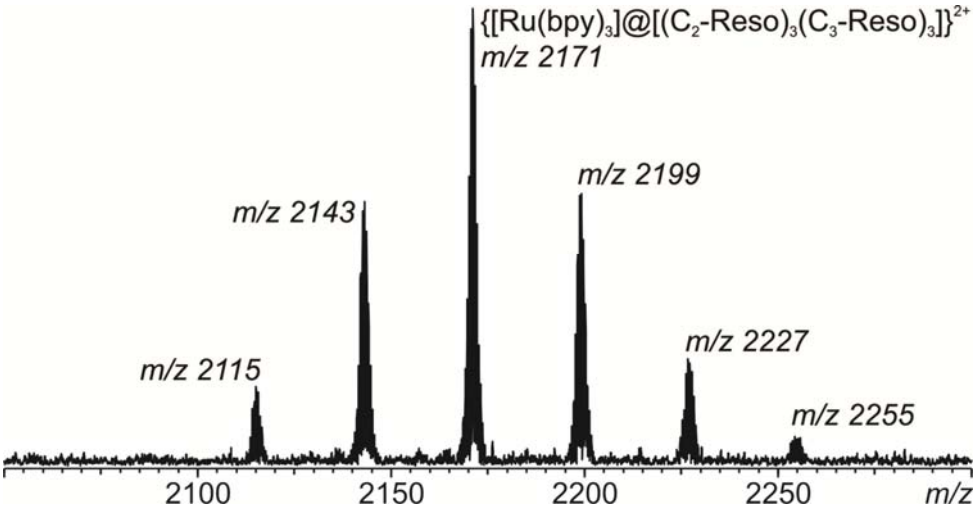

Figure 4.6.16 *ESI-FTICR mass spectrum obtained from a double-syringe experiment after a reaction time of 10 s. Syringe 1 contained a mixture of* $[Ru(bpy)_3][Al(OC(CF_3)_3)_4]_2$ *and* ***C_2-Reso*** *(1:6; concentration of* ***C_2-Reso*** *= 250 μM) in a solvent mixture of* $CHCl_3$ *and acetone (7:3), syringe 2 contained a mixture of* $[Ru(bpy)_3][Al(OC(CF_3)_3)_4]_2$ *and* ***C_3-Reso*** *(1:6; concentration of* ***C_3-Reso*** *= 250 μM) in the same solvent mixture. The spectrum shows an almost perfect statistical distribution of mixed hexamers.*

4.6.4 Conclusions drawn from the Comparison of the Solution and Gas-Phase Studies on Resorcinarene Hexamer Formation

The comparison of different pseudooctahedral metal complexes with different charge states (0, +I, +II) and different counter anions showed a clear trend for preferred encapsulation of the doubly charged $Ru(bpy)_3^{2+}$ complex in resorcinarene capsules in solution: Whereas no interactions with the resorcinarene could be observed for neutral $Ir(ppy)_3$ and singly charged $[Ir(ppy)_2(bpy)]^+$, the addition of **C_{11}-Reso** causes significant upfield shifts of the bpy protons in the $Ru(bpy)_3^{2+}$ complex. This is only observed with the extremely weakly coordinating anion $[Al(OC(CF_3)_3)_4]^-$, whereas hexafluorophosphate apparently prevents binding of $Ru(bpy)_3^{2+}$ to resorcinarenes. These results show that a) ion pairing – or to be more precise the absence or at least weakening of the latter – plays a crucial role in allowing resorcinarene/metal-complex encapsulation and that b) encapsulation requires at least *two* positive charges on the metal complex to provide sufficiently high cation-π interactions.

The importance of the second charge is impressively confirmed by ESI-MS experiments: Whereas $Ru(bpy)_3^{2+}$ preferably forms 6:1 complexes with resorcinarenes in the gas phase – regardless of which counteranion is used (PF_6^- or $[Al(OC(CF_3)_3)_4]^-$), this is not observed for the iridium complex $[Ir(ppy)_2(bpy)]^+$ with charge +1. In fact, only 1:1 to 5:1 aggregates are seen in the corresponding mass spectra.

The combination of the results shows that a) clear proofs for the formation of hexameric encapsulation complexes in solution could not be found – not even for doubly charged $Ru(bpy)_3^{2+}$ in combination with the $[Al(OC(CF_3)_3)_4]^-$ anion.
b) Further, the fact that these 6:1 encapsulation complexes are nevertheless observed – and even preferred – in the gas phase strongly indicates the hexameric capsules encapsulating the $Ru(bpy)_3^{2+}$ complex are most probably formed during the electropray ionization process. One reasonable mechanism for the formation of the hexamer would follow the path of resorcinarenes successively "clipping" to each one pyridine subunit of the ruthenium complex upon proceeding shrinking progress of the charged droplets.

4.7 The Influence of the counteranion on the Cation Binding towards Upper-Rim substituted Resorcinarenes[**]

Recognition motifs based on hydrogen bonds are by far the most frequently used tools in the design of organic supramolecular architectures with desired properties.[147, 148] Anions play an important role in a range of biological, chemical, environmental and medical processes, so the design and synthesis of ditopic multisite host systems for the simultaneous recognition of anionic and cationic guest species (ion pair recognition) is a quickly developing area of research.

Resorcinarenes,[149,150] generally considered one of the work horses in supramolecular chemistry, possess a multipurpose scaffold with potential for further functionalization. Their rich host-guest chemistry includes the formation of open inclusion complexes,[151,152] dimeric,[153,154] and hexameric[136,155,156,] capsules as well as nanotubes.[157] The encapsulation of guest molecules into reversibly formed, self-assembled capsules and reactions mediated or even catalyzed[158,159,160] by encapsulation mimic biological processes such as substrate recognition in enzymes and its conversion into metabolites. The aromatic rings of resorcinarenes are highly activated for electrophilic substitution leading to resorcinarenes with various functionalities.[161-167] The electron-rich nature of the aromatic rings of the bowl-shaped resorcinarene is mainly responsible for their ability to attract guest species fitting into the interior size of the resorcinarene cavity. Attaching different substituents to resorcinarenes varying in size and electronic nature provides the platform for fine-tuning the complexation abilities of these host compounds.

Tandem mass spectrometry is a tool used to examine the recognition properties of host compounds in the gas-phase. The fact that effects of solvents or counterions can be ruled out allows the study of the intrinsic properties of such non-covalently bound complexes.[168] Dimeric[154] and hexameric[136,155,156] capsules of resorcinarenes, pyrogallarenes and related compounds encapsulating small and large cations have been shown to prevail in the gas phase as isolated species and have been shown to be connected by a closed seam of hydrogen bonds.[169-177]

[**] The results presented in this chapter have been published in:

N. K. Beyeh, D. P. Weimann, L. Kaufmann, C. A. Schalley, K. Rissanen, *Chem. Eur. J.* **2012**, *18*, 5552

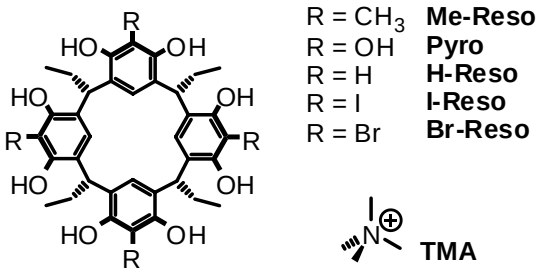

Figure 4.7.1 *Differently upper-rim substituted resorcinarene hosts and guest cation tetramethylammonium (**TMA**).*

The combination of both, tandem mass spectrometry and ^{1}H NMR titration, allows a precise determination of the influence of the counteranion on the binding behavior: NMR titration experiments reflect the binding processes in solution taking into account the presence of the counteranions, whereas tandem mass spectrometry experiments reveal the exclusive interactions between resorcinarene host and tetramethylammonium.

To investigate the relative binding ability of the differently substituted resorcinarene hosts (Figure 4.7.1) towards tetramethylammonium (**TMA**) in the gas phase, a solution of each two of the hosts and the guest in equimolar concentrations in acetonitrile with 1-5 % MeOH was electrosprayed and the corresponding heterodimeric complex encapsulating the guest cation **TMA** was isolated and fragmented by irradiation with an infrared multiphoton dissociation (IRMPD) laser. With this methodology, it is possible to determine even small differences in binding strength, as the peak intensity for the monomeric complexes is directly related to the binding strength of the host.

Figure 4.7.2 shows the isolation and fragmentation spectra of the capsule [**TMA@Me-Reso•H-Reso**]$^{+}$. The isolation and fragmentation of the heterodimeric capsule (*m/z* 1331) results in a much higher intensity for the monomeric complex [**TMA@Me-Reso**]$^{+}$ (*m/z* 730) than for [**TMA@H-Reso**]$^{+}$ (*m/z* 674).

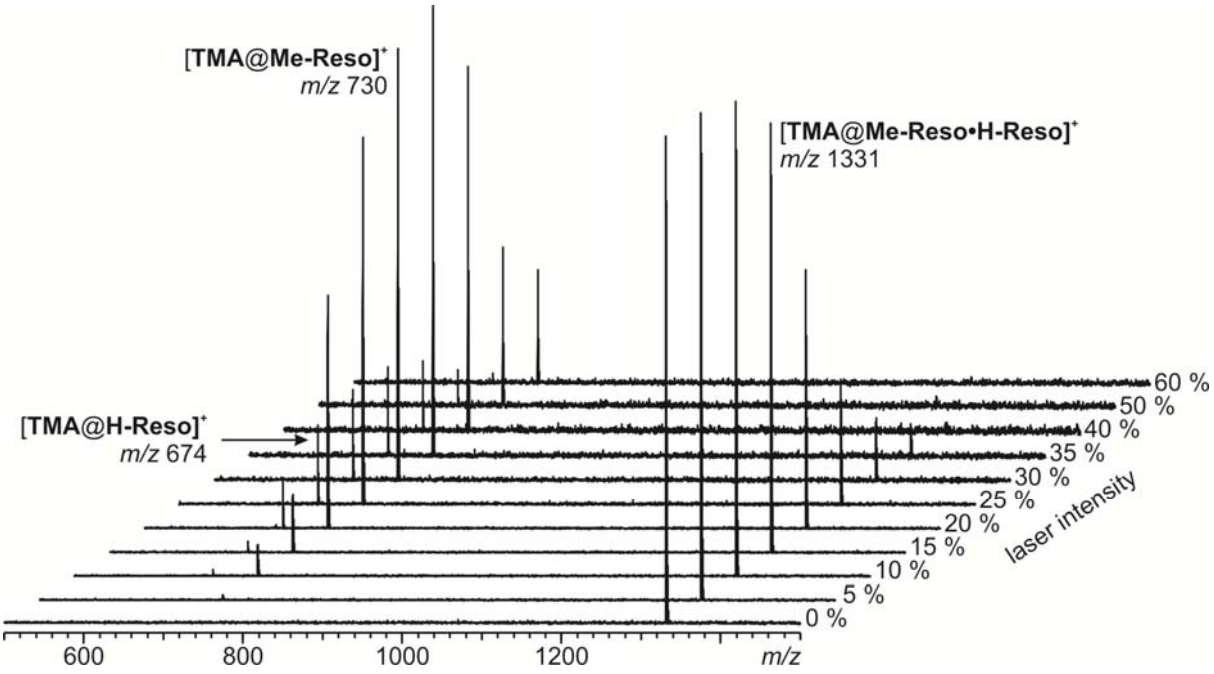

Figure 4.7.2 *Gas-phase isolation and laser-induced fragmentation spectra of heterodimeric complex* ***[TMA@Me-Reso•H-Reso]***$^{+}$*. After fragmentation by laser irradiation (t = 500 ms), the* ***TMA*** *cation preferably sticks to* ***Me-Reso*** *(m/z 730).*

Since the cation in the monomeric assembly is mainly bound by cation-π interactions, the inductive effect of the substituents on the aromatic ring of the resorcinarene is responsible for this discriminative behavior. The electron donating effect of the methyl group increases the electron density of the aromatic ring making it more susceptible to positively charged guest species through cation-π interactions. Therefore, the cation prefers to stick to **Me-Reso** instead of **H-Reso**. These experiments were performed accordingly with different equimolar mixtures of each two of the resorcinarenes and **TMA** (Figure 4.7.3 to 4.7.8):

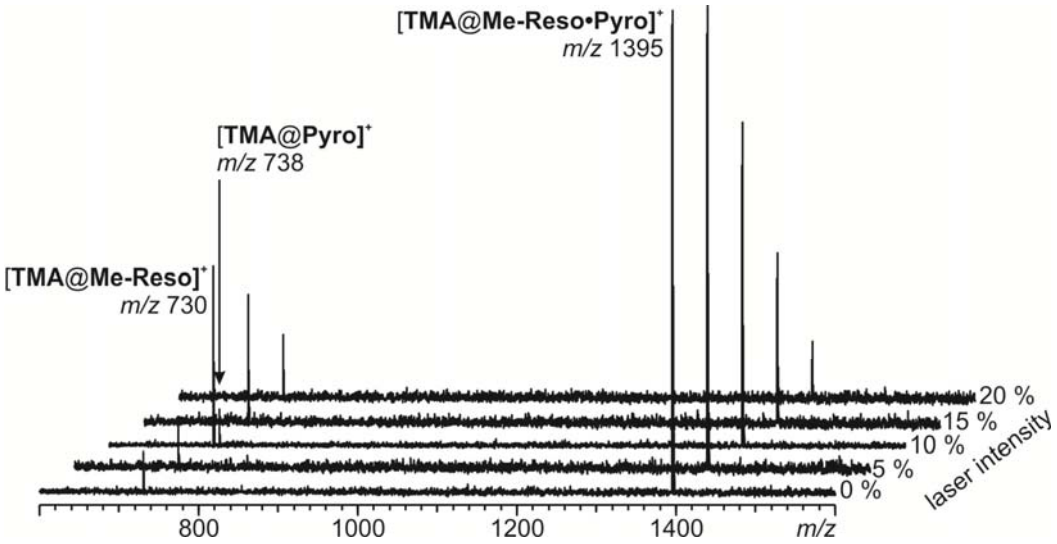

Figure 4.7.3 *Gas-phase isolation and laser-induced fragmentation spectra of heterodimeric complex* ***[TMA@Me-Reso•Pyro]***$^{+}$*. After fragmentation by laser irradiation (t = 500 ms), the* ***TMA*** *cation preferably sticks to* ***Me-Reso*** *(m/z 730).*

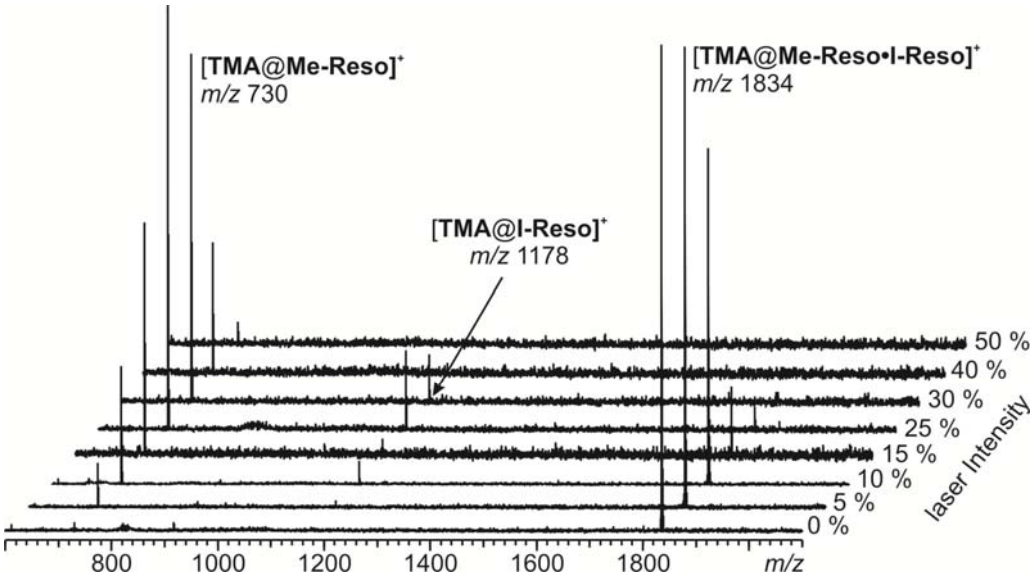

Figure 4.7.4 *Gas-phase isolation and laser-induced fragmentation spectra of heterodimeric complex* ***[TMA@Me-Reso•I-Reso]***$^{+}$*. After fragmentation by laser irradiation (t = 500 ms), the* ***TMA*** *cation preferably sticks to* ***Me-Reso*** *(m/z 730).*

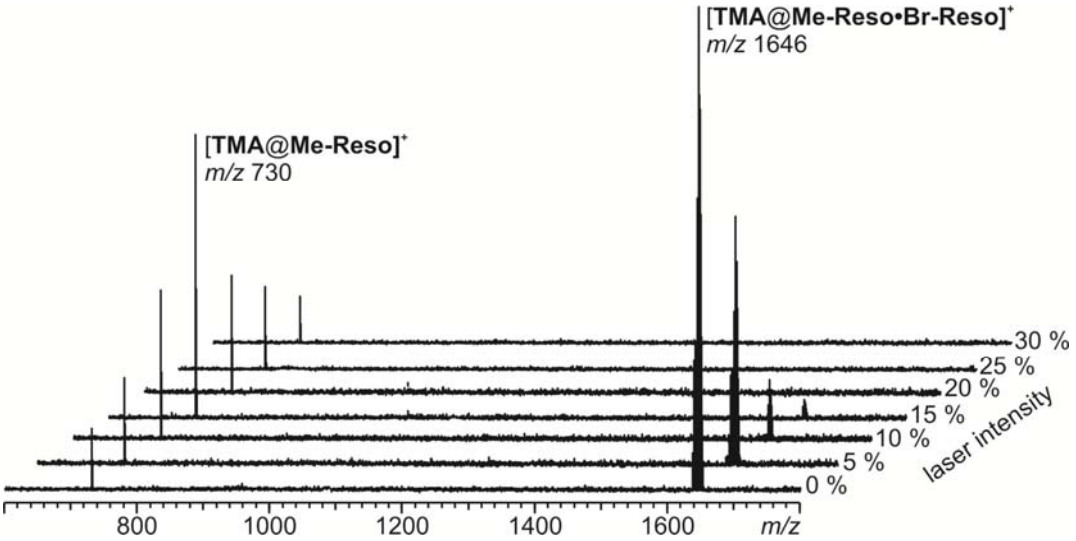

Figure 4.7.5 *Gas-phase isolation and laser-induced fragmentation spectra of heterodimeric complex* ***[TMA@Me-Reso•Br-Reso]***$^{+}$*. After fragmentation by laser irradiation (t = 500 ms), the* ***TMA*** *cation preferably sticks to* ***Me-Reso*** *(m/z 730), whereas a signal for the complex* ***[TMA@Br-Reso]***$^{+}$ *is not even observed.*

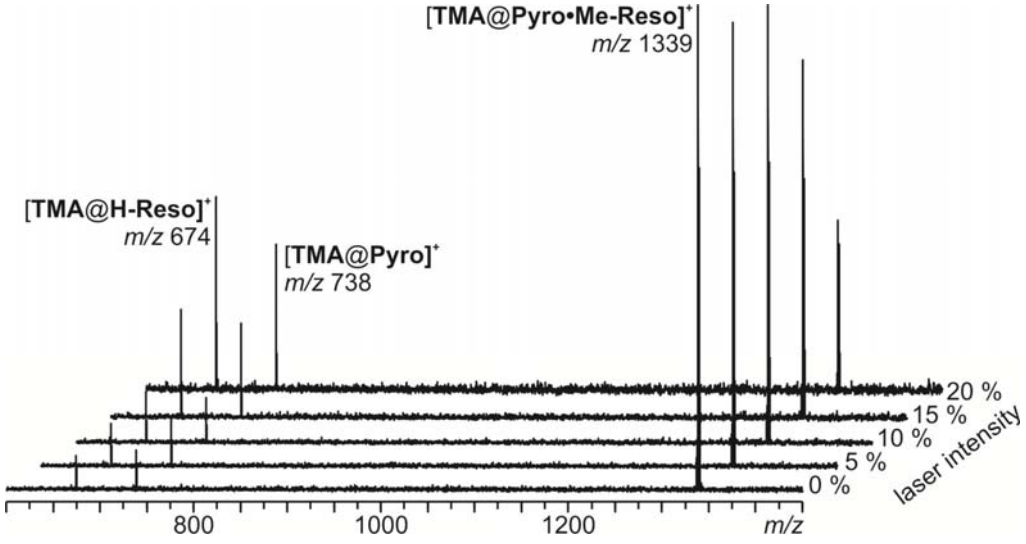

Figure 4.7.6 *Gas-phase isolation and laser-induced fragmentation spectra of heterodimeric complex* ***[TMA@Pyro•H-Reso]***$^{+}$*. After fragmentation by laser irradiation (t = 500 ms), the* ***TMA*** *cation does not preferably stick to either* ***Pyro*** *(m/z 738) or* ***H-Reso*** *(m/z 674).*

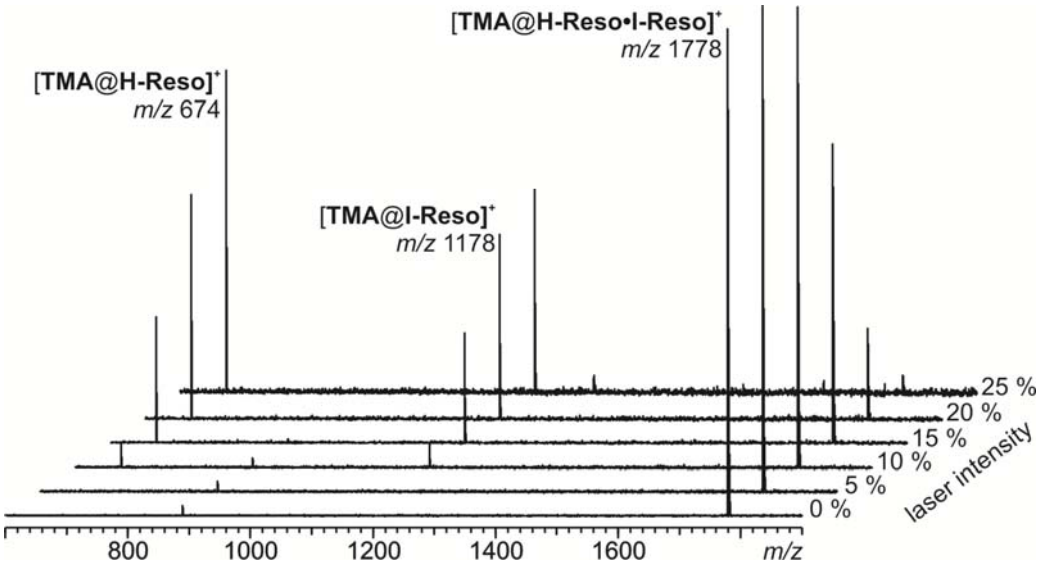

Figure 4.7.7 *Gas-phase isolation and laser-induced fragmentation spectra of heterodimeric complex* ***[TMA@H-Reso•I-Reso]***$^{+}$*. After fragmentation by laser irradiation (t = 500 ms), the* ***TMA*** *cation preferably sticks to* ***H-Reso*** *(m/z 674).*

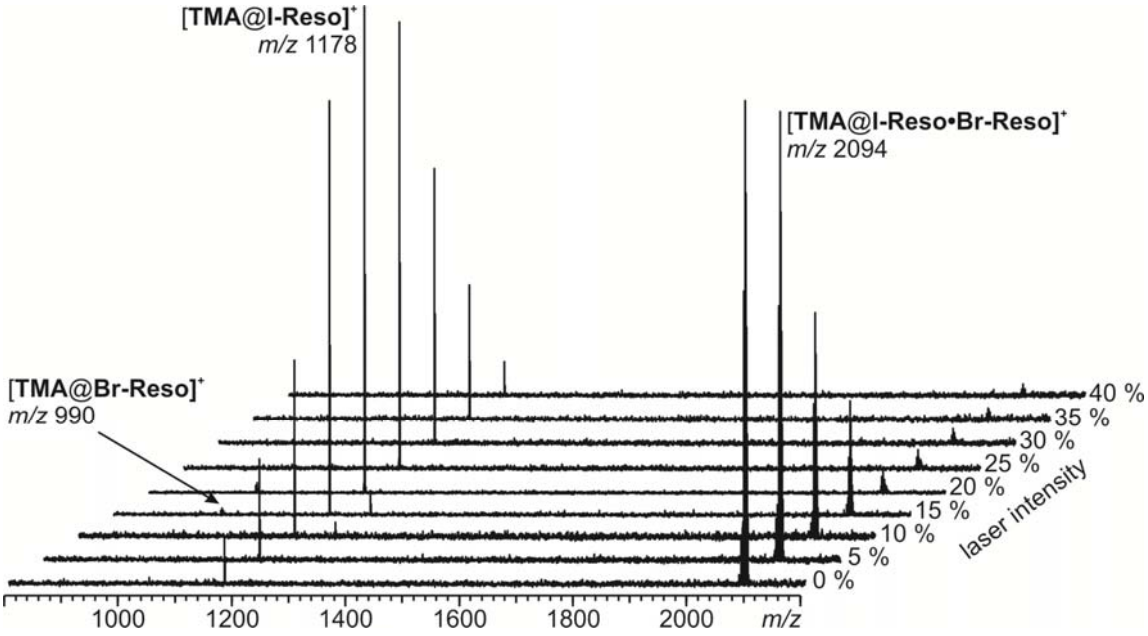

Figure 4.7.8 *Gas-phase isolation and laser-induced fragmentation spectra of heterodimeric complex* ***[TMA@I-Reso•Br-Reso]***$^{+}$*. After fragmentation by laser irradiation (t = 500 ms), the* ***TMA*** *cation preferably sticks to* ***I-Reso*** *(m/z 1178).*

From these experiments, a clear ranking of binding strength evolved. The ability to complex the tetramethylammonium cation (**TMA**) decreases in the following order of upper-rim substituents (R-group in Figure 4.7.1):

CH_3 (**Me-Reso**) > OH (**Pyro**) ≈ H (**H-Reso**) > I (**I-Reso**) >> Br (**Br-Reso**),

This mainly corresponds to the substituents' electronic effects. However, there might be additional effects on the binding energy that are caused by direct interactions with the upper-rim substituents, as even the rather small tetramethylammonium ion is not completely buried inside the cavity. Consequently, the more polarizable methyl substituents would stabilize the cation somewhat better than the hydroxy substituents.

Complexation studies in solution of the different resorcinarenes with **TMA**Br and **TMA**BF_4 were undertaken by ^{1}H NMR titration experiments via addition of increasing amounts of the salts to a solution of the resorcinarene hosts in methanol-d_4. For solubility reasons, less polar solvents could not be used in the titration experiments. For the same reason, solutions of the tetramethylammonium salts had to be added to the less soluble resorcinarenes Significant complexation-induced upfield shifts of the guest signals were observed as expected from the shielding effects of the aromatic rings of the bowl-shaped host cavity upon addition of the guest. This clearly points to a guest exchange fast on the NMR time scale at 303 K. Job plot experiments[178,179] indicate a 1:1 complex stoichiometry in methanol-d_4. The lack of formation of the dimer in solution is probably due to the efficiency with which the solvent competes with the hydrogen-bonding system of the hosts and also solvates the ions present. The saturation shift for the methyl protons of the **TMA** cation in methanol-d_4 differs accordingly with the respective hosts, whereas the largest shift is observed for **Pyro** as the host.

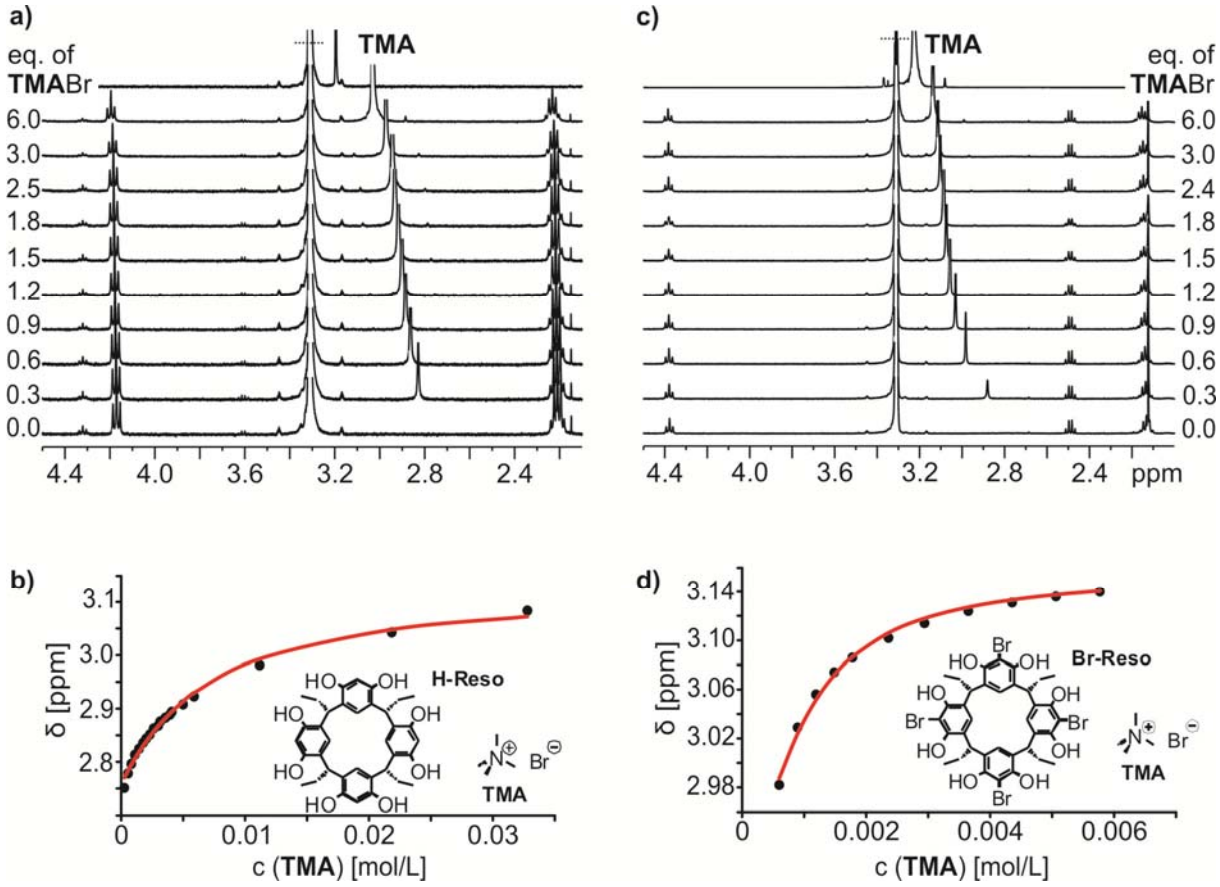

Figure 4.7.9 a) *Spectral changes observed upon the addition of up to 6 equivalents of* ***TMA****Br to* ***H-Reso*** *in CD_3OD and* ***b)*** *the corresponding ^1H NMR fitting.* ***c)*** *Spectral changes observed upon the addition of up to 6 equivalents of* ***TMA****Br to* ***Br-Reso*** *in CD_3OD and* ***d)*** *the corresponding ^1H NMR fitting. The amount of added* ***TMA*** *salt (in equivalents) is given by the numbers next to each NMR spectrum in panel a) and c). The top spectrum in panel a) and c) corresponds to free* ***TMA****Br in CD_3OD.*

The binding constants were obtained by non-linear least square titration curve fit of the respective titration data based on a 1:1 host-guest binding model using the spreadsheet software developed by K. Hirose.[179,180]

From the curvature of the titration curve, the binding constant was determined by non-linear curve fitting based on equation 4.7.1 using the spreadsheet software from Prof. Dr. Keiji Hirose. In this equation, δ_{obs} is the observed shift of the signals of **TMA** at each titration step as a function of the initial concentrations of host $[H]_0$ and guest $[G]_0$. δ_0 is the chemical shift of free **TMA** and $\Delta\delta_{max}$ is the difference between the theoretical signal shift at 100 % complexation and δ_0.

$$\delta_{obs} = \delta_0 + \frac{\Delta\delta_{max}}{2[H]_0}\left[\frac{1}{K_a} + [H]_0 + [G]_0 - \sqrt{\left(\frac{1}{K_a} + [H]_0 + [G]_0\right)^2 - 4[H]_0[G]_0}\right] \quad [4.7.1]$$

The results of these calculations are displayed in Table 4.7.1.

Table 4.7.1 *Binding constants K_a for the differently substitutred resorcinarene hosts with guests* ***TMA****Br and* ***TMA****BF_4.[a] Errors are within ± 10%.*

counteranion	Br^-	BF_4^-
	K_a $[M^{-1}]$[b]	K_a $[M^{-1}]$[b]
TMA@Me-Reso	121	213
TMA@Pyro	478	450
TMA@H-Reso	170[c]	120
TMA@I-Reso	2141	1246
TMA@Br-Reso	2549	1550

[a] In CD_3OD at 303 K. [b] Obtained from monitoring the **TMA** signals. [c] This binding constant is in close agreement with those previously reported in the literature.[154,181]

Surprisingly, the observed trend does not correspond to the one expected from the upper-rim substituents' electronic effects as observed in the gas-phase. In solution, the tetra-halogenated resorcinarenes **I-Reso** and **Br-Reso** gave much higher binding constants than the non-halogenated resorcinarenes (**Me-Reso**, **Pyro**, and **H-Reso**) regardless of whether the bromide or the tetrafluoroborate salt is used. This effect indicates an influence of the counter anion, which additionally might bind to the resorcinarene.

Considering the binding of **TMA** to the halogenated resorcinarenes **I-Reso** and **Br-Reso**, significantly lower binding constants are observed for **TMA**BF_4 as compared to **TMA**Br, which is expected due to the lower ion pairing energy of the tetrafluoroborate salt and confirms the assumption that the counteranion is involved in the binding process. However, this trend is not observed in case of the non-halogenated resorcinarene hosts.

The very different binding behavior of the tetrahalogenated resorcinarenes (**I-Reso** and **Br-Reso**) on the one hand and the non-halogenated resorcinarenes **Me-Reso, H-Reso** and **Pyro** on the other hand clearly indicates that the binding in solution involves the counteranions. The fact that the tetrabrominated host **Br-Reso** gave a higher binding constant than the tetraiodinated host **I-Reso** for both counteranions indicates that the host interacts with the counteranion through the hydrogen bonding motif O–H•••X^-.

The electronic effects of the halogens render the hydrogen on the hydroxyl group more acidic, which therefore is able to form stronger hydrogen bonds to the anions. This effect is more pronounced in case of **Br-Reso** as compared to **I-Reso** due to the higher electronegativity of bromine. Figure 4.7.10a schematically illustrates the cooperative interplay of all non-covalent interactions involved in the ion-pair binding.

An optimized geometry calculation on the AM1 MOZYME level (Figure 4.7.10b) gives an additional hint that the anion is bound to the resorcinarene by a combination of cation-anion interactions as well as hydrogen bonding. According to this calculation, the anion might sit in a pocket formed out of the **TMA** cation, two of the upper-rim bromine substituents, and the hydroxyl group pointing upwards.

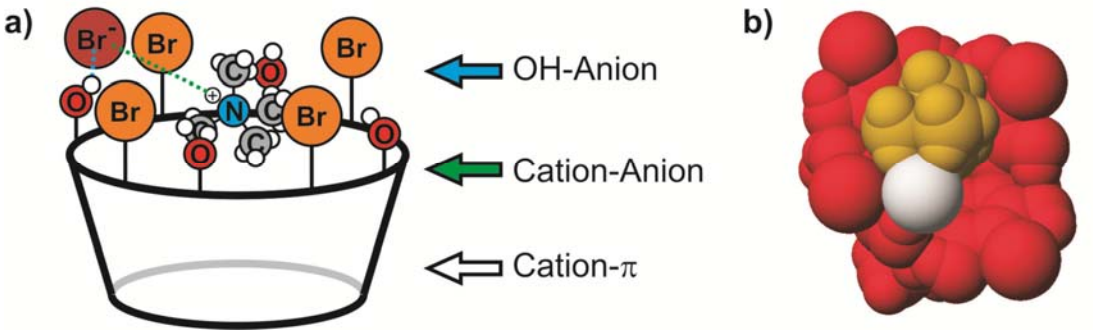

Figure 4.7.10 a) *Schematic illustration of the ion pair binding of tetramethylammonium bromide to quadruply brominated resorcinarene (**Br-Reso**) by the combination of cation-π and O-H•••anion interactions.* ***b)*** *AM1 MOZYME optimized structure of the same complex. The tetramethylammnium cation (orange) sits in the middle of the resorcinarene bowl (red), whereas the bromide anion (white) is located in a pocket formed out of the **TMA** cation, two of the upper-rim bromine substituents, and the hydroxyl group pointing upwards.*

In conclusion, these results highlight the importance to not only take into account the substituents of the host but also the counteranion of a cationic guest to tune the complexation ability of a host-guest-complex.

Whereas often the main focus for the design and the optimization of the binding behavior of a cation receptor lies only on the pure host-guest interactions, this study could show by combining gas-phase and solution studies that also the counteranion can and will play a crucial role in the recognition event.

Contrary to the gas phase, the incorporation of bromine and iodine substituents on the upper rim of resorcinarene receptors greatly enhances the binding of the tetramethylammonium cation (**TMA**) in solution. A change of the counteranion from Br^- to BF_4^- causes a significant reduction of the binding energy.

This clearly indicates that in solution the counter anion also actively plays a key role in the complexation behaviour and that the halogenated resorcinarenes are capable of binding ion-pairs through cation-π interactions and hydrogen bonding in a synergetic manner in a competitive solvent.

These results show how the complexation ability of cation receptors can be enhanced and fine-tuned by creating a means to additionally bind the corresponding counteranion, which might find an application in supramolecular ion pair receptors.

5. Conclusion and Outlook

The present thesis provides new insights on the field of the analysis and control of molecular motion as well as molecular recognition.

In the more synthetically oriented part, the well-known Hunter/Vögtle-type tetralactam macrocycle could be modified accordingly so that a change of the pH value from neutral to strongly basic allows the formation of a new intramolecular hydrogen bond between a macrocycle's amide proton and the now deprotonated phenolate on the macrocycle's isophthaloyl moiety. This intramolecular binding induces a conformational rearrangement of the macrocycle. The possibility to control the steric conformation of the macrocycle allows to affect the shuttling rate in bistationary [2]rotaxane-based molecular shuttles: Depending on the central spacer separating the two ethylene diamide stations, two different effects caused by the deprotonation-induced conformational switch may influence the shuttling rate.

The finding that the same external trigger – namely change of the pH value – can influence the shuttling rate in bistationary [2]rotaxane-based molecular shuttles in a completely opposite way depending on the nature of the central spacer moiety integrated in the axle could find possible applications in the design and construction of various molecular machines. One might possibly think about attaching similar systems to nanoparticles, depositing them on various surfaces, or extending the principle of the control over the shuttling rate to multivalent systems.

Furthermore, the potential of intramolecular hydrogen bonding could be applied to direct Hunter/Vögtle-type macrocyclization reaction towards the selective formation of octalactam macrocycles, which are not more than side products under the usual reaction conditions. This shows that intramolecular non-covalent interactions cannot only be applied for the control in dynamic processes, but also for the control over the outcome of the synthesis of large supramolecular receptor systems.

In the first project of the more analytically oriented part, intriguingly simple H/D exchange experiments conducted in the highly diluted gas phase provide evidence for the ability of 18-crown-6 to quickly move along oligolysine peptide chains and over the periphery of POPAM dendrimers. Furthermore, mechanistic studies of suitable model compounds showed the crown ethers to move together with a proton from an ammonium to an amino group. Finally,

the zwitterionic structure of crown complexes of acid-terminated oligolysine peptides is expressed by the isotope exchange behaviour.
The highly diluted gas phase inside a mass spectrometer provides the ideal conditions for the investigation of the dynamics within non-covalent complexes, as intermolecular processes that might likely occur in solution can be ruled out completely here.
Consequently, gas-phase experiments provide insight into a completely new reactivity of weakly bound supramolecular complexes and suggest many synthetic as well as biological non-covalent complexes to exhibit a more pronounced dynamic behaviour than commonly recognized. Unravelling the dynamics in non-covalent complexes will contribute significantly to the analysis of biomolecular function. The H/D exchange discussed here for the particular example of crown ether/oligolysine complexes establishes a novel and remarkably simple approach to address this mobility phenomenon. From a methodological point of view, the experiments discussed above extend the scope of H/D exchange experiments to the question of large-scale molecular motion.

The potential of mass spectrometry and gas-phase experiments was then extended to the investigation of the binding of anions to different receptor molecules through hydrogen bonding and anion-π interactions, respectively. It could be shown that mass spectrometric experiments are perfectly suited to complement results from experiments in solution (e.g. from NMR) or even to extend the view on recognition phenomena. Under environment-free conditions in the highly diluted gas phase, weak non-covalent interactions are more likely to be observed than in solution, especially in competing solvents. Thus, in both cases – resorcinarene scaffold with four *o*-phenylenediamine side arms as well as a class of several monomeric and dimeric naphthalene diimide systems – more anions could be found to bind to the anion receptors in the gas phase than in solution. Furthermore, the gas phase allows the exclusive study of the intrinsic properties of a receptor without any solvation effects.

The importance of taking into account more than just one analytical method for the investigation of supramolecular recognition and complexation events becomes even clearer during the study of a) hexamer formation from resorcinarenes encapsulating pseudooctahedral transition metal complexes and b) ion pair binding to upper-rim substituted resorcinarenes. In both cases, only the combination of different analytical methods – and in fact even the comparison of different results for the same systems in solution vs. gas phase – is able to

deliver valuable information about the formation pathway of resorcinarene hexamers and the binding mode of ion pairs to upper-rim substituted resorcinarenes.

In both cases, NMR studies in solution do not comply with the data obtained from MS and MS^2 experiments. However, the combination of solution and gas phase results opens a new view on the basic interactions taking place during the binding process so that it is of prime importance to always carefully investigate especially those results that initially may seem contradictory.

6. Experimental Section

6.1 General Methods

6.1.1 Analytical Methods

^{1}H NMR spectra were recorded with *Bruker* AC 250 (250 MHz), *Bruker* ECX (400 MHz), *Jeol* Eclipse 500 (500 MHz), *Bruker* Avance 500 (500 MHz), and *Bruker* AVANCE III (700 MHz) with $CDCl_3$, CD_3OD or [D_6]-DMSO as the solvent. Chemical shifts are expressed in ppm and are given relative to tetramethylsilane (δ = 0 ppm) as calibrated with the solvent signal ($CDCl_3$: δ = 7.26 ppm; CD_3OD: δ = 3.13 ppm; [D_6]-DMSO: δ = 2.50 ppm).

^{13}C NMR spectra were recorded with *Bruker* AC 250 (62.5 MHz), *Bruker* ECX (100 MHz), and *Bruker* AV 500 (125.5 MHz) with $CDCl_3$, CD_3OD or [D_6]-DMSO as solvent. The chemical shifts are expressed in ppm and are given relative to tetramethylsilane (δ = 0) as calibrated with the solvent signal (CDCl3: δ = 77.0 ppm; CD_3OD: δ = 49.0 ppm; d_6-DMSO: δ = 39.52 ppm).

Mass spectra were recorded with a Finnigan Mat 711 (EI, 80 eV, 8 kV), an Agilent 6210 ESI-TOF, and an Agilent QFT-7 FTICR mass spectrometer with Micromass Z-Spray ESI source.

IR spectra were measured with a Nicolet FTIR spectrometer 5 SXC with DTGS-detector.

Thin layer chromatography (TLC) analysis was performed on *Merck* silica gel 60 F_{254} plates.

Elemental analysis is not suitable for analysis of most of the compounds synthesized in this thesis, since usually solvent molecules are co-crystallized in the cavity of the tetralactam macrocycle. Instead, exact masses can be determined.

6.1.2 Preparative Methods

Purchased chemicals (from ALDRICH, ACROS, MERCK and LANCESTER) were used without further purification. If necessary, all solvents were dried by standard methods (CH_2Cl_2 over $CaCl_2$ and Et_2O over Na).

Column chromatography was conducted on silica gel 60 (230 - 400 mesh, 40 - 63 µm, *Fluka*).

6.1.3 Description of the Gas-Phase Experiments in Chapter 4.3 (Molecular "Spacewalk")

All gas-phase experiments described herein were conducted with an Ionspec QFT-7 FTICR mass spectrometer (Agilent, Lake Forest/USA), equipped with a 7 T superconducting magnet and a Micromass Z-Spray electrospray ionization (ESI) source (Waters Co., Saint-Quentin, France). The samples were introduced into the source as 50 µM solutions of 18-crown-6 and Lys_{15}, 1,12-diaminododecane, Lys_5, or **G1** - **G5** POPAM dendrimer, respectively, in methanol with 1 % formic acid at flow rates of 1 - 4 µL/min. A constant spray and highest intensities were achieved with a capillary voltage of 3800 V and a source temperature of 40 °C. The parameters for sample cone and extractor cone voltages as well as the ion optics were optimized for maximum intensities of the desired complex ions. Multiple scans (up to 20) were recorded and averaged for each spectrum in order to improve the signal-to-noise ratio.

For the gas-phase H/D exchange experiments, the hexapole ion accumulation/collision cell of the FTICR mass spectrometer was used as an ion trap and reaction chamber for the isotope exchange reaction. After ion accumulation in the hexapole collision cell, the entrance of new ions into the hexapole was blocked by switching off the radio frequency of the quadrupole in front of the hexapole. To conduct the isotopic exchange, CH_3OD was then introduced into the collision cell after a short delay. The reaction time was controlled with the help of a solenoid pulse valve, which can be controlled with high temporal precision (steps of down to ca. 25 µs caused reproducible changes in the exchange behavior in the early stages of the H/D

exchange). After the H/D exchange reaction, the ions were transferred into the instrument's FTICR analyzer cell and detected by a standard excitation and detection sequence with high mass accuracy and baseline resolution for the isotope patterns of all charge states.

6.1.4 Description of the Gas-Phase Experiments in Chapter 4.4 (Resorcinarene-based Anion Receptor)

All gas-phase experiments described in chapter 4.4 were conducted with an Ionspec QFT-7 FT-ICR mass spectrometer (Agilent, Lake Forest/USA), equipped with a 7 T superconducting magnet and a Micromass Z-Spray electrospray ionization (ESI) source (Waters Co., Saint-Quentin, France). The samples were introduced into the source as 50 μM solutions of **4** and the corresponding anion in acetonitrile (or methanol) at flow rates of 1–2 μL/min. A constant spray and highest intensities were achieved with a capillary voltage of 3800 V at a source temperature of 40 °C. The parameters for sample cone and extractor cone voltage were optimized for maximum intensitites of the desired complexes. Multiple scans (10–20) were recorded and averaged for each spectrum in order to improve the signal-to-noise ratio. After accumulation and transfer into the instrument's FTICR analyzer cell, the ions were detected by a standard excitation and detection sequence. For the fragmentation experiments, the ions of interest were mass selected in the ICR cell and irradiated with a 25 W CO_2 laser in the IR region (infrared multiphoton dissociation (IRMPD), 10.6 μm wavelength) to induce fragmentation. The H/D exchange experiments were conducted as described above (see 6.1.3).

6.1.5 Description of the Gas-Phase Experiments in Chapter 4.5 (Anion Binding to Naphthalene Diimides)

The (tandem) mass spectrometric experiments described in chapter 4.5 were conducted with an Ionspec QFT-7 FTICR mass spectrometer (Agilent, Lake Forest/USA), equipped with a 7 T superconducting magnet and a Micromass Z-Spray electrospray ionization source (Waters). The samples were introduced into the source as 50 μM solutions of NDI and the tetrabutyl ammonium salt of the corresponding anion in acetonitrile at flow rates of 1–2 μL/min. A constant spray and highest intensities were achieved with a capillary voltage of 3,000–3,800 V (depending on the used NDI and anion) and at a source temperature of 40 °C. The parameters for the sample cone (20–45 V) and extractor cone (8–10 V) voltages were optimized for maximum intensities of the desired complexes. Multiple scans (20–50) were recorded and averaged for each spectrum to improve the signal-to-noise ratio. After accumulation and transfer into the instrument's FTICR analyser cell, the ions were detected by a standard excitation and detection sequence. For the fragmentation experiments, the ions of interest were mass selected in the ICR cell and irradiated with a 25 W CO_2 laser in the infrared region (infrared multiphoton dissociation, 10.6 μm wavelength) to induce fragmentation.

6.1.6 Description of the Gas-Phase Experiments in Chapter 4.6 (Formation of Resorcinarene Hexamers)

The mass spectrometric experiments described in chapter 4.6 were performed with an Ionspec QFT-7 Fourier-Transform Ion-Cyclotron-Resonance (FTICR) mass spectrometer (Agilent, Lake Forest/USA), equipped with a 7 T superconducting magnet and a Micromass Z-Spray ESI-Source (Waters Co., Saint-Quentin/France). The samples were introduced into the source as solutions in either pure chloroform in case of the iridium complexes or in a mixture of chloroform/acetone (7:3) in case of the ruthenium complexes at flow rates of 4 μL/min. The solutions were 250 μM with respect to the concentration of the pyrogallarene and resorcinarenes and approx. 1/6 of that with respect to the concentration of the metal complexes. A constant spray and highest intensities were achieved with a capillary voltage of 3800 V at a source temperature of 40 °C. The parameters for sample cone and extractor cone

voltages as well as the ion optics were optimized for maximum intensities of the desired larger complex ions. After accumulation and transfer of the ions into the FTICR analyzer cell of the instrument, the ions were detected by a standard excitation and detection sequence. Multiple scans (up to 50) were recorded and averaged for each spectrum in order to improve the signal-to-noise ratio.

For the double syringe experiment, two solutions were prepared in two separate syringes: Solution 1 contained a mixture of $[Ru(bpy)_3][Al(OC(CF_3)_3)_4]_2$ and **C_2-Reso** in a ratio of 1:6 at a concentration of 250 μM for **C_2-Reso** in a solvent mixture of $CHCl_3$ and acetone (7:3). Solution 2 contained a mixture of $[Ru(bpy)_3][Al(OC(CF_3)_3)_4]_2$ and **C_3-Reso** in a ratio of 1:6 at a concentration of 250 μM for **C_3-Reso** in the same solvent mixture. Both solutions were then pumped simultaneously into a mixing T that is connected to the ion source. Ionization and detection were performed as described above.

6.1.7 Description of the Gas-Phase Experiments in Chapter 4.7 (Ion-Pair Binding to Halogenated Resorcinarenes)

The mass spectrometric experiments described in chapter 4.7 were performed with an Ionspec QFT-7 Fourier-Transform Ion-Cyclotron-Resonance (FTICR) mass spectrometer (Agilent, Lake Forest/USA), equipped with a 7 T superconducting magnet and a Micromass Z-Spray ESI-Source (Waters Co., Saint-Quentin/France). The samples were introduced into the source as 50 μm solutions in CH_3CN containing 1–5% MeOH to dissolve the guest salts at flow rates of 1–2 μL/min_1. A constant spray and highest intensities were achieved with a capillary voltage of 3800 V at a source temperature of 40 °C. The sample cone voltage was adjusted to –30 V. After accumulation and transfer of the ions into the FTICR analyzer cell of the instrument, the ions were detected by a standard excitation and detection sequence. Multiple scans (10–50) were recorded and averaged for each spectrum in order to improve the signal-to-noise ratio. To determine a ranking of binding strength, 1:1:1 solutions of two resorcinarenes and NMe_4OH were electrosprayed and the corresponding heterodimeric capsule was isolated and fragmented by irradiation with a CO_2 IR laser (λ = 10.6 μm). The laser power is tunable between 0 and 100% of 25 W.

6.2 Synthesis of Tetra- and Octalactam Macrocycles

6.2.1 Synthesis of Isophthaloyol Building Blocks

5-*tert*-Butyl-isophthaloyl dichloride

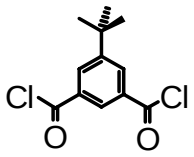

5 g (22.5 mmol / 222.2 g/mol) of 5-tert-butyl-isophthalic acid were suspended in 16.3 ml (26.8 g / 225 mmol / 119 g/mol / 10 eq.) of thionyl chloride and the mixture was refluxed for 6 h. Afterwards, the excess of $SOCl_2$ was removed in water-jet vacuum. The residue was washed with petrol ether. Recrystallisation from petrol ether yielded 5-*tert*-butyl-isophthaloyl dichloride as colourless crystals.

Yield: quant.

For NMR analysis, a small amount of 5-tert-butyl-isophthaloyl dichloride was converted to the corresponding ethyl ester by stirring it in some ethanol for 10 minutes.

$C_{12}H_{12}Cl_2O_2$ 259.13 g/mol

^{1}H NMR (250 MHz, $CDCl_3$, 298 K)
δ [ppm] = 1.33 (s, 9H, ^{t}Bu-H); 1.37 (t, 6H, CH_3); 4.36 (q, 4H, CH_2); 8.21 (s, 2H, H4 & H6); 8.44 (s, 1H, H2)

^{13}C NMR (62.5 MHz, $CDCl_3$, 298 K)
δ [ppm] = 14.10 (CH_3); 30.91 ($C(\mathbf{C}H_3)_3$); 34.71 ($\mathbf{C}(CH_3)_3$); 61.01 (CH_2); 127.64 (C2); 130.39 (C1 & C3); 130.55 (C4 & C6); 151.72 (C5); 166.01 (**C**=O)

The analytical data was consistent with the literature values.[182]

4-Methoxyisophthaloyl dichloride

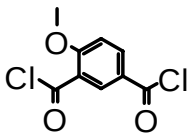

1.14 g (196.16 g/mol / 5.8 mmol) 4-Methoxyisophthalic acid were suspended in 15 ml $SOCl_2$ and 1 ml DMF and refluxed for 6 h. After evaporation of the $SOCl_2$, the brownish crude product was recrystallized from CH_2Cl_2/petrol ether (1:1).

Yield: quant. (colorless crystalline solid)

For NMR analysis, the product was converted to the corresponding ethyl ester.

$C_9H_6Cl_2O_3$ 233.05 g/mol

^{1}H NMR (400 MHz, $CDCl_3$, 298 K)

δ [ppm] = 1.34 (t, 6H, ethyl-CH_3); 4.32 (s, 6H, OCH_3); 6.96 (d, 1H, H5); 8.10 (dd, 1H, H6); 8.40 (d, 1H, H2)

MS (EI, 70 eV)

m/z = 232,0 ($[M+H]^{+\bullet}$); 197,0 ($[M-Cl]^+$)

The analytical data was consistent with the literature values.[183]

4,6-Dihydroxy-isophthalic acid

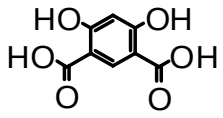

22 g resorcinol (110.11 g/mol / 200 mmol) were mixed with 40 g $KHCO_3$ (100.12 g/mol / 400 mmol) and heated in an autoclave to 220 °C for 6 h under 30-50 bar Ar pressure. The mixture was then dissolved in 200 ml H_2O and extracted with Et_2O. Upon addition of aqueous HCl the crude product precipitated from the solution, which was then recrystallized from 4 l H_2O. Yield: 40 %

$C_8H_6O_6$ 198.13 g/mol

^{1}H NMR (400 MHz, $CDCl_3$, 298 K)
δ [ppm] = 6.38 (s, 1H, H5); 8.27 (s, 1H, H2); 11.80 (br, OH)

MS (EI, 70 eV)
m/z = 198.0 ($[M]^{+\bullet}$); 180.0 ($[M - H_2O]^{+\bullet}$); 168.0 ($[M - 2\ H_2O]^{+\bullet}$); 134.0 ($[M - 2\ H_2O - CO]^{+\bullet}$); 106.2 ($[M - 2\ H_2O - 2\ CO]^{+\bullet}$)

The analytical data was consistent with the literature values.[184]

4,6-Dimethoxy-isophthalic acid dimethyl ester

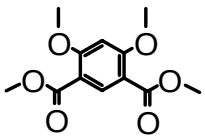

11.3 g 4,6-Dihydroxy-isophthalic acid (198.13 g/mol / 57 mmol) and 50 ml Me_2SO_4 (1.33 g/cm³ / 66.6 g / 126.13 g/mol / 540 mmol) were dissolved in 300 ml acetone and 82.8 g K_2CO_3 (138.21 g/mol / 600 mmol) were added. This mixture was refluxed for 4 d. After cooling to r.t. 100 ml CH_2Cl_2 were added and the solution was stirred for 30 minutes. The insoluble residue was filtered off and the organic layer was washed once with water. After evaporating the solvent, the residue was washed with water and dried *in vacuo*.
Yield: 91 %

$C_{12}H_{14}O_6$ 254.24 g/mol

^{1}H NMR (400 MHz, $CDCl_3$, 298 K)
δ [ppm] = 3.85 (s, 6H, OCH_3); 3.96 (s, 6H, $COOCH_3$); 6.46 (s, 1H, H5); 8.45 (s, 1H, H2)

MS (EI, 70 eV)
m/z = 254.0 ($[M]^{+\bullet}$); 223.0 ($[M - CH_3O]^+$); 196.0 ($[M - C_2H_2O_2]^+$); 165.0 ($[M - OCH_3 - COOCH_3]^+$); 134.8 ($[M - 2\ COOCH_3]^+$)

The analytical data was consistent with the literature values.[185]

4,6-Dimethoxy-isophthalic acid

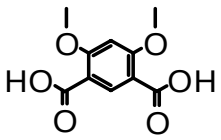

15.6 g 4,6-Dimethoxy-isophthalic acid dimethyl ester (254.24 g/mol / 61.3 mmol) were dissolved in 45 ml MeOH and a solution of 6 g NaOH in 15 ml H_2O was added. The mixture was refluxed for 4 h. The product precipitated upon acidification with HCL (24 %) and was collected by filtration.

Yield: 78 %

$C_{10}H_{10}O_6$ 226.18 g/mol

^{1}H NMR (400 MHz, $CDCl_3$, 298 K)

δ [ppm] = 3.89 (s, 6H, OCH_3); 6.67 (s, 1H, H5); 8.18 (s, 1H, H2); 12.41 (br, 2H, COOH)

MS (EI, 70 eV)

m/z = 226.1 ($[M]^{+\cdot}$); 209.0 ($[M - OH]^+$); 197.0 ($[M – CHO]^+$); 179.0 ($[M – CHO – H_2O]^+$)

The analytical data was consistent with the literature values.[185]

4,6-Dimethoxy-isophthaloyl dichloride

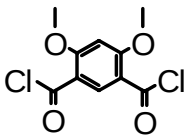

2.26 g 4,6-Dimethoxy-isophthalic acid (226.18 g/mol / 10 mmol) were suspended in 100 ml dry CH_2Cl_2 and 4.5 ml oxalyl chloride (1.48 g/cm³ / 6.66 g / 126.93 g/mol / 52.5 mmol) and 2 drops of DMF were added. The mixture was then refluxed for 1 h and then concentrated to dryness. Yield: 99 %

For ^{1}H-NMR analysis, the product was converted to the corresponding ethyl ester.

$C_{10}H_8Cl_2O_4$ 263.07 g/mol

^{1}H NMR (400 MHz, $CDCl_3$, 298 K)

δ [ppm] = 1.35 (t, 6H, ethyl-CH_3); 3.94 (s, 6H, OCH_3); 4.31 (q, 4H, ethyl-CH_2); 6.45 (s, 1H, H5); 8.41 (s, 1H, H2)

The analytical data was consistent with the literature values.[185]

4,6-Dibenzyloxy-isophthalic acid dibenzyl ester

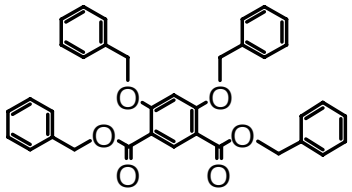

10 g 4,6-Dihydroxy-isophthalic acid (198.13 g/mol / 50.5 mmol) and 34.9 g K_2CO_3 (138.2 g/mol / 252 mmol) were dissolved in 100 ml DMF and heated to 60 °C for 2 h. After addition of 24.3 ml benzyl bromide (34.5 g / 171 g/mol / 202 mmol), the mixture was heated to 100 °C for 2 d. The reaction mixture was filtered while still hot and the residue was extracted with ethyl acetate. The combined organic phases were concentrated to dryness and redissolved in CH_2Cl_2, washed with brine and water and dried with Na_2SO_4. Evaporation of the solvent gives the product as a colourless solid.
Yield: 49 %

$C_{36}H_{30}O_6$ 558.62 g/mol

^{1}H NMR (400 MHz, $CDCl_3$, 298 K)
δ [ppm] = 5.15 (s, 4H, C**H**$_2$); 5.32 (s, 4H, C**H**$_2$); 6.57 (s, 1H, H5); 7,34 (br, 20H, Ph-**H**); 8.61 (s, 1H, H2)

^{13}C NMR (100 MHz, $CDCl_3$, 298 K)
δ [ppm] = 65.12 (**C**H_2); 70.93 (**C**H_2); 99.28 (C5); 112.59 (C1 & C3); 127.11 (Ph-C_{ortho}); 127.13 (Ph-C_{ortho}); 128.26 (Ph-C_{para}); 128.57 (Ph-C_{para}); 128.66 (Ph-C_{meta}); 128.83 (Ph-C_{meta}); 133.45 (C2); 135.85 (Ph-C_{ipso}); 136.22 (Ph-C_{ipso}); 163.08 (C4 & C6); 164.94 (**C**=O)

Note: The NMR spectra also show signals for an impurity - most probably benzylic alcohol from not reacted benzyl bromide - which could be removed easily in the following step.

MS ESI-TOF, positive mode, sprayed from MeOH
m/z = 581.1947 ($[M + Na]^+$); 1139.3999 ($[2M + Na]^+$); 1698.6080 ($[3M + Na]^+$)

4,6-Dibenzyloxy-isophthalic acid

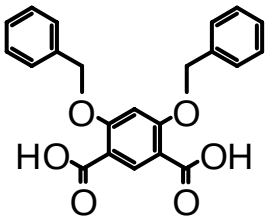

13.94 g 4,6-Dibenzyloxy-isophthalic acid dibenzyl ester (558.6 g/mol / 25 mmol) were dissolved in 45 ml MeOH and a solution of 6 g NaOH in 15 ml H_2O was added. The mixture was heated to reflux for 4 h. The product was precipitated by acidification of the solution with HCl (37 %), filtrated from the remaining solution, washed with water, and dried *in vacuo*.
Yield: 68 %

$C_{28}H_{18}O_6$ 378.37 g/mol

^{1}H NMR (400 MHz, [D_6]-DMSO, 298 K)
δ [ppm] = 5.27 (s, 2H, C**H**$_2$); 6.95 (s, 1H, H5); 8.21 (s, 1H, H2); 7.30 (t, 2H, H_{para}); 7.37 (t, 4H, H_{meta}); 7.48 (d, 4H, H_{ortho}); 12.48 (s, 2H, COO**H**)

^{13}C NMR (100 MHz, [D_6]-DMSO, 298 K)
δ [ppm] = 70.57 (**C**H_2); 100.25 (C5); 113.14 (C1 & C3); 127.68 (Ph-C_{ortho}); 128.33 (Ph-C_{para}); 128.97 (Ph-C_{meta}); 136.56 (C2); 136.99 (Ph-C_{ipso}); 162.62 (C4 & C6); 166.36 (**C**=O)

MS ESI-TOF, negative mode, sprayed from MeOH
m/z = 377.1040 ([M - H]$^-$)

4,6-Dibenzyloxy-isophthaloyl dichloride

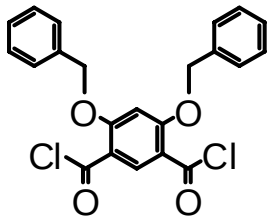

5.94 g 4,6-Dibenzyloxy-isophthalic acid (378.4 g/mol / 15.6 mmol) were dissolved in 120 ml CH_2Cl_2. After addition of 6,8 ml oxalyl chloride (1.48 g/cm^3 / 10 g / 126.9 g/mol / 78.7 mmol) and some drops of DMF, the solution was heated to reflux for 2 h. Evaporation of the solvent resulted in the product as an off-white solid.

Yield: 99 %

For NMR analysis, the product was converted to the ethyl ester by stirring with ethanol for 10 minutes.

$C_{22}H_{16}Cl_2O_4$ 415.27 g/mol

^{1}H NMR (400 MHz, $CDCl_3$, 298 K)

δ [ppm] = 1.32 (t, 6H, ethyl-C**H**$_3$); 4.33 (quart, 4H, ethyl-C**H**$_2$); 5.13 (s, 4H, Bn-C**H**$_2$); 6.53 (s, 1H, H5); 7.36 (m, 10H, Ph-**H**); 8.48 (s, 1H, H2)

^{13}C NMR (100 MHz, $CDCl_3$, 298 K)

δ [ppm] = 14.39 (ethyl-**C**H$_3$); 60.89 (ethyl-**C**H$_2$); 70.83 (**C**H$_2$); 99.25 (C5); 112.99 (C1 & C3); 126.98 (Ph-C$_{ortho}$); 128.17 (Ph-C$_{para}$); 128.73 (Ph-C$_{meta}$); 135.96 (C2); 137.07 (Ph-C$_{ipso}$); 162.68 (C4 & C6); 165.13 (**C**=O)

MS EI, 70 eV

m/z = 413.8 ($[M]^{+\bullet}$); 379.1 ($[M - Cl]^+$); 288.3 ($[M - Cl - toluene]^+$); 253.2 ($[M - 2Cl - toluene]^{+\bullet}$);

($[M - 2 Cl - CO]^{+\bullet}$); ($[M - 2 Cl - 2 CO]^{+\bullet}$); ($[M - 2 Cl - 2 CO - C_2H_2]^{+\bullet}$); ($[M - 2 Cl - 2 CO - C_2H_2 - C_4H_2]^{+\bullet}$)

6.2.2 Synthesis of Extended Diamine Building Blocks

4,4'-(Cyclohexane-1,1-diyl)bis(2,6-dimethylaniline) ("Hunter's diamine")

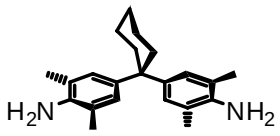

50.2 g Cyclohexanone (53 ml / 0.51 mol / 98.14 g/mol), 123.5 g 2,6-Dimethylaniline (126 ml / 1.02 mol / 121.18 g/mol), 83.8 ml Hydrochloric Acid 37 % (1.02 mol) and 210 ml EtOH were refluxed for 6 d. After cooling to r.t. 100 ml NaOH (10 N) were added, upon which a colorless precipitate formed. The precipitate was filtered from the brown solution and washed with cold EtOH.
Yield: 50 %

$C_{22}H_{30}N_2$ 322.49 g/mol

^{1}H NMR (400 MHz, $CDCl_3$, 298 K)
δ [ppm] = 1.46 (br, 2H, Cy-H); 1.53 (br, 4H, Cy-H); 2.14 (s, 12H, CH_3); 2.18 (br, 4H, Cy-H); 3.43 (br s, 4H, NH_2); 6.84 (s, 4H, Ar-H)

MS ESI-TOF, positive mode, sprayed from CH_3OH
m/z = 323.247 ($[M+H]^+$); 345.229 ($[M+Na]^+$)

The analytical data was consistent with the literature values.[16]

N^1,N^3-bis(4-(1-(4-amino-3,5-dimethylphenyl)cyclohexyl)-2,6-dimethylphenyl)-5-*tert*-butylisophthalamide (*t-Bu-EDA*)

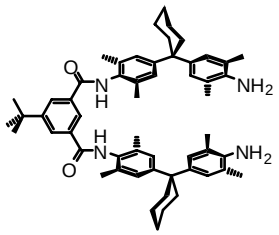

14.5 g (45 mmol / 322 g/mol / 6 eq.) of Hunter's diamine (1,1-bis(4-amino-3,5-dimethylphenyl)cyclohexane) were dissolved in 300 ml CH_2Cl_2 and 3 ml of triethylamine were added. 5-tert-butyl-isophthaloyl dichloride (1.9 g / 7.5 mmol / 258.9 g/mol) in 50 ml CH_2Cl_2 was slowly dropped to this solution.

The resulting mixture was stirred over night at r.t. and then concentrated to dryness in vacuo.

The extended diamine was separated from excess of Hunter's diamine by column chromatography using CH_2Cl_2/EE (6:1) as eluent.

Yield: 51 % (slightly brownish solid)

$C_{56}H_{70}N_4O_2$ 831.18 g/mol

^{1}H NMR (250 MHz, $CDCl_3$, 298 K):
δ [ppm] = 1.31 (s, 9H, ^{t}Bu-H); 1.54 (br s, 12H, Cy-CH_2); 2,11 (s, 24H, Ph-CH_3); 2,21 (br s, 8H, Cy-CH_2); 3.39 (4H, NH_2); 6.84 (s, 4H, Ph-H); 6.94 (s, 4H, Ph-H); 7.93 (s, 2H, NH); 8.12 (s, 2H, isophthal-H4 & H6); 8.40 (s, 1H, isophthal-H2)

^{13}C NMR (125 MHz, $CDCl_3$, 298 K)**:**
δ [ppm] = 17.82 (Ph-CH_3); 18.43 (Cy-CH_2); 20.77 (Cy-CH_2); 26.31 (Cy-CH_2); 30.96 (C(**C**H_3)$_3$); 34.86 (**C**(CH_3)$_3$); 37.04 (Cy-CH_2); 44.72 (Cy-C_{quart}); 121.27 (isophthal-C2); 122.67 (Ph-**C**-CH_3); 126.72 (Ph-**C**H); 126.86 (Ph-**C**H); 127.64 (isophthal-C4 & C6); 130.64 (Ph-**C**-NHR); 134,49 (isophthal-C1 & C3); 134.62 (Ph-**C**-CH_3); 137.61 (Ph-**C**-$C_{quart.}$); 139.81 (Ph-**C**-$C_{quart.}$); 148.31 (Ph-**C**-NH_2); 152.67 (isophthal-**C**-^{t}Bu); 165.44 (**C**=O)

MS ESI-FTICR, positive mode, sprayed from MeOH

m/z = 831.56 $[M+H]^+$; 416.28 $[M+2H]^{2+}$

(calc.: 831.55715 $[M+H]^+$; 416.28222 $[M+2H]^{2+}$)

The analytical data was consistent with the literature values.[18]

***N*,*N*-Bis-{4-[1-(4-amino-3,5-dimethyl-phenyl)-cyclohexyl]-2,6-dimethyl-phenyl}-4-methoxy-isophthalamide (*4-OMe-EDA*)**

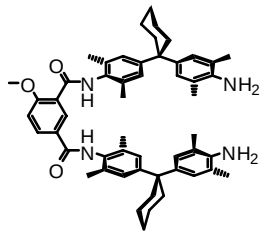

0.5 g (233.05 g/mol / 2.14 mmol) 4-Methoxyisophthaloyl chloride and 4.15 g (322.49 g / 12.9 mmol) Hunter's diamine were dissolved in 250 ml. After addition of 2 ml NEt_3, the mixture was stirred at r.t. for 5 d.

Column chromatography with EE/hexane (1:2) gradually increasing to pure EE could only separate the excess Hunter's diamine from a mixture of **4-OMe-EDA** and **4-OMe-EEDA** ("doubly" extended diamine building block). Column chromatography with CH_2Cl_2/EE (6:1) yielded the pure **4-OMe-EDA**.

Yield: 30 %

$C_{53}H_{64}N_4O_3$ 805.10 g/mol

^{1}H NMR (400 MHz, $CDCl_3$, 298 K)

δ [ppm] = 1.49 (s, 9H, ^{t}Bu-H); 1.56 (br s, 12H, Cy-CH_2); 2.14 (s, 24H, Ph-CH_3); 2.22 (br s, 8H, Cy-CH_2); 3.47 (br, 4H, NH_2); 4.01 (s, 3H, OCH_3); 6.87 (d, 4H, Ph-H); 6.94 (s, 4H, Ph-H); 7.93 (s, 2H, NH); 8.12 (s, 2H, 4,6-isophthal-H); 8.40 (s, 1H, 2-isophthal-H)

^{13}C NMR (125 MHz, $CDCl_3$, 298 K)

δ [ppm] = 18.15 (Ph-CH_3); 18.88 (Cy-CH_2); 19.16 (Cy-CH_2); 23.11 (Cy-CH_2); 26.59 (C(**C**H_3)$_3$); 37.33 (**C**(CH_3)$_3$); 37.36 (Cy-CH_2); 45.04 (Cy-C_{quart}); 56.52 (OCH_3); 121.37 (isophthal-C1); 121.57 (Ph-**C**-CH_3); 126.95 (Ph-**C**H); 127.18 (Ph-**C**H); 127.18 (isophthal-C2); 127.76 (isophthal-C2); 127.18 (isophthal-C3); 130.53 (Ph-**C**-NHR); 134,57 (isophthal-C); 134,94 (isophthal-C); 134.62 (Ph-**C**-CH_3); 137.65 & 137.87 (Ph-**C**-$C_{quart.}$); 140.18 (Ph-**C**-$C_{quart.}$); 148.41 & 148.61 (Ph-**C**-

NH_2); 152.67 (isophthal-**C**-^{t}Bu); 159.92 (**C**-OCH_3); 162.94 (**C**=O); 164.64 (**C**=O)

MS ESI-FTICR, positive mode, sprayed from CH_3OH (1 % formic acid)
m/z = 805.48 ($[M+H]^+$); 906,48 ($[M+NEt_3+H]^+$)

***N*,*N*-Bis-{4-[1-(4-amino-3,5-dimethyl-phenyl)-cyclohexyl]-2,6-dimethyl-phenyl}-4,6-dimethoxy-isophthalamide (*Di-OMe-EDA*)**

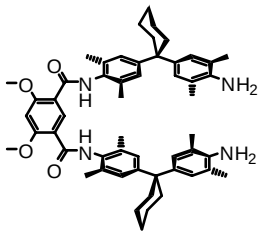

14.5 g (322.49 g / 45 mmol) Hunter's diamine were dissolved in 250 ml CH_2Cl_2 and 2 ml NEt_3 were added. A solution of 2.77 g (263.07 g/mol / 10.5 mmol) 4,6-dimethoxy-isophthaloyl dichloride in 50 ml CH_2Cl_2 was slowly dropped into this mixture, which was then stirred at r.t. over night. After evaporation of the solvent, the raw product was purified by column chromatography over silica gel using a mixture of DCM / ethyl acetate (6:1) as eluent. Yield: 58 %

$C_{54}H_{66}N_4O_4$ 835.13 g/mol

^{1}H NMR (400 MHz, $CDCl_3$, 298 K)
δ [ppm] = 1.48 (br, 12H, cy-H); 2.14 (s, 12H, CH_3); 2.20 (br, 6H, cy-H); 2.21 (s, 12H, CH_3); 3.96 (s, 4H, NH_2); 4,05 (s, 6H, CH_3);); 6.59 (s, 1H, 2-isophth); 6.85 (s, 4H, Ar-H); 6.98 (s, 4H, Ar-H); 8.61 (s, 2H, NH); 9.04 (s, 1H, 5-isophth)

^{13}C NMR (125 MHz, $CDCl_3$, 298 K)
δ [ppm] = 18.74 (Ph-CH_3); 19.19 (Cy-CH_2); 23.08 (Cy-CH_2); 26.53 (Cy-CH_2); 37.32 (Cy-CH_2); 45.01 (Cy-C_{quart}); 56.51 (O-CH_3); 115.95 (isophthal-C5); 121.53 (isophthal-C1 & C3); 126.86 (Ph-**C**H); 127.64 (isophthal-C2); 131.76 (Ph-**C**-NHR); 134,65 (Ph-**C**-CH_3); 134.65 (Ph-**C**-CH_3); 137.73 (Ph-**C**-$C_{quart.}$); 140.15 (Ph-**C**-$C_{quart.}$); 148.28 (Ph-**C**-NH_2); 160.07 (isophthal-C4 & C6); 162.53 (**C**=O)

MS ESI-TOF, positive mode, sprayed from MeOH
m/z = 835.1 ($[M + H]^+$)

***N*,*N*-Bis-{4-[1-(4-amino-3,5-dimethyl-phenyl)-cyclohexyl]-2,6-dimethyl-phenyl}-4,6-dibenzyloxy-isophthalamide (*Di-OBn-EDA*)**

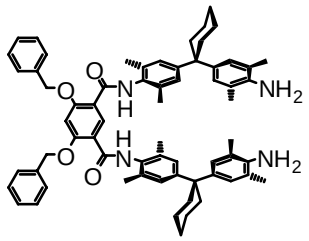

15 g (322.49 g/mol / 46.4 mmol) 4,4'-(Cyclohexane-1,1-diyl)bis(2,6-dimethylaniline) were dissolved in 250 ml CH_2Cl_2 and 2 ml NEt_3 were added. To this solution, a solution of 4.29 g 4,6-dibenzyloxy-isophthaloyl dichloride (415.27 g/mol / 10.3 mmol) in 50 ml CH_2Cl_2 was added slowly. The reaction mixture was stirred over night and then concentrated to dryness. The raw product was purified by column chromatography over silica gel using a mixture of DCM / ethyl acetate (6:1) as eluent. Yield: 60 %

$C_{66}H_{74}N_4O_4$ 987.32 g/mol

^{1}H NMR (400 MHz, $CDCl_3$, 298 K)
δ [ppm] = 1.42 (br, 4H, cy-**H**); 1.52 (br, 8H, cy-**H**); 2.07 (s, 12H, C**H**$_3$); 2.14 (s, 12H, C**H**$_3$); 2.19 (br, 8H, cy-**H**); 3.61 (br, 4H, N**H**$_2$); 5.20 (s, 4H, Bn-C**H**$_2$); 6.67 (s, 1H, H5); 6.84 (s, 4H, Ar-**H**); 6.92 (s, 4H, Ar-**H**); 7,37 (br, 10H, Bn-**H**); 8,58 (s, 1H, H2); 9,06 (s, 2H, N**H**)

^{13}C NMR (100 MHz, $CDCl_3$, 298 K)
δ [ppm] = 18.22 (**C**H$_3$); 19.10 (**C**H$_3$); 23.08 (Cy-C3 & Cy-C5); 26.58 (Cy-C4); 37.30 (Cy-C2 & Cy-C6); 45.00 (Cy-C$_{quart}$); 71.81 (Bn-**C**H$_2$); 100.00 (isophthal-C5); 116.44 (isophthal-C1 & C3); 121.71 (Ar-**C**-CH$_3$); 126.74 (Ar-**C**); 127.23 (Ar-**C**); 128.00 (Ar-**C**); 129.17 (Ar-**C**); 129.25 (Ar-**C**); 131.67 (Ar-**C**-NH); 134.56 (Ar-**C**- C$_{quart}$); 134.86 (Bn-**C**-CH$_2$); 139.99 (Ar-**C**); 159,58 (isophthal-C4 & C6); 162,57 (**C**=O)

MS ESI-TOF, positive mode, sprayed from MeOH
m/z = 987.5902 ([M + H]$^+$)

N^2,N^6-Bis(4-(1-(4-amino-3,5-dimethylphenyl)cyclohexyl)-2,6-dimethylphenyl)-pyridine-2,6-dicarboxamide (*Py-EDA*)

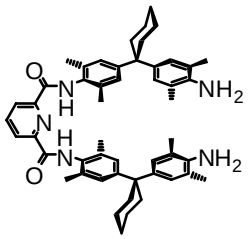

17.74 g (322.5 g/mol / 55 mmol) 4,4'-(cyclohexane-1,1-diyl)bis(2,6-dimethylaniline) were dissolved in 250 ml CH_2Cl_2 and 2 ml NEt_3 were added. To this solution, a solution of 2.04 g pyridine-2,6-dicarbonyl dichloride (204.0 g/mol / 10.3 mmol) in 50 ml CH_2Cl_2 was added slowly. The reaction mixture was stirred over night and then concentrated to dryness. The raw product was purified by column chromatography over silica gel using a mixture of DCM / ethyl acetate (4:1) as eluent. Yield: 55 %

$C_{51}H_{61}N_5O_2$ 776.06 g/mol

^{1}H NMR (400 MHz, $CDCl_3$, 298 K)
δ [ppm] = 1.48 (br, 4H, Cy-**H**); 1.56 (br, 8H, Cy-**H**); 2.06 (s, 12H, C**H**$_3$); 2.21 (br, 8H, Cy-**H**); 2.24 (s, 12H, C**H**$_3$); 3.53 (br, 4H, N**H**$_2$); 6.87 (s, 4H, Ar-**H**); 7.04 (s, 4H, Ar-**H**); 8.50 (d, 2H, H3 & H5); 8.58 (s, 1H, H2); 9.18 (s, 2H, N**H**)

^{13}C NMR (100 MHz, $CDCl_3$, 298 K)
δ [ppm] = 18.16 (**C**H$_3$); 19.06 (**C**H$_3$); 23.08 (Cy-C3 & Cy-C5); 26.56 (Cy-C4); 37.34 (Cy-C2 & Cy-C6); 45.06 (Cy-C$_{quart}$); 121.71 (Ar-**C**-CH$_3$); 125.61 (Ar-**C**); 127.12 (Ar-**C**); 127.20 (Ar-**C**); 130.47 (Ar-**C**); 134.51 (Ar-**C**); 140.20 (Py-C4); 149.56 (Py-C2 & C6); 161.56 (**C**=O)

MS ESI-TOF, positive mode, sprayed from MeOH
m/z = 776.4924 ($[M + H]^+$; calc. 776.4898)

The analytical data was consistent with the literature values.[186]

6.2.3 Synthesis of Macrocycles

10^5,23^5-Di-*tert*-butyl-7^3,7^5,13^2,13^6,20^3,20^5,26^3,26^5-octamethyl-8,12,21,23^2,25-tetraaza-7,13,20,26(1,4),10,23(1,3)-hexabenzenadispiro[5.7.5.7]hexa-cosaphan-9,11,22,24-tetrone (*Di-tert-butyl-tetralactam macrocycle*)

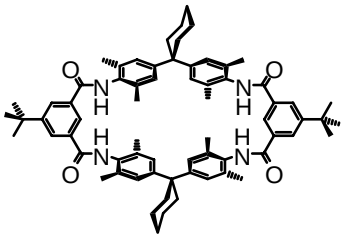

A solution of 1g (1.2 mmol / 830 g/mol) of **^{t}Bu-EDA** and 2 ml Et_3N in 250 ml CH_2Cl_2 and a solution of 312 mg (1.2 mmol / 258.9 g/mol) of 5-*tert*-butyl-isophthaloyl dichloride in 250 ml CH_2Cl_2 were slowly dropped into a flask with 1200 ml CH_2Cl_2 over a period of 14 h under Argon atmosphere. This mixture was stirred for at least another 3 d at r.t. and then concentrated to dryness.

The crude product was purified by column chromatography using CH_2Cl_2/EE (6:1) as eluent.

Yield: 25 % (slightly brownish solid)

$C_{68}H_{80}N_4O_4$ 1017.39 g/mol

^{1}H NMR (500 MHz, $CDCl_3$ + 10 % CD_3OD, 298 K)
δ [ppm] = 1.37 (s, 18H, ^{t}Bu-H); 1.47 (br s, 4H, Cy-CH_2); 1.60 (br s, 8 H, Cy-CH_2); 2,13 (s, 24H, Ph-CH_3); 2,29 (br s, 8H, Cy-CH_2); 6.94 (s, 4H, Ph-H); 6.95 (s, 4H, Ph-H); 7.27 (s, 2H, isophthal-H5); 8.12 (s, 2H, isophthal-H2); 8.14 (d, 4H, isophthal-H4,6); 8.57 (s, 4H, NH)

^{13}C NMR (125 MHz, $CDCl_3$ + 10 % CD_3OD, 298 K)
δ [ppm] = 16.09 (Ph-CH_3); 20.08 (Cy-CH_2); 20.32 (Cy-CH_2); 23.76 (Cy-CH_2); 27.08 (C(**C**H_3)$_3$); 29.32 (**C**(CH_3)$_3$); 32.60 (Cy-CH_2); 42.53 (Cy-C_{quart}); 121.27 (isophthal-C2); 123.63 (Ph-**C**-CH_3); 125.81 (Ph-**C**H); 128.82 (isophthal-C4 & C6); 131.67 (Ph-**C**-NHR); 132,44

(isophthal-C1 & C3); 145.39 (Ph-**C**-$C_{quart.}$); 150.87 (isophthal-**C**-^{t}Bu); 164.11 (**C**=O)

MS ESI-FTICR, positive mode, sprayed from MeOH

m/z = 1017.6249 $[M+H]^+$; 1039.6069 $[M+Na]^+$; 1055.5613 $[M+K]^+$ (calc.: 1017.62523 $[M+H]^+$; 1039.60718 $[M+Na]^+$; 1055.58112 $[M+K]^+$)

The analytical data was consistent with the literature values.[187]

10^4-Methoxy-7^3,7^5,13^2,13^6,20^3,20^5,26^3,26^5-octamethyl-8,12,21,23^2,25-tetraaza-7,13,20, 26(1,4),10,23(1,3)-hexabenzenadispiro[5.7.5.7]hexa-cosaphan-9,11,22,24-tetrone (*Py-OMe-Macrocycle*)

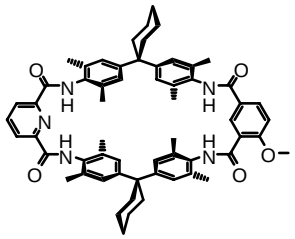

Two solutions of 776.1 mg **Py-EDA** (776.1 g/mol / 1 mmol) and 2 ml NEt_3 in 250 ml CH_2Cl_2 and 233.0 mg 4-methoxyisophthaloyl dichloride (233.0 g/mol / 1 mmol) in 250 ml CH_2Cl_2 were dropped simultaneously under Ar atmosphere into a flask with 1.2 l CH_2Cl_2 over a period of approx. 12 h. The resulting solution was stirred for 7 d. After evaporation of the solvent, the crude product was purified by column chromatography over silica gel using a mixture of DCM / ethyl acetate (6:1) as eluent.
Yield: 64 %

$C_{60}H_{65}N_5O_5$ 936.19 g/mol

MS ESI-TOF, positive mode, sprayed from MeOH
m/z = 936.5063 ($[M + H]^+$; calc. 936.5058); 958.4880 ($[M + Na]^+$; calc. 958.4878); 974.4612 ($[M + K]^+$; calc. 974.4617)

NMR analysis was not possible due to the extremely low solubility of the macrocycle.

10^4,10^6-Di-benzyloxy-7^3,7^5,13^2,13^6,20^3,20^5,26^3,26^5-octamethyl-8,12,21,23^2,25-tetraaza-7,13,20,26(1,4),10,23(1,3)-hexabenzenadispiro[5.7.5.7]hexa-cosaphan-9,11,22,24-tetrone (*Py-di-OBn-Macrocycle*)

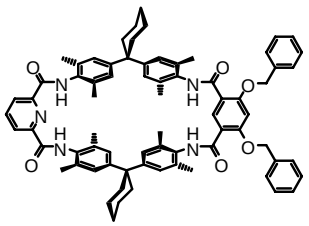

Two solutions of 776.1 mg **Py-EDA** (776.1 g/mol / 1 mmol) and 2 mL NEt_3 in 250 mL CH_2Cl_2 and 415.3 mg 4,6-dibenzyloxyisophthaloyl dichloride (415.3 g/mol / 1 mmol) in 250 mL CH_2Cl_2 were dropped simultaneously under Ar atmosphere into a flask with 1.2 L CH_2Cl_2 over a period of approx. 12 h. The resulting solution was stirred for 7 d. After evaporation of the solvent, the raw product was purified by column chromatography over silica gel using a mixture of DCM / ethyl acetate (6:1) as eluent (R_f = 0.34).
Yield: 76 %

$C_{73}H_{75}N_5O_6$ 1118.41 g/mol

^{1}H NMR (400 MHz, $CDCl_3$, 298 K)
δ [ppm] = 1.49 (br, Cy-**H**); 1.61 (br, Cy-**H**); 2.12 (s, 12H, C**H**$_3$); 2.19 (s, 12H, C**H**$_3$); 2.24 (br, Cy-**H**); 2.31 (br, Cy-**H**); 5.24 (s, 4H, Bn-C**H**$_2$); 6.69 (s, 1H, isophthal-H5); 6.95 (br s, 8H, Ar-H); 7.39 (m, 10H, Ph-H); 7.70 (br, 2H, N**H**); 8.12 (t, 1H, py-H5); 8.51 (d, 2H. py-H4 & H6); 8.61 (s, 1H, isophthal-H2); 8.87 (br, 2H, N**H**)

^{13}C NMR (100 MHz, $CDCl_3$, 298 K)
δ [ppm] = 19.10; 23.02; 26.49; 29.79; 35.79; 45.04; 71.40; 99.12; 116.28; 125.77; 126.43; 126.66; 127.43; 128.69; 129.04; 130.37; 131.71; 134.61; 134.78; 135.40; 139.39; 147.34; 148.41; 149.01; 160.86; 161.52; 164.15

MS	ESI-TOF, positive mode, sprayed from MeOH *m/z* = 1118.5751 ($[M + H]^+$; calc. 1118.5790; 100); 1140.5567 ($[M + Na]^+$; calc. 1140.5610; 17); 1156.5296 ($[M + K]^+$; calc. 1156.5349; 26)

10^5,36^5-Di-*tert*-butyl-23^4,$49^{4(\text{or 6 for the other isomer, respectively})}$-dimethoxy-$7^3$,$7^5$,$13^2$,$13^6$, 20^3,20^5,26^2,26^6,33^3,33^5, 39^2,39^6,46^3,46^5,52^2,52^6-hexadecamethyl-8,12,21,25,34,38, 47,51-octaaza-7,13,20,26,33,39,46,52(1,4),10,23,36,49(1,3)-dodecabenzenatetra-spiro[5.7.5.7.5.7.5.7]dopenta-contaphan-9,11,22,24,35,37,48,50-octone
(*Di-^{t}Bu-di-OMe-Octalactam Macrocycle*)

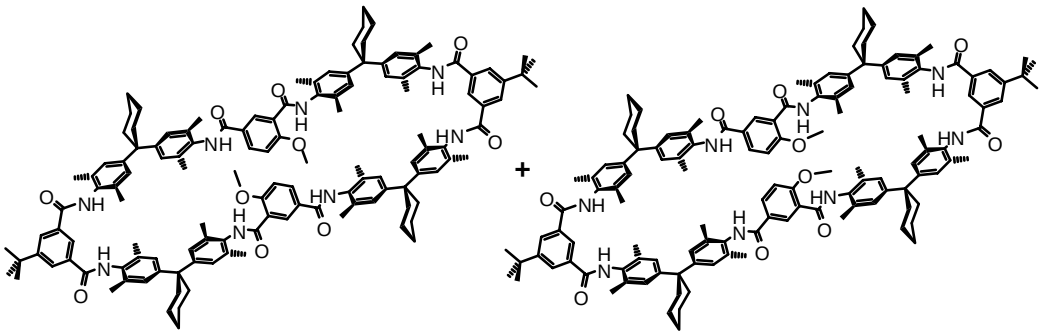

Two solutions of 831.2 mg **^{t}Bu-EDA** (831.2 g/mol / 1 mmol) and 2 ml NEt_3 in 250 ml CH_2Cl_2 and 233.0 mg 4-methoxyisophthaloyl dichloride (233.0 g/mol / 1 mmol) in 250 ml CH_2Cl_2 were dropped simultaneously under Ar atmosphere into a flask with 1.2 l CH_2Cl_2 over a period of approx. 12 h. The resulting solution was stirred for 7 d. After evaporation of the solvent, the raw product was purified by column chromatography over silica gel using a mixture of DCM / ethyl acetate (6:1) as eluent. Yield: 4 %

$C_{130}H_{148}N_8O_{10}$ 1982.61 g/mol

^{1}H NMR (500 MHz, $CDCl_3$, 298 K)
δ [ppm] = 0.64 (s); 1.08 (s); 1.39(s, ^{t}Bu-H); 1.41 (s); 1.94 (s); 2.30 (br); 2.52 (s); 3.96 (s); 4.07 (s, OC**H**$_3$); 6.29 (s); 6.67 (br); 6.95 (br); 6.97 (s); 6.99 (s); 7.12 (br); 7.61 (dd); 7.83 (s); 8.27 (t); 8.39 (t); 8.88 (s); 8.93 (s); 8.96 (s); 9.02 (s)

MS ESI-FTICR, sprayed from MeOH + 1% HCOOH
m/z = 992.043 ($[M + 2H]^{2+}$; calc.: 992.075)

Due to the high complexity of the ^{1}H NMR spectrum of the mixture of the two macrocycles, most of the signals cannot be assigned unambiguously, however, tandem MS experiments cearly unravel the identity of the octalactam macrocycle.

10^4,10^6,23^4,23^6,36^4,36^6,49^4,49^6,Octabenzyloxy-7^3,7^5,13^2,13^6,20^3,20^5,26^2,26^6,33^3,33^5, 39^2,39^6,46^3,46^5,52^2,52^6-hexadecamethyl-8,12,21,25,34,38,47,51-octaaza-7,13,20,26, 33,39,46,52(1,4),10,23,36,49(1,3)-dodecabenzenatetraspiro[5.7.5.7.5.7.5.7]dopenta-contaphan-9,11,22,24,35,37,48,50-octone (*$(OBn)_8$-Octalactam Macrocycle*)

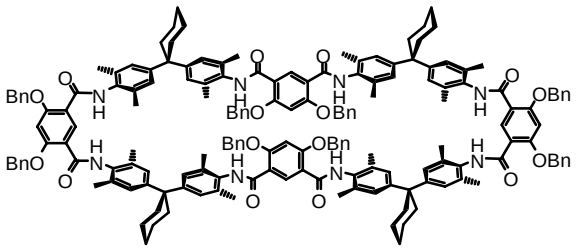

Two solutions of 987.3 mg **Di-OBn-EDA** (987.3 g/mol / 1 mmol) and 2 ml NEt_3 in 250 mL CH_2Cl_2 and 415.3 mg 4,6-dibenzyloxyisophthaloyl dichloride (415.3 g/mol / 1 mmol) in 250 mL CH_2Cl_2 were dropped simultaneously under Ar atmosphere into a flask with 1.2 L CH_2Cl_2 over a period of approx. 12 h. The resulting solution was stirred for 4-7 days. After evaporation of the solvent, the raw product was purified by column chromatography over silica gel using a mixture of DCM / ethyl acetate (5:1) as eluent. Yield: 19 %

$C_{176}H_{176}N_8O_{16}$ 2659.32 g/mol

^{1}H NMR (400 MHz, $CDCl_3$ + 5 % CD_3OD, 298 K)
δ [ppm] = 1.35 & 1.42 (br, 24H, Cy-**H**); 1.96 (s, 48H, C**H**$_3$); 2.09 (br, 16H, Cy-**H**); 5.16 (s, 16 H, Bn-C**H**$_2$); 6.66 (s, 4H, isophthal-H5); 6.84 (s, 16H, Ar-**H**); 7.25 & 7.27 (br, 40H, Bn-**H**); 8.81 (s, 4H, isophthal-H2)

MS ESI-TOF, posotive mode, sprayed from MeOH
m/z = 2682.3224 ($[M + Na]^+$; calc. 2682.3162); 1352.6536 ($[M + 2Na]^{2+}$; calc. 1352.6527); 909.4354 ($[M + 3Na]^{3+}$; calc. 909.4315)

10^4,10^6,23^4,23^6,36^4,36^6,49^4,49^6,Octahydroxy-7^3,7^5,13^2,13^6,20^3,20^5,26^2,26^6,33^3,33^5, 39^2,39^6,46^3,46^5,52^2,52^6-hexadecamethyl-8,12,21,25,34,38,47,51-octaaza-7,13,20,26, 33,39,46,52(1,4),10,23,36,49(1,3)-dodecabenzenatetraspiro[5.7.5.7.5.7.5.7]dopenta-contaphan-9,11,22,24,35,37,48,50-octone (*$(OH)_8$-Octalactam Macrocycle*)

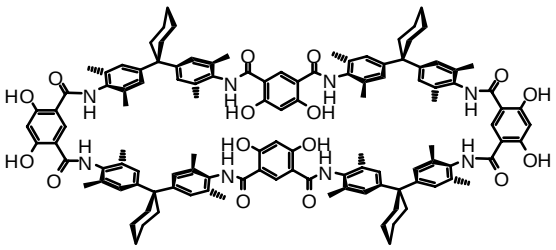

65 mg **$(OBn)_8$-octalactam macrocycle** (2659.3 g/mol / 24.4 μmol) were dissolved in 20 ml MeOH. After addition of 40 mg Pd/C (10 % Pd on carbon), the suspension was flushed with H_2 for 5 min and afterwards stirred over night. The suspension was filtered over celite. The celite was then extracted with $CHCl_3$/MeOH (10:1) to elute the product.
Yield: 30 %

$C_{120}H_{128}N_8O_{16}$ 1938.34 g/mol

^{1}H NMR (400 MHz, $CDCl_3$, 298 K)
δ [ppm] = 1.36 (br, 8H, Cy-**H**); 1.42 (br, 16H, Cy-**H**); 2.07 (s, 48H, C**H**$_3$); 2.11 (br, 16H, Cy-**H**); 6.32 (s, 4H, isophthal-H5); 6.88 (s, 16H, Ar-**H**); 8.48 (s, 4H, isophthal-H2)

MS ESI-FTICR, negative mode, sprayed from MeOH + 1% NEt_3
m/z = 967.9757 ($[M - 2H]^{2-}$; calc. 967.9668); 1936.9629 ($[M - H]^-$; calc.1936.9408)

6.3 Synthesis of Axle Components

N-Boc-N,N'-Dimethylethylenediamine

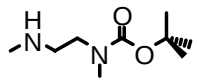

2 g (2.44 ml / 88.15 g/mol / 22.69 mmol) of *N*,*N*'-ethylenediamine were dissolved in 25 ml CH_2Cl_2 and cooled to 0 °C. After addition of 1.65 g (218.25 g/mol / 7.56 mmol / 0.33 eq.) of Boc_2O in 15 ml CH_2Cl_2, the solution was stirred over night and allowed to warm to r.t. Then, the solvent was removed *in vacuo*. The remaining solid was redissolved in ethyl acetate, washed with brine and H_2O and dried over $MgSO_4$. Evaporation of the solvent yielded a nearly colorless oily liquid.
Yield: 95 %

$C_9H_{21}N_2O_2$ 188.27 g/mol

^{1}H NMR (250 MHz, $CDCl_3$, 298 K)
δ [ppm] = 1.30 (s, 9H; ^{t}Bu-**H**); 1.88 (s, 1H, N**H**); 2.29 (s, 3H, NHC**H**$_3$); 2.57 (t, 2H C**H**$_2$NHCH$_3$); 2.72 (s, 3H, NBocC**H**$_3$); 3.18 (t, 2H C**H**$_2$NBocCH$_3$)

^{13}C NMR (125 MHz, $CDCl_3$, 298 K)
δ [ppm] = 28.38 (C(**C**H$_3$)$_3$); 34.60 (NBoc**C**H$_3$); 36,29 (NH**C**H$_3$); 48.37 (NHCH$_3$**C**H$_2$); 49.71 (**C**H$_2$); 79.26 (**C**(CH$_3$)$_3$); 155.84 (**C**=O)

MS ESI-FTICR, positive mode, sprayed from CH_3CN
m/z = 189.1598 ([M+H]$^+$)

The analytical data was consistent with the literature values.[188]

3.5 *tert*-Butyl-2-aminoethylcarbamate (*N-Boc-Ethylene Diamine*)

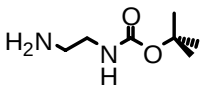

14.4 g of ethylene diamine (16 ml / 60 g/mol / 240 mmol) were dissolved in 20 ml CH_2Cl_2 and cooled to 0 °C. After addition of 9 g of Boc_2O (218.2 g/mol / 41 mmol / 0.16 eq.) in 100 ml CH_2Cl_2 over a period of 3 h, the solution was stirred over night and allowed to warm to r.t. Then, the solvent was removed *in vacuo*. The remaining solid was redissolved in saturated Na_2CO_3 solution. The resulting solution was extracted three times with CH_2Cl_2 (100 + 100 + 75 ml). The combined organic phases were dried over $MgSO_4$. Evaporation of the solvent yielded a slightly yellowish oily liquid Yield: 96 %

$C_7H_{16}N_2O_2$ 160.21 g/mol

^{1}H NMR (400 MHz, $CDCl_3$, 298 K)
δ [ppm] = 1.19 (br, 2H, N**H**$_2$); 1.42 (s, 9H, Boc-C**H**$_3$); 2.77 (t, 2H, C**H**$_2$); 3.14 (q, 2H, C**H**$_2$); 4.92 (br, 1H, N**H**)

MS ESI-TOF, positive mode, sprayed from MeOH
m/z = 161.1290 ($[M + H]^+$; calc. 161.1285)

The analytical data was consistent with the literature values.[189]

N^1,N^6-bis(2-*N*-Boc-aminoethyl)adipamide

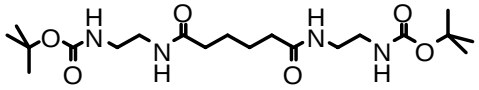

A solution of 1.027 g *N*-Boc-ethylene diamine (160.2 g/mol / 6.41 mmol) in 10 mL CH_2Cl_2 was cooled to 0°C and a solution of 586 mg adipoyl dichloride (183.0 g/mol / 3.20 mmol / 469 µL) was added slowly. The resulting solution was stirred over night and allowed to warm to room temperature meanwhile. The resulting mixture of dichloromethane solution and colourless precipitate was washed with saturated $NaHCO_3$ solution after what the biphasic solvent mixture was removed by filtration. The colourless residue was washed with water and dried *in vacuo*. Yield: 73 %

$C_{20}H_{38}N_4O_6$ 430.54 g/mol

^{1}H NMR (400 MHz, $CDCl_3$, 298 K)
δ [ppm] = 1.33 (s, 18H, ^{t}Bu-H); 1.40 (quint, 4H, adipoyl-CH_2 - C3 & C4); 1.99 (t, 4H, adipoyl-CH_2 - C2 & C5); 2.91 (quart, 4H, CH_2); 3.00 (quart, 4H, CH_2); 6.74 (t, 2H, NH); 7.75 (t, 2H, NH)

^{13}C NMR (125 MHz, $CDCl_3$, 298 K)
δ [ppm] = 25.83 (**C**H_2); 29.15 (**C**H_3); 36.14 (**C**H_2); 39.56 (**C**H_2); 40.70 (**C**H_2); 78.54 (C_{quart}); 156.52 (C=O); 173.02 (C=O)

MS ESI-TOF, positive mode, sprayed from MeOH
m/z = 431.2872 ($[M + H]^+$; calc. 431.2864; 100); 453.2694 ($[M + Na]^+$; calc. 453.2684; 100); 469.2430 ($[M + K]^+$; calc. 469.2423; 7); 532.4071 ($[M + NEt_3H]^+$; calc. 532.4069; 12)

4,4'-Biphenyldicarbonyldichloride

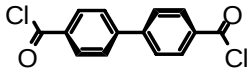

A mixture of 4,4'-biphenyldicarbonic acid (2.35 g / 242.2 g/mol / 9.7 mmol), 20 ml $SOCl_2$, and 0.5 ml DMF was refluxed for 4 h. Evaporation of the volatiles gave the product as a colorless solid. Yield: 99 %

For ^{1}H-NMR analysis, the product was converted to the corresponding ethyl ester.

$C_{14}H_8Cl_2O_2$ 279.12 g/mol

^{1}H NMR (400 MHz, $CDCl_3$, 298 K)

δ [ppm] = 1.40 (t, 6H, Et-CH_3); 4.39 (q, 4H, Et-CH_2); 7.66 (d, 4H, Ar-H); 8.12 (d, 4H, Ar-H)

^{13}C NMR *not possible due to extremely poor solubility*

MS (EI, 70 eV)

m/z = 278.1 ($[M]^{+\bullet}$); 243.1 ($[M - Cl]^+$); 215.0 ($[M - Cl - CO]^+$); 180.3 ($[M - 2\ Cl - CO]^{+\bullet}$); 151.9 ($[M - 2\ Cl - 2\ CO]^{+\bullet}$); 126.2 ($[M - 2\ Cl - 2\ CO - C_2H_2]^{+\bullet}$); 76.2 ($[M - 2\ Cl - 2\ CO - C_2H_2 - C_4H_2]^{+\bullet}$)

Terephthaloyldichloride

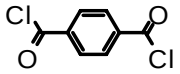

A mixture of terephthalic acid (5 g / 266.1 g/mol / 30 mmol), 21 ml $SOCl_2$, and 0.5 ml DMF was refluxed for 15 h. Evaporation of the volatiles gave the product as a colorless solid.
Yield: quant.
For ^{1}H NMR analysis, the product was converted to the corresponding ethyl ester.

$C_8H_4Cl_2O_2$ 203.02 g/mol

^{1}H NMR (400 MHz, $CDCl_3$, 298 K)
δ [ppm] = 1.39 (t, 6H, Et-CH_3); 4.38 (q, 4H, Et-CH_2); 8.08 (s, 4H, Ar-H)

^{13}C NMR (100 MHz, $CDCl_3$, 298 K)
δ [ppm] = 14.14 (CH_3); 61.52 (CH_2); 129.45 (C2 & C3); 134.12 (C1 & C4); 166.05 (C=O)

MS (EI, 70 eV)
m/z = 202.1 ($[M]^{+\bullet}$); 167.1 ($[M - Cl]^+$); 139.1 ($[M - Cl - CO]^+$); 104.0 ($[M - 2\ Cl - CO]^{+\bullet}$); 76.2 ($[M - 2\ Cl - 2\ CO]^{+\bullet}$); 50.2 ($[M - 2\ Cl - 2\ CO - C_2H_2]^{+\bullet}$)

N^4,$N^{4'}$-Bis(2-(tert-butoxycarbonyl-amino)ethyl)biphenyl-4,4'-dicarboxamide

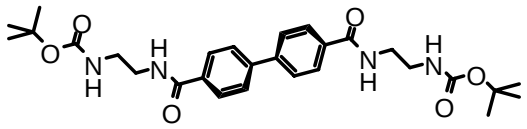

A solution of 1 g 4,4'-biphenyldicarbonyldichloride (279.1 g/mol / 3.58 mmol) in 70 ml CH_2Cl_2 was slowly dropped into a solution of 1.15 g *N*-Boc-ethylene diamine (160.2 g/mol / 7.2 mmol) in 20 ml CH_2Cl_2. The resulting solution was stirred over night, upon which a white solid precipitated. An excess of saturated $NaHCO_3$ solution was added. The precipitate was filtered off, washed with water, and dried *in vacuo*.
Yield: 83 %

$C_{28}H_{38}N_4O_6$ 526.62 g/mol

^{1}H NMR (400 MHz, $CDCl_3$, 298 K)
δ [ppm] = 1.34 (s, 18H, ^{t}Bu-H); 3.09 (q, 4H, CH_2); 3.28 (q, 4H, CH_2); 6.91 (t, 2H, NH); 7.80 (d, 4H, Ar-H); 7.92 (d, 4H, Ar-H); 8.52 (t, 2H, NH)

^{13}C NMR (100 MHz, $CDCl_3$, 298 K)
δ [ppm] = 28.81; 40.24; 40.43; 78.31; 127.24; 128.56; 134.44; 142.21; 156.38; 166.53

MS ESI-TOF, positive mode, sprayed from CH_3OH
m/z = 549.2697 ($[M+Na]^+$); 1075.5496 ($[2M+Na]^+$)

Triphenylacetylchloride

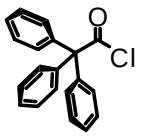

A mixture of 1 g of triphenylacetic acid (288.3 g/mol / 3.47 mmol), 10 ml $SOCl_2$ and 0.5 ml DMF was heated to reflux for 2 h. Evaporation of the solvent yielded in the product as a yellowish solid. Yield: quant.

For ^{1}H-NMR analysis, the product was converted to the corresponding ethyl ester.

$C_{20}H_{15}ClO$ 306.79 g/mol

^{1}H NMR (400 MHz, $CDCl_3$, 298 K)

δ [ppm] = 1.05 (t, 3H, CH_3); 4.17 (q, 2H, CH_2); 7.08 & 7.25 (m, 15H, Ph-**H**)

^{13}C NMR (100 MHz, $CDCl_3$, 298 K)

δ [ppm] = 11.07 (CH_3); 61.89 (c_{quart}); 67.39 (CH_2); 127.38 (C_{para}); 128.31 (C_{meta}); 130.42 (C_{ortho}); 143.72 (C_{ipso}); 176.30 (C=O)

MS EI, 70 eV

m/z = 305.8 ($[M]^{+\bullet}$); 243.0 ($[M\text{-}Cl\text{-}CO]^+$); 165.0 ($[M\text{-}Cl\text{-}CO\text{-}C_6H_6]^+$)

***tert*-Butyl 2-(2,2,2-triphenylacetamido)ethylcarbamate**

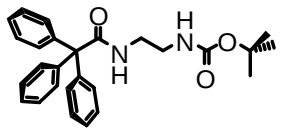

A solution of 520 mg of triphenylacetyl chloride (306.8 g/mol / 1.7 mmol) in 10 ml CH_2Cl_2 was added to a solution of 272 mg *N*-Boc-ethylene diamine (160.2 g/mol / 1.7 mmol) and 0.5 ml NEt_3 in 10 ml CH_2Cl_2 and stirred for 48 h. Afterwards, the solution was washed with saturated $NaHCO_3$ solution, dried with $MgSO_4$, concentrated to dryness. The product was dried in high vacuum. Yield: 88 %

$C_{27}H_{30}N_2O_3$ 430.54 g/mol

^{1}H NMR (400 MHz, $CDCl_3$, 298 K)
δ [ppm] = 1.38 (s, 9H, ^{t}Bu-CH_3); 3.19 (q, 2H, CH_2); 3.41 (q, 2H, CH_2); 4.75 (br t, 1H, NH); 6.14 (br t, 1H, NH); 7.26 (m, 15H, Ph-H)

^{13}C NMR (100 MHz, $CDCl_3$, 298 K)
δ [ppm] = 28.46 (CH_3); 40.41 (CH_2); 40.47(CH_2); 67.91 (**C**Ph_3); 79.50 (**C**$(CH_3)_3$); 127.13 (C_{para}); 128.09; 130.56; 143.36 (C_{ipso}); 156.28 (C=O); 174.27 (C=O)

MS ESI-TOF, positive mode, sprayed from MeOH
m/z = 431.2387 ($[M + H]^+$; calc. 431.2329); 453.2214 ($[M + Na]^+$; calc. 453.2149); 469.1954 ($[M + K]^+$; calc. 469.1888)

***N*-(2-Aminoethyl)-2,2,2-triphenylacetamide (*Trityl-Ethylene Diamine*)**

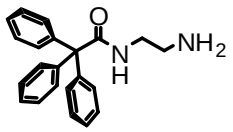

594 mg of *tert*-Butyl 2-(2,2,2-triphenylacetamido)ethylcarbamate (430.5 g/mol / 1.38 mmol) were dissolved in 10 ml CH_2Cl_2. 1 ml of trifluoroacetic acid was added and the mixture was stirred over night. The solution was then concentrated to dryness. The remaining yellowish viscous oil was sonicated after addition of water, which led to the precipitation of an off-white solid that was collected by filtration and dried in high vacuum.
Yield: 94 %

$C_{22}H_{22}N_2O$ 330.42 g/mol

^{1}H NMR (400 MHz, $CDCl_3$, 298 K)
δ [ppm] = 2.86 (t, 2H, CH_2); 3.38 (q, 2H, CH_2); 3.71 (br, 2H, NH_2); 6.95 (br t, 1H, NH); 7.15 (m, 15H, Ph-H)

^{13}C NMR (100 MHz, $CDCl_3$, 298 K)
δ [ppm] = 38.22 (CH_2); 39.08 (CH_2); 67.83 (**C**Ph_3); 127.20 (C_{para}); 128.07 (C_{meta}); 130.27 (C_{ortho}); 142.78 (C_{ipso}); 176.17 (C=O)

MS ESI-TOF, positive mode, sprayed from MeOH
m/z = 331.1822 ($[M + H]^+$; calc. 331.1805); 353.1652 ($[M + Na]^+$; calc. 353.1624); 369.1364 ($[M + K]^+$; calc. 369.1364)

6.4 Synthesis of Rotaxanes

[2]-{N^4,$N^{4'}$-Bis(4-tritylphenyl)biphenyl-4,4'-dicarboxamide}-{10^4,10^6-di-benzyloxy-7^3,7^5,13^2,13^6,20^3,20^5,26^3,26^5-octamethyl-8,12,21,23^2,25-tetraaza-7,13,20,26(1,4),10,23(1,3)-hexabenzenadispiro[5.7.5.7]hexa-cosaphan-9,11,22,24-tetrone}-Rotaxane (R1)

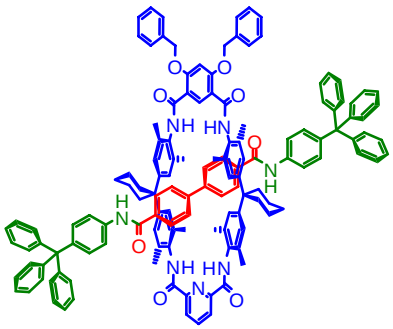

50 mg **Py-di-OBn-Macrocycle** (1118.4 g/mol / 45 µmol), 25.1 mg 4,4'-Biphenyldicarbonyldichloride (229.1 g/mol / 90 µmol), and 0.1 ml NEt_3 were dissolved in 10 ml CH_2Cl_2 and 60.4 mg 4-triphenylmethylaniline (335.4 g/mol / 180 µmol) in 10 ml CH_2Cl_2 were added. The resulting solution was stirred for 7 d at r.t. After evaporation of the solvent, the raw product was purified by column chromatography over silica gel using a mixture of DCM / ethyl acetate (10:1) as eluent (R_f = 0.5).

Yield: 15 %

$C_{137}H_{123}N_7O_8$ 1995.48 g/mol

^{1}H NMR (700 MHz, $CDCl_3$, 298 K)

δ [ppm] = 1.49 & 1.53 (br, 6H, Cy-**H**); 1.65 (br, 4H Cy-**H**); 1.79 (s, 12H, C**H**$_3$);1.99 (s, 12H, C**H**$_3$); 2.19 & 2.39 (br, 6H Cy-**H**); 5.24 (s, 4H, Bn-C**H**$_2$); 6.68 (s, 1H, isophthal-H5); 6.75 (s, 4H, Ar-H); 6.98 (s, 4H, Ar-H); 7.07 (d, 4H, axle); 7.13 (d, 4H, axle); 7.26 (m, 30H, trityl-H); 7.38 (t, 2H, Bn-H); 7.42 (t, 4H, Bn-H); 7.48 (t, 8H); 7.52 (d, 4H, Bn-H); 7.76 (br, 2H, N**H**); 7.98 (t, 1H); 8.12 (t, 1H, py-H5); 8.35 (s, 1H, isophthal-H2); 8.39 (br, 2H, NH); 8.47 (d, 2H. py-H4 & H6); 10.17 (s, 2H, ring-N**H**)

^{13}C NMR (125 MHz, $CDCl_3$, 298 K)

δ = 14.09; 18.48; 18.80; 22.89; 26.37; 29.69; 35.04; 44.86; 53.39; 64.64; 71.40; 76.82; 77.00; 77.19; 116.15; 119.24; 120.33; 125.14; 125.56; 126.00; 126.25; 127.03; 127.36; 127.52; 127.78; 128.69; 128.98; 131.00; 131.11; 131.13; 131.34; 131.48; 131.82; 134.02; 135.16; 135.55; 143.06; 143.14; 146.74; 147.99; 149.05; 160.63; 162.25; 165.43; 164.51

MS ESI-FTICR, positive mode, sprayed from MeOH

m/z = 1995.898 ($[M + H]^+$; calc. 1995.954)

[2]-{N^4,$N^{4'}$-Bis(2-(2,2,2-triphenylacetamido)ethyl)biphenyl-4,4'-dicarboxamide}-{10^4,10^6-di-benzyloxy-7^3,7^5,13^2,13^6,20^3,20^5,26^3,26^5-octamethyl-8,12,21,23^2,25-tetraaza-7,13,20,26(1,4),10,23(1,3)-hexabenzenadispiro[5.7.5.7]hexa-cosaphan-9,11,22,24-tetrone}-Rotaxane (R2)

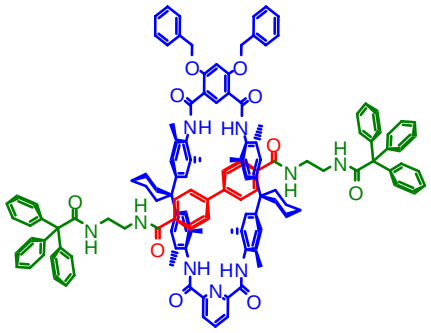

150 mg **Py-di-OBn-Macrocycle** (1118.4 g/mol / 134 µmol), 75 mg 4,4'-Biphenyldicarbonyldichloride (229.1 g/mol / 269 µmol), and 0.2 ml NEt_3 were dissolved in 20 ml CH_2Cl_2 and 180 mg N-(2-aminoethyl)-2,2,2-triphenylacetamide (330.4 g/mol / 545 µmol) in 20 ml CH_2Cl_2 were added. The resulting solution was stirred for 7 d at r.t.. After evaporation of the solvent, the raw product was purified by column chromatography over silica gel using a mixture of CH_2Cl_2 / ethyl acetate (1:1) as eluent (R_f = 0.5).
Yield: 19 %

$C_{131}H_{125}N_9O_{10}$ 1985.45 g/mol

^{1}H NMR (700 MHz, $CDCl_3$, 298 K)

δ [ppm] = 1.51 (br, 8H, Cy-**H**); 1.64 (br, 4H Cy-**H**); 1.86 (s, 12H, C**H**$_3$);1.96 (s, 12H, C**H**$_3$); 2.23 & 2.32 (br, 8H Cy-**H**); 2.95 (br, 4H, axle-C**H**$_2$); 3.06 (br, 4H, axle-C**H**$_2$); 5.23 (s, 4H, Bn-C**H**$_2$); 5.91 (br, 2H, axle-N**H**); 6.66 (s, 1H, isophthal-H5); 6.82 (s, 4H, Ar-**H**); 6.95 (s, 4H, Ar-**H**); 7.14 (m, 10H, Bn-**H**); 7.24 (m, 30H, trityl-**H**); 7.33 (t, 2H, axle-N**H**); 7.37 (d, 2H, biphenyl-**H**); 7.39 (d, 2H, biphenyl-**H**); 7.43 (d, 2H, biphenyl-**H**); 7.47 (d, 2H, biphenyl-**H**); 8.07 (t, 1H, py-H5); 8.21 (br, 2H, N**H**); 8.45 (d, 2H. py-H4 & H6); 8.57 (s, 1H, isophthal-H2); 10.18 (s, 2H, N**H**)

^{13}C NMR (175 MHz, $CDCl_3$, 298 K)

δ = 14.09; 22.68; 22.99; 25.51; 26.36; 27.16; 27.22; 29.59; 31.90; 31.92; 35.72; 38.71; 40.30; 45.03; 67.64; 71.34; 99.96; 116.66; 125.12; 125.99; 126.34; 127.00; 127.25; 127.30; 127.42; 128.10; 128.43; 128.88; 129.73; 130.02; 131.17; 131.65; 133.20; 134.93; 135.22; 135.69; 138.74; 142.88; 142.99; 147.99; 148.25; 148.97; 160.61; 162.20; 164.89; 167.57; 175.06

MS ESI-FTICR, positive mode, sprayed from MeOH

m/z = 1985.997 ($[M + H]^+$; calc. 1985.966)

[2]-{N^4,$N^{4'}$-Bis(2-(2,2,2-triphenylacetamido)ethyl)biphenyl-4,4'-dicarboxamide}-{10^4,10^6-di-hydroxy-7^3,7^5,13^2,13^6,20^3,20^5,26^3,26^5-octamethyl-8,12,21,23^2,25-tetraaza-7,13,20,26(1,4),10,23(1,3)-hexabenzenadispiro[5.7.5.7]hexa-cosaphan-9,11,22,24-tetrone}-Rotaxane (R4)

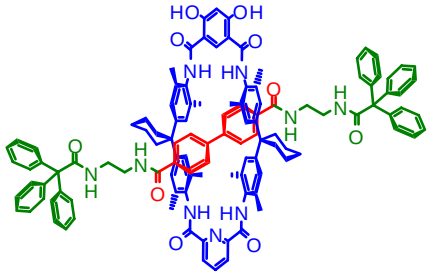

65 mg rotaxane **R2** (1985.5 g/mol / 24.7 µmol) were dissolved in 10 ml MeOH. After addition of 40 mg Pd/C (10 % Pd on carbon), the suspension was flushed with H_2 for 5 min and afterwards stirred for 40 h. Then, the suspension was filtered over celite. The celite was extracted with $CHCl_3$/MeOH (10:1) to elute the product.
Yield: 88 %

$C_{117}H_{113}N_9O_{10}$ 1805.20 g/mol

^{1}H NMR (400 MHz, $CDCl_3$, 298 K)

δ [ppm] = 1.52 & 1.56 (br, 4H, Cy-**H**); 1.67 (br, 8H Cy-**H**); 1.92 (s, 24H, C**H**$_3$); 2.22 & 2.32 (br, 8H Cy-**H**); 2.88 (br, 4H, axle-C**H**$_2$); 2.93 (br, 4H, axle-C**H**$_2$); 5.91 (br, 2H, axle-N**H**); 6.58 (s, 1H, isophthal-H5); 6.89 (s, 4H, Ar-**H**); 6.96 (s, 4H, Ar-**H**); 7.02 (d, 12H, trityl-**H**); 7.21 (t, 12H, trityl-**H**); 7.26 (d, 6H, trityl-**H**); 7.66 (d, 4H, biphenyl-**H**); 7.70 (d, 4H, biphenyl-**H**); 8.16 (t, 1H, py-H5); 8.21 (br, 2H, N**H**); 8.46 (d, 2H. py-H4 & H6); 8.79 (s, 1H, isophthal-H2); 10.18 (s, 2H, N**H**); 11.96 (s, 2H, O**H**)

^{13}C NMR (175 MHz, $CDCl_3$, 298 K)

δ [ppm] = 18.512; 18.680; 22.973; 26.260; 29.732; 36.662; 38.601; 45.257; 67.523; 105.160; 107.528; 124.986; 126.570; 127.055; 127.495; 127.575; 128.094; 130.291; 130.311; 130.532; 131.276; 134.899; 135.474; 139.236; 142.570; 148.897; 161.998; 166.307; 167.675; 168.747; 176.473

MS ESI-FTICR, positive mode, sprayed from MeOH

m/z = 1803.859 ($[M + H]^+$; calc. 1803.857)

[2]-{2-Hydroxy-N^1,N^3-bis(2-(2,2,2-triphenylacetamido)ethyl)isophthalamide}-{10^4,10^6-di-benzyloxy-7^3,7^5,13^2,13^6,20^3,20^5,26^3,26^5-octamethyl-8,12,21,23^2,25-tetraaza-7,13,20,26(1,4),10,23(1,3)-hexabenzenadispiro[5.7.5.7]hexa-cosaphan-9,11,22,24-tetrone}-Rotaxane (R3)

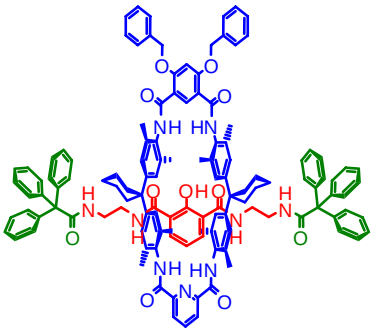

48 mg of N^1,N^3-bis(2-aminoethyl)-2-hydroxyisophthalamide (226.3 g/mol / 180 µmol) and 42 mg of P1 base (234.3 g/mol / 180 µmol / 0.921 g/mol / 46 µl) were stirred in 10 ml CH_2Cl_2 for 10 min until everything completely dissolved. 100 mg **Py-di-OBn-Macrocycle** (1118.4 g/mol / 89 µmol) and 0.2 ml NEt_3 were added in 3 ml CH_2Cl_2 followed by the addition of 111 mg of triphenylacetyl chloride (306.8 g/mol / 360 µmol) in 5 ml CH_2Cl_2. The resulting solution was stirred for 4 d at r.t. After evaporation of the solvent, the raw product was purified by column chromatography over silica gel using a mixture of CH_2Cl_2 / ethyl acetate (5:1 switching to 1:1 after elution of the free macrocycle) as eluent (R_f = 0.5).
Yield: 21 %

$C_{125}H_{121}N_9O_{11}$ 1925.35 g/mol

^{1}H NMR (400 MHz, $CDCl_3$, 298 K)
δ [ppm] =1.48 (br, 6H, Cy-**H**); 1.61 (br, 8H Cy-**H**); 1.81 (s, 12H, C**H**$_3$); 1.94 (s, 12H, C**H**$_3$); 2.17 (br, 8H Cy-**H**); 2.25 (br, 8H, axle-C**H**$_2$); 5.22 (s, 4H, Bn-C**H**$_2$); 6.65 (t, 1H; axle-phenol-**H**) 6.70 (s, 1H, isophthal-H5); 6.90 (br, 8H, Ar-**H** + 2H, N**H**); 7.18 (t, 30H, trityl-**H**); 7.28 (t,4H); 7.36 (t, 6H); 7.49 (d, 6H);7.81 (br, 2H, N**H**); 8.12 (t, 1H, py-H5); 8.43 (d, 2H. py-H4 & H6); 8.47 (s, 1H, isophthal-H2); 10.46 (s, 2H, N**H**); 15.04 (s, 1H, O**H**)

^{13}C NMR (100 MHz, $CDCl_3$, 298 K)

δ [ppm] = 18.46; 18.49; 23.07; 45.14; 70.97; 99.99; 117.81; 118.76; 124.83; 126.96; 127.50; 127.93; 128.12; 128.19; 128.21; 128.70; 130.33; 130.37; 130.41; 131.16; 131.52; 134.72; 135.61; 136.55; 142.58; 148.96; 160.53; 160.98; 162.02; 165.18

MS ESI-FTICR, negative mode, sprayed from MeOH

m/z = 1923.955 ($[M - H]^-$; calc. 1923.915)

[2]-{2-Hydroxy-N^1,N^3-bis(2-(2,2,2-triphenylacetamido)ethyl)isophthalamide}-{10^4,10^6-dihydroxy-7^3,7^5,13^2,13^6,20^3,20^5,26^3,26^5-octamethyl-8,12,21,23^2,25-tetraaza-7,13,20,26(1,4),10,23(1,3)-hexabenzenadispiro[5.7.5.7]hexa-cosaphan-9,11,22,24-tetrone}-Rotaxane (R5)

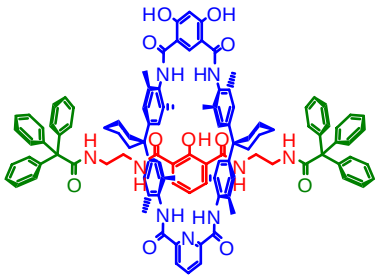

30 mg rotaxane **R3** (1925.4 g/mol / 15.6 µmol) were dissolved in 20 ml MeOH. After addition of 40 mg Pd/C (10 % Pd on carbon), the suspension was flushed with H_2 for 5 min and afterwards stirred for 42 h. Then, the suspension was filtered over celite. The celite was extracted with $CHCl_3$/MeOH (10:1) to elute the product (off-white solid).
Yield: 92 %

$C_{111}H_{109}N_9O_{11}$ 1745.11 g/mol

^{1}H NMR (500 MHz, $CDCl_3$, 298 K)
δ [ppm] = 1.47 (br, 6H, Cy-**H**); 1.53 & 1.61 (br, 8H Cy-**H**); 1.73; 1.97; 2.06 (4H, ethylene-CH_2); 2.23; 2.40; 3.56 (2H, ethylene-CH_2); 3.69 (2H, ethylene-CH_2); 6.54; 6.69; 6.71; 7.06; 7.23; 8.10; 8.12; 8.14; 8.41; 8.43; 8.84; 10.19 (s, 2H, N**H**); 12.00 (s, 2H, O**H**); 15.24 (s, 1H, O**H**)

^{13}C NMR (125 MHz, $CDCl_3$, 298 K)
δ [ppm] =14.22; 18.30; 18.67; 22.78; 23.07; 26.38; 29.45; 29.79; 32.02; 36.36; 37.05; 37.80; 39.16; 43.71; 45.56; 67.18; 68.03; 105.02; 107.63; 114.59; 119.16; 124.94; 127.53; 127.94; 128.37; 130.31; 130.54; 131.26; 139.15; 142.45; 142.66; 149.03; 161.15; 162.08; 166.28; 168.84; 170.59; 177.89

MS ESI-FTICR, positive mode, sprayed from MeOH
m/z = 1743.8045 ($[M + H]^+$; calc. 1743.8205)

6.5 Synthesis of Metal Complexes

2,2'-Bipyridyl-bis-(2,2'-phenylpyridyl)-iridium(III) Tetrakis-nonafluoro-*tert*-butyloxy-aluminate

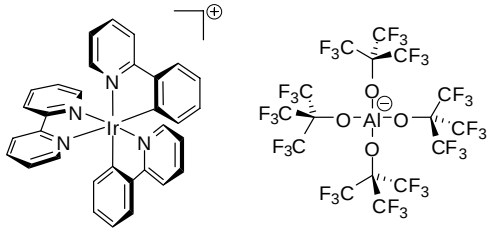

489 mg (0.455 mmol / 1074.96 g/mol) Silver tetrakis-nonafluoro-*tert*-butyloxy-aluminate 315 mg (0.455 mmol / 692.23 g/mol) and 2,2'-bipyridyl-bis-(2,2'-phenylpyridyl)-iridium(I) chloride were dissolved in 10 of CH_2Cl_2 and stirred over night in the dark. Afterwards, the AgCl formed was removed by filtration. The remaining orange solution was evaporated to dryness, yielding a bright yellow solid. Yield: 83 %

$C_{48}H_{24}AlF_{36}IrN_4O_4$ 1623.87 g/mol

^{1}H NMR (400 MHz, $CDCl_3$, 298 K)
δ [ppm] = 6.28 (dd, 2H, ppy-H3); 6.94 (m, 4H, ppy-H4 & ppy-H5'); 7.06 (dt, 2H); 7.41 (td, 2H); 7.47 (ddd, 2H); 7.70 (dd, 2H); 7.77 (dt, 2H); 7.94 (d, 2H); 8.04 (m, 4H); 8.30 (d, 2H, bpy-H3)

^{13}C NMR (125 MHz, $CDCl_3$, 298 K)
δ [ppm] = 115,37; 118,55; 118,71; 119,31; 120,50; 123,91; 126,62; 127,14; 133,85; 134,69; 138,77; 143,47; 144,88; 146,41; 150,91

^{19}F NMR (400 MHz, $CDCl_3$, 298 K)
δ [ppm] = -75.49

MS ESI-FTICR, positive mode, sprayed from CH_2Cl_2
m/z = 657.162 ($[Ir(bpy)(ppy)_2]^+$)
ESI-FTICR, negative mode, sprayed from CH_2Cl_2
m/z = 966.907 ($[Al(OC(C_4F_9)_3)_4]^-$)

Tris-(2,2'-phenylpyridyl)-iridium(III)

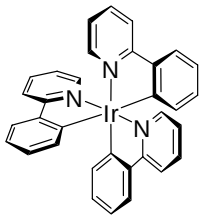

$IrCl_3 \cdot x\ H_2O$ [x = 3.69] (100 mg / 0.274 mmol / 365.04 g/mol) and 2-phenylpyridine (4.25 g / 3.9 ml / 27.4 mmol / 155.20 g/mol / 100 eq.) were heated in a standard household microwave for 1 minute. The orange solution was evaporated to dryness, yielding a bright yellow solid. Yield: 83 % (but still contains a small amount of $[Ir(ppy)_2Cl]_2$)

$C_{33}H_{24}IrN_3$ 654.78 g/mol

^{1}H NMR (400 MHz, $CDCl_3$, 298 K)
δ [ppm] = 6.84 (m, 4H); 7.51 (d, 1H); 7.53 (dt, 1H); 7.64 (d, 1H); 7.87 (d, 1H, py-H3)

MS (EI, 70 eV)
m/z = 655.2 ($[M]^{+\cdot}$); 501.2 ($[M\text{-}ppy]^+$)

The analytical data was consistent with the literature values.[190]

6.6 Synthesis of Oligolysine Peptides[††]

Peptides $Lys_{15}COOH$ and $Lys_{15}CONH_2$ were synthesized using a SyroXP-I peptide synthesizer (Multi-SynTech GmbH, Germany) on a 0.05 mM scale according to standard Fmoc-strategy. Peptide $Lys_{15}COOH$ was synthesized on a preloaded Fmoc-Lys(Boc)-Wang resin (0,60 mmol/g; Novabiochem® - Merck, Germany) while Lys_{15}-NH_2 was synthesized on a unloaded Rink Amide MBHA resin (0,78 mmol/g; Novabiochem® - Merck, Germany). For all amino acid couplings, a fourfold excess of Fmoc-Lys(Boc)-OH and coupling reagents TBTU and HOBt (Fa. Gerhardt, Germany) as well as an eightfold excess of DIEA (Acros Organics, Belgium) relative to resin loading was used. All couplings were performed as double couplings (30 minutes). The coupling mixture contained 0.23 M $NaClO_4$ to prevent on-resin aggregation. A mixture of DBU and piperidine (2% each) in DMF was used for Fmoc-deprotection (4 x 5 minutes). $Lys_{15}COOH$ was cleaved from resin by treatment with 2 mL TFA/TIS/H_2O (90/9/1) for three hours. The resin was washed twice with TFA (1 mL) and DCM (dry, 1 mL) and excess solvent was removed by evaporation. Peptide $Lys_{15}CONH_2$ was cleaved from resin by a two-stage procedure. At first the resin was washed slowly with a mixture of 5% TFA and 5% TIS in DCM (25 mL). Additionally, the resin was treated afterwards according to the same cleaved procedure like peptide $Lys_{15}COOH$. The peptides were precipitated with cool diethyl ether, centrifuged and dried in vacuum.

Purification was carried out by preparative reversed-phase HPLC on a Knauer Smartline system (manager 5000, 2 × pump 1000, UV detector 2500; Knauer GmbH, Germany) equipped with a Luna™ C8 (10u, 250×21.20 mm) column (Phenomenex, USA). Eluation solvents were ACN/0.1% TFA (gradient grade; Acros Organics, Belgium) and water Millipore/0.1% TFA. The flowrate was 20 mL min^{-1}. Purified peptides were characterized by analytical HPLC and ESI-MS. The analytic HPLC was carried out with a VWR-Hitachi Elite LaChrome system (L-2200 autosampler, 2 × L-2130 pump, L-2455 diode array detector; VWR International GmbH, Germany) equipped with a Luna™ C8 (5u, 250×4.6 mm) column (Phenomenex, USA). The flowrate was 1 mL min^{-1}.

[††] performed by Jessica Falenski (group of Prof. Beate Koksch, FU Berlin)

7. Acknowledgements

First, I want to thank my supervisor Prof. Dr. Christoph A. Schalley for the opportunity to work in his group on the challenging projects described above and several others more, for the possibility to learn so many interesting things about science, and for his constant support.
I also would like to thank Prof. Dr. Rainer Haag for being my second supervisor and for his time to review this thesis.
Further, I am thankful to Prof. Kari Rissanen for hosting me in his group in Jyväskylä.

I am very thankful to the whole Schalley group for their valuable discussions during numerous coffee sessions and of course for the pleasant and inspiring atmosphere during the last years, especially to my labmates Johannes Poppenberg, Sophia Möhl, Julian Sklorz, Christian Timper, and particularly Ralf Troff and Dominik Sattler whom I spent most of my lab time with.

Definitely, many of the results described in this thesis would not have been possible without the fruitful cooperation with other scientists from the Freie Universität Berlin and other institutes. I therefore would like to express my thanks to the following people:

- Henrik D. F. Winkler, Jessica A. Falenski, and Prof. Beate Koksch (all FU Berlin) for their cooperation on the „spacewalk“ project and Prof. Bert Meijer (TU Eindhoven) and Dr. Henk M. Janssen (SyMO-Chem B.V., Eindhoven) for providing the POPAM dendrimers,
- Kirsi Salorinne and Maija Nissinen (University of Jyväskylä, Finland) for their cooperation on the investigation of the resorcinarene-based anion receptor,
- Ryan E. Dawson, Andreas Hennig, Daniel Emery, Velayutham Ravikumar, Javier Montenegro, Toshihide Takeuchi, Jiri Mareda, Prof. Stefan Matile (all University of Geneva, Switzerland), Sandro Gabutti, and Prof. Marcel Mayor (both University of Basel, Switzerland) for their cooperation on the NDI anion-π project,
- Lena Kaufmann (FU Berlin), Kodiah Beyeh, and Prof. Kari Rissanen (both University of Jyväskylä, Finland), Byron Purse (University of Denver, CO), and Prof. Ingo Krossing (University of Freiburg) for their cooperation on the resorcinarene related projects,
- Dominik Sattler and Ahmet Gökkaya for their first attempts on the synthesis of alkyloxy-substitutes tetra- and octalactam macrocycles.

I am also thankful to Dr. Andreas Springer and his team for measuring the ESI-TOF and EI mass spectra and for keeping the ESI-FTICR mass spectrometer as one of my most important tools in a working condition.
Further, I wish to thank the NMR team and especially Dr. Andreas Schäfer for measuring numerous NMR spectra and for fulfilling also my more special wishes regarding the more complex analyses.
Also, I would like to thank Prof. Dieter Lentz for performing the singly crystal X-ray analysis of my shuttle rotaxane.

Finally, I am deeply grateful to Larissa von Krbek for finding (hopefully all of) the spelling mistakes in this thesis and for bringing back the smile to my face.

8. List of Publications

1. *Host-guest chemistry of self-assembling supramolecular capsules in the gas phase*
   D. P. Weimann, C. A. Schalley
   Supramol. Chem. **2008**, *20*, 117-128

2. *Dynamic Motion in Crown Ether-Dendrimer Complexes: A Spacewalk on the Molecular Scale*
   H. D. F. Winkler, D. P. Weimann, A. Springer, C. A. Schalley
   Angew. Chem. **2009**, *121*, 7382-7386; *Angew. Chem. Int. Ed.* **2009**, *48*, 7246-7250

3. *Highly dynamic motion of crown ethers along oligolysine peptide chains*
   D. P. Weimann, H. D. F. Winkler, J. A. Falenski, B. Koksch, C. A. Schalley
   Nature Chem. **2009**, *1*, 573-577

4. *Resorcinarene Podand with Amine Functionalized Side Arms - Synthesis, Structure and Binding Properties of a Neutral Anion Receptor*
   K. Salorinne, D. P. Weimann, C. A. Schalley, M. Nissinen
   Eur. J. Org. Chem. **2009**, 6151-6159

5. *Experimental evidence for the functional relevance of anion-pi interactions*
   R. E. Dawson, A. Hennig, D. P. Weimann, D. Emery, V. Ravikumar, J. Montenegro, T. Takeuchi, S. Gabutti, M. Mayor, J. Mareda, C. A. Schalley, S. Matile
   Nature Chem. **2010**, *2*, 533-538

6. *Mass Spectrometry and Gas Phase Chemistry of Supramolecules*
   D. P. Weimann, M. Kogej, C. A. Schalley
   in „Analytical Methods in Supramolecular Chemistry“, 2. Auflage, C. A. Schalley (Ed.), *Wiley-VCH, Weinheim,* **2012**

7. *Ion Pair Recognition of Tetramethyl Ammonium Salts by Halogenated Resorcinarenes*
   N. K. Beyeh, D. P. Weimann, L. Kaufmann, C. A. Schalley, K. Rissanen
   Chem. Eur. J **2012**, *18*, 5552

9. References

1 a) A. J. Goshe, J. D. Crowley, B. Bosnich, *Helv. Chim. Acta* **2001**, 2971; b) J. W. Steed, D. R. Turner, K. Wallace, *Core Concepts in Supramolecular Chemistry and Nanochemistry* **2007,** Wiley-VCH; c) B. L. Schottel, H. T. Chifotides, K. R. Dunbar*, Chem. Soc. Rev.* **2008**, *37*, 68; d) J. W. Steed, J. L. Atwood, *Supramolecular Chemistry*, Wiley, Chichester/England, **2000**..

2 J.-M. Lehn, *Angew. Chem. Int. Ed.* **1990**, *29*, 1304.

3 E. Fischer, *Ber. Deutsch. Chem. Ges*. **1984**, *3*, 2985.

4 a) T. S. Moore, T. F. Winmill, *J. Chem. Soc.* **1912**, *101* 1635; b) W. M. Latimer, W. H. Rodebush, *J. Am. Chem. Soc.* **1920***, 42*, 1419.

5 J. D. Watson, F. Crick, *.Nature* **1953**, *171*, 737.

6 A. L. Lehninger, „Principles of Biochemistry“ 3rd Ed. **2000**, Freeman.

7 C. A. Schalley, K. Beizai, F. Vögtle, *Acc. Chem. Res.* **2001**, *34*, 465.

8 C. A. Schalley, A. Lützen, M. Albrecht, *Chem. Eur. J.* **2004**, *10*, 1072.

9 J. E. Green, J. W. Choi, A. Boukai, Y. Bunimovich, E. Johnston-Halperin, E. Delonno, Y. Luo, B. A. Sheriff, K. Xu, Y. S. Shin, H.-R. Tseng, J. F. Stoddart, J. R. Heath, *Nature* **2007**, *445*, 414.

10 O. Safarowsky, B. Windisch, A. Mohry, F. Vögtle, *J. Prakt. Chem.* **2000**, *5*, 342.

11 A. Sobanski, R. Schmieder, F. Vögtle, *Chem. uns. Zeit* **2000**, *34*, 160.

12 a) C. Yamamoto,Y. Okamoto, T. Schmidt, R. Jaeger, F. Vögtle, *J. Am. Chem. Soc.* **1997**, *119*, 10547; b) C. Reuter, A. Mohry, A. Sobanski, F. Vögtle, *Chem. Eur. J.* **2000**, *6*, 1674.

13 C. O. Dietrich-Buchecker, J.-P. Sauvage, *Chem. Rev.* **1987**, 87, 795.

14 C. A. Schalley, T. Weilandt, J. Brüggemann, F. Vögtle, *Top. Curr. Chem.* **2004**, *248*, 141-200.

15 I. T. Harrison, S. Harrison, *J. Am. Chem. Soc.* **1967**, *89*, 5723.

16 C. A. Hunter, *J. Chem. Soc., Chem. Commun.* **1991**, 749.

17 C. A. Schalley, W. Reckien, S. Peyerimhoff, B. Baytekin, F. Vögtle, *Chem. Eur. J.* **2004**, *10*, 4777.

18 F. Vögtle, M. Haendel, S. Meier, S. Ottens-Hildebrandt, F. Ott, T. Schmidt, *Liebigs Ann.* **1995**, *5*, 739.

19 Examples for rotaxane formation via amide template can be found in: a) C. Heim, A. Affeld, M. Nieger, F. Vögtle, *Helv. Chim. Acta* **1999**, *82*, 746; b) F. Vögtle, T. Dünnwald, T. Schmidt, *Acc. Chem. Res.* **1996**, *29*, 451; c) C. Seel, A. Parham, O. Safarowsky, G. Hübner, F. Vögtle, *J. Org. Chem.* **1999**, *64*, 7236; d) O. Braun, A. Huenten, F. Vögtle, *J. Prakt. Chem.* **1999**, *341*, 542; e) F. Vögtle, R. Jaeger, M. Haendel, S. Ottens-Hildebrandt, W. Schmidt, *Synthesis* **1996**, *3*, 353; f) F. Vögtle, F. Ahuis, S. Baumann, J. L. Sessler, *Liebigs Ann.* **1996**, 921; g) C. Fischer, M. Nieger, O. Mogck, V. Boehmer, R. Ungaro, F. Vögtle, *Eur. J. Org. Chem.* **1997**, 155; h) R. Jaeger, S. Baumann, M. Fischer, O. Safarowsky, M. Nieger, F. Vögtle, *Liebigs Ann.* **1997**, 2269; i) C. A. Hunter, C. Low, M. Packer, S. Spey, J. Vinter, M. Vysotsky, C. Zonta, *Angew. Chem. Int. Ed.* **2001**, *40*, 2678; j) R. Schmieder, G. Huebner, C. Seel, F. Vögtle, *Angew. Chem. Int. Ed.* **1999**, *38*, 3528; k) C. Yamamoto, Y. Okamoto, T. Schmidt, R. Jaeger, F. Vögtle, *J. Am. Chem. Soc.* **1997**, *119*, 10547; l) C. Reuter, A. Mohry, A. Sobanski, F. Vögtle, *Chem. Eur. J.* **2000**, *6*, 1674; m) C. Reuter, W. Wienand, C. Schmuck, F. Vögtle, *Chem. Eur. J.* **2001**, *7*, 1728.

20 a) D. A. Leigh, A. Murphy, J. P. Smart, A. M. Z. Slawin, Angew. *Chem. Int. Ed.* **1997**, *36*, 728; b) F. G. Gatti, D. A. Leigh, S. A. Nepogodiev, A. M. Z. Slawin, S. J. Teat, J. K. Y. Wong, *J. Am. Chem. Soc.* **2001**, *123*, 5983; c) G. Brancato, F. Coutrot, D. A. Leigh, A. Murphy, J. K. Y. Wong, F. Zerbetto, *Proc. Natl. Acad. Sci. USA* **2002**, *99*, 4967; d) J. S. Hannam, T. J. Kidd, D. A. Leigh, A. J. Wilson, *Org. Lett.* **2003**, *5*, 1907; e) k) T. J. Kidd, T. J. A. Loonjens, D. A. Leigh, J. K. Y. Wong, *Angew. Chem. Int. Ed.* **2003**, *42* , 3379.

21 a) G. M. Hübner, J. Gläser, C. Seel, F. Vögtle, *Angew. Chem.* **1999**, *111*, 395; *Angew. Chem. Int. Ed.* **1999**, *37*, 3031; b) C. Reuter, W. Wienand, G. M. Hübner, C. Seel, F. Vögtle, *Chem. Eur. J.* **1999**, *5*, 2692; c) C. Seel, F. Vögtle, *Chem. Eur. J.* **2000**, *6*, 21.

22 P. Ghosh, O. Mermagen, C. A. Schalley, *Chem. Commun.* **2002**, 2628.

23 P. Ghosh, G. Federwisch, M. Kogej, C. A. Schalley, D. Haase, W. Saak, A. Lützen, R. M. Gschwind, *Org. Biomol. Chem.* **2005**, *3*, 2691.

24 a) J. A. Wisner, M. G. B. Drew, P. D. Beer, *Angew. Chem.,Int. Ed.* **2001**, *40*, 3606; b) M. Sambrook, J. A. Wisner, R. L. Paul, M. G. B. Drew, A. R. Cowley, F. Szemes, P. D. Beer, *J. Am. Chem. Soc.* **2005**, *127*, 2292; c) D. Curiel, M. Sambrook, R. L. Paul, A. R. Cowley, F. Szemes, P. D. Beer, *Chem. Commun.* **2004**, 1162; d) J. A. Wisner, M. Sambrook, M. G. B. Drew, P. D. Beer, *J. Am. Chem. Soc.* **2002**, *124*, 12469; e) D. Curiel, P. D. Beer, *Chem. Commun.* **2005**, *14*, 1909; f) M. Sambrook, J. A. Wisner, R. L. Paul, A. R. Cowley, F. Szemes, P. D. Beer, *J. Am. Chem.Soc.* **2004**, *126*, 15364; g) K.-Y. Ng, A. R. Cowley, P. D. Beer, *Chem. Commun.* **2006**, 3676.

25 I. Poleschak, J.-M. Kern, J.-P. Sauvage, *Chem. Commun.* **2004**, 474.

26 a) T. Chang, A. M. Heiss, S. J. Cantrill, M. C. T. Fyfe, A. R. Pease, S. J. Rowan, J. F. Stoddart, D. J. Williams, *Org. Lett.* **2000**, *2*, 2943; b) T. Chang, A. M. Heiss, S. J. Cantrill, M. C. T. Fyfe, A. R. Pease, S. J. Rowan, J. F. Stoddart, A. J. P. White, D. J. Williams, *Org. Lett.* **2000**, *2*, 2847; c) S. J. Cantrill, D. A. Fulton, A. M. Heiss, A. Pease, J. F. Stoddart, A. J. P. White, D. J. Williams, *Eur. J. Chem.* **2000**, *6*, 2274; d) F. Diederich, L. Echogoyen, M. G. Gómez-López, R. Kessinger, J. F. Stoddart, *J. Chem. Soc.; Perkin Trans. 2* **1999**, 1577; e) T. Clifford, A. Abushamleh, D. H. Busch, *Proc. Nat. Acad. Sci. USA* **2002**, *99*, 4830; f) P. R. Ashton, M. C. T. Fyfe, M. V. Martínez-Días, S. Menzer, C. Schiavo, J. F. Stoddart, A. J. P. White, D. J. Williams, *Chem. Eur. J.* **1998**, *4*, 1523; g) V. Balzani, M. Clemente-León, A. Credi, J. N. Lowe, J. D. Badjic, J. F. Stoddart, *Chem. Eur. J.* **2003**, *9*, 5348.

27 a) S. H. Chiu, S. J. Rowan, S. J. Cantrill, J. F. Stoddart, *Chem. Eur. J.* **2002**, *8*, 5170; b) J. Cao, M. C. T. Fyfe, J. F. Stoddart, *J. Org. Chem.* **2000**, *65*, 1937; c) A. F. M. Kilbinger, S. J. Cantrill, A. W. Waltman, M. W. Day, R. H. Grubbs, *Angew. Chem. Int. Ed.* **2003**, *42*, 3281; d) T. Chang, A. M. Heiss, S. J. Cantrill, M. C. T. Fyfe, A. R. Pease, S. J. Rowan, J. F. Stoddart, A. J. P. Williams, *Org. Lett.* **2000**, *2*, 2947; e) M. Horn, J. Ihringer, P. T. Glink, J. F. Stoddart, *Chem. Eur. J.* **2003**, *9*, 4046; f) A. G. Kolchinski, N. W. Alcock, R. A. Roesner, D. H. Busch, *Chem. Commun.* **1998**, 1437; g) J. D. Badjic, V. Balzani, A. Credi, J. N. Lowe, S. Silvi, J. F. Stoddart, *Chem. Eur. J.* **2004**, *10*, 1926; h) J. D. Badjic, S. J. Cantrill, J. F. Stoddart, *J. Am. Chem. Soc.* **2004**, *126*, 2288; i) P. R. Ashton, P. J. Campbell, E. J. T. Chrystal, P. T. Glink, S. Menzer, D. Philp, N. Spencer, J. F. Stoddart, P. A. Tasker, D. J. Williams, *Angew. Chem. Int. Ed. Engl.* **1995**, *34*, 1865.

28 a) W. Jiang, H. D. F. Winkler, C. A. Schalley, *J. Am. Chem. Soc.* **2008**, *130*, 13852; b) W. Jiang, C. A. Schalley, *Proc. Natl. Acad. Sci. USA* **2009**, *106*, 10425; c) W. Jiang, P. C. Mohr, A. Schäfer, C. A. Schalley, *J. Am. Chem. Soc.* **2010**, *132*, 2309; d) W. Jiang, C. A. Schalley, *J. Mass Spectrom.* **2010**, *45*, 788; e) W. Jiang, D. Sattler, K. Rissanen, C.A. Schalley, *Org. Lett.* **2011**, *13*, 4502; f) W. Jiang, K. Nowosinski, N. L. Löw, E. V. Dzyuba, F. Klautzsch, A. Schäfer, J. Huuskonen, K. Rissanen, C. A. Schalley, *J. Am. Chem. Soc.* **2012**, *134*, 1860.

29 J. D. Badjic, V. Balzani, A. Credi, S. Silvi, J. F. Stoddart, *Science* **2004**, *303*, 1845.

30 *Templated Synthesis of Interlocked Molecules,* C. A. Schalley, J. Illigen in: *Bottom-up Nanofabrication: Supramolecules, Self-Assemblies, and Organized Films*, K. Ariga, H.S. Nalwa (Eds.), American Scientific Publishers, Valencia/USA, **2009**.

31 C. A. Hunter, J. K. M. Saunders, *J. Am. Chem. Soc.* **1990**, *112*, 5525.

32 J. O. Jeppesen, K. A. Nielsen, J. Perkins, S. A. Vignon, A. Di Fabio, R. Ballardini, M. T. Gandolfi, M. Venturi, V. Balzani, J. Becher, J. F. Stoddart, *Chem. Eur. J.* **2003**, 9, 2982.

33 H.-R. Tseng, S. A. Vignon, P. C. Celestre, J. Perkins, J. O. Jeppesen, A. Di Fabio, R. Ballardini, M. T. Gandolfi, M. Venturi, V. Balzani, J. F. Stoddart, *Chem. Eur. J.* **2004**, *10*, 155.

34 W. R. Dichtel, O. S. Mijanic, J. M. Spruell, J. R. Heath, J. F. Stoddart, *J. Am. Chem. Soc.* **2006**, *128*, 10388.

35 I. Aprahamian, W. R. Dichtel, T. Ikeda, J. R. Heath, J. F. Stoddart, *Org. Lett.*. **2007**, *9*, 1287.

36 a) J. O. Jeppesen, J. Perkins, J. Becher, J. F. Stoddart, *Angew. Chem.* **2001**, *113*, 1256; *Angew. Chem. Int. Ed.* **2001**, *40*, 1216; b) H.-R. Tseng, S. A. Vignon, J. F. Stoddart, *Angew. Chem.* **2003**, *115*, 1529; *Angew. Chem. Int. Ed.* **2003**, *42*, 1491.

37 a) E. Cordova, R. A. Bissell, N. Spencer, P. R. Ashton, J. F. Stoddart, A. E. Kaifer, *J. Org. Chem.* **1993**, *58*, 6550; b) D. B. Amabilino, P. R. Ashton, S. E. Boyd, M. Gomez-Lopez, W. Hayes, J. F. Stoddart, *J. Org. Chem.* **1997**, *62*, 3062.

38 *Mass Spectrometry and Gas-Phase Chemistry of Non-Covalent Complexes*, C.A. Schalley, A. Springer, Wiley, Hoboken/NJ **2009**.

39 *Mass Spectrometry and Gas-Phase Chemistry of Supramolecules: A Primer,* E. V. Dzyuba, J. Poppenberg, S. Richter, R.W. Troff, C.A. Schalley in: *Supramolecular Chemistry - From Molecules to Nanomaterials*, pp. 347-378, J. W. Steed, P. Gale (Eds.), Wiley, Chichester, **2012**.

40 B. Baytekin, H. T. Baytekin, C. A. Schalley, *Org. Biomol. Chem.* **2006**, *4*, 2825.

41 C. A. Schalley, *Mass Spectrom. Rev.* **2001**, *20*, 253.

42 T. D. Märk (Ed.), G. H. Dunn (Ed.), *Electron Impact Ionization*, **1985**, Springer, Berlin.

43 a) M. S. B. Munson, F. H. Field, *J. Am. Chem. Soc.* **1966**, *88*, 2621; b) R. C. Dougherty, *Biomed. Mass Spectrom.* **1981**, *8*, 283; c) G. S. Ghaderi, P. S. Kulkarni, E. B. Ledford, C. L. Wilkins, M. L. Gross, *Anal. Chem.* **1981**, *53*, 428; d) B. Munson, Int. J. Mass. Spectrom. **2000**, *200*, 243.

44 a) E. C. Horning, D. I. Carroll, I. Dzidic, K. D. Haegele, M. G. Horning, R. N. Stillwell, *J. Chromatogr. Sci.* **1974**, *12*, 725; b) E. C. Horning, D. I. Carroll, I. Dzidic, K. D. Haegele, M. G. Horning, R. N. Stillwell, *J. Chromatogr.* **1974**, *99*, 13; c) D. I. Carroll, I. Dzidic, R. N. Stillwell, K. D. Haegele, E. C. Horning, *Anal. Chem.* **1975**, *47*, 2369; d) V. G. Zaikin, J. M. Halket, *Eur. J. Mass Spectrom.* **2006**, *12*, 79; e) P. Terrier, B. Desmazières, J. Tortajada, W. Buchmann, *Mass Spectrom. Rev.* **2001**, *30*, 854.

45 a) H. R. Morris, M. Panico, M. Barber , R. S. Bordoli, R. D. Sedgwick, A. Tyler, *Biochem. Biophys. Res. Commun.***1981**, *101*, 623; b) M. Barber , R. S. Bordoli, R. D. Sedgwick, A. Tyler, *J. Chem. Soc., Chem. Commun.* **1981**, 325; c) M. Barber , R. S. Bordoli, R. D. Sedgwick, A. N. Tyler, *Nature* **1981**, *293*, 270; d) M. Barber, R. S. Bordoli, G. J. Elliott, R. D. Sedgwick, A. N. Tyler, *Anal. Chem.* **1982**, *54*, 645A; e) K. B. Tomer, *Mass Spectrom. Rev.* **1989**, *8*, 445.

46 for reviews on MALDI see: a) R. Zenobi, R. Knochenmuss, *Mass Spectrom. Rev.* **1999**, 17, 337; b) C. Menzel, K. Dreisewerd, S. Berkenkamp, F. Hillenkamp, *Int. J. Mass Spectrom.* **2001**, 207, 73; c) K. Dreisewerd, S. Berkenkamp, A. Leisner, A. Rohlfing, C. Menzel, *Int. J. Mass Spectrom.* **2003**, 226, 189; d) K. Dreisewerd, *Chem. Rev.* **2003**, 103, 395; e) M. Karas, R. Krüger, *Chem. Rev.* **2003**, 103, 427; f) K. Tanaka, *Angew. Chem.* **2003**, 115, 3989; *Angew. Chem. Int. Ed.* **2003**, 42, 3989.

47 a) B. H. Wang, K. Dreisewerd, U. Bahr, M. Karas, F. Hillenkamp, *J. Am. Soc. Mass Spectrom.* **1993**, 4, 393; b) P. Juhasz, C. E. Costello, *Rapid Commun. Mass Spectrom.* **1993**, 7, 343; c) M. Glückmann, A. Pfenninger, R. Krüger, M. Thierolf, M. Karas, V. Horneffer, F. Hillenkamp, *Int. J. Mass Spectrom.* **2001**, 210/211, 121.

48 a) J. B. Fenn, M. Mann, C. K. Meng, S. F. Wong, C. M. Whitehouse, *Mass Spectrom. Rev.* **1990**, 9, 37; b) P. Kebarle, L. Tang, *Anal. Chem.* **1993**, 65, 972A; c) S. J. Gaskell, *J. Mass Spectrom.* **1997**, 32, 677; d) J. B. Fenn, *Angew. Chem.* **2003**, 115, 3999; *Angew. Chem. Int. Ed.* **2003**, 42, 3871.

49 a) M. Dole, L. L. Mack, R. L. Hines, R. C. Mobley, L. D. Ferguson, M. B. Alice, *Macromolecules* **1968**, 1, 96; b) M. Dole, L. L. Mack, R. L. Hines, R. C. Mobley, L. D. Ferguson, M. B. Alice, *J. Chem. Phys.* **1968**, 49, 2240.

50 a) M. Dole, L. L. Mack, R. L. Hines, R. C. Mobley, L. D. Ferguson, M. B. Alice, *J. Chem. Phys.* **1968**, 49, 2240; b) F. W. Röllgen, E. Bramer-Wegner, L. Buttering, *J. Phys. Colloq.* **1984**, 45, Suppl. 12, C9-297.

51 a) J. V. Iribarne, B. A. Thomson, *J. Chem. Phys.* **1976**, 64, 2287; b) B. A. Thomson, J. V. Iribarne, *J. Chem. Phys.* **1979**, 71, 4451.

52 *Mass Spectrometry and Gas Phase Chemistry of Supramolecules*, D. P. Weimann, M. Kogej, C. A. Schalley in *Analytical Methods in Supramolecular Chemistry, 2nd Edition*, C.A. Schalley (ed.), Wiley-VCH, Weinheim, **2012**.

53 A. G. Marshall, C. S. Hendrickson, G. S. Jackson, *Mass Spectrom. Rev.* **1998**, *17*, 1.

54 a) *Tandem Mass Spectrometry*, F. W. McLafferty (Ed.), Wiley, New York, **1983**; b) *Mass Spectrometry*, K. L. Busch, G. L. Glish, S. A. McLuckey, Wiley, New York, **1988**.

55 a) F. W. McLafferty, P. F. Bente, R. Kornfeld, S.-C. Tsai, I. Howe, *J. Am. Chem. Soc.* **1973**, 95, 2120; b) K. Levsen, H. Schwarz, *Angew. Chem.* **1976**, *88*, 589; Angew. Chem. Int. Ed. **1976**, *15*, 509; c) K. Levsen, H. Schwarz, Mass Spectrom. Rev. **1983**, *2*, 77; d) C. D. Bradley, P. J. Derrick, *Org. Mass Spectrom.* **1991**, *26*, 395; e) S. A. McLuckey, *J. Am. Soc. Mass Spectrom.* **1992**, *3*, 599; f) A. K. Shukla, J. H. Futrell, *J. Mass Spectrom.* **2000**, *35,* 1069.

56 J. W. Gauthier, T. R. Trautman, D. B. Jacobson, *Anal. Chim. Acta* **1991**, *246*, 211.

57 a) N. G. Basov, E. P. Markin, A. N. Oraevski, A. V. Pankratov, A. N. Shachkov, *JETP Lett.* **1971**, *14*, 165; b) R. L. Woodin, D. S. Bomse, J. L. Beauchamp, J. Am. Chem. Soc. **1978**, *100*, 3248; c) C. H.

Watson, G. Baykut, J. R. Eyler, *Anal. Chem.* **1987**, *59*, 1133; d) D. P. Little, J. P. Speir, M. W. Senko, P. B. O'Connor, F. W. McLafferty, *Anal. Chem.* **1994**, *66*, 2809.

58 N. C. Polfer, J. Oomens, *Phys. Chem. Chem. Phys.*, **2007**, *9*, 3804.

59 M. Przybylski and M. O. Glocker, *Angew. Chem. Int. Ed.,* **1996**, *35*, 806.

60 J. S. Brodbelt, *Int. J. Mass Spectrom.,* **2000**, *200*, 57.

61 C. A. Schalley, *Int. J. Mass Spectrom.,* **2000**, *194*, 11.

62 C. B. Lebrilla, *Acc. Chem. Res.,* **2001**, *34*, 653.

63 C. A. Schalley, *Mass Spectrom. Rev.,* **2001**, *20*, 253.

64 C. A. Schalley, W. Reckien, S. Pexerimhoff, B. Baytekin, F. Vögtle, *Chem. Eur. J.* **2004**, *10*, 4777.

65 B. Baytekin, S. S. Zhu, B. Brusilowskij, J. Illigen, J. Ranta, J. Huuskonen, L. Russo, K. Rissanen, L. Kaufmann, C. A. Schalley, *Chem. Eur. J.* **2008**, *14*, 10012.

66 H. Tian, Q.-C. Wang, *Chem. Soc. Rev.* **2006**, *35*, 361.

67 L. Yuan, A. R. Sanford, W. Feng, A. Zhang, J. Zhu, H. Zeng, K. Yamato, M. Li, J. S. Ferguson, B. Gong, *J. Org. Chem*. **2005**, *70*, 10660.

68 E. J. Corey *J. Am. Chem. Soc.* **1972**, *94*, 6192.

69 S.-Y. Chang, H. S. Kim, K.-J. Chang, K.-S. Jeong, *Org. Lett.* **2004**, *6*, 181.

70 a) P. V. Santacroce, J. T. Davis, M. E. Light, P. A. Gale, J. C. Iglesias-Sanchez, P. Prados, R. Quesada, *J. Am. Chem. Soc.* **2007**, *129*, 1886; b) G. W. Bates, P. A. Gale, *Structure & Bonding* **2008***, 129,* 1; c) D. Makuc, J. R. Hiscock, M. E. Light, P. A. Gale, Janez Plavec, *Beilstein J. Org. Chem.* **2011,** *7,* 1205.

71 M. Hesse, B. Meier, B. Zeeh, *Spektroskopische Methoden in der organischen Chemie*, 7th Ed., **2005**, Thieme, Stuttgart, New York.

72 J. Jeener, B. H. Meier, P.Bachmann, R. R. Ernst, *J. Chem. Phys.* **1979**, *71*, 4546.

73 H. Günther, *NMR-Spektroskopie, 3rd ed.*, Thieme, Stuttgart, **1992**, 314.

74 S. S. Zhu, M. Nieger, J. Daniels, T. Felder, I. Kossev, T. Schmidt, M. Sokolowski, F. Vögtle, C. A. Schalley, *Chem. Eur. J.* **2009**, *15*, 5040.

75 C. A. Hunter, *J. Am. Chem. Soc.* **1992**, *114*, 5303.

76 F. J. Carver, C. A. Hunter, R. J. Shannon, *J. Chem. Soc., Chem. Commun.*, **1994**, 1277.

77 M. Yamaguchi, H. Okubo, M. Hirama, *Chem. Commun.*, **1996**, 1771.

78 C. A. Hunter, D. H. Puvvis, *Angew. Chem. Int. Ed.* **1996**, *31*, 792.

79 H. Okubo, M. Yamaguchi, C. Kabuto, *J. Org. Chem.*, **1998**, *63*, 9500.

80 O. Safarowsky, E. Vogel, F. Vögtle *Eur. J. Org. Chem.* **2000**, 499.

81 F. Schwanke, O. Safarowsky, C. Heim, G. Silva, F. Vögtle, *Helv. Chim. Acta* **2000**, *83*, 3279.

82 G. M. Hübner, J. Gläser, C. Seel, F. Vögtle, *Angew. Chem. Int. Ed.* **1999**, *38*, 383.

83 C. A. Schalley, J. Hoernschemeyer, X.-Y. Li, G. Silva, P. Weis *Int. J. Mass Spectrom.* **2003**, *228*, 373.

84 M. Meot-Ner (Mautner), *Chem. Rev.* **2005***, 105*, 213.

85 C. Lifshitz, *Int. J. Mass Spectrom.* **2004**, *234*, 63.

86 K. A. Kellersberger, C. Desjupa, Y. J. Liang, R. M. Pope, D. V. Dearden, *Int. J. Mass Spectrom.* **1999**, *193*, 181.

87 E. Ventola, K. Rissanen, P. Vainiotalo, *Chem. Eur. J.* **2004**, *10*, 6152.

88 E. Ventola, A. Hyyryläinen, P. Vainiotalo, *Rapid Commun. Mass Spectrom.* **2006,** *20*, 1218.

89 E. Kalenius, D. Moiani, E. Dalcanale, P. Vainiotalo, *Chem. Commun.* **2007**, 3865.

90 T. D. Wood, R. A. Chorush, F. M. Wampler III, D. P. Little, P. B. O'Connor, F. W. McLafferty, *Proc. Natl. Acad. Sci. USA* **1995**, *92*, 2421.

91 T. Wyttenbach, M. T. Bowers, *J. Am. Soc. Mass Spectrom.* **1999**, *10*, 9.

92 S.-W. Lee, H.-N. Lee, H. S. Kim, J. L. Beauchamp, *J. Am. Chem. Soc.* **1998**, *120*, 5800.

93 S. G. Lias, *J. Phys. Chem.* **1984**, *88*, 4401.

94 D. J. Cram, J. M. Cram, *Acc. Chem. Res.* **1978**, *11*, 8.

95 V. Rüdiger, H.-J. Schneider, V. P. Solov'ev, V. P. Kazachenko and O. A. Raevsky, *Eur. J. Org. Chem.* **1999**, 1847.

96 S. Maleknia, J. Brodbelt, *J. Am. Chem. Soc.* **1993**, *115*, 2837.

97 D. V. Dearden, Y. J. Liang, J. B. Nicoll, K. A. Kellersberger, *J. Mass Spectrom.* **2001**, *36*, 989.

98 D. V. Dearden, C. Desjupa, Y. J. Liang, J. S. Bradshaw, R. M. Izatt, *J. Am. Chem. Soc.* **1997**, *119*, 353.

99 H. F. Wu, J. S. Brodbelt, *J. Am. Soc. Mass Spectrom.* **1993**, *4*, 718.

100 C.-C. Liou, J. S. Brodbelt, *J. Am. Chem. Soc.* **1992**, *114*, 6761.

101 D. V. Dearden, I.-H. Chu, *J. Incl. Phenomena Mol. Recogn.* **1997**, *29*, 269.

102 R. R. Julian, J. L. Beauchamp, *J. Am. Soc. Mass. Spectrom.* **2002**, *13*, 493.

103 R. R. Julian, J. A. May, B. M. Stoltz, J. L. Beauchamp, *Int. J. Mass Spectrom.* **2003**, *228*, 851.

104 J. B. Fenn, M. Mann, C. K. Meng, S. F. Wong, C. M. Whitehouse, *Science* **1989**, *246*, 64.

105 S. A. Hofstadler, K. A. Sannes-Lowery, R. H. Griffey, *Rapid Commun. Mass. Spectrom.* **1999**, *13*, 1971.

106 S. A. Hofstadler, K. A. Sannes-Lowery, R. H. Griffey, *J. Mass. Spectrom.* **2000**, *35*, 62.

107 a) J. C. Hummelen, J. L. J. van Dongen, E. W. Meijer, *Chem. Eur. J.* **1997**, *3*, 1489; b) B. Baytekin, N. Werner, F. Luppertz, M. Engeser, J. Brüggemann, S. Bitter, R. Henkel, T. Felder, C. A. Schalley, *Int. J. Mass Spectrom.* **2006**, *249*, 138.

108 J. W. Weener, J. L. J. van Dongen, E. W. Meijer, *J. Am. Chem. Soc.* **1999**, *121*, 10346.

109 a) C. A. Schalley, C. Verhaelen, F.-G. Klärner, U. Hahn, F. Vögtle, *Angew. Chem. Int. Ed.* **2005**, *44*, 477; b) M. A. C. Broeren, J. L. J. van Dongen, M. Pittelkow, J. B. Christensen, M. H. P. van Genderen, E. W. Meijer, *Angew. Chem. Int. Ed.* **2004**, *43*, 3557.

110 a) D. J. Cram, J. M. Cram, *Acc. Chem. Res.* **1978**, *11*, 8; b) V. Rüdiger, H. J. Schneider, V. P. Solov'ev, V. P. Kazachenko, O. A. Raevsky, *Eur. J. Org. Chem*. **1999**, 1847.

111 a) S. Maleknia, J. Brodbelt, *J. Am. Chem. Soc.* **1993***, 115*, 2837; b) D. V. Dearden, Y. J. Liang, J. B. Nicoll, K. A. Kellersberger, *J. Mass Spectrom.* **2001**, *36*, 989; c) D. V. Dearden, C. Desjupa, Y. J. Liang, J. S. Bradshaw, R. M. Izatt, *J. Am. Chem. Soc.* **1997**, *119*, 353; d) H. F. Wu, J. S. Brodbelt, *J. Am. Soc. Mass Spectrom.* **1993**, *4*, 718; e) C.-C. Liou, J. S. Brodbelt, *J. Am. Chem. Soc.* **1992**, *114*, 6761; f) D. V. Dearden, I.-H. Chu*, J. Incl. Phenomena Mol. Recogn.* **1997**, *29*, 269.

112 J. B. Fenn, M. Mann, C. K. Meng, S. F. Wong, C. M. Whitehouse, *Science* **1989**, *246*, 64.

113 a) M. Meot-Ner (Mautner*), J. Am. Chem. Soc.* **1983**, *105*, 4912; b) NIST Chemistry WebBook, NIST Standard Reference Database 69, Eds. P.J. Linstrom, W.G. Mallard, National Institute of Standards and Technology, Gaithersburg MD, 20899, http://webbook.nist.gov, (retrieved April 16, 2009).

114 a) C. Lifshitz, *Int. J. Mass Spectrom.* **2004**, *234*, 63; b) K. A. Kellersberger, C. Desjupa, Y. J. Liang, R. M. Pope, D. V. Dearden, *Int. J. Mass Spectrom.* **1999**, *193*, 181; c) E. Ventola, K. Rissanen, P. Vainiotalo, *Chem. Eur. J.* **2004**, *10*, 6152; d) E. Ventola, A. Hyyryläinen, P. Vainiotalo, *Rapid Commun. Mass Spectrom.* **2006**, *20*, 1218; e) E. Kalenius, D. Moiani, E. Dalcanale, P. Vainiotalo, *Chem. Commun.* **2007**, 3865.

115 T. Wyttenbach, M. T. Bowers, J. Am. Soc. Mass Spectrom. 1999, 10, 9.

116 a) S. Campbell, M. T. Rodgers, E. M. Marzluff, J. L. Beauchamp, *J. Am. Chem. Soc.* **1995**, *117*, 12840; b) H. A. Cox, R. R. Julian, S. W. Lee, J. L. Beauchamp,. *J. Am. Chem. Soc.* **2004**, *126*, 6485; c) M. A. Freitas, A. G. Marshall, *Int. J. Mass Spectrom.* **1999**, *182-183*, 221; d) N. C. Polfer, R. C. Dunbar, J. Oomens, *J. Am. Soc. Mass Spectrom.* **2007**, *18*, 512.

117 For an intriguing example of covalent bond formation in a non-covalent complex, also see: R. R. Julian, J. A. May, B. M. Stoltz, J. L. Beauchamp, *Angew. Chem. Int. Ed.* **2003**, *42*, 1012.

118 C. Blondel, C. Delsart, F. Goldfarb, *J. Phys. B* **2001**, *34*, L281.

119 J. E. Bartmess, J. A. Scott, R. T. McIver Jr., *J. Am. Chem. Soc.* **1979**, *101*, 6046.

120 T. Becherer, D. Meshcheryakov, A. Springer, V. Böhmer. C. A. Schalley, *J. Mass. Spectrom.* **2009**, *44*, 1338.

121 B. L. Schottel, H. T. Chifotides, K. R. Dunbar, *Chem. Soc. Rev.* **2008**, *37*, 68.

122 H. Y. Au-Yeung, G. D. Pantos, J. K. M. Sanders, *Proc. Natl. Acad. Sci.* **2009**, *106*, 10466.

123 H. Y. Au-Yeung, G. D. Pantos, J. K. M. Sanders, *J. Am. Chem. Soc.* **2009**, *131*, 16030.

124 H. Shao, T. Nguyen, N. C. Romano, D. A. Modarelli, J. R. Parquette, *J. Am. Chem. Soc.* **2009**, *131*, 16374.

125 N. Sakai, R. Bhosale, D. Emery, J. Mareda, S. Matile, *J. Am. Chem. Soc.* **2010**, *132*, 6923.

126 N. Sakai, J. Mareda, E. Vautheyb, S. Matile, *Chem. Commun.* **2010**, 46, 4225.

127 V. Gorteau, G. Bollot, J. Mareda, S. Matile, *Org. Biomol. Chem.* **2007**, *5*, 3000-3012.

128 S. Gabutti, M. Knutzen, M. Neuburger, G. Schull, R. Berndt, M. Mayor, *Chem. Commun.* **2008**, 2370.

129 R. G. Cooks, J. S. Patrick, T. Kotiaho, S. A. McLuckey, *Mass Spectrom. Rev.* **1994**, *13*, 287.

130 B. A. McNally, A. V. Koulov, B. D. Smith, J.-B. Joos, A. P. Davis, *Chem. Commun.* **2005**, 1087.

131 S. Gabutti, S. Schaffner, M. Neuburger, M. Fischer, G. Schäfer, M. Mayor, *Org. Biomol. Chem.*, **2009**, *7*, 3222.

132 S. S. Zhu, H. Staats, K. Brandhorst, J. Grunenberg, F. Gruppi, E. Dalcanale, A. Lützen, K. Rissanen, C. A. Schalley, *Angew. Chem.* **2008**, *120*, 800; *Angew. Chem. Int. Ed.* **2008**, *47*, 788.

133 A. Shivanyuk, J. Rebek, Jr, *J. Am. Chem. Soc.* **2003**, *125*, 3432.

134 L. Avram, Y. Cohen, *J. Am. Chem. Soc.* **2004**, *126*, 11556

135 L. R. MacGillivray, J. L. Atwood, *Nature* **1997**, *389*, 469.

136 N. K. Beyeh, M. Kogej, A. Åhman, K. Rissanen, C. A. Schalley, *Angew. Chem. Int. Ed.* **2006**, *45*, 5214.

137 a) A. Shivanyuk, J. Rebek, Jr, *Chem. Commun.* **2001**, 2424; b) S. Shimizu, T. Kiuchi, N. Pan, *Angew. Chem. Int. Ed.* **2007**, *46*, 6442.

138 I. Philip, A. E. Kaifer, *J. Org. Chem.* **2005**, *70*, 1558.

139 T. Evan-Salem, I. Baruch, L. Avram, Y. Cohen, L. C. Palmer, J. Rebek, Jr., *Proc. Natl. Acad. Soc.* **2006**, *103*, 12296.

140 L. Avram, Y. Cohen, *J. Am. Chem. Soc.* **2002**, *124*, 15148.
141 N. K. Beyeh, unpublished results.
142 a) I. Krossing, *Chem. Eur. J.* **2001**, *7*, 490; b) A. Bihlmeier, M. Gonsior, I. Raabe, N. Trapp, I. Krossing, *Chem. Eur. J.* **2004**, *10*, 5041.
143 Safety data sheet of chloroform, Fisher Scientific UK, 26.4.2011.
144 Byron Purse et al., unpublished results.
145 Y. Cohen , T. Evan-Salem, L. Avram, *Supramol. Chem.* **2008**, *20*, 71.
146 a) R. E. Maples, *Petroleum Refinery Process Economics* (2nd ed.), Pennwell Books, Tulsa, OK, 2000; b) http://en.wikipedia.org/wiki/Viscosity#Liquids.
147 J.-M. Lehn, in *Supramolecular Chemistry: Concepts and Perspectives,* Wiley-VCH, Weinheim, **1995**.
148 G. Desiraju, *Angew. Chem. Int. Ed.* **1995**, *34*, 2311.
149 P. Timmerman, W. Verboom, and D. Reinhoudt, *Tetrahedron,* **1996**, *52*, 2663.
150 A. Jasat and J. C. Sherman, *Chem. Rev.* **1999**, *99*, 931.
151 D. Rudkevich, J. Rebek, *Eur. J. Org. Chem.,* **1999**, 1991.
152 M. Nissinen, K. Rissanen, *Supramol. Chem.*, **2003**, *15*, 581.
153 M. Luostarinen, A. Åhman, M. Nissinen, K. Rissanen, *Supramol. Chem.*, **2004**, *16*, 505.
154 H. Mansikkamäki, C. A. Schalley, M. Nissinen, K. Rissanen, *New J. Chem.*, **2005**, *29*, 116.
155 A. Shivanyuk, J. Rebek, *J. Am. Chem. Soc.*, **2003**, *125*, 3432.
156 J. Atwood, L. Babour, A. Jerga, *Proc. Natl. Acad. Sci. USA*, **2002**, *99*, 4837.
157 H. Mansikkamäki, M. Nissinen, K. Rissanen, *Angew. Chem. Int. Ed.* **2004**, *43*, 1243.
158 J. Kang, J. Rebek, Jr., *Nature* **1997**, *385*, 50.
159 H. Ito, T. Kusukawa, M. Fujita, *Chem. Lett.*, **2000**, 598.
160 J. Chen, S. Kärner, S. L. Craig, D. M. Rudkevich, J. Rebek, Jr., *Nature,* **2002**, *415*, 385.
161 H. Konishi, O. Morikawa, K. Kobayashi, K. Abe, A. Ohkubo, *Tetrahedron Lett.,* **2003**, *44*, 7425
162 W. Iwanek, J. Mattay, *Liebigs Ann. Chem.,* **1995**, 1463.
163 K. Airola, V. Böhmer, E. F. Paulus, K. Rissanen, C. Schmidt, I. Thondorf, W. Vogt, *Tetrahedron,* **1997**, *53*, 10709.
164 C. Schmidt, K. Airola, V. Böhmer, W. Vogt, K. Rissanen, *Tetrahedron,* **1997**, *53*, 17691.
165 G. Arnott, H. Heaney, R. Hunter, P. C. B. Page, *Eur. J. Org. Chem.,* **2004**, 5126.
166 C. Schmidt, I. Thondorf, E. Kolehmainen, V. Böhmer, W. Vogt, K. Rissanen, *Tetrahedron Lett.* **1998**, *39*, 8833.
167 N. K. Beyeh, A. Valkonen, K. Rissanen, *Org. Lett.* **2010**, *12*, 1392.
168 D. P. Weimann, C. A. Schalley, *Supramol. Chem.* **2008**, *20*, 117.
169 H. D. F. Winkler, E. V. Dzyuba, J. A. W. Sklorz, N. K. Beyeh, K. Rissanen, C. A. Schalley, *Chem. Sci.* **2011**, *2*, 615.
170 J. A. Bryant, M. T. Blanda, M. Vincenti, D. J. Cram, *J. Am. Chem. Soc.,* **1991**, *113*, 2167.
171 L. M. Nuwaysir, J. A. Castoro, C. L.-C. Yang, C. L.Wilkins, *J. Am. Chem. Soc.,* **1992**, *114*, 5748.
172 F. Inokuchi, Y. Miyahara, T. Inazu, S. Shinkai, *Angew. Chem. Int. Ed.* **1995**, *34*, 1364.
173 P. S. H. Wong, X. Yu, D. V. Dearden, *Inorg. Chim. Acta,* **1996**, *246*, 259.
174 E. Ventola, K. Rissanen, P. Vainiotalo, *Chem. Commun.,* **2002**, 1110.

175 M. Mäkinen, P. Vainiotalo, K. Rissanen, *J. Am. Soc. Mass Spectrom.,* **2002**, *7*, 851.

176 M. Mäkinen, M. Nissinen, K. Rissanen, P. Vainiotalo, *J. Am. Chem. Soc.,* **2003**, *14*, 143.

177 M. C. Letzel, B. Decker, A. B. Rozhenko, W. W. Schoeller, J. Mattay, *J. Am. Chem. Soc.,* **2004**, *126*, 9669.

178 K. A. Connors, *Binding Constants*, Wiley, New York, **1987**.

179 K. Hirose, *J. Inclusion Phenom. Macrocyclic Chem.*, **2001**, *39*, 193.

180 K. Hirose, *Determination of Binding Constants*, in: C. A. Schalley (Ed.), *Analytical Methods in Supramolecular Chemistry*, Wiley-VCH, Weinheim, 2007, pp 17-54.

181 J. L. Atwood, A. Szumna, *J. Supramol. Chem.* **2002**, ***2***, 479.

182 C. Heim, A. Affeld, M. Nieger, F. Vögtle, *Helv. Chim. Acta* **1999**, *82*, 746.

183 S. Q. Wang, X. J. Liu, Z. M. Yi, K. Zhao, *Chinese Chem. Lett.* **2003**, *14*, 581-584.

184 L. Yuan, A. R. Sanford, W. Feng, A. Zhang, J. Zhu, H. Zeng, K. Yamato, M. Li, J. S. Ferguson, B. Gong, *J. Org. Chem*. **2005**, *70*, 10660.

185 A. Zhang, J. S. Ferguson, K. Yamato, C. Zheng, B. Gong *Org. Lett.* **2006**, *8*, 5117.

186 O. Braun, A. Hunten, F. Vögtle, *J. Prakt. Chem.* **1999**, *341*, 542.

187 C. Fischer, M. Nieger, O. Mogck, V. Böhmer, R. Ungaro, F. Vögtle, *Eur. J. Org. Chem.* **1998**, 155.

188 R. J. Amir, N. Pessah, M. Shamis, D. Shabat, *Angew. Chem. Int. Ed.* **2003**, *42*, 4494.

189 a) D. M. Kneeland, K. Ariga, V. M. Lynch, C. Y. Huang, E. V. Anslyn, *J. Am. Chem. Soc.* **1993**, *115*, 10042; b) O. M. New, D. Dolphin, *Eur. J. Org. Chem.* **2009**, 2675.

190 H. Konno, Y. Sasaki, Chem. Lett. **2003**, *32*, 252.